The 12th International Symposium on Water Environment Systems
---with Perspective of Global Safety

21st ~ 23rd November, 2024

Department of Civil and Environmental Engineering
Graduate School of Engineering
Tohoku University

GP-RSS
International Joint Graduate Program in Resilience and Safety Studies

SyDE
WISE Program for Sustainability in the Dynamic Earth
変動地球共生学卓越大学院プログラム

SPONSORS

International Joint Graduate Program in Resilience and Safety Studies of Tohoku University

http://gp-rss.tohoku.ac.jp/

WISE Program for Sustainability in the Dynamic Earth of Tohoku University
https://syde.tohoku.ac.jp/

Department of Civil and Environmental Engineering, Graduate School of Engineering, Tohoku University

http://www.eng.tohoku.ac.jp/

ORGANIZERS

Dr. So KAZAMA	Professor, Tohoku Univ
Dr. Yu-You LI	Professor, Tohoku Univ
Dr. Daisuke SANO	Professor, Tohoku Univ
Dr. Keiko UDO	Professor, Tohoku Univ
Dr. Kengo KUBOTA	Associate Professor, Tohoku Univ
Dr. Mohan AMARASIRI	Associate Professor, Tohoku Univ
Dr. Rajapaksha Mudiyansekage Janaka Bamunawala	Assistant Prof., Tohoku Univ

SECRETARIATS

Dr. Yusuke HIRAGA	Assistant Professor, Tohoku Univ
Dr. Yu QIN	Assistant Professor, Tohoku Univ
Dr. Wakana OISHI	Assistant Professor, Tohoku Univ
Juntong HA	DC Student, Tohoku Univ
Zhafirah Meuthia Ardhana	DC Student, Tohoku Univ
Qingkang ZENG	DC Student, Tohoku Univ
Weiyi WANG	DC Student, Tohoku Univ

PARTICIPANTS

University of Illinois at Urbana-Champaign, USA

    Helen Nguyen   Ivan Racheff Professor

Nanjing Tech University, China

Yong Hu	Professor
Liwen Cao	Student
Xiang Li	Student

Kumoh National Institute of Technology, South Korea

Seong Jin Noh	Associate Professor
Bomi Kim	Student
Yaewon Lee	Student
Hyuna Woo	Student

Suzhou University of Science and Technology, China

Zhe Kong	Associate Professor
Guangyi Ma	Student
Chende Sun	Student

University of Science and Technology Beijing, China

    Yan Guo   Associate Professor

Universidad Técnica Federico Santa María, Chile

    Joaquin Meza   Assistant Professor

National Institute of Ecology, South Korea

    Ji Hyun Kang   Senior Researcher

Kasetsart University, Thailand

Prem Rangsiwanichpong	Assistant Professor
Jinnaphrot Chalatthanyakit	Student
Khatthaleeya Prommit	Student

Fukushima University, Japan

    Asim Hussain   Student

Erina Yamagata	Student
Sheikh Hefzul Bari	Student

Miyazaki University, Japan

Chen Xu	Student

Tohoku Institute of Technology, Japan

Keitaro Susukida	Student
Mutsuki Kodama	Student

Tongji University, China

Yafei Zhang	Student

Tohoku University, Japan

Yusuke Hiraga	Assistant Professor
Amalia Nafisah Rahmani Irawan	Post-Doc researcher
Jacqueline Muthoni Mbugua	Post-Doc researcher
Jose Angelo Hokson	Post-Doc researcher
Atsuya Ikemoto	Student
Chang Liu	Student
Daniel Martua	Student
Hongjun Zhao	Student
Kumudu Madhawa Kurugama	Student
Muthiah SADIDAH	Student
Putri Shafa KAMILA	Student
Qingkang Zeng	Student
Ruixin Wu	Student
Ryotaro Tahara	Student
Sakina Ahmed	Student
Shimon Suzuki	Student
Takaya Kaneko	Student
Takuya Matsumoto	Student
Tomoaki Matsuura	Student
Wasitha Dilshan	Student
Weiyi Wang	Student
Y Liu	Student
Zhaolong Gu	Student

FIELDWORK

21 Nov (Thu)

Fieldwork I: Arahama Elementary School and Natori-Denshokan

・**Arahama Elementary School**

This facility preserves and maintains the school building of the Arahama Elementary School in Sendai, which was damaged by the Great East Japan Earthquake on March 11, 2011, as a relic of the disaster, with the aim of raising awareness of disaster prevention and disaster mitigation among many people. The school building, which still retains clear traces of the disaster, is open to the public and exhibits images and videos of the immediate aftermath of the disaster so that visitors can experience the power and threat of the tsunami.

・**Natori-Denshokan**

The museum aims to pass on the memories and lessons of the Great East Japan Earthquake to the rest of the world and to future generations, to keep the disaster from fading away, and to foster awareness of disaster prevention. We are grateful for all the support we have received and will continue to work together with storytellers and local residents involved in disaster prevention activities to help realize a society that is resilient to natural disasters.

Fieldwork II: Sen-en purification center and JNEX bioplant

Gathering: 8:50 at Aobayama bus stop (青葉山駅前) (reserved only)

・**Sen-en purification center**

Sen-en purification center, receiving 120,000 m^3/day of wastewater, is the second largest wastewater treatment plant in Miyagi-ken. The A/O and A/A/O methods are used to treat the wastewater and the sewage sludge is effectively digested for biogas, which is further converted to low-carbon electricity in the plant.

・**Jnex bioplant**

Jnex has been the largest biogas plant in Japan. This plant receives organic solid wastes from local areas and produces biogas, electricity and fertilizers. Jnex is making contributions to sustainable society in Sendai by reducing solid wastes, recycling bio-energy and reusing organic matters and nutrients.

SYMPOSIUM

22 Nov (Fri) (GMT +9)

8:50 - 9:00 Opening Speech & Group Photo

9:00-12:05 Oral Session I : *Water & Wastewater treatment*

9:00 - 10:00	[Plenary Lecture] *Legionella pneumophila* and lead: the weakest link in drinking water safety in the US **Helen NGUYEN**, *University of Illinois at Urbana-Champaign*
10:00-10:10	*Coffee break*
10:10-10:25	Murine Norovirus Inactivation and Adaptation Mechanism to Ammonia **Putri Shafa KAMILA**, *Tohoku University*
10:25-10:40	A novel technology on hydrothermal mineralization of CO_2 capture solution into $CaCO_3$-based functional building materials **Yafei ZHANG**, *Tongji University*
10:40-10:55	Enhanced anaerobic digestion performance of mesophilic and thermophilic siphon-driven self-agitated reactor for food waste treatment by intermittent micro-aeration **Xiang LI**, *Nanjing Tech University*
10:55-11:05	*Coffee break*
11:05-11:20	Denitrification-enhanced anaerobic digestion for low-carbon and effective treatment of DMF-containing industrial wastewater **Zhe KONG**, *Suzhou University of Science and Technology*
11:20-11:35	Advanced nitrogen and phosphorus removal by Anammox-HAP in IC reactors **Liwen CAO**, *Nanjing Tech University*
11:35-11:50	Characteristics and mechanisms of partial denitrification-anammox granular sludge floating in upflow reactor **Ruixin WU**, *Tohoku University*
11:50-12:05	The exploration of efficient nitritation through granular sludge in the continuous mode reactor **Hongjun ZHAO**, *University of Science and Technology Beijing*

12:05-13:00 *Lunch Break*

12:30-14:30 Poster Session

Towards carbon-neutral biotechnologies for rural wastewater: A review of current treatment processes and future perspectives
- **Guangyi MA**, *Suzhou University of Science and Technology*

Biofiltration for low-carbon rural wastewater treatment: a review of advancements and opportunities towards carbon neutrality
- **Chende SUN**, *Suzhou University of Science and Technology*

Upgrading of Nitrogen Removal Process by Hybrid Anammox Reactor with Functional Carriers
- **Weiyi WANG**, *Tohoku University*

Effects of pH Control and Sludge Recirculation on Hydrogen Production in Two-Phase Anaerobic Digestion of Food Waste and Paper Waste
- **Qingkang ZENG**, *Tohoku University*

Evaluation of ensemble post-processing methods to improve high-resolution short-term streamflow prediction based on LDAPS and WRF-Hydro
- **Yaewon Lee**, *Kumoh National Institute of Technology, Republic of Korea*

Developing deep learning-based urban inundation prediction model with physical information for real-time applications
- **Hyuna Woo**, *Kumoh National Institute of Technology, Republic of Korea*

Evaluating Downstream Flood Hazards Using Dam Break Simulation: A Case Study of Khlong Luang Rachalothorn Reservoir, Thailand
- **Jinnaphrot Chalatthanyakit**, *Kasetsart University, Thailand*

Future Projections of Dengue Fever Risk in Chiang Mai Under Climate Change
- **Prem Rangsiwanichpong**, *Kasetsart University, Thailand*

Multiphase dolomitization in Kingriali formation of Namal Gorge section in Western Salt Range, Pakistan
- **Asim Hussain**, *Fukushima University, Japan*

Suspended sediment transport in the Abukuma River estuary

- **Sheikh Hefzul Bari**, *Fukushima University, Japan*

Implementation of disaster prevention education method using three-dimensional digital space: Focusing on the subject's independence

- **Keitaro Susukida**, *Tohoku Institute of Technology, Japan*

Effectiveness analysis of 3D disaster education content using text mining of free response questionnaire data

- **Mutsuki Kodama**, *Tohoku Institute of Technology, Japan*

Can sampling during rain events improve the detection rate of eDNA metabarcoding?

- **Chen Xu**, *University of Miyazaki, Japan*

What are the differences between the two rivers in different climatic zones? -Focusing on the Abukuma River and Mogami River in Japan

- **Erina Yamagata**, *Fukushima University, Japan*

Analysis of Future Changes and the Impact of Historical Warming on Localized Heavy Rainfall Using the Pseudo-Global Warming Method

- **Ryotaro Tahara**, *Tohoku University*

Effects of wetland loss on the regional temperature: Case study of 2023 heatwave event in Southeast Asia

- **Chang Liu**, *Tohoku University*

High-resolution spatial estimation of soil moisture using UAV aerial photography and machine learning algorithms

- **Takuya Matsumoto**, *Tohoku University*

The Impact of Sea Level Rise and Wave Driven by Climate Change on Indonesia Coastal Flood Condition

- **Daniel Martua**, *Tohoku University*

Understanding relationship between land use change and fluvial inundation frequency in Chiang Mai, Thailand

- **Zhaolong Gu**, *Tohoku University*

Effects of updating frequency and observation network density in hydrological data assimilation
- **Kumudu Madhawa Kurugama**, *Tohoku University*

Development of hazard assessment methods capable of simulating the discharge of large woody debris at dam catchments
- **Y Liu**, *Tohoku University*

Effects of Climate Change and Population Change on Exposed Population to Fluvial Flood, Pluvial Flood, and Slope Failure
- **Tomoaki Matsuura**, *Tohoku University*

SRGAN-based downscaling of GRACE groundwater storage for improved aquifer management
- **Sakina Ahmed**, *Tohoku University*

Relationship between long-term river-to-coast sediment supply and channel characteristics
- **Shimon Suzuki**, *Tohoku University*

Modeling Post-Wildfire Hydrological Responses: Assessing Flood Risk Amplification in California's Watersheds
- **Wasitha Dilshan**, *Tohoku University*

An Integrated Evaluation of the Potential for Hydropower Generation and Flood Damage Reduction in Irrigation Reservoirs Across Japan
- **Atsuya Ikemoto**, *Tohoku University*

Assessing the effectiveness of reducing the amount of damage to trees in river channels throughout Japan
- **Takaya Kaneko**, *Tohoku University*

Modeling The Interaction of Flood Hazard and Society in Citarum Watershed, Indonesia: A Socio-hydrological Perspective
- **Muthiah SADIDAH**, *Tohoku University*

14:45-18:00 Oral Session II : *Hydrology & Hydro-ecology*

14:45-15:05	Integrated WRF and WRF-Hydro approaches for assessing climate change impacts on extreme flood events
	Seong Jin NOH, *Kumoh National Institute of Technology*, Republic of Korea
15:05-15:25	Assessing Probable Maximum Precipitation (PMP) Estimates in Chile Using Statistical GEV Distribution and Physically Based Approaches
	Joaquin Meza, *Universidad Técnica Federico Santa María*, Chile
15:25-15:45	Analysis on the inundation vulnerability of coastal dunes depending on a scenario of sea level rise
	Jihyun Kang, *National Institute of Ecology*, Republic of Korea
15:45-16:05	Enhancing physics-based inundation modeling through ensemble data assimilation: impacts of multivariate observations
	Bomi Kim, *Kumoh National Institute of Technology*, Republic of Korea
16:05-16:25	Assessing Soil Erosion under Climate Change Using CMIP6 Models in the Mun River Basin
	Khatthaleeya Prommit, *Kasetsart University*, Thailand
16:25-16:45	*Coffee break*
16:45-17:05	Predicting typhoon rainfall using image-based similarity of atmospheric fields
	Jose Angelo Hokson, *Tohoku University*
17:05-17:25	Sensitivity analysis of cloud seeding methods for rainfall suppression: A WRF model-based study of the 2014 Hiroshima rainfall event
	Jacqueline Muthoni Mbugua, *Tohoku University*
17:25-17:45	Using census and model-based approach to develop 1-km crop yield of paddy in Indonesia
	Amalia Nafisah Rahmani Irawan, *Tohoku University*

## 17:45 - 18:00 General discussion & Closing Remarks

18:00 - 20:00 Network Dinner

Full Proceeding: [Click Here]

VENUE of SYMPOSIUM

Aobayama Campus, Graduate School of Engineering, Tohoku University
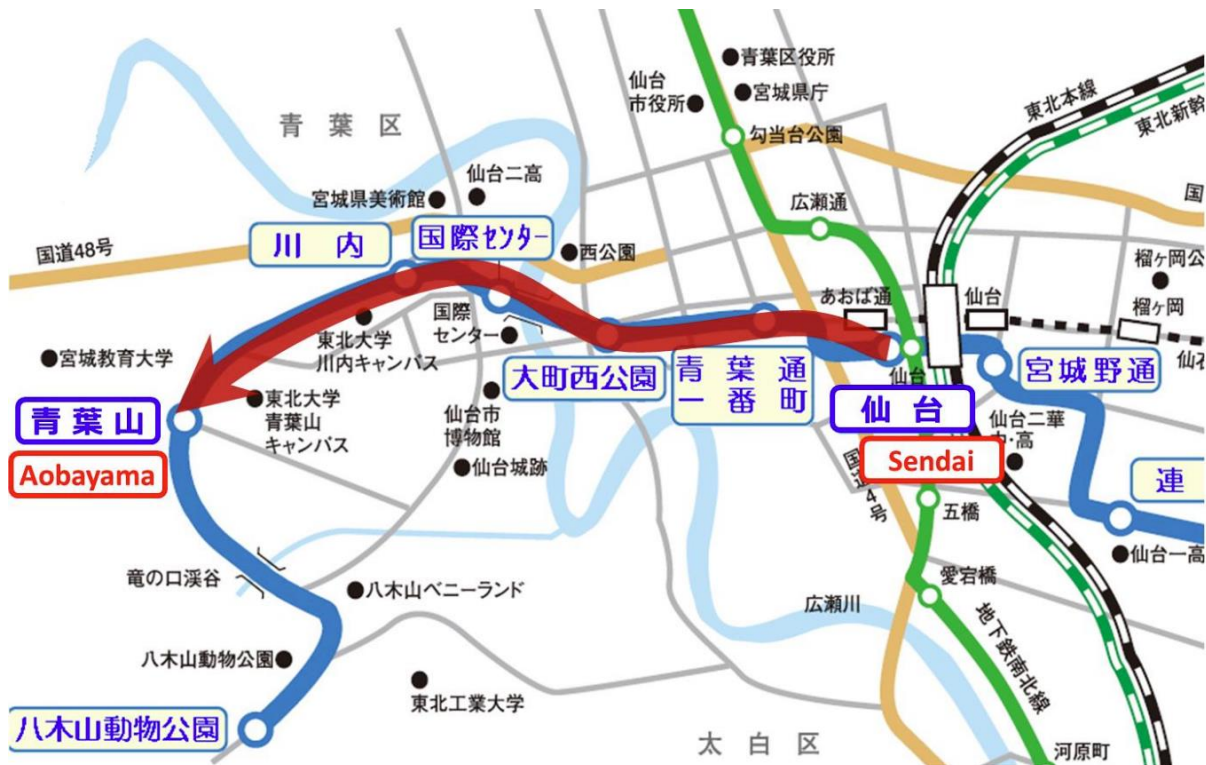（東北大学大学院工学研究科・青葉山キャンパス）

- Lectures & Posters: Room 401, Aoba Memorial Hall（C03）

  （講演、口頭・ポスターの発表：青葉記念会館(C03)，401号室）

- Network Dinner: 1F, Engineering Laboratory Complex Building（C10）

  （懇親会：総合研究棟(C10)，1階）
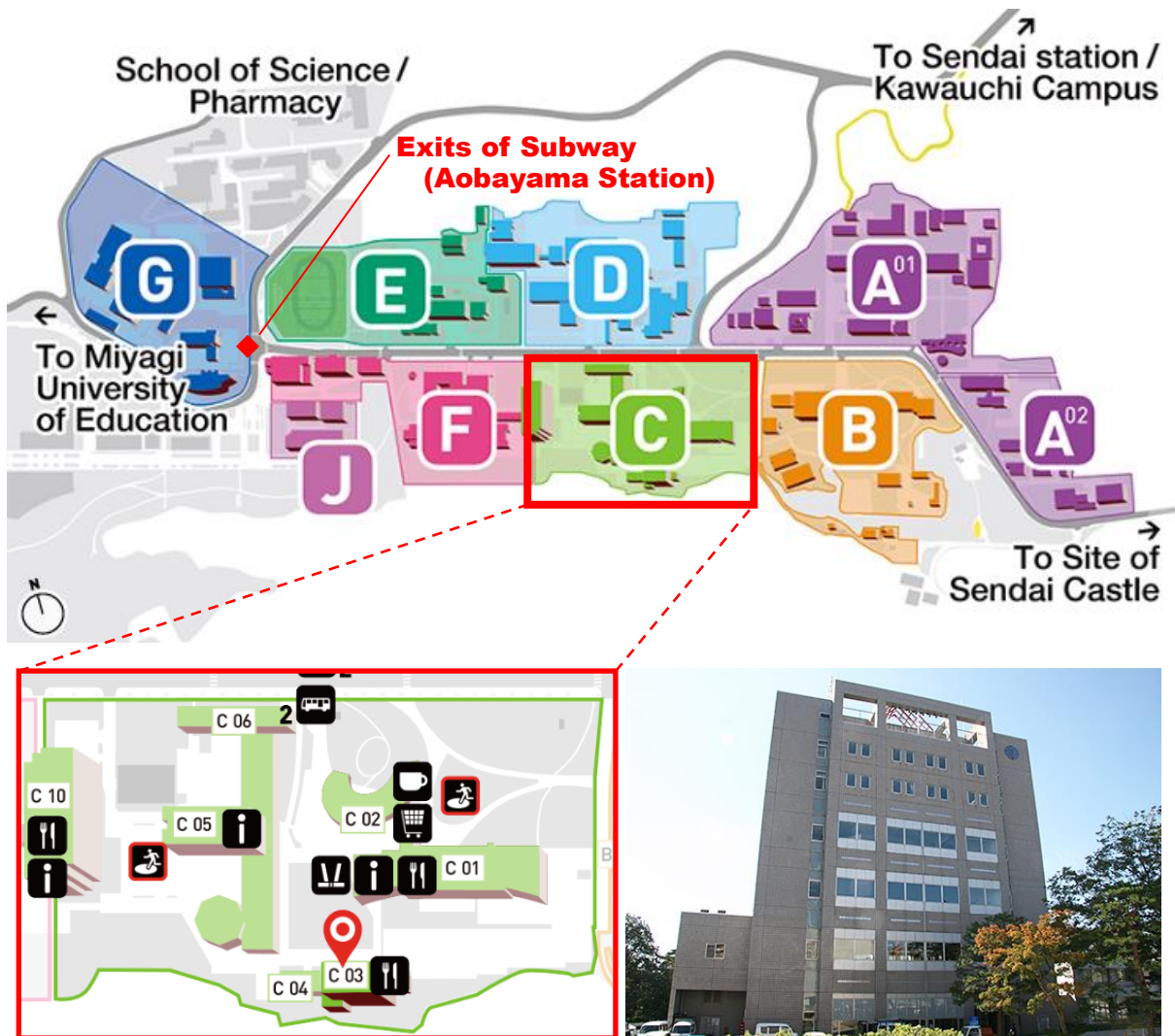
Aoba Memorial Hall（C03）（青葉記念会館）

ACCESS

to Aobayama Campus, Tohoku Univ.

Public access: Only Subway **Tozai Line** is recommended.

If you start from **Sendai Sation** (or Aoba-dori Ichiban-cho), please take the direction of Yagiyama Zoological Park (Yagiyama Dobutsu Koen) and get off at **Aobayama**. (Ticket fee: 250 Yen)

公共交通機関：　地下鉄・東西線はオススメ

「仙台駅」（又は「青葉通一番町」）から「八木山動物公園」方面に「青葉山」まで。

（運賃：250 円）

The 12th International Symposium on Water Environment Systems
----- with Perspective of Global Safety   (Nov. 21st～23rd , 2024)

GP-RSS & SyDE
Tohoku University

Legionella pneumophila and lead: the weakest link in drinking water safety in the US

○ Helen Nguyen

Ivan Racheff Professor, Civil and Environmental Engineering, University of Illinois at Urbana-Champaign

Abstract

Drinking water distribution system infrastructure in the United States is aging and degrading, contributing to numerous public health crises and a rise in concern over chemical and microbiological water quality. Point-of-use (POU) filters certified to remove lead (Pb), many of which are composed of porous solid block activated carbon media, have become increasingly popular as a temporary solution to address drinking water quality problems. Unfortunately, these filters can release high concentrations of bacteria and fail to effectively remove particulate Pb. For their rapid rise in usage, these POU filters are understudied, and some unintended consequences go overlooked in the pursuit of an inexpensive and convenient solution to decrease Pb exposure in drinking water. I will present the findings of a recent project that captured a holistic view of the contributions activated carbon POU filters make to drinking water quality. First, we quantified the risk posed by *Legionella pneumophila* (*L. pneumophila*) in homes supplied by private wells and studied the role POU filters play on the microbial risk of drinking water. *L. pneumophila* was detected in about 30% of samples in rural homes. Systems without filters and without chlorine had the highest risk, followed by those with ripe filters (>1 week old), those without filters and with chlorine, and finally, those with new filters. Acquiring quantitative data and understanding the factors influencing the microbial risk in understudied water systems and from using these ubiquitous POU filters is essential for risk management in indoor environments. Second, we examined the impacts of water hardness and biofilm in the filters on the Pb removal efficiency of activated carbon POU filters. Adding calcium and dissolved biomass diminished the repulsion of negatively charged Pb phosphate nanoparticles, increasing aggregation and improving POU filter performance. This study provides important insights into how well filters will remove Pb as bacteria accumulate and grow, the contribution of aggregation to this Pb removal efficiency, and to what extent additional measures need to be taken to minimize bacterial growth.

The 12th International Symposium on Water Environment Systems
----- with Perspective of Global Safety   (Nov. 21st ~ 22nd , 2024)

GP-RSS & SyDE
Tohoku University

Murine Norovirus Inactivation and Adaptation Mechanism to Ammonia

○ Putri Shafa KAMILA[1*], Wakana OISHI[2] & Daisuke SANO[1,2]

[1]Department of Frontier Sciences for Advanced Environment, Graduate School of Environmental Studies, Tohoku University, Miyagi 980-8579, Japan.

[2]Department of Civil and Architecture, School of Engineering, Tohoku University, Miyagi 980-8579, Japan.

*E-mail: putri.shafa.kamila.p7@dc.tohoku.ac.jp

Abstract

Discrepancies in safe sanitation services between and within countries are a concerning issue. Aside from facilitating the spread of waterborne pathogens, particularly viruses, these viruses can rapidly adapt to various environmental stresses. Therefore, relying on a single disinfection strategy for safe sanitation services may not be sufficient to prevent infectious disease outbreaks. This research investigates disinfection treatment of murine norovirus using ammonia, a known in-situ sanitizer. Murine norovirus was inactivated by 3-log reduction using 328 mM ammonia with a 90-minute contact time. While experimental adaptation studies are currently underway, future research will explore the ammonia inactivation mechanism and the adaptation mechanism of population with decreased susceptibility.

Keywords: murine norovirus, ammonia, inactivation, disinfection, adaptation

1 Introduction

Global access to safe sanitation increased from 49% to 57% between 2015 and 2022. However, 3.5 billion people still lack safe sanitation services, including 419 million who practice open defecation [1]. Challenges are not only related to accessibility but disparities between and within countries [2]. Thirty-seven percent of the urban population is not connected to sewers, a trend that is becoming more common in low- and middle-income countries. As a result, non-sewered sanitation, which involves on-site treatment or storage and transport to a treatment facility, is an alternative option. However, there is a misconception that containment equates to safely managed treatment. In reality, many containment systems are inappropriately constructed without standardization [3]. This significantly contributes to the transmission of waterborne pathogens, including norovirus.

Norovirus is highly contagious, relatively stable in the environment for over two weeks, and can cause gastroenteritis outbreaks through fecal-oral route transmission [4]. In contrast, ammonia, a natural component of excreta, has the capability to inactivate viruses [5]. This research will focus on norovirus inactivation by ammonia. Additionally, genetic variation and high adaptability, particularly RNA viruses, can lead to the emergence of less susceptible populations that are not sufficiently inactivated during treatment, particularly disinfection processes [6]. This is a major concern in virus inactivation efforts. As the virus adaptation mechanism is likely linked to virucidal agent's inactivation mechanism, this research will not only investigate the adaptation mechanism of norovirus to repeated ammonia exposure, but also confirm the inactivation mechanism itself.

2 Materials and methods

In this research, murine norovirus (MNV) S7 PP3 strain was propagated and enumerated according to published procedures [7]. The host cell is RAW 264.7 cells (ATCC TIB-71) and it was cultured in Dulbecco's Modified Eagle Medium (DMEM)-2 (Shimadzu) with additional HEPES 10 mM, 10% (v/v) fetal bovine serum (Gibco), 0.1% (w/v) sodium bicarbonate, 2 mM L-glutamine (Gibco), and Antibiotic-Antimycotic (Gibco). For susceptibility test and experimental adaptation, ammonia buffer solution was used and prepared by dissolving 1 M 25% (w/w) $NH_3(aq)$ and 1 M NH_4Cl with ratio of 1:1. In addition, ammonia concentration was obtained using the indophenol blue method [8] and MNV infectivity was determined using plaque assay [7].

Before conducting serial passage for experimental adaptation, MNV was inactivated to know log-reduction value (LRV) for certain contact times. One-hundred microliters MNV suspension with initial concentration 10^6-10^7 PFU (Plaque Forming Unit)/mL was exposed to 900 μL ammonia buffer solution containing 328 mM NH_3 with pH approximately 9.6 in 25°C for 0-, 5-, 30-, 90-minutes, and 24-hours contact times.

Serial passages of MNV with and without disinfection treatment were conducted for obtaining less susceptible population. A virus population was taken from MNV S7 PP3 laboratory strain as ancestor with initial concentration 10^6-10^7 PFU/mL. For treatment with disinfection (test), 100 μL MNV suspension was exposed to 900 μL ammonia buffer solution and incubated at room temperature 25°C for approximately 60 minutes to achieve 3-log reduction. Subsequently, 100 μL of MNV and ammonia buffer suspension was given into 900 μL culture medium and 25 μL HCl to stop disinfection. Final MNV suspension with approximately 10^3 PFU/mL was inoculated to 85-90% confluent RAW 264.7 cells cultured in T75 flask (ThermoFisher Scientific) containing 15 mL of culture medium. While for treatment without disinfection (control), a virus population was taken from the same ancestor and diluted with culture medium so that the final infectious titer was 10^3 PFU/mL. Ammonia buffer solution 900 μL was mixed with 100 μL culture medium and given into the mixture of 900 μL culture medium and 25 μL HCl. After that, 1 mL of virus suspension was inoculated to confluent RAW 264.7 cells cultured in T75 flask containing 14 mL of culture medium and the final mixture of ammonia buffer, culture medium and HCl solution was also added to mimic the same condition as disinfection treatment. The multiplicity of infection (MOI) was approximately 10^{-4}. MNV was finally incubated at 37°C with 5% CO_2 for 2 days. To collect MNV suspension, 50 ml falcon tube was used and centrifuged at 8,000 g for 10 min at 4°C to separate cells pellet. The

The 12th International Symposium on Water Environment Systems
----- with Perspective of Global Safety   (Nov. 21st ~ 22nd , 2024)

GP-RSS & SyDE
Tohoku University

supernatant was passed through a 0.22 μm PVDF membrane filter (Merck) and stored in -80ºC for disinfection susceptibility test. The serial passage was conducted until the 10th passage, and the entire process will be conducted in two replicates.

The susceptibility test was evaluated for each virus population in three replicates by exposing 100 μL MNV *n*th (control/test) population suspension to 900 μL ammonia buffer solution containing 338 ± 33.8 mM NH_3 with pH approximately 9.6 in 25ºC and observed 0-, 30-, and 90-minutes contact times. Moreover, statistical analysis was performed and visualized in RStudio (Version 2024.04.1), with p-value < 0.05 considered to be statistically significant.

3 Results and discussion

MNV was inactivated by 3-log reduction using a 328 mM ammonia buffer solution with a 90-minute contact time. Furthermore, the virus inactivation rate constant (k) was determined using a first-order kinetics model [5] and found to be 0.074/minute.

For the experimental adaptation results, the susceptibility test of MNV *n*th population with a 90-minute contact time, both with (test) and without (control) disinfection treatment, revealed no significant difference in susceptibility to ammonia, as indicated by a p-value of 0.28 from the Wilcoxon test (Fig. 1).
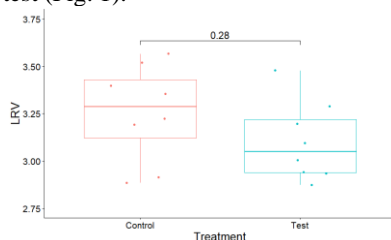
Fig. 1. Wilcoxon test between treatments.

In terms of statistical difference between populations, a p-value of 0.41 was obtained from the Kruskal Wallis test, indicating no significant difference in susceptibility between populations up to the eighth passage. However, it is worth noting that there is a greater than 0.5-log reduction difference in susceptibility between the test and control populations in the fifth population (Fig. 2).
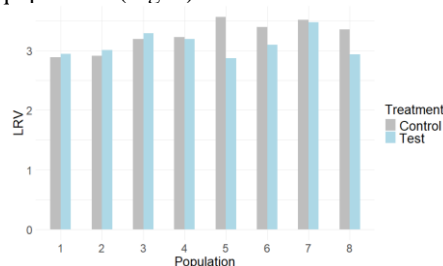
Fig. 2. Log-reduction value comparisons between populations and treatments

Previous studies have shown that MNV can adapt to various disinfection treatments, such as chlorine and calcium hydroxide. Sequencing analysis has been conducted to understand the difference in nucleotide diversity and mutation in susceptible and less susceptible MNV populations. These studies have identified specific mutations in VP1 and VP2 of MNV after repeated exposure to calcium hydroxide and chlorine, respectively [6, 9]. Additionally, another study found that increased nonsynonymous genetic diversity in VP1 was the primary factor contributing to MNV adaptation to chlorine disinfection [10]. Furthermore, cross-resistance has been observed in Echovirus 11 to free chlorine after exposure to ClO_2, as both disinfectants share a similar inactivation mechanism: inhibiting virus binding to host cells by cleaving capsid proteins [11, 12]. While ammonia is known to inactivate MS2 bacteriophage through a single-hit mechanism that causes loss of genome integrity, as evidenced by genome electrophoresis and host-binding investigations [5], the specific mechanisms of capsid protein degradation and MNV adaptation to ammonia remain unclear. Therefore, to confirm whether these adaptation mechanisms align with inactivation mechanism, further analysis, such as genome and protein degradation studies, is crucial.

4 Conclusions

The current result demonstrates that MNV can be inactivated by 99.9% using ammonia within 90 minutes. While the experimental adaptation study did not reveal significant differences in susceptibility between the test and control populations, a greater than 0.5-log reduction in susceptibility was observed in the 5th population. Further investigation into the inactivation mechanism and the reasons for decreased susceptibility is necessary.

Reference

[1] United Nations, The Sustainable Development Goals Report 2024, (2024).

[2] Dickin and Gabrielsson, Inequalities in water, sanitation and hygiene: Challenges and opportunities for measurement and monitoring, Water Security, 20 (2023), 1-10.

[3] Strande, Linda, Integrating recent scientific advances to enhance non-sewered sanitation in urban areas, Nature Water, 2 (2024), 405-418.

[4] Lopman, et al., Environmental transmission of norovirus gastroenteritis, Current Opinion in Virology, 2, 1 (2012), 96-102.

[5] Decrey, et al., Ammonia as an In Situ Sanitizer: Inactivation Kinetics and Mechanisms of the ssRNA Virus MS2 by NH_3, Environ. Sci. Technol., 49, 2 (2015), 1060-1067.

[6] Oishi, et al., Experimental Adaptation of Murine Norovirus to Calcium Hydroxide, Front. Microbiol., 13 (2022), 1-11.

[7] Gonzalez-Hernandez, et al., Plaque assay for murine norovirus, J. Vis. Exp (2012), 1-6.

[8] Scheiner, Determination of ammonia and Kjeldahl nitrogen by indophenol method, Water Research, 10, 1 (1976), 31-36.

[9] Rachmadi, et al., Free-Chlorine Disinfection as a Selection Pressure on Norovirus, Appl. Environ. Microbiol., 84 (2018), 1-14.

[10] Wanguyun, et al., Genetic diversity of murine norovirus populations less susceptible to chlorine, Front. Microbiol., 15 (2024), 1-12.

[11] Wigginton, et al., Virus Inactivation Mechanisms: Impact of Disinfectants on Virus Function and Structural Integrity, Environ. Sci. Technol., 46, 21 (2012), 12069-12078.

[12] Zhong, et al., Cross-Resistance of UV- or Chlorine Dioxide-Resistant Echovirus 11 to Other Disinfectants, Front. Microbiol., 8 (2017), 1-12.

The 12th International Symposium on Water Environment Systems
----- with Perspective of Global Safety   (Nov. 21st ~ 22nd , 2024)

GP-RSS & SyDE
Tohoku University

A novel technology on hydrothermal mineralization of CO_2 capture solution into $CaCO_3$-based functional building materials

◯ Yafei ZHANG[1,2*], Zhenzi JING[1] & Yu-You LI[2]

[1]Key Laboratory of Advanced Civil Engineering Materials of Ministry of Education, School of Materials Science and Engineering, Tongji University, Shanghai, China.
[2]Department of Civil and Environmental Engineering, Graduate School of Engineering, Tohoku University, Sendai, Miyagi, Japan.
*E-mail: zyf1997@tongji.edu.cn.

Abstract

Inspired by natural CO_2 carbonation underground, a novel hydrothermal mineralization technology was developed to convert CO_2 capture solutions and industrial solid wastes into $CaCO_3$-based functional building materials. In-situ CO_2 solidification in capture solution using calcium carbide residue (CCR) into carbonates achieved a high carbonation rate of nearly 90% at 25 °C for 1 hour with a liquid-solid ratio of 4 mL/g. High-crystalline calcite was uniformly distributed in carbonated CCR through the spontaneous precipitation of $CaCO_3$ from dissolved Ca^{2+} ions in CCR and free CO_3^{2-} in capture solution. To further enhance CO_2 utilization, real carbonated CCR rich in $CaCO_3$ was utilized to hydrothermally synthesize a tough $CaCO_3$-based building material, achieving a high flexural strength of 23.4 MPa at 200 °C for 9 hours. Its superior strength compared to common concrete was attributed to the formation of C-S-H/tobermorite on the stable mineralized calcite matrix through hydrothermal dissolution and reconstitution. The material also demonstrated excellent humidity regulation performance, enabling stable CO_2 sequestration and valuable utilization in building materials.

Keywords: hydrothermal mineralization, CCUS, CO_2 solidification, CO_2 capture solution, calcium carbide residue, functional building materials.

1 Introduction

Massive emissions of CO_2 from energy-intensive industries are inducing global warming. To reduce carbon emissions, carbon capture, utilization and storage technology (CCUS) has been acknowledged as the only feasible option for realizing industrial low-carbon transformation. In CCUS routes (**Fig.1**), the CO_2 storage underground only realizes carbon sequestration without utilizing CO_2 as a valuable resource, and it appears unsustainable due to high energy consumption and leakage risks. Additionally, gaseous CO_2 curing requires prior separation and purification of CO_2 for better mineralization efficiency, and also typically occurs only on the surface of materials due to the limitation in gas-solid reaction dynamics, resulting in a low degree of CO_2 mineralization. Therefore, the direct in-situ fixation and utilization of CO_2 in capture solution remain significant challenges.
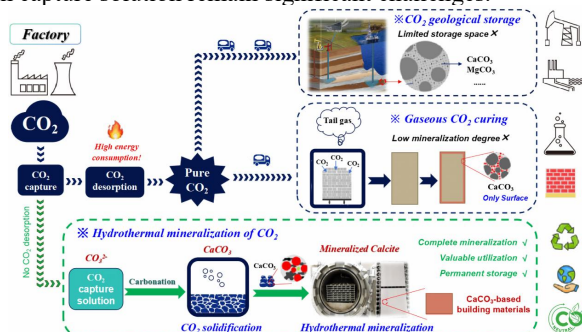
Fig. 1. Comparison of common pathways for CO_2 utilization and storage

Inspired by the geological sequestration of CO_2 as carbonates and the hydrothermal phenomenon for diagenesis in nature [1], this study proposed a novel hydrothermal mineralization technology to solidify CO_2 capture solutions and industrial solid wastes into $CaCO_3$-based functional building materials, enabling effective CO_2 utilization and sequestration in situ with low energy consumption.
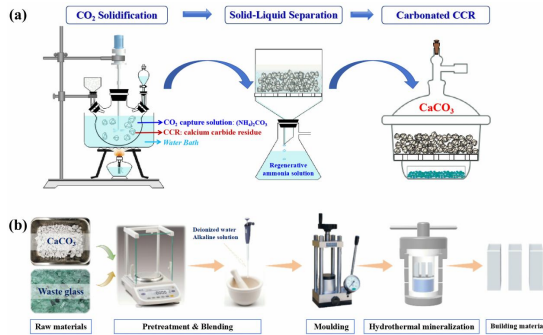
2 Materials and methods

2.1 Raw materials

The calcium carbide residue (CCR) used in the CO_2 solidification experiment was collected from a large-scale coal-to-chemical factory. It was oven-dried and finely powdered, with main components of CaO (~93.9 wt%) and portlandite ($Ca(OH)_2$). A solution of ~33 wt% $(NH_4)_2CO_3$ was used to simulate the CO_2 capture solution that has completed CO_2 capture.

2.2 CO_2 solidification reaction

The $(NH_4)_2CO_3$ solution and CCR powder were added to the reactor in specified liquid-to-solid ratios (1-10 mL/g). The CO_2 solidification reaction was conducted at 25-80℃ for 1-16 hours with a constant stirring rate of ~1000 r/min. Afterwards, the solid-liquid mixture was filtered using a sand core funnel. Then the solid product was dried at 80 °C for 24 hours as the final carbonated CCR products, while the filtrate was recycled as regenerated ammonia solution for next CO_2 capture, as shown in **Fig.2a**.

2.3 Hydrothermal mineralization reaction

The carbonated CCR was mixed with waste glass powder for hydrothermal mineralization (**Fig.2b**). The mixture with 10 wt% deionized water was compressed to green bodies (40*15*5 mm^3) in mold, and then they were hydrothermally cured for 0-24 hours at 200℃ in a Teflon-lined stainless-steel autoclave. Finally, all cured specimens were oven-dried and stored for further analysis.

The 12th International Symposium on Water Environment Systems
----- with Perspective of Global Safety   (Nov. 21st ~ 22nd , 2024)

GP-RSS & SyDE
Tohoku University

**Fig. 2. Experimental processing of CO₂ solidification and hydrothermal mineralization**

3 Results and discussion

3.1 Solidification of CO₂ in capture solution

In the CO_2 solidification reaction, as L/S ratio increased at 25 °C, the carbonation rate (R_c) gradually rose to nearly 90% at 4 mL/g, corresponding to a CO_2 fixation rate (R_f) of ~40%, and then remained stable. The XRD patterns also indicated that almost all $Ca(OH)_2$ in raw CCR was fully converted into calcite ($CaCO_3$) above 4 mL/g, indicating a continuous high degree of carbonation in this case. As the time extended from 1 h to 16 h, the R_c increased slightly and stabilized within 82%~88%, suggesting that a saturated CO_2 solidification (carbonation) in capture solution could be achieved within 1 hour at room temperature (**Fig.3**).
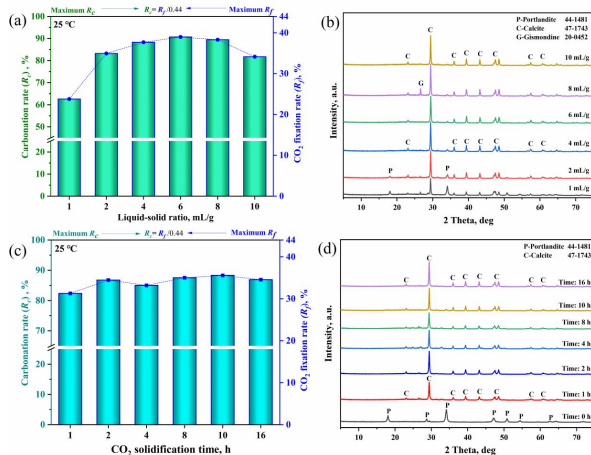
Fig. 3. Carbonation rate (*Rc*) and CO₂ fixation rate (*Rf*) at different conditions
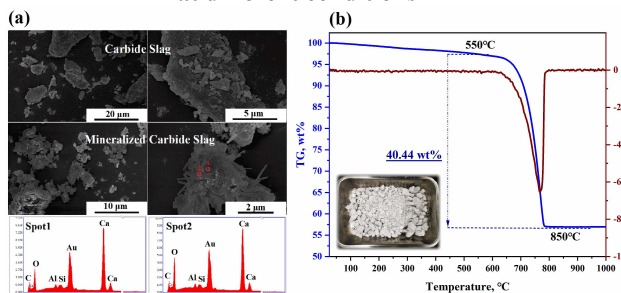
**Fig. 4. Characteristics of carbonated CCR products**

The initial irregular portlandite in CCR transformed into typical plate/strip-like calcite after CO_2 solidification reaction (**Fig.4a**). Calcite crystals were widely distributed in the carbonated CCR. EDS results confirmed a high Ca content with certain C and O, corresponding to the primary elemental composition. TG analysis (**Fig.4b**) also showed a

CO₂ content of 40 wt% in carbonated CCR, closely aligning with the theoretical value of 44 wt% in pure $CaCO_3$.

3.2 Hydrothermal mineralization of CO₂

The carbonated CCR rich in $CaCO_3$ was used as a calcium resource at a 60 wt% proportion for hydrothermal synthesis of building materials, enabling final CO_2 mineralization and stable sequestration as minerals in building materials.

As the hydrothermal time extended, the flexural strength of materials continuously increased, reaching a maximum of 23.4 MPa at 9 hours (**Fig.5a**). In XRD patterns, calcite peaks remained dominant due to its great stability, indicating the characteristic of $CaCO_3$-based materials. Besides, C-S-H peaks also appeared near calcite peaks at 9 hours (**Fig.5b**). The C-S-H or tobermorite formed on calcite matrix could densely fill the pores, thereby improving the mechanical performance of materials [2]. In this way, the captured CO_2 was effectively mineralized into stable calcite, and reliably sequestered within the $CaCO_3$-based building materials by hydrothermal dissolution and reconstitution (**Fig.5c**) [2]. The $CaCO_3$-based materials also exhibited significant performance for regulating indoor humidity, with the moisture adsorption of ~195.3 g/m² within 24 hours.
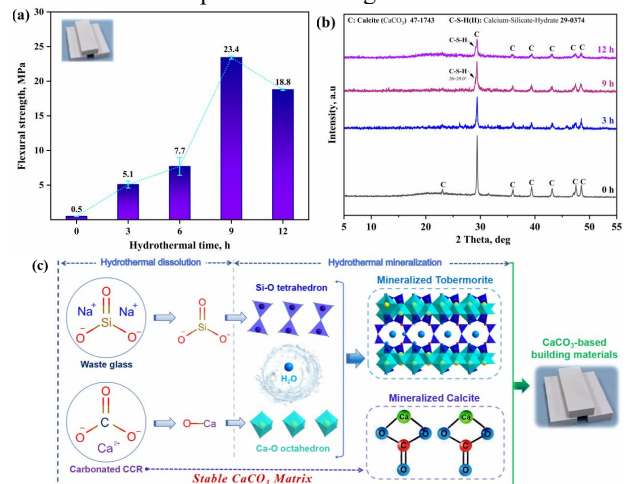
Fig. 5. Mechanism of hydrothermal mineralization

4 Conclusions

A novel hydrothermal mineralization technology was developed to convert CO_2 capture solutions and industrial solid wastes into $CaCO_3$-based functional building materials. In situ CO_2 solidification in capture solution was achieved effectively, with a high carbonation rate of nearly 90 % was reached at 25°C for 1 hour at a liquid-solid ratio of 4 mL/g. The carbonated CCR were utilized and hydrothermally mineralized into tough $CaCO_3$-based materials, with a high flexural strength of 23.4 MPa and excellent humidity regulation performance, thus enabling stable in-situ CO_2 sequestration and effective utilization in building materials.

Reference

[1] Y Zhang, et al. Hydrothermal solidification of underground construction wastes into building materials: Waste slurry recycling, industrial application and evaluation J. Clean. Prod. 2023, 426: 139091.

[2] Y Zhang, et al. Self-regulated immobilization behavior of multiple heavy metals via zeolitization towards a novel hydrothermal technology for soil remediation. Environ. Res. 2023, 216: 114726.

The 12th International Symposium on Water Environment Systems
----- with Perspective of Global Safety   (Nov. 21st ~ 23rd , 2024)

GP-RSS & SyDE
Tohoku University

Enhanced anaerobic digestion performance of mesophilic and thermophilic siphon-driven self-agitated reactor for food waste treatment by intermittent micro-aeration

◯ Xiang Li[1,2], Yong Hu[1]

[1] School of Environmental Science and Engineering, Nanjing Tech University, Nanjing 211816, PR China
[2] School of Material Science and Engineering, Nanjing Tech University, Nanjing 211816, PR China

Abstract

Micro-aeration based anaerobic digestion technology has presented tremendous potential in food waste treatment including strengthening food waste hydrolysis and acidogenic efficiency and regulating biogas production. Four siphon-driven self-agitated anaerobic reactors (SDSAR), which contained two SDSARs (R1 and R3) with 200 mL-oxygen intermittent aeration every day and other two SDSARs (R2 and R4) without aeration, were successfully activated during the start-up phase at the organic loading rate of 1 and 2 g-COD/L d. R1 and R2 were operated under mesophilic condition, while R2 and R4 were operated under thermophilic condition. In general, the highest COD removal efficiency and methane production in stable-running phase were obtained in R2 which indicated that micro-aeration during mesophilic condition can promote methanogenesis process to some extends. Future prospects can be laid in improving organic loading rate to over 10 g-COD/L d and aeration intensity to obtain the optimal condition for food waste micro-aeration digestion.

Keywords: micro-aeration, anaerobic digestion, food waste, methane production, biodegradation efficiency

The 12th International Symposium on Water Environment Systems
----- with Perspective of Global Safety   (Nov. 21th ~ 23th , 2024)

GP-RSS & SyDE
Tohoku University

Denitrification-enhanced anaerobic digestion for low-carbon and effective treatment of DMF-containing industrial wastewater

XINZHENG ZHANG, ZIXUAN DENG, ○ZHE KONG[1, 2*]

[1] School of Environmental Science and Engineering, Suzhou University of Science and Technology, Suzhou, 215009, China

[2] Suzhou National Joint Laboratory of Green and Low-carbon Wastewater Treatment and Resource Utilization, Suzhou University of Science and Technology, Suzhou, 215009, China

[*]E-mail: zhekong@mail.usts.edu.cn

Abstract

The feasibility of anaerobic membrane bioreactor (AnMBR) for the treatment of N, N-dimethylformamide (DMF)-containing wastewater was theoretically compared with the conventional activated sludge (CAS) process in this study. The electricity consumption and expenditure, bio-energy production and CO_2 emission were investigated using the operational results of a lab-scale AnMBR operated in a long-term operation. The AnMBR was capable of producing bio-methane from wastewater and generated 3.45 kWh/m^3 of electricity as recovered bio-energy while the CAS just generated 1.17 kWh/m3 of electricity from the post-treatment of excessive sludge disposal. The large quantity of bio-methane recovered by the AnMBR can also be sold as sustainable bioresource for the use of household natural gas with a theoretical profit gain of 29,821 US$/year, while that of the CAS was unprofitable. The AnMBR was also demonstrated to significantly reduce the carbon emission by obtaining a theoretical negative CO_2 production of -2.34 kg CO_2/m^3 with the recycle of bio-energy while that for the CAS was 4.50 kg CO_2/m^3. The results of this study demonstrate that the AnMBR process has promising potential for the carbon-neutral treatment of high-strength DMF-containing wastewater in the future.

Keywords: Anaerobic digestion; AnMBR; anaerobic membrane bioreactor; industrial wastewater; bio-energy production; carbon neutrality.

1 Introduction

DMF is hazardous and toxic to humans due to its hepatotoxicity and potential carcinogenicity, which is also likely to cause eutrophication since this organic matter is a nitrogenous compound. Since the high-strength industrial wastewater typically contains various types of organic pollutants and its total COD concentration can be up to 10,000-30,000 mg/L, in which the concentration of DMF is typically over 10,000 mg DMF/L, accounting for the majority of the total COD. DMF is considered as a persistent organic matter with a low degradability, thus, it is quite essential to realize the effective treatment of industrial DMF-containing wastewater (DCW). With the rapid spread of the concept of carbon neutrality in wastewater treatment process in recent years, which aims at succeeding in energy conservation and recovery along with the reduction of carbon emission during the processing of wastewater treatment, the development of a sustainable and low-carbon treatment process for DCW has been on the list of concerns for the carbon-neutral goal.

In this study, a lab-scale AnMBR fed the synthetic DCW was conducted for a long-term operation to investigate the feasibility of the AnMBR. The operational results and data were processed for evaluating the potential of energy recovery, CO_2 emission reduction and electricity expenditure based on theoretical calculations. The performance results of the AnMBR were compared with the empirical results of a theoretical CAS process, which were assumed to share the same operational conditions, parameters and efficiencies with that of the AnMBR. A comparison was conducted between the two processes to give new insights into the engineering application of the AnMBR process in the treatment of DCW. The objectives of this study are to: 1) Demonstrate the sustainability of energy conservation in the carbon-neutral treatment of DCW through the AnMBR process; 2) Quantitatively compare the reduction of carbon emission during the treatment of DCW through the AnMBR and CAS process; 3) Assess the theoretical expenditure cost and potential profit for the treatment of DCW through the AnMBR and CAS process. The new findings of this work facilitate the popularization of this promising bio-technology in the future treatment of high-strength industrial wastewater.

2 Materials and methods

2.1 Experimental apparatus

A small lab-scale flat-sheet AnMBR was designed and set up for the long-term treatment of synthetic DCW. A flowchart of CAS process is assumed in comparison with the AnMBR system. A long-term continuous operation of 200 days was conducted for both the AnMBR and CAS system. The AnMBR obtains an operational volume of 7 L and a headspace of 8 L. The reactor was made of polyvinylidene fluoride (PVDF), in which a flat-sheet membrane module with a total area of 0.122 m^2, made of chlorinated polyethylene (CPE) (Kubota Membrane Cartridge, Japan), was inserted and settled inside the AnMBR. The sludge produced from both systems was further digested using a lab-scale continuous stirred tank reactor (CSTR) with an operational volume of 12 L for the post-treatment of wasted sludge. It should be noted that the CAS process in this study was assumed as a conceptual process, which had the ability to effectively degrade DMF. Since the CAS process is commonly used as a biological treatment process for industrial wastewater and has been investigated for years, the results obtained from the CAS process in this study is based on the same data of DMF concentration, removal efficiency and other parameters obtained from a lab-scale AnMBR. Some of the results are even "ideal" assumptions for the CAS process, so as to estimate the maximum ability of this process

The 12th International Symposium on Water Environment Systems
----- with Perspective of Global Safety   (Nov. 21th ~ 23th , 2024)

GP-RSS & SyDE
Tohoku University

for the treatment of DCW. The CSTR process is also assumed to have the reported performance of an effective digestion of the excessive sludge yielded during the treatment of DCW.

2.2 Chemical reagents and synthetic wastewater

All the analytically pure chemical reagents used in this study were purchased from Wako Co. Ltd., Japan. As can be seen in the supplementary information, an average concentration of approximately $2,105 \pm 82$ mg DMF/L (equivalent to $3,219 \pm 124$ mg COD/L) was obtained for the synthetic high-strength DCW, which was reserved in a 120 L plastic bucket that played the role of a substrate reserve tank. It should be noted that although the real typical concentration of DMF can be up to over 10,000 mg/L, it might be too high for a lab-scale experiment. It is improper to set the initial concentration too high in case that the AnMBR is unable to degrade the high-concentration COD or that toxic organic matters might inhibit the microbial activity when the concentration is too high. Therefore, for the lab-scale experiment in this study, it is common to use a relatively low concentration like 2,000 mg/L for theoretical investigations. The synthetic wastewater was prepared using DMF as the sole substrate, which was diluted with tap water.

3 Results and discussion

3.1. Operational results

The lab-scale attempt on the application of an AnMBR to the anaerobic treatment of high-strength DCW was proved successful, and the detailed operational results were also discussed in a previous study. At a relatively long HRT of 12-24 h, a high COD removal of over 97% was obtained through the AnMBR. The HRT of 8 h was considered as the shortest HRT for the stable operation of the AnMBR with an affordable limit OLR of 10.2 kg COD/m^3/d. Under this circumstance, the AnMBR was capable of degrading the majority of DMF contained in the synthetic wastewater from $2,105 \pm 82$ mg/L to 52.5 ± 9.1 mg/L, and a high methane yield of 990 L/m3 was simultaneously obtained, demonstrating an effective methanogenic degradation of DMF. The majority of influent COD was converted into bio-methane which accounted for 80% of the total COD, and the residual COD in the effluent just accounted for 5%. It is known that the biomass growth during the AD process is much lower than that through the aerobic CAS process, with a determined coefficient of 1.035 g MLSS/g COD, the sludge-COD conversion efficiency of DMF was calculated as a very low level of 5.4-6.5% (selected as 6.5%). In contrast, it has been widely reported that 30-50% of the influent COD turns out to be sludge instead of being degraded through the CAS process. In this study, the sludge-COD conversion efficiency was assumed as a high level of 50%, suggesting that under an ideal condition that a thorough aerobic degradation of DMF was obtained through the CAS process, half of the total influent COD of DCW was converted into CO_2 while the rest of it directly became part of the sludge.

3.2. Bio-methane and bio-energy recovery

As shown in **Fig. 1**, in this study, since the AnMBR process was designed as a lab-scale reactor, the flowchart of the entire system was simplified. The electricity consumed for maintaining the AnMBR at the mesophilic condition of 35 °C was calculated as 13.95 kWh/m^3. While the reactor heating accounted for the largest energy consumption, which could be majorly covered by the rest of combustion heat. As

is mentioned previously, the CSTR for the post-treatment of excessive sludge was typically operated at a higher thermophilic temperature of 55 °C to realize a higher COD removal and biogas production, and the electricity consumed for heating the CSTR was up to 1.58 kWh/m3. The electricity consumed by digester heating for the AnMBR was summed as 13.78 kWh/m^3, while that of the CAS was 1.22 kWh/m^3.
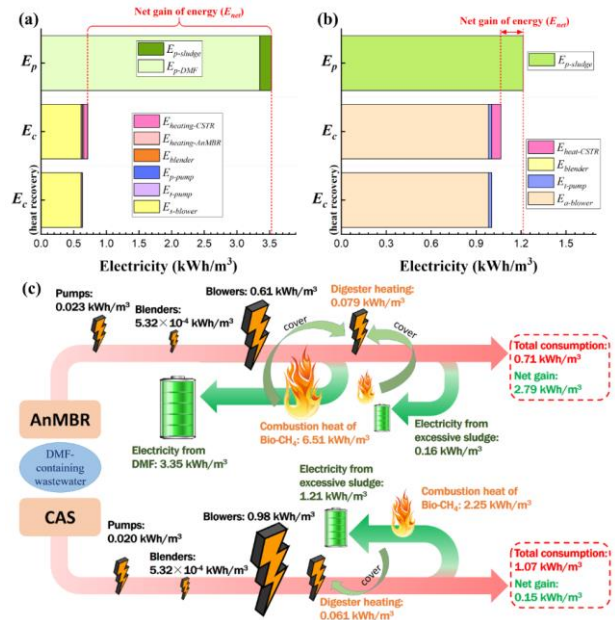
Fig. 1. A brief evaluation of energy conservation for the treatment of high-strength DMF-containing wastewater by the AnMBR (a) and CAS (b) processes along with the energy flowchart (c) for the comparison of two process.

4 Conclusions

The AnMBR process was proved as a promising alternative of the CAS process for carbon-neutral treatment of DCW with theoretical evaluation of energy, economy and carbon reduction. The AnMBR process could significantly save electricity in comparison with the energy-intensive CAS process. The future application of wastewater treatment process engineering for the AnMBR is considerd to have the potential of gaining net profit by selling the recycled bio-methane as household natural gas. The AnMBR process could also significantly reduce the carbon emission by lowering the CO_2 production during the wastewater treatment process. This study revealed the remarkable merits of the AnMBR process, also helping to popularize this carbon-neutral technology to the anaerobic treatment of industrial wastewater.

Reference

[1] Kong, Z., Xue, Y., Hao, T., Zhang, Y., Wu, J., Chen, H., Song, L., Rong, C., Li, D., Pan, Y., Li, Y., Li, Y.-Y., 2022. Carbon-neutral treatment of N, N-dimethylformamide-containing industrial wastewater by anaerobic membrane bioreactor (AnMBR): Bio-energy recovery and CO2 emission reduction. Bioresour. Technol. 358, 127396.

[2] Kong, Z., Xue, Y., Zhang, Y., Hao, T., Chen, H., Sun, J., Pan, Y., Li, D., Li, Y., Huang, Y., 2022. Insights into the carbon neutrality for the treatment process engineering of municipal wastewater by anaerobic membrane bioreactor integrated with partial nitritation-anammox: CO2 reduction and energy recovery. J. Water Process Eng. 49, 102996.

The 12th International Symposium on Water Environment Systems
----- with Perspective of Global Safety   (Nov. 21st ～ 23rd , 2024)

GP-RSS & SyDE
Tohoku University

Advanced nitrogen and phosphorus removal by Anammox-HAP in IC reactors

○ Liwen Cao, Yong Hu

School of Environmental Science and Engineering, Nanjing Tech University, Nanjing 211816, PR China

Abstract

Two alternative sludge (Anaerobic granular sludge (AGS) and activated flocculent sludge (AFS)) were employed to start up the anammox process in internal circulation (IC) reactors with the hydroxyapatite (HAP) strategy. Both reactors achieved rapid start-up on days 83 and 53, respectively. The analysis of granular properties revealed that the anammox granular sludge (AMXGS) transformed from AGS exhibited superior granular size distribution and settling performance. Furthermore, the assessment of microbial community structure demonstrated that inoculating AFS was capable of enriching AnAOB in a shorter time. Last but most importantly, this study provides a comprehensive analysis of the distinct granulation routes of AGS and AFS. AGS predominantly underwent a "broken-adsorption-granulation" process, whereas AFS exhibited not only a typical "adsorption-granulation" process but also a "biofilm growth-granulation" cycle process.

Nevertheless, when the nitrogen loading rate (NLR) was elevated to 2.26 gN/L/d, the AFS-Anammox system exhibited significant fluctuations, resulting in a reduction of the total nitrogen removal efficiency (TNRE) to 56%. In contrast, the TNRE of the AGS-Anammox system remained stable at 86%, indicating that the physical characteristics of granules is a crucial factor determining the stability of the system. Consequently, we performed experiments on the high-load Anammox-HAP process, utilizing the AGS-Anammox system as the experimental object. Finally, the NRR and PRR of 26.13 gN/L/d and 0.86 gP/L/d were obtained under the nitrogen and phosphorus load of 26.40 gN/L/d and 1.09 gP/L/d, respectively.

Keywords: Anammox; IC reactor; HAP; Start-up; Granulation routes; High-load.

The 12th International Symposium on Water Environment Systems
----- with Perspective of Global Safety (Nov. 21th ~ 23th , 2024)

GP-RSS & SyDe
Tohoku University

Characteristics and mechanisms of partial denitrification-anammox granular sludge floating in upflow reactor

Ruixin WU[1*], Morita Koudai[1], Zibin Luo[2] & Yu-You Li[1,2]

1Department of Frontier Science for Advanced Environment, Graduate School of Environmental Studies, Tohoku University, Miyagi 980-8579, Japan.

2Department of Civil and Environmental Engineering, Tohoku University, Graduate School of Engineering, Miyagi 980-8579, Japan

*E-mail: wu.ruixin.r6@dc.tohoku.ac.jp

Abstract

Partial denitrification (PD) coupled with anammox (PDA) is a promising nitrogen removal process. However, sludge flotation remains a prevalent instability issue in previous PDA process, which can lead to the loss of anammox bacteria and deteriorated nitrogen removal efficiency (NRE). In this study, as the nitrogen loading rate (NLR) increased from 0.5 to 1.0 g N/L/d, the sludge flotation and loss became more pronounced, and the TSS in the effluent rose from 4.2 mg/L to 25.0 mg/L. The mechanisms reveal that EPS and bubble content contribute significantly to flotation, while excessive growth of denitrifying bacteria further exacerbates the issue. These results provide valuable insights for controlling sludge flotation, ultimately enhancing the stability and efficiency of PDA processes in wastewater treatment applications.

Keywords: Partial denitrification; Anammox; granular sludge; floating

1 Introduction

Partial denitrification (PD) coupled with anammox (PDA) is an emerging nitrogen removal process that offers advantages over partial nitrification-anammox (PNA), such as adaptability to low temperatures and the potential for 100% nitrogen removal efficiency (NRE). However, sludge flotation is a common instability phenomenon in previous PDA processes. Sludge flotation can lead to the loss of anammox and deteriorating mass transfer, resulting in deteriorated nitrogen removal performance. However, the reasons for flotation remain unclear. This study investigates the phenomenon and mechanisms of PDA granular sludge flotation in an EGSB reactor, providing references for controlling flotation to prevent reactor deterioration.

2 Materials and methods

2.1 Reactor Setup and Operation

The PDA reactor (EGSB, 5 L) employed in this study contained a low speed stirring. The sludge inoculated in was PDA granular sludge in previous study. The influent of the reactor was synthetic wastewater, including NH_4^+-N ((NH_4)$_2SO_4$), NO_3^--N ($NaNO_3$) and other minerals, sodium acetate was fed into the reactor by a peristaltic pump to provide COD for PDA reaction. The average temperature was maintained at 25 °C, and the operation condition is shown in Table 1.

Table 1 Operation condition

Phase	I	II	III
Duration (day)	1-76	77-126	127-155
NH_4^+-N_{inf}(mg/L)	26.9 ± 3.7	38.1 ± 2.4	52.0 ± 3.2
NO_3^--N_{inf}(mg/L)	33.2 ± 2.7	51.0 ± 1.8	70.1 ± 1.8
COD/NO_3^--N	2.2 ± 0.2	2.2 ± 0.1	2.1 ± 0.1
HRT (h)	2.88	2.88	2.88
NLR (g N/L/d)	0.51 ± 0.03	0.78 ± 0.03	1.04 ± 0.04

2.2 Sampling and analytical methods

The influent and effluent samples were taken daily and analyzed after being filtered through 0.45 membrane. The concentration of NH_4^+-N, NO_2^--N, and NO_3^--N were determined using capillary electrophoresis (Agilent 7100; Agilent Technologies, Santa Clara, CA). The pH, COD and total suspended solids (TSS) and volatile suspended solids (VSS) were measured according to the standard methods [1].

3 Results and discussion

The system was operated for 155 days treating low C/N ratio synthetic municipal wastewater, with three phases divided by the NLR (Table 1). In phase I (day 1-76), the concentrations of NH_4^+-N, NO_3^--N in the influent were 26.9 ± 3.7 mg/L and 33.2 ± 2.7 mg/L, corresponding to the NLR was 0.51 ± 0.03 kg N/ m³/d (Fig. 1 a, c, d). After NLR was increased to 0.78 ± 0.03 in phase II (day 77-126), the TN removal efficiency slightly increased to 76.0 %, and the effluent TN increased to 22.6 ± 5.4 mg/L. In phase III (day

The 12th International Symposium on Water Environment Systems
----- with Perspective of Global Safety (Nov. 21th ~ 23th , 2024)

GP-RSS & SyDe
Tohoku University

127-155), influent NH_4^+-N and NO_3^--N was increased to 52.0 $\pm$ 3.2 and 70.1 $\pm$ 1.8 mg/L accompanied with NLR upgraded to the 1.04 $\pm$ 0.04 kg N/ m³/d. Subsequently, the effluent of TN and NRE were 27.4 $\pm$ 8.2 and 78.1 %, which were like phase I and II. The contribution of anammox to NRE was maintained at 74.5-78.0 % during reactor operation.
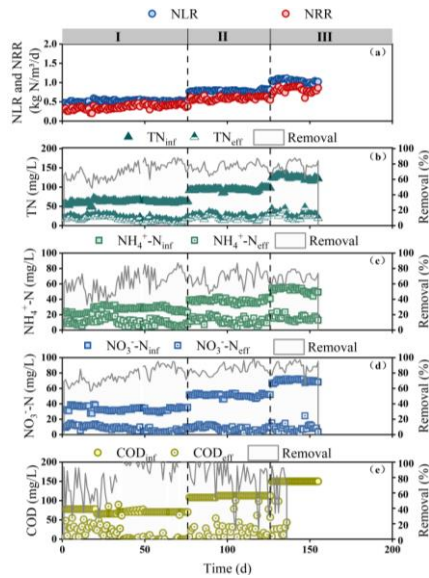

Fig.1. Reactor performance

With the increase of NLR, the TSS in the reactor increased from 27.2 to 36.2 g/L. The amount of sludge loss in the effluent gradually increased from 4.2 to 25.0 mg/L with the VSS/TSS ratio continued to decrease (0.8-0.6-0.5). This suggests that as the NLR increases, more sludge with good settling performance will be lost in the effluent, potentially leading to excessive sludge loss in the reactor and disrupting its normal operation.

There are three main reasons for sludge flotation and loss in the PDA reactor. First is the secretion of EPS, which aggregates small particles, increasing their surface area and then floating. This is the primary cause of sludge flotation under low load conditions. When the NLR was 0.5, the EPS content in the floating sludge (297.9 $\pm$ 16.8) was significantly higher than that in the stable sludge (217.0 $\pm$ 0.4) within the reactor, especially S-EPS and L-EPS. The second reason is the bubble content. As the NLR increases, the rate of bubble production in granular sludge rises. Excessive bubbles attach to the surface of the granular sludge, causing it to float upward. Additionally, some internal bubbles were unable to escape, reducing the settling performance of the granular sludge, which also leads to sludge flotation. The

third reason is the excessive proliferation of denitrifying bacteria. Since denitrifying bacteria grow on the outer layer of anammox bacteria, the excessive growth of denitrifying bacteria makes it difficult for the produced nitrogen gas to be released. Moreover, this outer layer of denitrifying bacteria may carry anammox bacteria along with it when lost. This is also reflected in Fig. 2, where the increased anammox activity is observed in the floating sludge. Over time, this may lead to excessive loss of anammox bacteria, reducing the reactor's nitrogen removal performance through anammox.
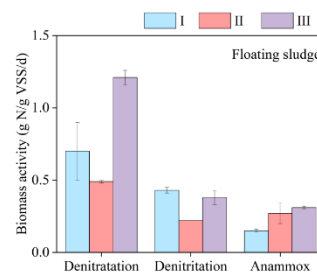

Fig.2. Biomass activity of floating sludge

4 Conclusions

(1) During the operation of a PDA reactor, as the NLR increased from 0.5 to 1.0 g N/L/d, the NRE remained between 70.8% and 78.1%, with the contribution of anammox ranging from 74.5% to 78.0%. As the NLR increased, sludge flotation and loss became more pronounced, and the TSS in the effluent rose from 4.2 mg/L to 25.0 mg/L.

(2) Sludge flotation and loss in the PDA reactor are caused by three main factors: EPS secretion, which increases surface area and promotes flotation, especially under low NLR; excessive bubble formation, which attaches to granular sludge and hampers settling; and the overgrowth of denitrifying bacteria, trapping nitrogen gas and causing anammox bacteria to be lost, ultimately reducing nitrogen removal efficiency.

Reference

[1] L. Lin, Z. Luo, Y. Zhang, Y. Ren, Y.-Y. Li, Partial denitrification-anammox granular sludge domesticated from high-strength anammox granules and the high-efficiency performance in treating low-nitrogen wastewater, Chemical Engineering Journal 477 (2023) 147281. https://doi.org/10.1016/j.cej.2023.147281.

The 12th International Symposium on Water Environment Systems
----- with Perspective of Global Safety   (Nov. 21st ~ 22nd , 2024)

GP-RSS & SyDE
Tohoku University

The exploration of efficient nitritation through granular sludge in the continuous mode reactor

○Hongjun Zhao [1, 2], Yan Guo [2], * & Yu-You Li [1, 3]

[1] Department of Frontier Sciences for Advanced Environment, Graduate School of Environmental Studies, Tohoku University, Miyagi 980-8579, Japan.

[2] School of Energy and Environmental Engineering, University of Science and Technology Beijing, Beijing 100083, China.

[3] Department of Civil and Environmental Engineering, Graduate School of Engineering, Tohoku University, Miyagi, 980-8579, Japan.

*E-mail: ustbgy2015@163.com

Abstract

Anammox has attracted considerable attention as a more environmentally friendly nitrogen removal process. However, nitritation, the prerequisite step for anammox, faces several challenges, with the most significant being the low nitrite production rate (NPR), which limits the nitrogen removal efficiency of anammox. In this study, a continuous mode reactor was employed to investigate the maximum NPR by adjusting the hydraulic retention time (HRT) and ammonia concentration in the influent. The NPR reached a maximum value of 1.89 kg/m³/d at an ammonia concentration of 1250.0 mg/L and an HRT of 12.0 h. Clear formation of granular sludge was observed in the reactor, with *Nitrosomonas* being the sole ammonia-oxidizing bacteria successfully enriched within the sludge. The production of free nitrous acid and low dissolved oxygen effectively inhibited nitrite-oxidizing bacteria. However, a significant presence of denitrifying bacteria in the sludge may have influenced the nitritation process. This study suggests that the continuous mode reactor holds potential for achieving a high NPR, compatible with the anammox process.

Keywords: High ammonium concentration; airlift reactor; Nitrosomonas; NOB inhibition.

1 Introduction

Wastewater treatment plants commonly employ the nitrification-denitrification process for biological nitrogen removal. However, with advancements in technology, novel biological nitrogen removal processes are emerging. Among them, the anammox (AMX) process, discovered in the 1990s, has garnered significant global attention for its high efficiency and low energy consumption [1]. Compared to traditional processes, AMX requires less aeration and does not rely on external carbon sources, making it particularly promising in the context of energy conservation and the pursuit of carbon neutrality. AMX is typically operated in tandem with nitritation process, where ammonium in wastewater is partially oxidized to nitrite, which serves as a substrate for the AMX process.

Recent studies have shown that the nitrite production rate (NPR) is a key limiting factor for the nitrogen removal rate (NRR) in AMX systems [1]. However, current methods to enhance NPR often introduce operational complexities, such as the use of magnetic fields or ultrasound [2], which hinder practical application. In contrast, controlling dissolved oxygen (DO) levels to regulate oxygen supply, based on the different oxygen affinities of ammonia-oxidizing bacteria (AOB) and nitrite-oxidizing bacteria (NOB), offers a simple, energy-efficient, and effective way to enhance NPR [3]. Therefore, exploring how to optimize nitritation through DO regulation to match the efficiency of the AMX process has both theoretical and practical significance.

Research into nitritation has led to the development of various types, including sequencing batch reactors (SBR) and continuous flow reactors, with the latter, continuous stirred-tank reactors (CSTR) and air-lift reactors (ALR) [4], being widely used. While early studies focused on SBR and membrane bioreactors (MBR) [5], these systems require complex control and are costly for large-scale wastewater treatment. In contrast, granular sludge continuous flow reactors (AGSCR) offer simpler operation and higher capacity, making them a growing focus of nitrogen wastewater treatment research. Therefore, this study will investigate nitritation process using AGSCR.

In conclusion, this study aims to explore maximum NPR in nitritation process by adjusting aeration to control DO concentration, thereby enhancing the overall nitrogen removal efficiency of the AMX process. By analyzing the properties, activity, and microbial community of sludge, this research will provide insights into the underlying mechanisms of microbial community changes under different operational conditions, ultimately advancing the practical application and optimization of the AMX process.

2 Materials and methods

2.1 The nitritation reactor

An airlift reactor was used in this study. The whole experiment was divided into nine phases depending on the different hydraulic residence times (HRTs) and ammonium concentrations. The reactor was controlled by heaters at a temperature of around 25 °C.

2.2 Chemical analysis

Temperature, DO, pH and ORP were analyzed by portable equipment. NH_4^+, NO_2^-, NO_3^-, MLSS and MLVSS were analyzed according to APHA standards.

3 Results and discussion

The experiment was divided into nine stages. In the first four stages, the HRT was shortened, and the NLR was

The 12th International Symposium on Water Environment Systems
----- with Perspective of Global Safety   (Nov. 21st～22nd , 2024)

GP-RSS & SyDE
Tohoku University

increased. In the subsequent five stages, the NLR was further raised by increasing the influent ammonium concentration. By continuously increasing the NLR, a higher NPR was achieved, matching the requirements of the AMX process. Instead of partial oxidation to control the ratio of ammonium to nitrite in the effluent, full nitritation was used to achieve a higher NPR. This significantly improved the NPR, and it also met the influent requirements for the AMX process by mixing the effluent with the original wastewater. Additionally, full nitritation resulted in higher concentrations of nitrite in the effluent, which led to an increase in FNA in the reaction zone, thereby exerting an inhibitory effect on NOB to some extent.
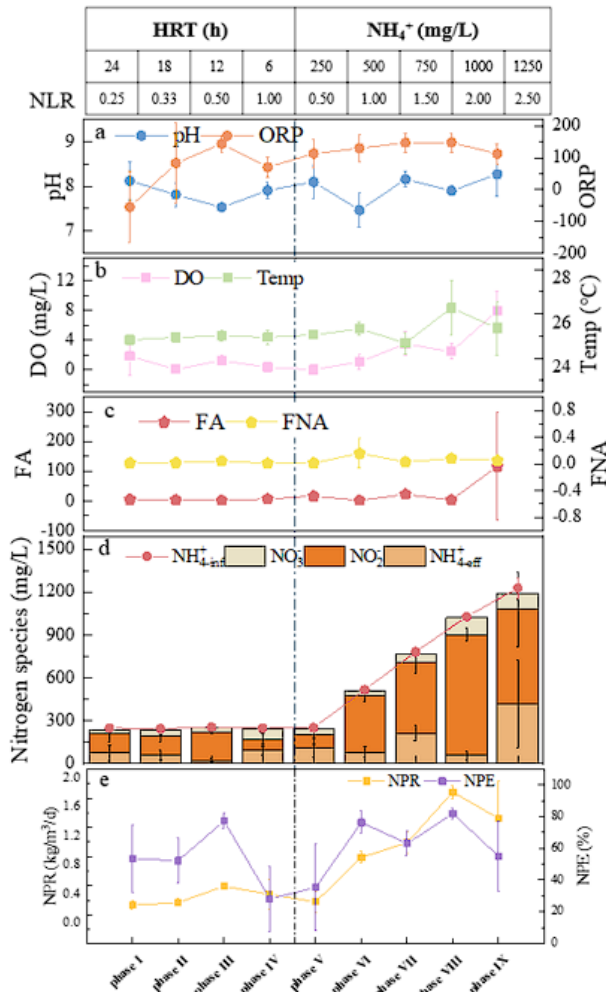
Figure 1. The condition of the reactor and variation of the influent and effluent.

During the first part of the experiment, nitrogen loss was minimal, achieving stable operation of the nitritation process. In both the first and second stages, the average NPE was 53%. However, as seen in Figure 1e, after the nitritation process strated, the NPE significantly exceeded 70%. In the third stage, the nitrite concentration in the effluent remained stable, with an average NPE of 78%, achieving minimal residual ammonium and nitrogen loss in this part of the study. In the fourth stage, the aeration rate was reduced due to excessive disturbances, resulting in an average NPE of only 24%, and a higher concentration of residual ammonium in the effluent. However, at the beginning of the fourth stage, despite instability in granular sludge caused by excessive aeration,

the NPR remained above 0.6 kg/m³/d. Throughout the third stage, performance was both stable and efficient. With an HRT of 12 h, the nitrite concentration in the effluent reached 208.0 mg/L, and the NPR concentration reached 0.42 kg/m³/d. By controlling the DO concentration, NOB was completely inhibited. Additionally, during the third stage, FNA levels increased, contributing to the suppression of NOB.

In the second part of the experiment, the production of nitrate gradually increased with the rise in ammonia concentration, as shown in Figure 1d. However, its proportion remained small and had little impact on overall performance. From the seventh to the eighth stage, the proportion of nitrate in the effluent increased. This was likely due to the higher AFR in the eighth stage, which led to an increase in DO concentration, weakening the inhibition of NOB and resulting in higher nitrate production. In this part of the experiment, the maximum NPR was reached at 1.89 kg/m³/d, with an NPE of 78.2%. Compared to the first part (NLR 1.00 kg/m³/d), the NPR increased by 2.9 times. Overall, the nitritation process under high loading remained relatively stable and was able to achieve a high NPR.

4 Conclusions

In this study, by adjusting the aeration rate and controlling oxygen supply, ammonia was oxidized to nitrite. As the nitrite concentration gradually increased, combined with the low DO concentration, NOB growth was successfully inhibited, allowing the nitritation process to be initiated and stabilized. Initially, NLR in the influent was increased by gradually shortening the HRT, during which the NPR reached up to 0.65 kg/m³/d, with an NPE of 63.49%. While maintaining an HRT of 12 h, the influent ammonia concentration was gradually increased, and when the NLR reached 2.42 kg/m³/d, the NPR increased to 1.89 kg/m³/d.

Reference

[1] Guo, Y., Chen, Y., Webeck, E., & Li, Y. Y. (2020). Towards more efficient nitrogen removal and phosphorus recovery from digestion effluent: Latest developments in the anammox-based process from the application perspective. Bioresource Technology, 299, 122560.

[2] Zheng, M., Liu, Y. C., Xin, J., Zuo, H., Wang, C. W., & Wu, W. M. (2016). Ultrasonic Treatment Enhanced Ammonia-Oxidizing Bacterial (AOB) Activity for Nitritation Process. Environmental Science and Technology, 50(2), 864–871.

[3] Wang, S., Deng, L., Zheng, D., Wang, L., Zhang, Y., Yang, H., Jiang, Y., & Huang, F. (2018). Control of partial nitrification using pulse aeration for treating digested effluent of swine wastewater. *Bioresource Technology*, *262*, 271–277.

[4] Gu, X.-D., Huang, W.-H., Li, Y.-Z., Huang, Y., & Zhang, M. (2023). Regulation of partial nitrification by influent N loading and sludge discharge in mainstream sewage treatment. *Journal of Water Process Engineering*, 52, 103536.

[5] Erguder, T. H., Boon, N., Vlaeminck, S. E., & Verstraete, W. (2008). Partial nitrification achieved by pulse sulfide doses in a sequential batch reactor. *Environmental Science and Technology*, *42*(23), 8715–8720.

[6] E.W. Rice, R.B. Baird, A.D. Eaton, E. (2017). Standard Methods for the Examination of Water and Wastewater. *American Public Health Association, American Water Works Association, Water Environment Federation*, 1496.

The 12th International Symposium on Water Environment Systems
----- with Perspective of Global Safety   (Nov. 21th ~ 23th , 2024)

GP-RSS & SyDE
Tohoku University

Towards carbon-neutral biotechnologies for rural wastewater: A review of current treatment processes and future perspectives

GUANGYI MA, ○ZHE KONG[1, 2*]

[1] School of Environmental Science and Engineering, Suzhou University of Science and Technology, Suzhou, 215009, China

[2] Suzhou National Joint Laboratory of Green and Low-carbon Wastewater Treatment and Resource Utilization, Suzhou University of Science and Technology, Suzhou, 215009, China

*E-mail: zhekong@mail.usts.edu.cn

Abstract

This study summarized and reviewed the significance and necessity in carbon-neutral treatment of rural wastewater by investigating the advantages and flaws of currently implemented treatment processes. Some state-of-the-art bioprocesses which accord with the principle of carbon neutrality are specifically introduced due to their potential of realizing carbon neutrality in wastewater treatment. Advanced biotechnologies like anaerobic membrane bioreactor, sulfur-based autotrophic denitrification and anammox are recognized as future directions and highly recommended for the carbon-neutral treatment of rural wastewater for the removal of both organic and inorganic pollutants. This study provides new insights into the development of biotechnologies for rural wastewater treatment from the perspective of popularizing the concept of carbon neutrality in the field of wastewater treatment with energy conservation and emission reduction.

Keywords: Rural wastewater; carbon neutrality; AnMBR; sulfur-based autotrophic denitrification; anammox.

1 Introduction

In recent years, the escalation of industrial and agricultural activities, coupled with population growth, has led to an increased consumption of natural resources such as coal, oil, natural gas, and fresh water. This has resulted in heightened carbon emissions and a looming energy and water scarcity crisis. The situation is particularly concerning as predictions suggest a 40% global water deficit by 2030 if current consumption patterns persist[1]. The necessity of water for human well-being and industrial processes underscores the urgent need for efficient wastewater treatment to safeguard public health and the environment.

China, as a developing nation with a vast rural population, faces significant challenges in managing water resources. Despite improvements in living standards, issues of water scarcity and pollution have become critical. Approximately 2.68 billion rural residents lack access to clean drinking water due to inadequate sanitation infrastructure[2]. As shown in **Fig.1**，China 's total wastewater discharge has been on the rise, with rural contributions exceeding 25%[3]. The absence of centralized treatment systems in rural areas has led to widespread, unregulated wastewater discharge, exacerbating ecological degradation. To address these issues, there is a growing focus on developing appropriate wastewater treatment systems for rural areas in developing countries like China.
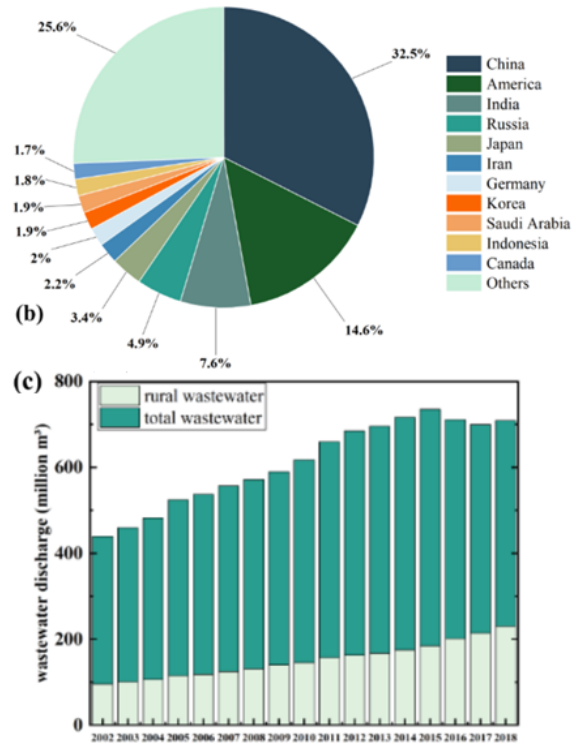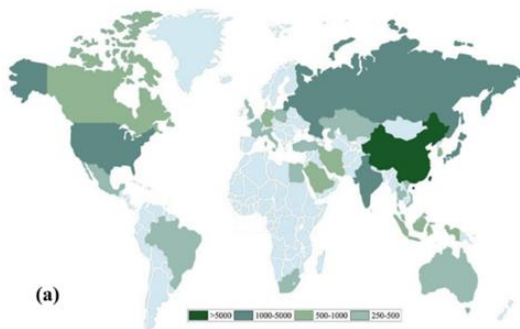
Fig. 1. Statistical data of global CO_2 emission of 2022: (a) Top 15 countries with highest CO_2 emission all over the world; (b) Contribution of CO_2 emission by country sector;(c) Rural wastewater and total wastewater discharge in China.

2 Carbon neutrality in rural wastewater treatment

Global warming poses a significant threat to human and ecological survival due to rising temperatures, prompting nations to pursue carbon neutrality by reducing greenhouse gas emissions. Carbon neutrality in wastewater treatment, which contributes 1.3% to global emissions and 3-4% of the world's electricity usage, is crucial for achieving this goal [4].

The 12th International Symposium on Water Environment Systems
----- with Perspective of Global Safety   (Nov. 21th ~ 23th , 2024)

GP-RSS & SyDE
Tohoku University

The concept involves minimizing energy consumption and carbon emissions, with a focus on energy conservation and reduction strategies.   While urban wastewater treatment often adopts centralized methods, rural areas face greater challenges due to decentralized pollution sources, leading to higher energy use and carbon emissions. Advanced biotechnologies offer a sustainable, low-carbon solution for rural wastewater treatment, reducing energy consumption, operational costs, and carbon emissions, making them particularly suitable for small communities in developing countries.   Despite the growing interest in carbon neutrality in wastewater treatment, there is a lack of comprehensive studies on the carbon-neutral potential of biotechnologies for rural wastewater management, with existing research primarily focusing on energy recovery and low carbon emissions.

## 3 Conventional treatment processes for rural wastewater treatment

In rural areas, where operational and maintenance costs are low, traditional treatment processes, predominantly simplistic and rudimentary biological technologies, have been extensively utilized for several decades, particularly in developing and underdeveloped countries. While these conventional treatment methods can remove a significant portion of pollutants from rural wastewater to a certain extent, their limited pollutant removal capacity, low efficiency, and weak performance relegate them to serving as basic sanitary facilities, playing a foundational role in rural wastewater management. Moreover, these conventional processes are often challenging to manage and maintain on a daily basis, exhibiting sensitivity to environmental fluctuations such as temperature, water quality, and humidity. For instance, septic tanks and soil treatment systems, though easy to maintain, have a limited capability to remove contaminants and may pose health and safety risks. Waste stabilization ponds, despite their high cost-effectiveness, require substantial land area, are susceptible to seasonal variations, and could potentially contribute to greenhouse gas emissions. Conventional activated sludge processes, while effective in treatment, consume high energy, making them unsuitable for the dispersed needs of rural areas.

4 Currently implemented biotechnologies for rural wastewater treatment

There is a contradiction that the energy-saving necessity urges manufactories to implement new strategies and devices with sustainability, but the more stringent environmental requirements and stricter discharge standards have driven researchers towards advanced wastewater treatment process that are more energy-consuming. Consequently, with the rapid development of wastewater treatment process in the past few years, more advanced and enhanced biotechnologies are brought about with merits of high effectiveness, low-carbon properties, eco-friendliness and sustainability, and are also suitable to the decentralized wastewater treatment in rural areas. Currently, a number of advanced biotechnologies that possess the potential to significantly reduce energy consumption and carbon emissions, in accordance with the principles of carbon neutrality, have been effectively applied in the treatment of rural wastewater for several years, as depicted in **Fig. 2**. Technologies such as constructed wetlands, biological contact oxidation, and moving bed biofilm reactors (MBBR) have demonstrated efficacy in managing rural wastewater.   However, they are not without challenges, as they often entail high costs and energy consumption.

Biological filters capitalize on natural or synthetic materials that serve as the primary framework and structure for biological media. These media facilitate the attachment of a substantial microbial population, resulting in the formation of robust biofilms that are capable of effectively removing a spectrum of pollutants, including SS, chroma, turbidity, COD, BOD_5, TN and TP [5,6]. Biofilters are extensively applied in the treatment of municipal or domestic wastewater owing to its fabulous merits of strong treatment capacity, small footprint, cost-effectiveness in operation and maintenance, low energy consumption and good effluent quality. As a result, it is recommended that biofilters are likely to have significant potential in future treatment of rural wastewater according with the principle of carbon neutrality.
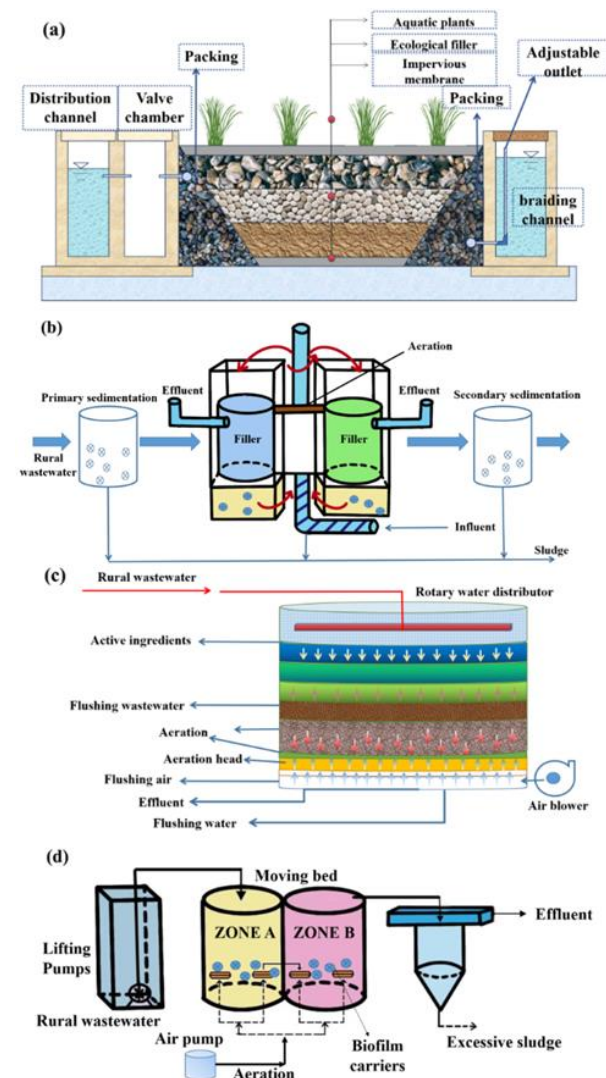
Fig. 2. Currently implemented biotechnologies for rural wastewater treatment which are used in recent years: (a) Constructed wetland; (b) Biological contact oxidation; (c) Moving bed biofilm reactor; (d) Biofilter (biofiltration system).

The 12th International Symposium on Water Environment Systems
----- with Perspective of Global Safety   (Nov. 21th~23th, 2024)

GP-RSS & SyDE
Tohoku University

5 State-of-the-art biotechnologies for carbon-neutral treatment of rural wastewater

A state-of-the-art biotechnology which is conformed with the principle of carbon neutrality for wastewater treatment should be satisfied with the following aspect: Effective utilization of CO_2 as the sole or major carbon source and reducing the relying on organic compounds or the consumption of coal/fossil fuel ; Availability in the production of high value-added and high energy-density products like bio-gas, bio-fuels and bio-resources which improve economic and social benefits ; Reduction in the consumption of water, soil, energy, fertilizers and other resources to relieve the negative impact on the ecological environment; Excellent convenience in maneuverability, sustainability and flexibility for different areas and climates. At present, for the field of rural wastewater treatment, the feasibility of carbon neutrality can be reflected in developing effective, eco-friendly, sustainable and low-carbon biotechnologies. Some state-of-the-art biotechnologies put forward in recent years has gradually demonstrated their merits in order to realizing the goal of carbon neutrality in rural wastewater treatment.

In the realm of contemporary technologies, Sulfur-Autotrophic Denitrification (SAD) and Anaerobic Ammonium Oxidation (anammox) have emerged as innovative approaches that leverage inorganic carbon sources and autotrophic microorganisms, thereby diminishing reliance on organic carbon sources. This strategy not only mitigates greenhouse gas emissions and reduces sludge production but also enhances the efficiency of nitrogen removal. Concurrently, nutrient recovery technologies are being developed with a focus on the recovery of phosphorus from wastewater, addressing the impending scarcity of this vital resource. Anaerobic biological treatment technologies, including Anaerobic Digestion (AD), Upflow Anaerobic Sludge Blanket (UASB), Extended Granular Sludge Bed (EGSB), and Anaerobic Membrane Bioreactors (AnMBR), are recognized for their proficiency in converting organic matter into biogas, a process that significantly reduces carbon emissions while simultaneously generating renewable energy. These technologies not only augment the economic and environmental benefits of wastewater treatment but also bolster the sustainability of the systems, offering carbon-neutral solutions for rural wastewater management.

6 Perspectives and challenges of carbon-neutral treatment of rural wastewater

Despite the potential for carbon neutrality demonstrated by the most advanced biotechnologies in various treatment processes for rural wastewater, the pursuit of low-carbon and sustainable wastewater management in rural areas continues to confront numerous challenges. One such challenge is the necessity for minimization and in-situ treatment, which necessitates the adoption of compact, decentralized treatment technologies suitable for small-scale applications, such as Johkasou and underground integrated processes. Concurrently, there is a critical need to consider cost-effectiveness and ease of maintenance to ensure the viability of these technologies in developing and underdeveloped countries. Furthermore, the byproducts generated during the treatment process, including excess sludge and harmful gases, must be effectively managed to mitigate potential environmental and health impacts. In terms of treatment technologies, there is a requirement for the enhancement of bioreactor design and materials, as well as the integration of diverse biotechnologies to augment the efficiency of pollutant removal, in order to meet increasingly stringent emission standards and achieve the goal of carbon neutrality.

4 Conclusions

This study summarized those widely implemented and currently used biotechnologies for rural wastewater treatment, also providing new insights into the carbon-neutral treatment processing and future perspectives on rural wastewater treatment with the following key findings. While conventional treatment processes which have been applied for decades are still so far available for rural wastewater, their further application and development are significantly limited due to the consensus of carbon neutrality, and are no longer suitable to the future low-carbon treatment of rural wastewater with the consideration of carbon emission reduction and energy conservation. State-of-the-art biotechnologies like sulfur-based autotrophic denitrification, anammox and advanced anaerobic biotechnologies are conformed with the principle of carbon neutrality due to their availability in energy conservation, bioresource recovery and carbon reduction during the wastewater treatment process. Carbon-neutral treatment processes are recognized as the suitable solutions to the future direction of rural wastewater treatment with the concern of minimalization and in-situ treatment, reduction in expenditure and maintenance, control of byproducts and future upgrades. This study facilitates the popularizing of the concept of carbon neutrality in the field of wastewater treatment.

Reference

[1] Z.-Y. Zhao, J. Zuo, G. Zillante, Transformation of water resource management: a case study of the South-to-North Water Diversion project, J. Clean. Prod. 163 (2017) 136–145. https://doi.org/10.1016/j.jclepro.2015.08.066.

[2] Y. Huang, L. Wu, P. Li, N. Li, Y. He, What's the cost-effective pattern for rural wastewater treatment?, J. Environ. Manage. 303 (2022) 114226. https://doi.org/10.1016/j.jenvman.2021.114226.

[3] P. Song, G. Huang, C. An, J. Shen, P. Zhang, X. Chen, J. Shen, Y. Yao, R. Zheng, C. Sun, Treatment of rural domestic wastewater using multi-soil-layering systems: Performance evaluation, factorial analysis and numerical modeling, Sci. Total Environ. 644 (2018) 536–546. https://doi.org/10.1016/j.scitotenv.2018.06.331.

[4] X. You, L. Yang, X. Zhou, Y. Zhang, Sustainability and carbon neutrality trends for microalgae-based wastewater treatment: A review, Environ. Res. 209 (2022) 112860. https://doi.org/10.1016/j.envres.2022.112860..

[5] T.C. Guarin, K.R. Pagilla, Microbial community in biofilters for water reuse applications: A critical review, Sci. Total Environ. 773 (2021) 145655. https://doi.org/10.1016/j.scitotenv.2021.145655.

[6] L. Zhang, B. Cui, B. Yuan, A. Zhang, J. Feng, J. Zhang, X. Han, L. Pan, L. Li, Denitrification mechanism and artificial neural networks modeling for low-pollution water purification using a denitrification biological filter process, Sep. Purif. Technol. 257 (2021) 117918. https://doi.org/10.1016/j.seppur.2020.117918.

The 12th International Symposium on Water Environment Systems
----- with Perspective of Global Safety   (Nov. 21th ~ 23th , 2024)

GP-RSS & SyDE
Tohoku University

Biofiltration for low-carbon rural wastewater treatment: a review of advancements and opportunities towards carbon neutrality

CHENGDE SUN, GUANGYI MA, ZHEMING XI, ○ZHE KONG[1, 2*]

[1] School of Environmental Science and Engineering, Suzhou University of Science and Technology, Suzhou, 215009, China

[2] Suzhou National Joint Laboratory of Green and Low-carbon Wastewater Treatment and Resource Utilization, Suzhou University of Science and Technology, Suzhou, 215009, China

*E-mail: zhekong@mail.usts.edu.cn

Abstract

In this study, benefits and advancements of implementing biofiltration process and its derivatives as good alternatives to the low-carbon treatment of rural wastewater towards carbon neutrality. Challenges of rural wastewater treatment and limitations of existing biological treatment processes were investigated. Advanced biofiltration technologies integrated with the concept of carbon neutrality present advantages such as promoted removal performance of pollutants, energy conservation, lower operational expenses, and minimal greenhouse gas emissions were recommended. These systems have the potential for extension and modification to accommodate various circumstances. Newly developed biotechnologies for the enhancements of biofiltration process include combinations like improvements on filter media, exogenous additives for enhanced removal, integration with carbon-neutral processes for effective nitrogen and phosphorus removal like sulfur-based autotrophic denitrification, pyrite-based autotrophic denitrification and anaerobic ammonium oxidation process with its upgrades and derivatives. In the future, developments in biofiltration process can be pursued through various avenues for the aim of achieving low-carbon treatment of pollutants from rural wastewater. This study offers a novel perspective on the utilization of biofiltration and popularize the carbon-neutral treatment of rural wastewater.

Keywords: Rural wastewater; carbon neutrality; biofiltration system; filter media; autotrophic denitrification; anammox.

1 Introduction

The escalating consumption of fossil fuels and freshwater, coupled with the intensification of carbon emissions, has led to a critical depletion of energy and water resources worldwide. Despite global efforts to curb carbon emissions, levels remain high, with social projections forecasting a significant decrease in water availability by 2030, potentially leading to severe shortages. In China, with over 500 million farmers constituting 36.11% of the population[1], the expanding irrigated land area has increased water usage and exacerbated wastewater treatment challenges in rural regions. These areas, characterized by dispersed wastewater sources and complex water quality, face difficulties in centralized treatment due to the absence of established drainage and treatment networks. The high biodegradability of rural wastewater, which contains elevated levels of chemical oxygen demand, nitrogen, and phosphorus, presents an opportunity for biological treatment processes. However, the treatment process itself contributes to greenhouse gas emissions, estimated to be around 1.3% of the global total[2]. The adoption of carbon-neutral strategies in wastewater treatment, focusing on energy conservation and emission reduction, is crucial. Biofiltration systems, with their low carbon footprint and high efficiency, offer a promising solution for sustainable and low-carbon wastewater management in rural areas, aligning with the global push towards carbon neutrality.

The purpose of this study is to provide a comprehensive assessment of the feasibility, advantages, limitations, sustainability, and carbon efficiency of biofiltration systems in achieving carbon neutrality in rural wastewater treatment, and to explore the development, improvement and progress of these systems, with a view to providing strategic and methodological new insights into the challenges of achieving carbon neutrality in rural wastewater treatment in the future. In this study, the latest developments in biofiltration processes that can be utilized for the carbon-neutral of rural wastewater are investigated. The strengths and limitations of biofiltration systems, as well as their sustainability and carbon efficiency, are also evaluated. This study presents novel viewpoints on the evolution, improvement, and progress of biofiltration systems, providing strategic and methodological insights to address the forthcoming challenges of achieving carbon-neutral treatment in rural wastewater settings. The aim of this study is to offer novel insights into the feasibility of utilizing biofiltration systems for the treatment of rural wastewater, with a focus on achieving carbon neutrality.

2 Challenges for rural wastewater treatment

A small lab-scale flat-sheet AnMBR was designed and set up In China, the rural population, comprising over 500 million individuals across more than 2.33 million villages, represents 36.11% of the nation's total population[1]. These rural areas are responsible for generating an estimated 8 billion tons of wastewater annually, with a consistent upward trend in volume[3]. As shown in **Fig. 1 (a) to (c)**, statistics from 2022 reveal that the emissions of COD, total nitrogen (TN), and total phosphorus (TP) from agricultural wastewater in China amounted to approximately 1,785.7, 174.4, and 27.7 thousand tons, respectively. The challenge of managing high levels of COD, TN, and TP in rural wastewater is further complicated by the dispersed nature of point sources[4], which, along with variable water quality and quantity, makes it impractical to apply urban wastewater treatment methods in rural settings. Additionally, rural areas often lack the extensive infrastructure necessary for

The 12th International Symposium on Water Environment Systems
----- with Perspective of Global Safety   (Nov. 21th ~ 23th , 2024)

GP-RSS & SyDE
Tohoku University

wastewater treatment, including collection systems, treatment facilities, and pipeline networks, making large-scale centralized treatment plants economically and logistically unfeasible. The study compares the carbon emissions and energy consumption of conventional rural wastewater treatment processes with biofiltration technologies, as depicted in **Fig. 1 (d) and (e)**, and highlights the need for a cost-effective, implementable, and carbon-reducing wastewater treatment solution that is suitable for diffused pollution sources in rural areas.
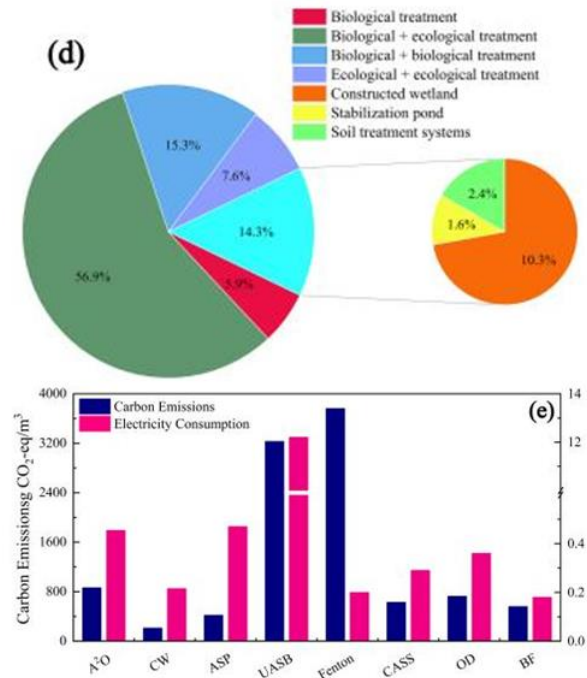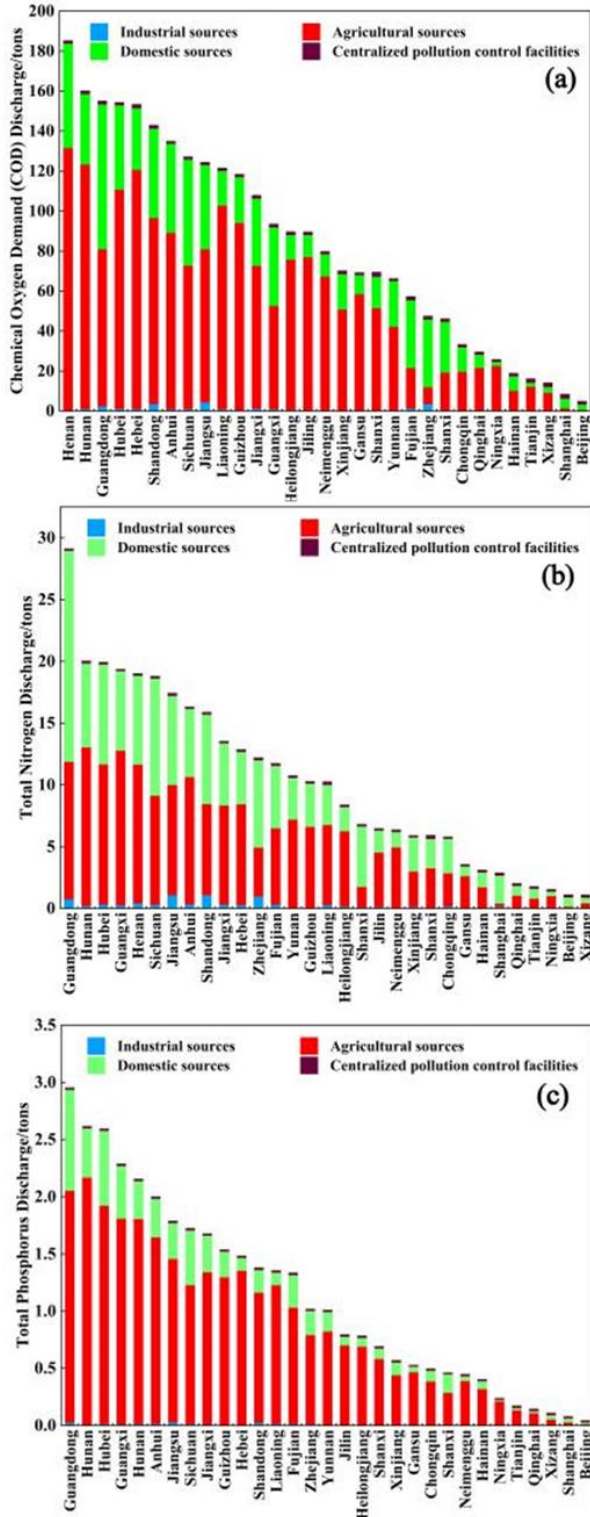

Fig. 1. Statistical data of (a) Discharge amount of chemical oxygen demand (COD) by regions in China, 2022; (b) Total nitrogen discharge by regions in China, 2022; (c) Total phosphorus discharge by regions in China in 2022 (Data from the 2022 Annual Report of the People's Republic of China on Ecological and Environmental Statistics). (d) Percentage of rural wastewater treatment processes used (e) Comparison of carbon emissions and electricity consumption of biofilters and other conventional rural wastewater treatment processes; A2O: Anaerobic-anoxic-oxic; CW: Constructed wetland; ASP: Activated sludge process; UASB: Up-flow anaerobic sludge bed; Fenton: Fenton process; CASS: Cyclic activated sludge system; OD: Oxidation ditch; BF: Biological filter.

3 Conventional treatment processes for rural wastewater

In summary, traditional biological treatment methods for rural wastewater, such as Conventional Activated Sludge (CAS), Soil Treatment Systems (STSs), Constructed Wetlands (CWs), Stabilization Ponds (SPs), and Upflow Anaerobic Sludge Blanket (UASB) reactors, each have their merits but also present limitations. The CAS process, as depicted in **Fig.2(a)**, generates activated sludge flocs through aeration, effectively treating COD, nitrogen, and phosphorus in wastewater, yet its complexity and high energy consumption make it unsuitable for rural areas. As shown in **Fig.2 (b),** STSs leverage the natural treatment capabilities of soil, but their efficiency is influenced by soil composition and wastewater quality, and their denitrification efficiency is limited by the low carbon-to-nitrogen ratio in rural wastewater[5]. **Fig. 2 (c)** illustrates that CWs use aquatic plants and natural ecological processes to treat wastewater, but they require substantial land and are prone to clogging. SPs, as shown in **Fig. 2 (d)**, operate without mechanical equipment, reducing operational and maintenance energy needs, but they demand large land areas and have limited phosphorus removal efficiency [6]. UASB reactors, depicted

The 12th International Symposium on Water Environment Systems
----- with Perspective of Global Safety   (Nov. 21th ~ 23th , 2024)

GP-RSS & SyDE
Tohoku University

in **Fig.2(e)**, are adept at treating high-strength wastewater but are not well-suited for the dispersed, low-pollutant concentration wastewater typical of rural settings [7]. Consequently, these traditional methods, while effective in certain contexts, may not be the most appropriate for the unique challenges of rural wastewater treatment.

Compared with these processes mentioned above, biofiltration systems are considered more suitable to the wastewater treatment in rural areas. A biofilter is capable of reducing energy consumption, enhancing pollutants removal efficiency, and ensuring the quality of the effluent for rural wastewater treatment. This process resembles a natural ecosystem and leads to a decrease in energy consumption thereby reducing operating costs and simplifying the sludge management process. Moreover, the filter media employed in biofiltration systems improve stability and performance due to their low density and resistance to clogging, ensuring smooth operation [8]. Additionally, the media support the formation of biofilms, providing an optimal environment for microbial growth. Biofiltration systems require minimal maintenance, with simple cleaning and upkeep procedures. Their superior adaptability allows them to handle fluctuations in water quality and changes in pollutant loads, maintaining effective treatment results for rural wastewater.
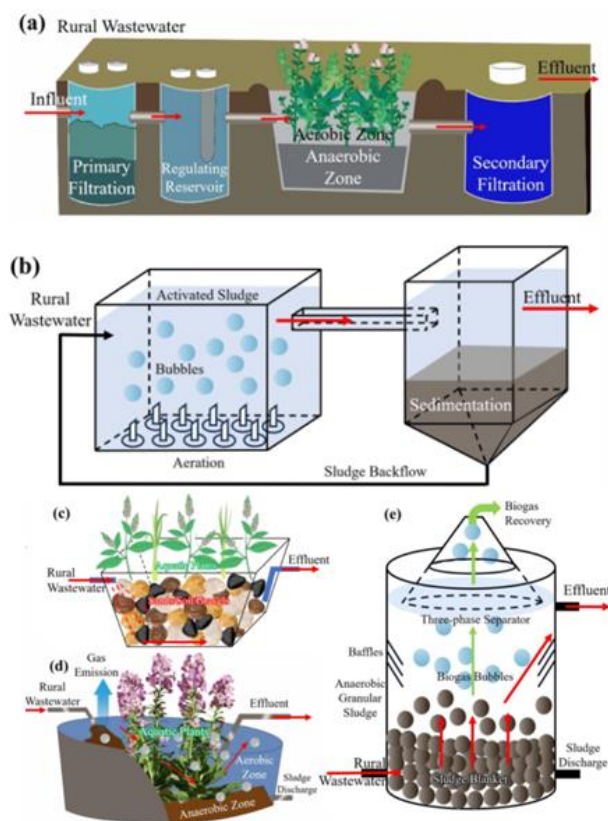
Fig. 2. Currently implemented conventional treatment processes for rural wastewater treatment which are used in recent years: (a) Soil treatment system; (b) Constructed wetland; (c) Conventional activated sludge process; (d) Wastewater stabilization pond; (e) Up-flow anaerobic sludge blanket reactor.

4 Development and applications of biofiltration process

Biofiltration systems, in contrast to traditional physical/chemical filtration methods, leverage biological reactions to break down and convert pollutants through microbial activity, offering a mature and environmentally friendly approach to wastewater treatment with low energy consumption and high efficiency, particularly suitable for rural applications. These systems operate through three primary mechanisms: separation, adsorption, and biodegradation, with the latter distinguishing them from conventional filters by enhancing water quality through microbial metabolism. The integration of biofiltration into decentralized sanitation systems is economically viable and strategically important, requiring an analysis of wastewater pollution indices and the selection of appropriate systems based on economic conditions. For instance, anammox biofilters are ideal for wastewater with a low carbon-to-nitrogen ratio, while denitrification biofilters are suitable for mildly polluted industrial and urban/rural wastewater. Operational parameters must be controlled, and regular maintenance conducted to ensure the effectiveness of biofilters, which are simple to operate and hold promise for developing countries.

Categorized into Biological Aerated Filters (BAF), Denitrification Biofilters (DNBF), and Integrated Bioreactors (IB), biofilters consist of essential components like inflow, container, filter media, outflow, and aeration systems. BAFs, requiring air supply for biofilms, are effective in removing BOD, COD, TSS, pathogens, and NH_4^+-N but have limited TN and TP removal, necessitating additional treatment stages. DNBFs, being anaerobic, focus on denitrification to reduce NO_3-N levels, converting them into N_2 and requiring additional carbon sources to enhance denitrifying bacteria. Integrated Bioreactors merge BAF and DNBF processes, allowing for simultaneous aerobic and anaerobic reactions, achieving high removal efficiencies for COD, NH_4^+-N, NO_3-N, and TP, albeit with increased construction and management costs. These systems, when applied to rural wastewater treatment, demonstrate high removal efficiencies and cost-effectiveness, providing a viable pathway for future enhancements in wastewater management.

5 Current advancements of biofiltration process

Filter media are of paramount importance within biofiltration systems, providing a porous structure that serves as a habitat for microbial growth and facilitates the removal of pollutants. A variety of common materials, including zeolite, volcanic rock, ceramics, and activated carbon, are utilized for their high specific surface areas, which are essential for microbial attachment and diversity. Advanced materials such as graphene and metal-organic frameworks (MOFs) have also shown potential in wastewater treatment due to their excellent specific surface areas, chemical stability, and tunable surface chemistry, demonstrating efficacy in the removal of heavy metals, aromatic compounds, and other pollutants [9,10].

In the current landscape of wastewater treatment technologies, sulfur-based autotrophic denitrification (SAD) and pyrite-based autotrophic denitrification (PAD) are considered advanced approaches that enhance the efficiency of biofilters and diminish reliance on external carbon inputs. SAD employs reduced sulfur compounds as electron donors, offering a cost-effective and environmentally benign alternative to conventional heterotrophic denitrification. Conversely, PAD utilizes pyrite minerals to remove both

The 12ᵗʰ International Symposium on Water Environment Systems
----- with Perspective of Global Safety   (Nov. 21ᵗʰ～23ᵗʰ , 2024)

GP-RSS & SyDE
Tohoku University

nitrogen (N) and phosphorus (P), rendering it an efficient and eco-friendly method.

Furthermore, anaerobic ammonium oxidation (anammox)-based processes represent a sustainable nitrogen removal technology, involving anaerobic ammonium-oxidizing bacteria that utilize inorganic carbon under anaerobic conditions. Compared to traditional denitrification methods, the anammox process significantly reduces energy consumption and greenhouse gas emissions. The anammox-hydroxyapatite (HAP) process couples anammox with HAP crystallization for the simultaneous removal of N and P, offering an energy-efficient and effective method for wastewater treatment. However, this technology is still in the developmental stage, and its practical implementation necessitates consideration of various factors, including process stability, biofilter reactor design, environmental conditions, and cost implications.

6 Future perspectives on upgrades and enhancements on biofiltration

In the realm of rural wastewater treatment, filter media upgrades are pivotal for enhancing the efficiency of biofilters, which are tasked with the concurrent biological conversion of chemical oxygen demand (COD) and ammonium (NH_4^+), as well as the physical filtration of phosphorus (P) compounds. The choice of media, whether natural like sand or gravel, or engineered with adsorptive properties, directly influences biofilter performance. Innovations in media, such as carbon foam and composite materials, have shown promise in improving treatment outcomes and reducing operational costs. Advanced biofiltration technologies, including integrated autotrophic denitrification processes like pyrite-sulfur (PSAD) and manganese-based (MAD) systems, not only boost treatment efficiency but also align with carbon-neutral objectives by minimizing carbon emissions. Post-treatment strategies, such as anaerobic digestion for sludge management, further contribute to the sustainability of biofiltration systems. The integration of anammox processes with other denitrification methods presents a cutting-edge approach to nitrogen removal, offering a cost-effective and environmentally friendly solution. Collectively, these advancements in biofiltration media and processes underscore the ongoing evolution and optimization of rural wastewater treatment technologies.

7 Conclusions

This study systematically explored and investigated the contemporary developments and forthcoming obstacles in the research area of rural wastewater treatment by outlining the adopted biofiltration technologies and their future perspectives, delving into emerging carbon-neutral processes and offering a glimpse into the future direction of rural wastewater treatment with the following findings:

(1) Biofiltration systems are acknowledged to hold promising feasibility for achieving carbon-neutral treatment of rural wastewater by exhibiting the potential to significantly decrease carbon emissions, energy usage, and operational expenses.

(2) Advanced carbon-neutral processes such as SAD, PAD and anammox-based technologies which have the potential of improving and enhancing the removal performance of both organic and inorganic substances from rural wastewater are considered suitable to be integrated with biofiltration system.

(3) Future direction of the development of biofiltration process should focus on the upgrading of filter media, low-carbon autotrophic denitrification, mixotrophic denitrification and enhanced anammox-based processes to achieve carbon neutrality in rural wastewater treatment.

Reference

[1] Communiqué of the Seventh National Population Census (No. 1), (2021). https://www.gov.cn/guoqing/2021-05/13/content_5606149.htm (accessed August 29, 2024).

[2] X. You, L. Yang, X. Zhou, Y. Zhang, Sustainability and carbon neutrality trends for microalgae-based wastewater treatment: A review, Environ. Res. 209 (2022) 112860. https://doi.org/10.1016/j.envres.2022.112860.

[3] MEE, Yearbook of ecological and environmental s tatistics of China in 2022, Minist. Ecol. Environ. Peopl es Repub. China (2023). https://www.mee.gov.cn/hjzl/sth jzk/sthjtjnb/202312/t20231229_1060181.shtml.

[4] MOHURD, Yearbook of urban and rural constructi on of China in 2022, Minist. Hous. Urban-Rural Dev. Peoples Repub. China (2023). https://www.mohurd.gov.c n/gongkai/fdzdgknr/sjfb/index.html.

[5] P. Song, G. Huang, Y. Hong, C. An, X. Xin, P. Zhang, A biophysiological perspective on enhanced nitrate removal from decentralized domestic sewage using gravitational-flow multi-soil-layering systems, Chemosphere 240 (2020) 124868. https://doi.org/10.1016/j.chemosphere.2019.124868.

[6] Z.N. Norvill, A. Toledo-Cervantes, S. Blanco, A. Shilton, B. Guieysse, R. Muñoz, Photodegradation and sorption govern tetracycline removal during wastewater treatment in algal ponds, Bioresour. Technol. 232 (2017) 35–43. https://doi.org/10.1016/j.biortech.2017.02.011.

[7] F. Rodrigues-Silva, G.P. Masceno, P.P. Panicio, R. Imoski, L.D.T. Prola, C.B. Vidal, C.R. Xavier, W.A. Ramsdorf, F.H. Passig, M.V.D. Liz, Removal of microp ollutants by UASB reactor and post-treatment by Fento n and photo-Fenton: Matrix effect and toxicity response s, Environ. Res. 212 (2022) 113396. https://doi.org/10.1 016/j.envres.2022.113396.

[8] V.S. Koutnik, A. Borthakur, J. Leonard, S. Alkidim, H.C. Koydemir, D. Tseng, A. Ozcan, S. Ravi, S.K. Mohanty, Mobility of polypropylene microplastics in stormwater biofilters under freeze-thaw cycles, J. Hazard. Mater. Lett. 3 (2022) 100048. https://doi.org/10.1016/j.hazl.2022.100048.

[9] K. Rana, H. Kaur, N. Singh, T. Sithole, S.S. Siw al, Graphene-based materials: Unravelling its impact in wastewater treatment for sustainable environments, Mate r. 3 (2024) 100107. https://doi.org/10.1016/j.nxmate.2024. 100107.

[10] S.S.A. Shah, M. Sohail, G. Murtza, A. Waseem, A.U. Rehman, I. Hussain, M.S. Bashir, S.S. Alarfaji, A. M. Hassan, M.A. Nazir, M.S. Javed, T. Najam, Recent trends in wastewater treatment by using metal-organic f rameworks (MOFs) and their composites: A critical vie w-point, Chemosphere 349 (2024) 140729. https://doi.or g/10.1016/j.chemosphere.2023.140729.

The 12th International Symposium on Water Environment Systems
----- with Perspective of Global Safety   (Nov. 21th ~ 23th , 2024)

GP-RSS & SyDe
Tohoku University

Upgrading of Nitrogen Removal Process by Hybrid Anammox Reactor with Functional Carriers

○Weiyi WANG[1*] & Yu-You Li [1,2]

[1]Department of Frontier Science for Advanced Environmental, Graduate School of Environmental Studies, Tohoku University, Miyagi 980-8579, Japan.
[2]Department of Civil and Environmental Engineering, Tohoku University, Graduate School of Engineering, Miyagi 980-8579, Japan.
*E-mail: wang.weiyi.s5@dc.tohoku.ac.jp

Abstract

Hybrid Anammox reactors combining carriers and granules have been proposed to enhance nitrogen removal efficiency. The selection of functional carriers is crucial for achieving rapid startup and stable nitrogen removal in hybrid reactors. In this study, two identical hybrid anammox reactors with different functional carriers of hollow cylindrical polypropylene and acryl-fiber net fabric were conducted to investigate start-up and nitrogen removal performance. Compared to hollow cylindrical polypropylene carrier, the hybrid reactor with acryl-fiber carrier exhibited excellent capacities in nitrogen removal performance, microbial retention ability, and biofilm formation speed. Starting with an nitrogen loading rate of 0.25 g-N/L/d, the hybrid reactor achieved an nitrogen removal rate of over 2.0 g-N/L/d within 90 days, indicating a 10-fold increase in capacity.

Keywords: hybrid anammox reactor; start-up; biofilm; granular; carriers.

1 Introduction

The anaerobic ammonium oxidation (anammox) reaction is an anaerobic biological process in which ammonium and nitrite react directly to produce nitrogen gas, mediated by anaerobic ammonium oxidation bacteria (AnAOB). The anammox process does not require oxygen supply or an organic carbon source, making it a resource- and energy-efficient biological nitrogen removal process. However, challenges such as a slow growth rate of AnAOB, substrate inhibition, prolonged startup times, difficulties in maintaining microbial activity, and unstable reactor operation have been pointed out.

The accumulation and retention of AnAOB bacteria have thus far been studied through carrier-based biofilm methods and the formation of granules, both of which have been applied in practice. However, biofilm formation requires a long time, and granules present issues such as flotation and washout, each having its pros and cons. Recently, hybrid anammox reactors that combine carriers and granules have been proposed, showing improved performance. [1]

The selection of functional carriers is crucial for achieving rapid startup and stable nitrogen removal in hybrid reactors. In this study, two identical hybrid anammox reactors with different functional carriers of hollow cylindrical polypropylene (R1) and acryl-fiber net fabric (R2), were conducted to investigate start-up and nitrogen removal performance.

2 Materials and methods

2.1 Inoculated sludge and Substrate

In this study, HAP (hydroxyapatite)-Anammox granules cultivated in our laboratory were used as the seed sludge. A total of 800 mL of HAP-Anammox granules, with a concentration of 1.54 g-VSS/L, was introduced into each reactor. The composition of the synthetic wastewater used in this study was as follows: NH_4Cl 116-380 mg-N/L, $NaNO_2$ 134-495 mg-N/L, $NaHCO_3$ 0.5 g/L, KCl 0.57 g/L, KH_2PO_4 10 mg/L, $CaCl_2$ $2H_2O$ 10 mg/L, $MgCl_2$ $2H_2O$ 10 mg/L, $FeCl_2$ $4H_2O$ mg/L, Trace element 0.5 ml/L.

2.2 Reactor configuration and operation conditions

A hybrid Anammox reactor with an effective volume of 5.5 L was used. The operating temperature was maintained at 25 ℃. The functional carrier filling rate was 11%, calculated based on overflowed water. The pH was adjusted to 7.9-8.3 using 0.05 M sulfuric acid.
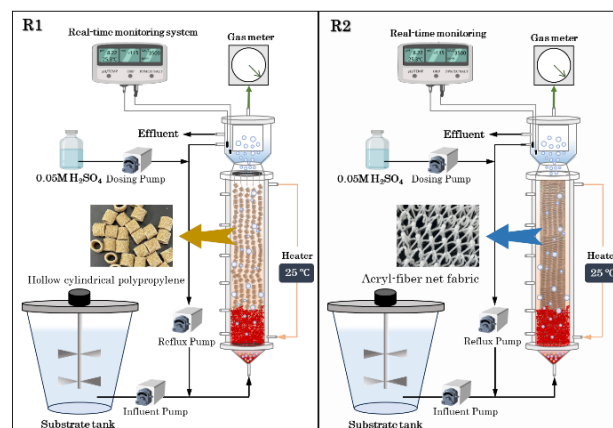

Fig. 1. Hybrid anammox reactor

2.3 Analytical Methods

Influent and effluent samples were collected every other day, filtered using a 0.45 μm membrane filter, and used for various analyses. The water quality parameters analyzed included six items: nitrogen concentration in the influent and effluent, pH, and FA (free ammonia) and FNA (free nitrous acid) concentrations in the effluent. Additionally, to evaluate the characteristics of the granules and biofilm during continuous operation, analyses were conducted for four items: measurement of suspended solids (SS) and volatile suspended solids (VSS), activity tests, and microscopic observations.

3 Results and discussion

The 12th International Symposium on Water Environment Systems
----- with Perspective of Global Safety   (Nov. 21th ~ 23th , 2024)

GP-RSS & SyDe
Tohoku University

3.1 Nitrogen removal performance

Table 1. Nitrogen removal performance in 1-90 days

Phase		I	II	III
Time (d)		1-24d	25-52d	53-90d
NRR	R1	0.25 ±0.25	0.62 ±0.14	1.32 ±0.32
(g-N/L/d)	R2	0.25 ±0.25	0.66 ±0.15	1.84 ±0.68
TNRE	R1	91.33 ±4.09	77.75 ±4.68	73.1 ±3.28
(%)	R2	90.7 ±3.39	82.63 ±2.58	79.26 ±3.15

The average NRR (Nitrogen Removal Rate) and average TN (Total Nitrogen) removal rates at each stage are shown in Table 1. In this study, the operation started under a condition of NLR (Nitrogen Loading Rate) at 0.25 g-N/L/d. The NLR was gradually increased, and after a startup period of 90 days, R1 achieved an NLR of 2.7 g-N/L/d and an NRR of 2.0 g-N/L/d. The total nitrogen removal rate was approximately 77.1% throughout the operating period. R2 achieved an NLR of 3.6 g-N/L/d and an NRR of 3.0 g-N/L/d, with a total nitrogen removal efficiency of about 81.5%. No inhibition from FA (free ammonia) or FNA (free nitrous acid) was observed. The pH was maintained at 8.1 ± 0.2, indicating stable reactor operation. The startup of the hybrid reactor using functional carriers was achieved within 90 days. In the hybrid reactor, the acryl-fiber net fabric carriers (R2) showed better nitrogen removal performance when coupled with granular sludge compared to the hollow cylindrical carriers (R1).

3.2 Start-up Kinetics of Hybrid Anammox Reactor

During the 90-day startup operation of the hybrid reactor, the activity of AnAOB increased; however, it is necessary to analyze how the reaction capability has grown. Therefore, to understand the rate of increase in reaction capability during the startup period, the relationship between total nitrogen removal rate and cultivation time was analyzed, as shown in Figure 2. It was assumed that the nitrogen removal rate in the reactor, corresponding to the growth of AnAOB, could be expressed with an exponential function concerning cultivation time (assuming logarithmic growth), allowing for the calculation of the doubling time. Under conditions of 25 ℃, the rate of increase in NRR for the two hybrid reactors with different carriers was calculated as 0.024 d^{-1} and 0.038 d^{-1}, resulting in doubling times of 29 days and 18 days, respectively.
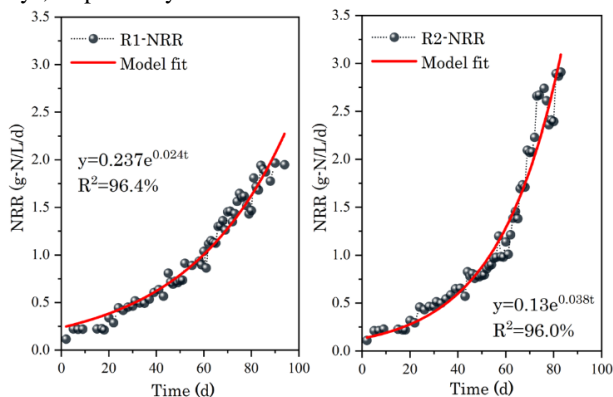

Fig. 2. NRR Increase Rate Analysis

3.3 Analysis of anammox growth rate

The changes in microbial biomass within the reactor during the 90-day startup period are shown in Figure 3. R1 granular sludge concentration increased from 1.5 to 8.89 g VSS/L and R2 granular sludge concentration increased from 1.5 to 10.57 g VSS/L in 90d of operation. On the 30th day,

no biomass was detected on the HC carriers; the biofilm biomass on the AF carriers reached 0.37 g VSS/L. On the 90th day, the biomass of the AF carriers was significantly higher, reaching 2.5 g VSS/L, compared to the HC carriers, which reached 0.4 g VSS/L.
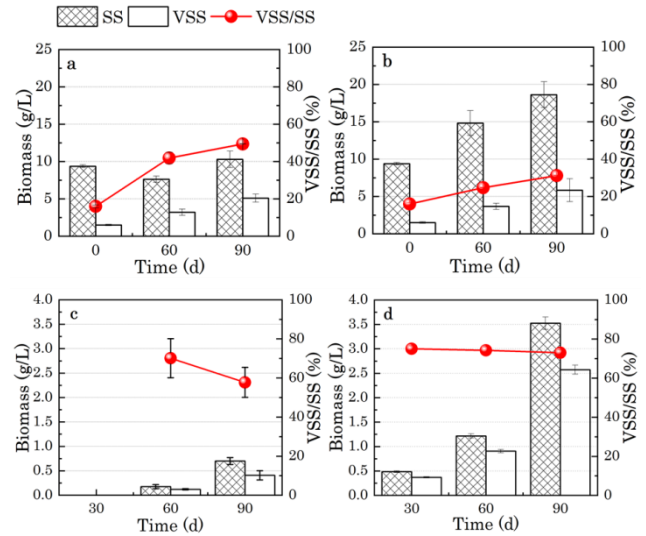
Fig. 3. Sludge Growth Rates: a. Granular Sludge of R1 b. Granular Sludge of R2 c. Biofilm of R1 d. Biofilm of R2

3.4 Morphological Characteristics of Biofilm

During the operational period, an increase in granular sludge and biofilm growth on the carriers was observed from the HAP granule inoculum. The growth of biofilm on different carrier surfaces varied. On the hollow cylindrical carrier, a red biofilm was observed by day 90, while on the acryl-fiber net fabric carriers, a red biofilm was detected by day 30. The biofilm conditions on the carriers at day 90 are compared in Figure 4. The biofilm on the hollow cylindrical carrier was found internally, whereas the biofilm on the
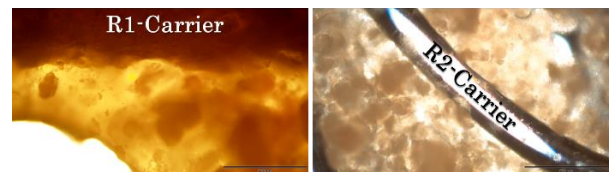
acryl-fiber carriers was attached around the fibers.

Fig. 4. 90-Day Biofilm Morphology on Carriers

4 Conclusions

1. Starting with an NLR of 0.25 g-N/L/d, the hybrid reactor achieved an NRR of over 2.0 g-N/L/d within 90 days (R1 2.0 g-N/L/d; R2-3.0 g-N/L/d), indicating a 10-fold increase in capacity;

2. Two identical hybrid anammox reactor both achieved short anammox reaction capacity doubling times (25 days and 18 days) at 25℃ operation.

3. Acryl-fiber net fabric carrier was better than hollow cylindrical carrier to couple with granular sludge for hybrid anammox reactor.

Reference

[1] Song, Y., Ni, J., Guo, Y., Kubota, K., Qi, W. K., & Li, Y. Y. (2023). Anammox upflow hybrid reactor: Nitrogen removal performance and potential for phosphorus recovery. Chemosphere, 313, 137580.

The 12th International Symposium on Water Environment Systems
----- with Perspective of Global Safety   (Nov. 21st ~ 22nd , 2024)

GP-RSS & SyDE
Tohoku University

Effects of pH Control and Sludge Recirculation on Hydrogen Production in Two-Phase Anaerobic Digestion of Food Waste and Paper Waste

○ QINGKANG ZENG*, YU QIN[1] & YU-YOU LI[1,2]

[1]Department of Civil Engineering, Tohoku University, Miyagi 980-8579, Japan.
[2]Department of Environment Engineering, Tohoku University, Miyagi 980-8579, Japan.
*E-mail:zeng.qingkang.q4@dc.tohoku.ac.jp.

Abstract

Two-phase anaerobic digestion (TPAD) could treat paper waste (PW) and food waste (FW)to generate H_2 and CH_4. However, the high hydrolysis and acidogenesis rates of FW in H_2 producing phase would always lead to acidification. Therefore, the pH of H_2 production phase should be controlled within a specific range. In this research, two different pH controlling methods were used in the TPAD system(adding alkaline solution or sludge recirculation). When the pH was controlled between 5.0 and 6.0 by adding alkaline solution, the H_2 production rates was 1.18 L/L/d and meanwhile excessive or insufficient pH values could both inhibit anaerobic H_2 fermentation process. On the other hand, the TPAD system combined with sludge recirculation could also achieve continuous and stable H_2 production. As the recirculation ratio was 1:1, the H_2 production rate was 1.25 L/L/d and the system outperformed in terms of VS removal efficiency, anaerobic reaction rate, and system stability than those in pH controlling by alkaline solution which suggested sludge recirculation would be a better choice.
Keywords: Paper waste; Food waste; Sludge recirculation; pH control; Co-digestion.

1 Introduction

In December 2022, the IEA report announced that "renewable energy will overtake coal as the world's largest power source by the beginning of 2025. From the perspective of preventing global warming, soaring fossil fuel prices, and building a decarbonized society, methods for generating hydrogen and methane from organic waste through the action of anaerobic microorganisms are attracting attention. H_2 is one kind of the cleanest energy, how to produce H_2 from anaerobic reaction has been a hot topic in the world. The two-phase anaerobic digestion (TPAD) system can achieve simultaneous production of H_2 and CH_4 separately. But there were still many operation and system questions such as the pH controlling. It was known than high H_2 production efficiency would be achieved as the pH range of 5.0 and 6.0[1]. Therefore, this research compared the effects of two different pH controlling methods (adding alkaline solution and sludge recirculation) on H_2 production to find the optimal pH controlling way.
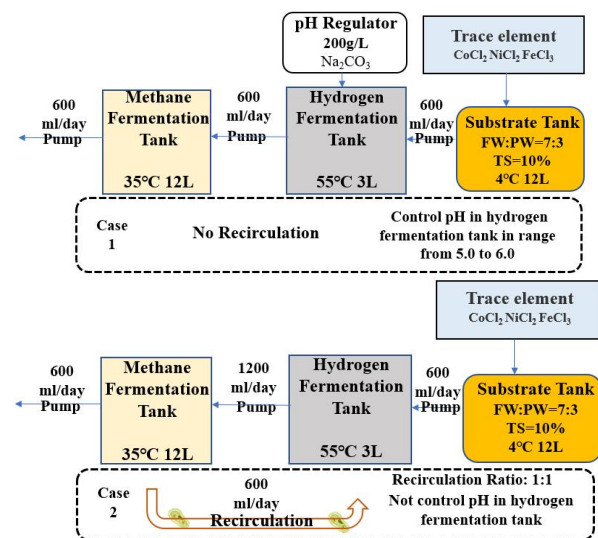
2 Materials and methods

The inoculum was taken from anaerobically digested sludge from the Senen Purification Center. After loading into the reactors, the air inside the reactors was expelled by nitrogen aeration blowtorch to make it anaerobic. The food waste used in this paper was artificially prepared food waste and paper waste was used by copy paper from the laboratory. The prepared artificial food waste and paper waste were mixed at a TS based ratio of 7:3, and some water was added to adjust the total TS of the mixed substrate to about 10%. The specific characteristics of the mixed substrate were shown in Table 1. Two comparative experiments were shown in Fig.1. Experimental apparatus were shown in Fig.2. In case 1, the pH was controlled between 5.0-6.0 by adding Na_2CO_3 solution. In case 2, 600mL methane sludge was recirculated into H_2 production phase every day. The HRT of H_2 production phase were 5d

and 2.5d, respectively. Each case was continuously operated on for around 30 days.

Table 1 Characteristics of substrate

Parameter	Value
pH	4.20
TS (%)	8.86
VS (%)	8.50
NH_4^+—N(mg/L)	11.2
Soluble COD (g/L)	41.1
Soluble CH_2O (g/L)	13.1
Soluble protein (g/L)	3.25
Total COD (g/L)	126
Total CH_2O (g/L)	80.8
Total protein (g/L)	14.6
Alkalinity (g-$CaCO_3$/L)	0

Fig. 1. Experiment processes of adding alkaline solution or sludge recirculation.

The 12th International Symposium on Water Environment Systems
----- with Perspective of Global Safety   (Nov. 21st ~ 22nd , 2024)

GP-RSS & SyDE
Tohoku University

Fig. 2. Two anaerobic fermentation reactors(left) and pH regulator system(right).

3 Results and discussion

Fig.3 showed H$_2$ composition, H$_2$ production rate and TS/VS under two different cases. It could be found that when adding recirculation, the H$_2$ production rate was faster (increasing by 6%) and TS/VS of sludge was much lower (decreasing by 52%) than those in case of controlling pH by adding alkaline solution. Meanwhile, the H$_2$ yield increased by 15.47% indicating that the TPAD system combined with sludge recirculation would have a better biogas production efficiency. Table 2 showed the organic removal capacity of the whole system under the two conditions. It also suggested that the higher organic removal efficiency would be achieved after adding recirculation. The reaction rates of four stages in H$_2$ production phase were all improved as shown in Table3, especially the rates of hydrolysis and acidogenesis. It might be due to the recirculated sludge from CH$_4$ production phase played a complementary role and gave the enhancement of the microbial population in H$_2$ production phase. COD and mass balance were conducted to determine the conversion efficiency of system as shown in Fig.4. After adding sludge recirculation, 3.33% of total input COD was converted to hydrogen which was almost the same as 3.29% under adding alkaline solution. However, the proportion of solid COD and dissolved COD was relatively decreased from 23.2% to 20.4%. When adding sludge recirculation, each 1L of substrate was input into system, an average of 6.3 L of H$_2$ could be generated under standard conditions. In contrast, when pH was controlled by alkaline solution, an average of 5.9 L of hydrogen was produced which suggested the addition of sludge recirculation could increase the H$_2$ yield .

4 Conclusions

Controlling pH between 5.0-6.0 is necessary for stable hydrogen production in TPAD system. Both sludge recirculation and adding alkaline solution could control pH in hydrogen fermentation tank. But sludge recirculation could dilute sludge and promote anaerobic reaction rate in hydrogen fermentation tank thus finally get higher hydrogen production rate (increasing by around 6%).

Reference

[1] Lu Li, et al.Temperature-phased anaerobic co-digestion of food waste and paper waste with and without recirculation: Biogas production and microbial structure, Science of The Total Environment, Volume 724,2020.
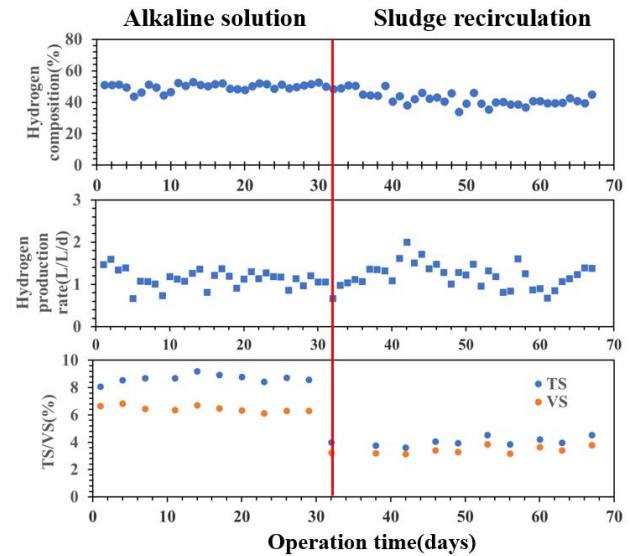
Fig. 3. H$_2$ composition (%), H$_2$ production rate (L/L/d) and TS/VS (%).

Table 2 degradation efficiency of organic matters.

Degradation efficiency	Unit	Sludge Recirculation	Alkaline solution
TS	%	77.07	71.83
VS	%	85.02	83.57
COD	%	79.57	76.78
Carbohydrate	%	94.68	94.52
Protein	%	60.39	30.08

Table 3 Reaction rate in hydrogen producing phase.

Average rates of anaerobic reactions(g-COD/L/d)	Alkaline solution	Recirculation
Hydrolysis	2.88	3.37
Acidogenesis	5.84	8.90
Acetogenesis	3.03	3.63
Methanogenesis	0	0.05
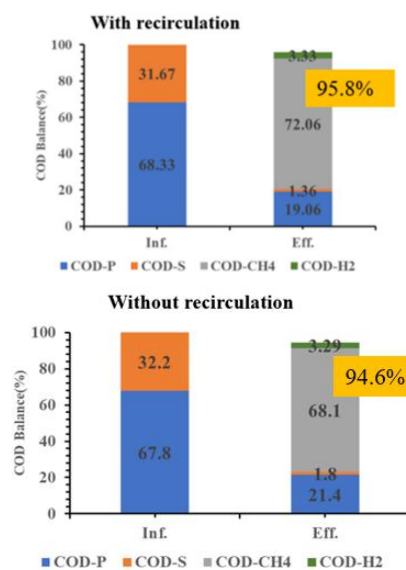
Fig. 4. COD and mass balance calculations.

The 12th International Symposium on Water Environment Systems
----- with Perspective of Global Safety   (Nov. 21st ~ 22nd , 2024)

GP-RSS & SyDE
Tohoku University

Integrated WRF and WRF-Hydro approaches for assessing climate change impacts on extreme flood events

Seong Jin NOH[1*], Bomi KIM[1], Yaewon LEE[1], Hyeonjin Choi[1], Minyoung KIM[1], Hyuna WOO[1] & Yusuke HIRAGA[2]

[1]Department of Civil Engineering, Kumoh National Institute of Technology, Gumi 39177, Republic of Korea.
[2]Department of Civil Engineering, Tohoku University, Miyagi 980-8579, Japan.
*E-mail: seongjin.noh@kumoh.ac.kr

Abstract

This study investigates the impact of climate change on extreme flooding using the Weather Research and Forecasting (WRF) model and its hydrological extension, WRF-Hydro, to simulate flood dynamics in the Nakdong River basin in South Korea. Traditional hydrological and atmospheric models fall short in simulating the complex interactions between climate and hydrology, highlighting the need for an integrated modeling approach. This research utilizes WRF to simulate high-resolution precipitation and WRF-Hydro to model flood responses, focusing on an extreme flood event triggered by Typhoon Hinnamnor in 2022. Preliminary results from the WRF-Hydro model setup provide insights into rainfall distribution and hydrological response under extreme conditions, though further research integrating WRF is required to fully capture atmospheric and land surface processes. The study aims to support adaptive flood management strategies by offering projections of future flood scenarios, crucial for policymakers and urban planners in East Asia.

Keywords: Climate change impact; Extreme flooding; WRF-Hydro; WRF; Integrated modeling.

1 Introduction

Climate change has increasingly intensified extreme weather events, including extreme precipitation and flooding, with severe impacts on both urban and rural communities. Rising global temperatures accelerate the hydrological cycle, leading to more frequent and intense rainfall, which, in turn, heightens flood risk [1]. As flooding causes significant economic losses, disrupts ecosystems, and threatens infrastructure and human lives, understanding how climate change influences flood dynamics is essential for developing effective adaptation strategies. This challenge is compounded by the need to assess not only current flood risks but also those under future climate scenarios, which are expected to worsen due to a faster hydrological cycle and increased atmospheric moisture capacity.

Traditional hydrological models, while useful for simulating historical flood events, generally lack the complexity required to incorporate the dynamic atmospheric conditions affected by climate change. Conversely, atmospheric models may predict precipitation but often fail to capture land surface processes and flood generation mechanisms comprehensively. This limitation underscores the need for integrated modeling approaches that couple atmospheric and hydrological components to provide a robust assessment of future flood risks. The Weather Research and Forecasting (WRF) model, widely used for high-resolution weather simulations, and its hydrological extension, WRF-Hydro, which models water movement across the land surface, together offer a promising framework to bridge this gap [2].

This study aims to assess the impact of climate change on extreme flooding through the integrated use of WRF and WRF-Hydro models. Specifically, it seeks to simulate extreme precipitation and flood events under various climate scenarios, analyze shifts in flood behavior—such as changes in frequency, intensity, and duration—and identify the key factors driving these changes. By comparing simulation outputs across scenarios, this research aims to uncover emerging trends that could shape future flood risks in vulnerable regions. Moreover, the study demonstrates the value of the WRF and WRF-Hydro system for supporting adaptation strategies by providing insights into potential flood scenarios under projected climate conditions.

2 Materials and methods

This study utilizes WRF and WRF-Hydro models to assess climate change impacts on extreme flooding. WRF, developed by the National Center for Atmospheric Research (NCAR), is a robust numerical weather prediction model capable of simulating a wide range of atmospheric phenomena. Configured with nested grids, WRF provides high-resolution precipitation data essential for understanding extreme weather patterns that influence flood events. WRF-Hydro, also developed by NCAR, is used here as a standalone hydrological model to simulate surface and subsurface water dynamics, including infiltration, overland flow, and channel routing. The model operates on a grid-based framework representing land features such as soil type, land cover, and elevation. By employing both models, we independently analyze the atmospheric and hydrological aspects of flooding. WRF provides insights into precipitation under climate scenarios, while WRF-Hydro enables simulation of flood response based on generalized precipitation inputs. This dual-model setup allows for a comprehensive assessment of climate change impacts on extreme flooding by leveraging the strengths of each model separately.

The study area for this research is the Nakdong River basin, the second-largest river basin in South Korea, which is highly vulnerable to extreme flooding events due to its geographical

The 12th International Symposium on Water Environment Systems
----- with Perspective of Global Safety　　(Nov. 21st ~ 22nd , 2024)

GP-RSS & SyDE
Tohoku University

and climatic conditions. To simulate flood dynamics accurately within this basin, WRF-Hydro is configured with a high-resolution 500-meter grid, enabling detailed representation of hydrological processes across varied landscapes. Input data for WRF-Hydro were generated using high-resolution topography, soil, and land cover maps, ensuring that the model captures the unique surface characteristics of the region, including elevation changes, soil permeability, and vegetation types (Fig. 1). The model targets an extreme flood event caused by Typhoon Hinnamnor, which struck the area in 2022, bringing record-breaking rainfall and severe flooding. By focusing on this event, the study assesses the hydrological response of the Nakdong River basin under extreme conditions, providing insights into how similar future events might affect the region under evolving climate scenarios.
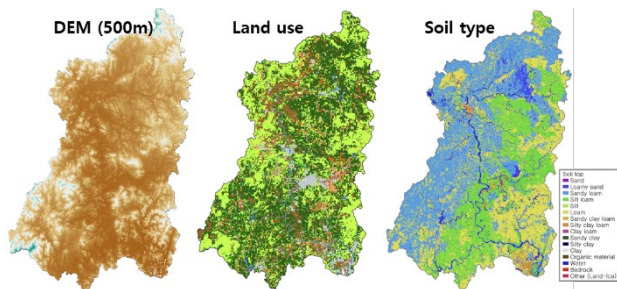

Fig. 1. Maps of hydrological characteristics of the Nakdong River basin

3 Tentative results and discussion

As a preliminary step, ground-measured precipitation data was analyzed, and WRF-Hydro hydrologic modeling was implemented, driven by ground-observed weather data. The map shows cumulative rainfall during Typhoon Hinnamnor from September 1 to 9, 2022, over a portion of South Korea (Fig. 2). The color gradient indicates rainfall intensity, with values ranging from 30 mm (in blue) to over 300 mm (in red). The heaviest rainfall occurred in the southern region, particularly concentrated in areas near the coast, as seen in the deep red zones. Blue dots mark observation points, indicating rainfall distribution across the region. This spatial pattern suggests that Typhoon Hinnamnor brought significant rainfall to southern South Korea, potentially increasing the risk of flooding, especially in coastal areas. Analyzing these patterns can provide insights into flood-prone regions and aid in future typhoon impact assessments.
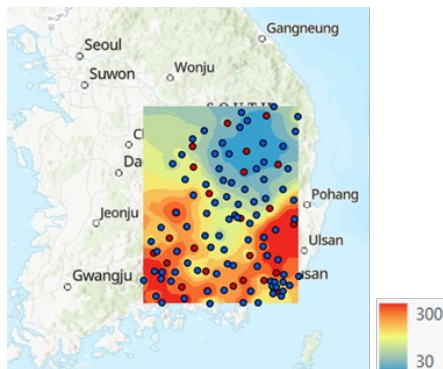
Fig. 2. Cumulative precipitation from 1 to 9 Sep. 2022
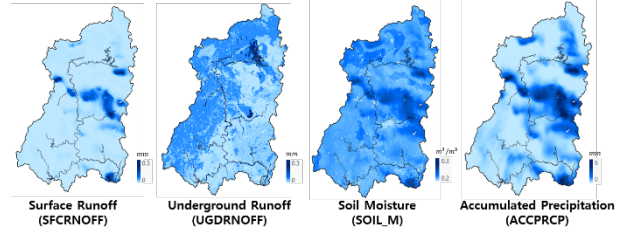
Fig. 3. Example simulation results of WRF-Hydro

Fig. 3 displays tentative WRF-Hydro simulation results, showing variations in water levels or soil moisture across a region over different time steps or conditions, with darker blue areas indicating higher values. Further simulations will be conducted to calibrate the model and to project future climate conditions using outputs from the WRF model, enhancing the accuracy and reliability of hydrological predictions.

4 Conclusions

This study emphasizes the need for integrated modeling approaches to assess the impact of climate change on extreme flooding. While the current results focus on precipitation analysis and initial WRF-Hydro setup, further research using an integrated WRF and WRF-Hydro system is essential to capture both atmospheric and hydrological processes, enabling a more comprehensive analysis of future flood scenarios. This approach holds promise for supporting adaptive flood management strategies, offering insights that can aid policymakers and urban planners. Continued model calibration and validation will be crucial to ensure accurate predictions, reinforcing the importance of proactive adaptation to protect vulnerable communities and infrastructure in East Asia.

Reference

[1]　B. Kim, G. Lee, Y. Lee, S. Kim, and S. J. Noh, Assessment of the Impact of Spatial Variability on Streamflow Predictions Using High-Resolution Modeling and Parameter Estimation: Case Study of Geumho River Catchment, South Korea, Water, 16(4), (2024) Art. no. 4.

[2]　Y. Wehbe et al., Analysis of an extreme weather event in a hyper-arid region using WRF-Hydro coupling, station, and satellite data, Natural Hazards and Earth System Sciences, 19(6), (2019) 1129–1149.

The 12th International Symposium on Water Environment Systems
----- with Perspective of Global Safety　　(Nov. 21st ~ 22nd , 2024)

GP-RSS & SyDE
Tohoku University

Enhancing physics-based inundation modeling through ensemble data assimilation: impacts of multivariate observations

Bomi KIM[1*], Yaewon LEE[1] & Seong Jin NOH[1]

[1]Department of Civil Engineering, Kumoh National Institute of Technology, Gumi 39177, Republic of Korea.

[*]E-mail: kimbom3835@kumoh.ac.kr

Abstract

In this study, we present a probabilistic urban flood modeling framework that integrates high-resolution process-based modeling with ensemble data assimilation (DA) to evaluate the impact of multivariate flood observations through synthetic experiments. This framework incorporates data from both sewer systems and urban surfaces into a 1D/2D inundation model (H12) using non-Gaussian sequential DA methods like particle filtering. The experiments, conducted in an urban catchment in Osaka, Japan, begin with a sensitivity analysis to explore uncertainties in model inputs, including surface roughness and overland-sewer flow interactions. Model ensembles are generated by perturbing effective components and are selectively updated as new observations are integrated. This DA setup examines how various observation types and locations, such as urban surface inundation depths and sewer water levels, influence the model's accuracy. Findings highlight how incorporating diverse observation sources and optimized observation locations can improve urban flood predictions with DA, supporting more effective data-driven flood forecasting strategies.

Keywords: Urban inundation; Ensemble data assimilation; Particle filtering; Synthetic experiments.

1 Introduction

Deterministic inundation analysis based on a single scenario often fails to adequately capture input uncertainties, limiting prediction reliability. Probabilistic inundation analysis addresses this by considering multiple scenarios and variable input conditions, producing a spectrum of potential outcomes. This probabilistic approach is particularly valuable for assessing the range and likelihood of inundation risks under varied conditions, enabling decision-makers to make informed choices. By integrating uncertainties in weather forecasts, terrain data, and hydrological conditions, probabilistic modeling provides more realistic and robust predictions.

Data assimilation (DA) methods further enhance model accuracy by merging predictions with observational data, effectively addressing uncertainties in both input data and the model. Among DA techniques, probabilistic methods like the Ensemble Kalman Filter (EnKF) and Particle Filter (PF) are particularly effective for managing uncertainty through probabilistic scenarios. The EnKF captures uncertainty by updating weights across multiple model states, while the PF adapts to non-Gaussian distributions by adjusting individual particle weights based on observations. Due to the Kalman Filter's Gaussian assumptions, PF techniques offer flexibility for complex hydrodynamic systems and have shown promise in probabilistic urban flood modeling.

Studies on DA in urban flooding emphasize the effectiveness of EnKF and PF in probabilistic mapping and modeling. However, previous studies often focus solely on 2D surface modeling, neglecting sewer network integration.

In this study, we apply a probabilistic DA method based on particle filters to a fully coupled 1D-2D urban inundation model in Nakahama, Japan, examining how different observational data types, specifically surface inundation depth and sewer water levels, affect model updates.

2 Materials and methods

To assess the proposed probabilistic inundation modeling, we selected Osaka's Nakahama area, covering 18.1 km² in eastern Osaka, Japan. The study utilized data from 3,026 sewer pipes (diameters 0.3–8.5 m), 2,903 manholes, and 4 pumping stations, along with a 5 m resolution Digital Elevation Model (DEM) converted into an unstructured triangular mesh for topographical input. This low-lying area, with reverse-gradient stormwater pipes, is highly prone to inundation, as demonstrated in the significant 2008 flood event analyzed by Lee and Nakagawa (2015).
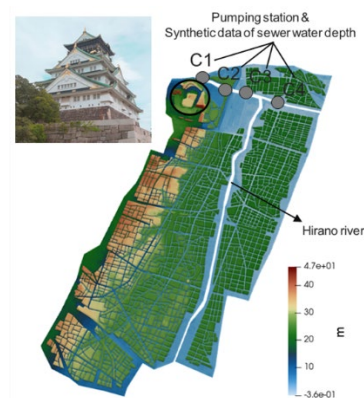

Fig. 1. Study area.

The 1D-2D integrated inundation model (Lee et al., 2015; Noh et al., 2018) combines sewer network and surface flow analyses, enabling high-resolution urban flood simulation. This model assumes runoff exchange between surface and sewer networks through catchments, with inflow and outflow simulated as weir and orifice flows. Coupling 1D sewer analysis with 2D surface flow captures complex urban flood dynamics, including sewer overflow and rapid overland flow

The 12th International Symposium on Water Environment Systems
----- with Perspective of Global Safety   (Nov. 21st ~ 22nd , 2024)

GP-RSS & SyDE
Tohoku University

paths. Extensively validated domestically and internationally, this model demonstrates high adaptability across urban environments. The model's integration of hybrid parallel computing technology enables it to perform at high resolutions without sacrificing computational efficiency, a critical advantage when simulating detailed urban landscapes and intricate drainage systems (Lee et al., 2013; Noh et al., 2018).
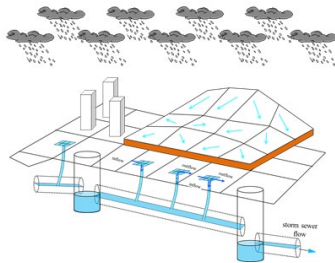
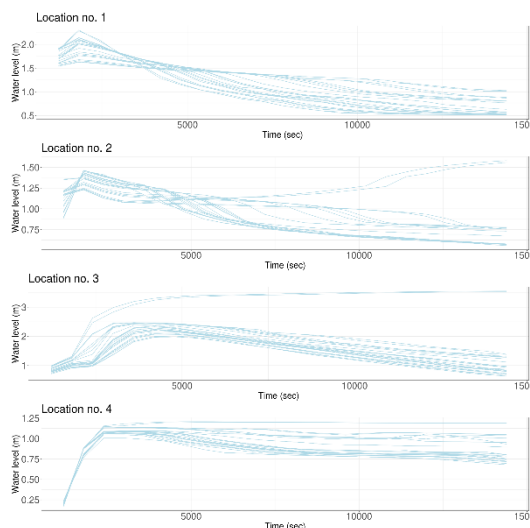**Fig. 2. H12 model concept diagram.**

The particle filter, also referred to as the Sequential Monte Carlo (SMC) method, is a simulation-based sequential data assimilation technique. This method predicts information by weighting the relationship between simulated outcomes and observed data, providing a flexible approach for use with nonlinear and non-Gaussian models. Unlike the widely-used Kalman filter techniques, which rely on assumptions of normal distributions and linearity, the particle filter accommodates more complex model dynamics. In nonlinear stochastic model systems, it operates within a dynamic state-space framework, incorporating state transition and observation equations to handle uncertainty and variability effectively. This flexibility makes the particle filter particularly useful for real-time applications where model assumptions may not hold consistently.

3 Tentative results

Fig. 3. Simulated uncertainty in storm sewer water levels with catchment inlet size perturbations.

We combined the ensemble particle filter with the H12 urban inundation analysis model to analyze the impact of state updates when using sewer water levels as observational data versus surface inundation depths. This figure shows the

results for storm sewer water levels, simulated by applying a perturbation range of 0.5 to 1 to the storm sewer inlet size. It illustrates water level variations over time at four locations, with the x-axis representing time (sec) and the y-axis representing water level (m) in each graph. We analyze the effects of these updates by comparing the perturbed results with observations. Observations include surface inundation depths and storm sewer water levels. The discussion will focus on understanding how incorporating different types of surface observations, such as inundation depth and extent, may enhance the model's accuracy and robustness.

Reference

[1] Lee, S., Nakagawa, H., Kawaike, K., Zhang, H., Experimental Validation of Interaction Model at Storm Drain for Development of Integrated Urban Inundation Model, Annual Journal of Hydraulic Engineering, JSCE, 57, (2013) 1-13.

[2] Lee, S., Nakagawa, H., Kawaike, K., Zhang, H., Urban inundation simulation considering road network and building configurations, Journal of Flood Risk Management, 9(3), (2015), 224-233.

[3] Noh, S. J., Lee, J., Lee, S., Kawaike, K., Seo, D.-J., Hyper-resolution 1D-2D urban flood modelling using LiDAR data and hybrid parallelization, Environmental Modelling and Software (2018), 1-37.

The 12th International Symposium on Water Environment Systems
----- with Perspective of Global Safety   (Nov. 21st ~ 22nd , 2024)

GP-RSS & SyDE
Tohoku University

Assessing Probable Maximum Precipitation (PMP) Estimates in Chile Using Statistical GEV Distribution and Physically Based Approaches

○ Joaquin Meza[1*], Yusuke Hiraga[2] , Alvaro Ossandon[1] & Ignacio Villavicencio[1]

[1]Department of Civil Engineering, Santa Maria Technical University, Valparaiso, Chile.
[2]Department of Civil Engineering, Tohoku University, Sendai, Japan.
[*]E-mail: joaquin.meza@usm.cl

Abstract

The Probable Maximum Precipitation (PMP) is a critical parameter for the design and safety assessment of hydraulic structures. This study explores two different approaches for estimating the PMP in Chile: a statistical method using the Generalized Extreme Value (GEV) distribution and a physically based method utilizing the Weather Research and Forecasting (WRF) model. Both methods resulted in less conservative PMP estimates compared to the traditional Hershfield method, suggesting that the latter may overestimate extreme precipitation in this region. While the statistical method is easier to implement and requires less computational effort, the physically based approach offers detailed spatial and temporal precipitation patterns, which are crucial in areas with complex terrain and climatic variability. The findings highlight the importance of selecting appropriate methodologies for PMP estimation, balancing practicality with the need for detailed analysis.

Keywords: Probable Maximum Precipitation; PMP; GEV distribution; WRF model; Extreme events.

1 Introduction

Estimating the Probable Maximum Precipitation (PMP) is essential for the design and risk assessment of hydraulic infrastructures like dams and flood defenses. The World Meteorological Organization (WMO) defines PMP as "the greatest depth of precipitation for a given duration that is meteorologically possible for a given size storm area at a particular location at a particular time of year" [1].

Traditional methods, such as the statistical approach proposed by Hershfield [2], estimate PMP using historical precipitation records and frequency factors. However, several studies have reported deficiencies in the Hershfield method. Koutsoyiannis [3] questioned its validity for estimating the upper bound of precipitation, arguing that the frequency factor does not stabilize and may not represent a physical limit. Micovic et al. [4] noted that while statistical methods like Hershfield's can be useful for quick estimates, they do not account for meteorological processes and may lead to overestimations, especially in regions with complex terrain or limited data. Additionally, the Hershfield method may not adequately capture the tails of the precipitation distribution, which are critical for estimating extreme events.

Alternatively, physically based models like the Weather Research and Forecasting (WRF) model can simulate extreme precipitation events by modifying atmospheric conditions, offering a process-based estimation of PMP [5]. These models incorporate physical atmospheric processes leading to extreme events and provide detailed spatial and temporal precipitation patterns under complex topography and climatic variability.

This study aims to compare two approaches: an alternative statistical method using the GEV distribution to enhance the estimation of extreme precipitation tails, and a physically based method utilizing the WRF model. By evaluating the benefits and limitations of each method, we seek to provide more accurate and reliable PMP estimates for the region, balancing practicality with the need for detailed analysis.

2 Materials and methods

2.1 Statistical Approach with GEV Distribution

The statistical method proposed involves fitting a Generalized Extreme Value (GEV) distribution to annual maximum daily precipitation (AMDP) data across Chile. Given the country's extensive latitudinal range and diverse topography—from the arid deserts in the north to the rainy temperate forests in the south—precipitation patterns vary significantly throughout the region. To account for this spatial heterogeneity, a clustering analysis was performed to group meteorological stations with similar precipitation characteristics.

The variables used for clustering included geographical coordinates (latitude and longitude) to capture spatial proximity, elevation due to its strong influence on precipitation patterns, and coefficient of variation of the AMDP. By clustering the stations, we were able to regionalize extreme precipitation, enhancing the reliability of the GEV parameter estimates by pooling data from stations within the same cluster. This approach reduces sampling variability and improves the estimation of the tails of the distribution, which is crucial for modeling extreme events.

Parameters of the GEV distribution for each cluster were estimated using L-moments, which are less sensitive to outliers and provide more robust estimates for small sample sizes. This method addresses the sensitivity of the shape parameter (ξ) to sample size and improves the estimation of extreme quantiles, as highlighted by Papalexiou and Koutsoyiannis [6]. For estimating the PMP for each cluster, we focus on adjusting the maximum observed precipitation by incorporating a regional frequency factor ψ that accounts for the upper limit of extreme precipitation in the area.

$$\psi_m = [1/\xi] \, ln\{1 + \xi \, [X_m - \mu]/\sigma\}$$

The 12th International Symposium on Water Environment Systems
----- with Perspective of Global Safety   (Nov. 21st ~ 22nd , 2024)

GP-RSS & SyDE
Tohoku University

where μ is the location parameter, σ is the scale parameter, and ξ is the shape parameter. By applying this regionalized statistical approach, we aim to improve upon traditional methods like Hershfield's by providing less conservative PMP estimates that better capture the behavior of extreme precipitation in different climatic regions of the country.
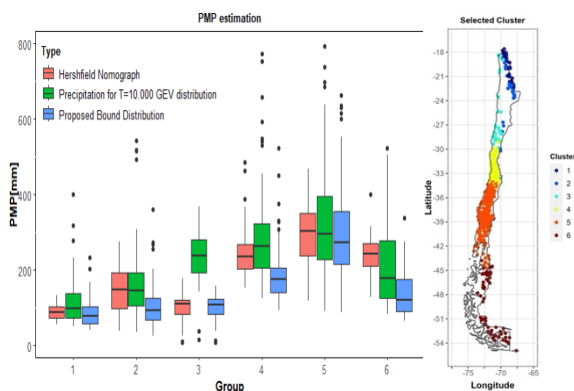
2.2 Physically Based Approach with WRF Model

The physically based method employs the Weather Research and Forecasting (WRF) model to simulate extreme precipitation events in the study area. Historical heavy precipitation events associated with Atmospheric Rivers (ARs) were selected for analysis.

To estimate the PMP, two key techniques were applied within the WRF model simulations. First, moisture maximization was performed by proportionally increasing the relative humidity in the initial and boundary conditions within the AR structure [7]. This approach enhances the moisture content available for precipitation without altering the overall dynamics of the atmospheric system. Second, geospatial shifting of the atmospheric fields was conducted by shifting them latitudinally. This technique optimizes the positioning of the moisture flux relative to the basin, effectively simulating how slight changes in the path of ARs could impact precipitation over the area [7].

Ensemble simulations were conducted by combining these two techniques to explore a range of possible scenarios. By varying the degree of moisture maximization and the extent of geospatial shifting, we were able to determine the scenario that produced the maximum basin-averaged precipitation.

3 Results and discussion

The statistical approach using the GEV distribution was applied to precipitation data across Chile. The results indicated that this method provided less conservative PMP estimates compared to the traditional Hershfield method. The GEV-based method, by accounting for the specific statistical properties of the precipitation data and regional characteristics through clustering yields values that are more physically plausible and tailored to the local climate.

Fig. 1. Comparison between the 24-hour PMP proposed method, Hershfield method, and T=10.000 years magnitude for GEV distribution

The physically based approach was applied specifically to the Maipo River Basin, a critical region that encompasses 42% of Chile's population. Using the optimal configuration of the WRF model identified in our methodology, we simulated and maximized extreme precipitation events associated with Atmospheric Rivers. The maximum 72-hour basin-averaged precipitation estimated using this method was **323.7 mm**. This value reflects a realistic yet extreme scenario of precipitation for the basin, incorporating both enhanced moisture conditions and optimal positioning of weather systems that contribute to heavy rainfall.

Comparing the two methods, we found differences in the PMP estimates for the Maipo River Basin, which corresponds to Cluster 4 in our statistical analysis. The statistical method provided PMP estimates for 24-hour storms. To compare these with the 72-hour PMP obtained from the physically based method, we used the duration coefficient to adjust for the longer storm duration (C_d=1.545 derived from the Chilean flooding manual). After applying this coefficient, the statistical method yielded a 72-hour PMP values between 160 and 800 [mm] in the stations located within the Maipo River Basin. These PMP estimations were less conservative than the Hershfield method but still higher than the physically based estimate from the WRF model. This suggests that while the statistical method proposed has a good behavior upon traditional approaches, the physically based method provides a more comprehensive understanding of potential extreme precipitation events by incorporating atmospheric processes. Therefore, for regions like the Maipo River Basin with significant population and infrastructure, utilizing the physically based method could enhance the reliability of PMP estimates for design and safety assessments.

4 Conclusions

This This study demonstrated that both the statistical approach using the GEV distribution and the physically based approach utilizing the WRF model provide valuable methodologies for estimating the PMP in Chile. The statistical method, enhanced by clustering and regional frequency factors, yielded less conservative and more region-specific PMP estimates compared to the traditional Hershfield method, particularly improving accuracy in arid regions like northern Chile.

In the Maipo River Basin, the physically based approach estimated a 72-hour PMP of 323.7 mm. This method offers detailed spatial and temporal insights into extreme precipitation events by simulating atmospheric processes, making it especially useful in regions with complex terrain and significant population and infrastructure.

Comparing the two methods, the statistical approach is more practical and easier to implement but may produce higher PMP estimates. The physically based approach, while more complex and computationally intensive, provides more realistic and spatially coherent estimates. Therefore, selecting the appropriate methodology depends on balancing practicality with the need for detailed analysis. Future work should focus on integrating both methods to capitalize on the strengths of each and on assessing the impacts of climate change on PMP estimates to ensure the resilience of infrastructure in the face of evolving climatic conditions.

The 12th International Symposium on Water Environment Systems
----- with Perspective of Global Safety   (Nov. 21st ~ 22nd , 2024)

GP-RSS & SyDE
Tohoku University

Reference

[1] World Meteorological Organization (2009). *Manual on Estimation of Probable Maximum Precipitation*. WMO-No. 1045.

[2] Hershfield, D. M. (1961). Estimating the Probable Maximum Precipitation. *Journal of the Hydraulics Division*, 87(5), 99–116. https://doi.org/10.1061/JYCEAJ.0000651

[3] Koutsoyiannis, D. (1999). A probabilistic view of Hershfield's method for estimating probable maximum precipitation. *Water Resources Research*, 35(4), 1313–1322. https://doi.org/10.1029/1999WR900002

[4] Micovic, Z., Schaefer, M. G., & Taylor, G. H. (2015). Uncertainty analysis for probable maximum precipitation estimates. Journal of Hydrology, 521, 360–373. https://doi.org/10.1016/j.jhydrol.2014.12.033

[5] Hiraga, Yusuke and Meza, Joaquin, Pmp Estimation by the Numerical Model-Based and Conventional Approaches for Maipo River Basin in Chile: Reconstruction and Maximization of Extreme Precipitation Using the Wrf Model. Available at SSRN: https://ssrn.com/abstract=4914546

[6] Papalexiou, S. M., & Koutsoyiannis, D. (2013). Battle of extreme value distributions: A global survey on extreme daily rainfall. *Water Resources Research*, 49(1), 187–201. https://doi.org/10.1029/2012WR012557

[7] Toride, K., et al. (2019). Model-based probable maximum precipitation estimation: How to estimate the worst-case scenario induced by atmospheric rivers? *Journal of Hydrometeorology*, 20(12), 2383–2400. https://doi.org/10.1175/JHM-D-19-0039.1

The 12th International Symposium on Water Environment Systems
----- with Perspective of Global Safety   (Nov. 21st ~ 22nd , 2024)

GP-RSS & SyDE
Tohoku University

Analysis on the inundation vulnerability of coastal dunes depending on a scenario of sea level rise

○ Jihyun Kang[1*], Changwan Seo[1] & Hoshang Rhew[2]

[1]National Institute of Ecology, 1210 Geumgang-ro, Maseo-myeon, Seocheongun, Republic of Korea
[2]Jeonbuk National University, 567 Baekjedaero, Daokjingu, Jeonjusi, Republic of Korea.
[*]E-mail: kjhb612@nie.re.kr

Abstract

The purpose of this study is to analyze the inundation areas in coastal dunes and vulnerable areas among land covers by applying the long-term sea level change scenario of SSP5-8.5. The changes in the approximately highest high water (AHHW) due to the sea level change and extreme highest tide level with 100-year cycle were analyzed at two coastal dunes (Sohwang dune and Goraebul dune) located on the east and west coasts of South Korea. In Sohwang Dune, the AHHW rises to approximately 8.24 m, which causes approximately 88% of the dune to be inundated, and coastal wetlands, artificial grasslands, and rice paddies in the near wetland may be subject to flood damage. In Goraebul Dune, the AHHW rises to 1.02 m, which causes most of the beach and natural bare land in front of the dune to be flooded. Most areas that will be inundated due to sea level rise are areas where coastal dune ecosystems appear, so it is considered necessary to analyze areas vulnerable to flooding in terms of the future decline in coastal dune ecosystems.

Keywords: inundation vulnerability, coastal dune, sea level change, dune ecosystem

1 Introduction

According to the IPCC 6th Assessment Report, the global average sea level rose by 1.9 mm (0.8–2.9 mm) per year from 1971 to 2006, and has been rising steeply by 3.7 mm (3.2–4.2 mm) per year from 2006 to 2018 (IPCC, 2021). In comparison, the rate of sea level rise along the coast of Korea was 2.2 mm per year from 1971 to 2006, which is higher than the global average, and has been rising similarly by 3.6 mm per year from 2006 to 2018 (KHOA). Even in the lowest climate change-induced sea level rise scenario, sea level rise is expected to continue due to heat absorption in the deep ocean and melting of the Greenland and Antarctic ice sheets. Sea level rise leads to an increase in the frequency and intensity of storm surges, which increases the occurrence of disasters. Therefore, it is very important to identify flooded areas that may occur due to sea level rise in advance and prepare long-term response measures. This study aims to analyze flooded areas by applying the predicted sea level rise along the coast of Korea to coastal sand dunes according to climate scenarios and to analyze vulnerable areas in terms of land cover.

2 Materials and methods

This study analyzed the 100yr extreme tide levels at Goraebul Dune on the east coast and Sohwang Dune on the west coast based on the tidal data of South Korea. The scenario of the long-tern sea level rise was added to the present AHHW to compare with the 100yr extreme tide levels, and the inundated area was analyzed using a 5mx5m DEM. In addition, the inundated area and landuse were overlapped to analyze the types of landuse vulnerable to flooding. The extreme tide level data measured at adjacent tide stations were used to analyze the 100yr extreme tide levels at Goraebul and Sohwang dunes. For Goraebul dune, the Gumbel function was applied using the extreme tide level data from Hupo tide station, and for Sohwang dune, the GEV function was applied using the data from

Boryeong tide station (Jung et al., 2008). For the analysis of sea level rise by climate change scenario, the long-term change values presented by KHOA were used. In the West Coast, it was reported that the sea level would rise by 80.8 cm in the SSP5-8.5 (2015-2200) scenario, and in the case of the East Coast, it would rise by 82.2 cm in the same scenario (KHOA). This increase was added to the AHHW to calculate the sea level height.

3 Results and discussion

3.1 100yr extreme tides and sea level rise by scenario

The 100yr extreme tide of Sohwang Dune was analyzed to be 8.57 m height, and the AHHW was confirmed to rise to 8.24 m under the climate change scenario (SSP5-8.5). The 100yr extreme tide level of Goraebul Dune was analyzed to be 1.01 m, and the sea level rise under the climate change scenario (SSP5-8.5) was analyzed to be 1.02 m, which is higher than the 100yr extreme tide level (Table 1).

Table 1 Sea level at Sohwang and Goraebul dunes

Sea level(m)	Sohwang dune	Goraebul dune
Mean Sea level(m)	3.61	0.06
AHHW(m)	7.43	0.20
100yr extreme tide(m)	8.57	1.01
Sea level by SSP1-2.6(m)	7.89	0.67
Sea level by SSP2-4.5(m)	8.01	0.78
Sea level by SSP3-7.0(m)	8.14	0.91
Sea level by SSP5-8.5(m)	8.24	1.02

3.2 Areas vulnerable to flooding in SSP5-8.5 Scenario

In SSP5-8.5 (2015-2100), the AHHW due to sea level rise was analyzed to be 8.24 m in Sohwang dune and 1.02 m in Goraebul dune. Assuming that there is no change in the current topography, the flooded area due to sea level rise was predicted to be 88% in Sohwang dune and 34% in Goraebul dune. In terms of landuse in the flooded area, it

The 12th International Symposium on Water Environment Systems
----- with Perspective of Global Safety   (Nov. 21st ~ 22nd , 2024)

GP-RSS & SyDE
Tohoku University

was confirmed that the coastal wetlands developed in front of the sand dune, the artificial grassland with low elevation in the center of the dune, and the rice fields behind it were flooded in Sohwang dune (Table 2). In addition, flooding was confirmed in the surrounding areas of relatively high-altitude coniferous forests due to sea level rise. In Goraebul dune, the natural beach and forndune area were flooded, and it was confirmed that the inland wetlands around the rivers flowing from the inland to the ocean were flooded at a high rate. These two dunes do not have a high proportion of residential and commercial facilities, so the damage to artificial structures due to sea level rise was not significant. However, as the wetlands and natural bare in front of the dunes and the natural grasslands connected to the back were flooded, the coastline was confirmed to advance to the coniferous forests that were created as windbreaks. In the case of coniferous forests close to the coastline, coastal erosion can be further accelerated and the resilience of the dunes can be reduced (Choi, et al., 2013). Therefore, it is necessary to secure a buffer zone by expanding the width of the beach and the entire dune by managing the coniferous forests close to the coastline.

Table 2 Proportion by landuse type

Landuse type	Sohwang dune	Goraebul dune
Residential	0.1	
Transportation	1.7	1.1
Rice paddy	10.9	4.4
Farm	0.6	2.2
Plantation		0.4
Decideous forest	2.3	
Coniferous forests	13.5	2.9
Mixed forest	0.1	
Natural grasslands	1.0	1.2
Artificial Grassland	24.2	2.6
Inland Wetlands	0.1	13.7
Coastal wetlands	44.4	
Natural bare		46.6
Artificial bare	1.1	0.1
Inland water		11.5
Ocean water		13.2
Total (%)	100	100

4 Conclusions

This study analyzed the flooded areas of Sohwang and Goraebul dunes according to the long-term sea level change scenario of SSP5-8.5, and analyzed the flood-vulnerable areas by overlapping the landuse map. In the case of Sohwang dune on the west coast, coastal wetlands and artificial grasslands were found to be vulnerable to flooding, and it was confirmed that low-altitude rice paddies in the hind dune could also be flooded. In the case of Goraebul dune on the east coast, it was confirmed that most of the beach in front of the sand dune was flooded. The flood-vulnerable areas in the two sand dunes are areas where the characteristics of the coastal sand dune ecosystem are shown. Therefore, it needs to analyze the flood-vulnerable areas in terms of the decline of the coastal sand dune ecosystem in the future. In addition, although this study applied the sea level rise rate of the longest scenario among the scenarios, it is judged necessary to find more

sensitive areas in terms of time by applying the sea level rise rate in time series units and to establish management measures.

Reference

[1] Choi, K.H., Kim, Y., and Jung, P.M., 2013, Adverse effect of planting pine on coastal dunes, Korea, Journal of Coastal Research, SI65, 909-914.

[2] IPCC, Climate change 2021: The physical science basic, IPCC.

[3] Jung, S.T., Kim, J.D., Ko, D.H., and Yoon, G.L., 2008, Parameter Estimation and Analysis of Extreme Highest Tide Level in Marginal Seas around Korea, Journal of the Korean Society of Ocean Engineers, 20(5), 482-490.

[4] Korea Hydrographic and Oceanographic Agency(KHOA), (http://www.khoa.go.kr/oceangrid/gis/category/observe/observeSearch.do?type=EYS#none)

The 12th International Symposium on Water Environment Systems
----- with Perspective of Global Safety   (Nov. 21st ~ 22nd , 2024)

GP-RSS & SyDE
Tohoku University

Assessing Soil Erosion under Climate Change Using CMIP6 Models in the Mun River Basin

○ Khatthaleeya Prommit [1], Prem Rangsiwichapong[1*]

[1]Department of Water Resources Engineering, Faculty of Engineering, Kasetsart University, Thailand.
[*]E-mail: prem.r@ku.th.

Abstract

Climate change is intensifying, significantly impacting the lives and properties of the population, particularly concerning soil erosion. In Thailand, soil erosion affects agricultural land use across approximately 17.42 million hectares. This study aims to investigate and predict the extent of soil erosion due to climate change impacts using the CMIP6 model. Additionally, it seeks to create a map depicting changes in soil erosion using the Revised Universal Soil Loss Equation (RUSLE). In addition too, focused on Thailand's Mun River Basin, used the RUSLE model to assess sediment output and considering factors such as rainfall, terrain, and soil properties. Furthermore, the changes in climate were examined using the CMIP6 models and then compared with precipitation data from monitoring stations operated by the Royal Irrigation Department of Thailand. The study examines the SSP245 and SSP585 scenarios, using monthly rainfall data from the baseline period of 2000-2014 and comparing it with projected monthly rainfall data for three future periods: 2024-2050, 2051-2075, and 2076-2100. The results indicate that soil erosion rates in SSP585 are more severe than in SSP245. The period from 2024-2050 shows the lowest erosion rates, while the highest rates occur from 2076 to 2100. However, compared to the thresholds set by the Land Development Department of Thailand, the soil erosion rates are categorized as low to moderate, which may lead to reduced agricultural productivity but is unlikely to result in loss of life.

Keywords: CMIP6; precipitation; soil erosion; Thailand

1 Introduction

Currently, climate change has intensified, and the amount of rainfall in Thailand has become more variable both spatially and temporally. The accumulated monthly rainfall from November to April has significantly increased at a rate of 10.8 mm per decade. Additionally, changes in monsoon winds have led to an increased likelihood of heavy rainfall events in Thailand, with certain areas facing a higher risk of flash floods.

One of the issues affecting the population is soil erosion, with approximately 17.42 million hectares of agricultural land in Thailand impacted by this problem. Therefore, this research aims to predict the amount of soil washout resulting from the impacts of climate change under the CMIP6 model and to create a map of changes in soil erosion using the Revised Universal Soil Loss Equation (RULSE)

2 Materials and methods

This research study focuses on predicting sediment quantities in the Mun Basin. The Mun Basin is located in the northeastern region of Thailand It spans an area of approximately 24,169 square kilometers
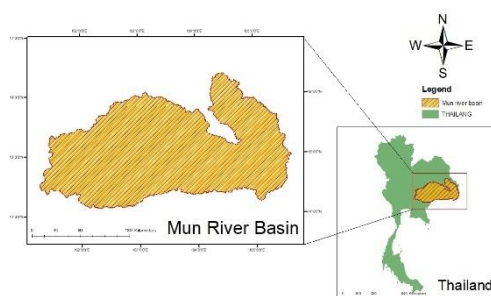

Fig. 1. Stay Area

This research study utilizes the Revised Universal Soil Loss Equation (RULSE) to calculate sediment quantities. The method incorporates various factors such as rainfall amounts, topography, soil properties, and land use. which can be expressed as:

$$\text{Soil erosion rate} = (R \times LS \times K \times P \times C)$$

Factors for calculating soil erosion include:

1. Rainfall Erosivity Factor (R)

Rainfall is a critical factor in soil erosion, In this study, the formula from the Land Development Department (2002) will be used to determine the rainfall erosivity factor (R):

$$R = 0.4669V - 12.141559$$

When V represents the annual rainfall amount, this study will use annual rainfall data from the Irrigation Department, historical records from GCM, and four CMIP6 models—AWI-CM-1-1-MR, EC-EARTH3-Veg, GFDL-ESM4, and MPI-ESM2-0—to estimate rainfall amounts under the SSP245 and SSP585 scenarios for calculating annual soil erosion quantities. The analysis will cover three future periods: 2024–2050, 2051–2075, and 2076–210

2. Soil Erodibility Factor (K)

The differences in soil texture, structure, density, infiltration rates, and surface water permeability determine the soil's resistance to erosion. For this study, the K-factor values derived from nomographs, based on data from soil series in Thailand, will be utilized. This information is available on the Land Development Department's website.

3.Slope Length and Slope Gradient Factor (LS)

Topography is a significant factor influencing soil erosion. This study utilizes the LS factor equation developed by Wischmeier and Smith (1965) to calculate soil erosion.

4. Cropping Management Factor (C Factor)

Plants and ground cover play a crucial role in preventing soil erosion by absorbing raindrop impact and slowing surface

The 12th International Symposium on Water Environment Systems
----- with Perspective of Global Safety   (Nov. 21st~22nd , 2024)

GP-RSS & SyDE
Tohoku University

runoff. This helps reduce the force that causes erosion and binds soil particles, increasing porosity and enhancing biological activity.

5. Conservation Practice Factor (P Factor)

The conservation practice factor (P factor) is defined by Wischmeier (1978) as the ratio of soil loss from a plot using a specific conservation practice to soil loss from a plot tilled up and down the slope under similar conditions. While other factors, such as soil improvement systems and plant residues, also affect soil loss, they are included in the P factor.

For the P factor, areas without any conservation practices have a P value of 1, while forest soils rich in organic matter have a P factor of 0.7

3 Results and discussion

The assessment of soil erosion in the Mun River Basin using RUSLE revealed that the rainfall erosivity factor in the area ranges between 521.88 and 963.638. The Soil Erodibility Factor (K) ranges from 0.004 to 0.37. The slope length and slope gradient factor (LS) range between 0 and 0.406. Since the Mun River Basin mainly consists of lowlands and uplands, the LS factor values are similar but increase in higher areas. The Cropping Management Factor (C) ranges from 0.0413 to 0.9332. The Conservation Practice Factor (P), ranges from 0.55 to 1.

The study found that, during the period from 2012 to 2021, the average annual soil erosion rate was 25.75 tons/ha/year. The highest erosion rate occurred in 2012, at 30.63 tons/ha/year, while the lowest occurred in 2017, at 5.63 tons/ha/year. According to the soil erosion criteria set by the Land Development Department, the erosion rate is considered slight.

The study found that, across all four models, the SSP585 scenario shows a higher soil erosion rate compared to SSP245, with a tendency to increase in the future. During the period 2024–2025, the lowest soil erosion rate is observed in the GFDL-ESM4 model at 25.6952 tons/ha/year. It is evident that the erosion rate is considered slight. In the period 2075–2100, the highest soil erosion rate is observed in the EC-EARTH3-Veg model at 40.2574 tons/ha/year. It is evident that the erosion rate is considered moderate

Table 1 Average soil erosion rate of the four models

year	Average of the four models	
	SSP245	SSP585
2024-2050	25.98	31.11
2051-2075	28.94	33.66
2076-2100	31.81	37.33
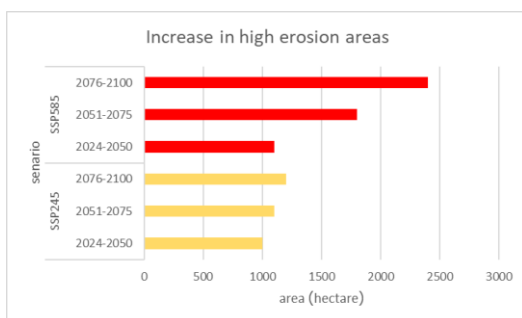
Fig. 2. Increase in high erosion areas chart
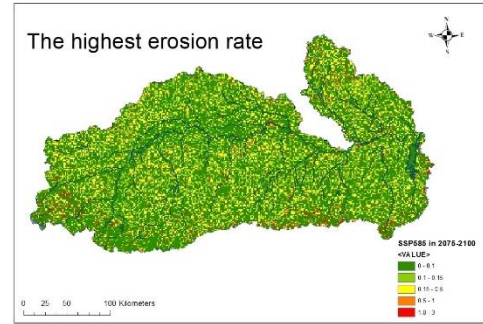
Fig. 3. The highest erosion rate

4 Conclusions

This study assessed soil erosion in the Mun River Basin using the Revised Universal Soil Loss Equation (RUSLE). It was found that the historical soil erosion rate averaged 25.75 tons per hectare per year. For future erosion rates, during the period 2024–2025, the lowest rate was 25.6952 tons per hectare per year, which is considered low, while in the period 2075–2100, the highest rate was 40.2574 tons per hectare per year, classified as moderate severity.

This level of severity will result in reduced agricultural productivity and the loss of fertile topsoil, though it will not affect the quality of life for people in surrounding areas. The study also found that the area impacted in the SSP585 scenario is larger than in SSP245. However, due to the mostly flat and agricultural landscape of the Mun River Basin, overall soil erosion rates remain low. Additionally, elevated areas in the basin have abundant forests, which help reduce soil erosion. Therefore, the overall soil erosion rate in the Mun River Basin remains low.

Reference

Chuenchum, P., Xu, M., & Tang, W. (2020). Estimation of soil erosion and sediment yield in the Lancang-Mekong River using the modified revised universal soil loss equation and GIS techniques. Water, 12(1), 135

Farhan, Y., Zregat, D., & Farhan, I. (2013). Spatial estimation of soil erosion risk using RUSLE approach, RS, and GIS techniques: A case study of Kufranja watershed, Northern Jordan. Journal of Water Resource and Protection, 5, 1247–1261.

Panditharathne, D. L. D., Abeysingha, N. S., Nirmanee, K. G. S., & Mallawatantri, A. (2019). Application of revised universal soil loss equation (RUSLE) model to assess soil erosion in the Kalu Ganga River Basin in Sri Lanka. Applied Environmental Soil Science, 2019, 4037379.

Land Development Department. (2002). Soil loss assessment in Thailand. Ministry of Agriculture and Cooperatives.

Rangsiwanichpong, P., Kazama, S., & Gunawardhana, L. (2018). Assessment of sediment yield in Thailand using revised universal soil loss equation and geographic information system techniques. River Research and Applications, 34(9), 1113-1122.

The 12ᵗʰ International Symposium on Water Environment Systems
----- with Perspective of Global Safety   (Nov. 21ˢᵗ ~ 22ⁿᵈ , 2024)

GP-RSS & SyDE
Tohoku University

Using census and model-based approach to develop 1-km crop yield of paddy in Indonesia

◯ Amalia Nafisah Rahmani IRAWAN[1*] & Daisuke KOMORI[1,2]

[1] Green Goals Initiative, Tohoku University, Miyagi 980-8572, Japan.
[2]Graduate School of Environmental Studies, Tohoku University, Miyagi 980-0845, Japan.
[*]E-mail: amalia.nafisah.rahmani.irawan.e2@tohoku.ac.jp

Abstract

This study aims to develop a comprehensive dataset on paddy crop yields during the dry season at 1-km resolution in Indonesia, covering the period from 2001 to 2021. Crop yield, a key indicator of agricultural productivity, is vital for understanding food security, economic stability, and environmental sustainability. Despite significant increases in global crop yields over the past century, driven by advancements in agricultural practices and technology, challenges such as climate change and water scarcity continue to threaten productivity. These challenges highlight the need for high-resolution crop yield data to effectively monitor agricultural conditions and to develop accurate assessments and mitigation strategies. In response, this research employs a hybrid approach, integrating census-based data from government agricultural observations with model-based data from remote sensing products. Indonesia is chosen as the study area due to its high agricultural activity, featuring three cropping seasons—two of which take place in the dry season—accounting for around 55% of the nation's annual rice production. The gridded crop yield of this study has a good correlation with the Earthstat Crop Yield dataset ($R^2 = 0.79$). The gridded crop yield dataset developed in this research demonstrates a strong correlation with the Earthstat Crop Yield dataset ($R^2 = 0.79$). This new dataset is anticipated to provide valuable insights into yield patterns and trends, facilitate the assessment of climate-related hazards such as floods and droughts, and inform strategies to improve agricultural resilience.

1 Introduction

Crop yield, a critical measure in agriculture, refers to the amount of crop harvested per unit area of land, usually provided in a ton per hectares (ton/ha). It is a fundamental indicator of agricultural productivity and efficiency, directly impacting food security, economic stability, and sustainability. Compared to harvested areas, crop yields vary annually due to weather conditions and have significantly increased over the past century. Additionally, advancements in agricultural practices, technological innovations, and scientific research have significantly improved crop yields over the past century. However, challenges such as soil degradation, water scarcity, pest infestations, and climate change continue to threaten agricultural productivity. Over the last fifty years, yield growth has been the primary driver of increased production, rather than the expansion of harvested areas (Blomqvist et al., 2020). This trend will continue to be crucial in the coming decades to feed growing populations while minimizing environmental impact from land-use changes.

To address these challenges, many researchers have been developing a detailed, accurate, and comprehensive datasets that provide insights into crop yield patterns and trends across different regions and time periods. A review paper by Kim et al., (2021) offers a summary of global gridded cropping system data products and **Table A.1.** on the appendix show the relatable dataset with this study. Generally, the methodology to develop the crop yield is divided into two approaches as follows: (1) census–based, which uses multiple ground observation data, such as surveys, samplings, or expert opinions, and (2) model–based, which uses remote–sensing data, such as climate data, vegetation indices to examine crop phenology, and land cover.

This research will combine census-based data, utilizing observed agricultural datasets from the government, with model-based data derived from various remote sensing products to create a gridded crop yield dataset for paddy during the dry season in Indonesia from 2001 to 2021. Indonesia is selected for this study due to its intensive agricultural activities, which include three cropping seasons, two of which occur during the dry season, contributing approximately 55% of the country's annual rice production.

2 Materials and methods
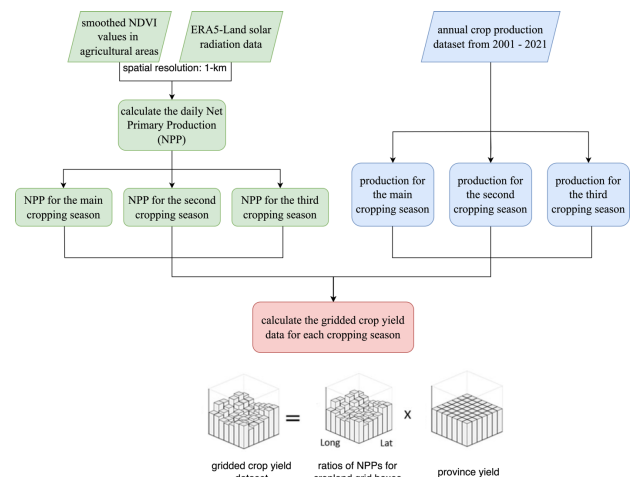
Fig. 1. Flowchart to develop gridded crop yield dataset.

Fig. 1. show the flowchart to develop the gridded crop yield dataset at 1-km resolution. Generally, the methodology is adapting the same approach used to develop the GDHY dataset (Iizumi et al., 2006; Iizumi & Sakai., 2020), but the

The 12th International Symposium on Water Environment Systems
----- with Perspective of Global Safety   (Nov. 21st ~ 22nd , 2024)

GP-RSS & SyDE
Tohoku University

observed yield dataset was obtained from the Ministry of Agriculture and the Statistic Bureau of Indonesia at the regency level instead of FAO dataset at the country level. Additionally, the Net Primary Productivity (NPP) is used as an indicator for estimating the crop yield on a grid cell. NPP was selected mainly because it quantifies the amount of biomass produced by plants, which directly relates to the amount of crop yield. Higher NPP typically means more biomass, and consequently, more potential crop yield. The detail procedure to calculate the NPP can refer to Iizumi et al., 2006, but in principle, it required the daily Normalized Difference Vegetation Index (NDVI) and solar radiation data.

3 Results and discussion

The main result of this study is the gridded dry cropping seasons production from 2001 – 2021 at 1-km resolution. **Fig. 2.** shows the example of the second and third cropping season production of rice in Java Island as detailed visualization because the high percentage of agricultural area in those regions, in year 2003, 2010, and 2019.
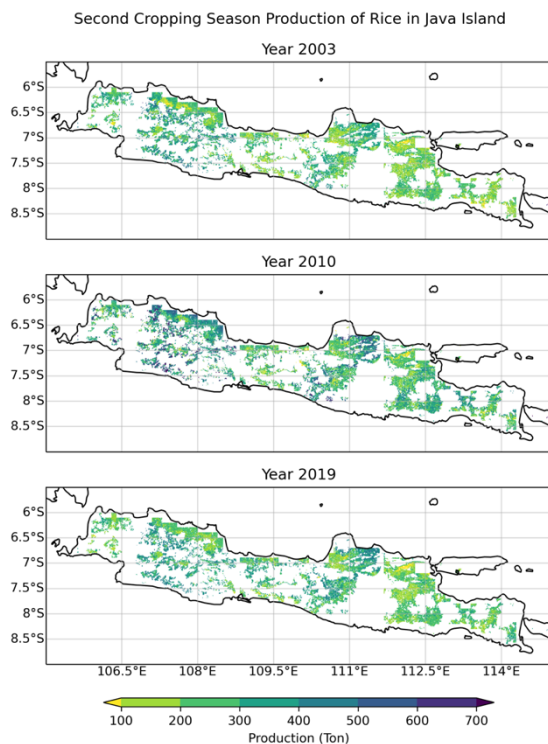

Fig. 2. Example of the second cropping season production in Java Island.

Currently, no other dataset matches the temporal and spatial resolution of this study. To validate the results, the following approaches were employed: a) assessing the correlation between the average of dry cropping season yield data from this study and the second crop yield data from GDHY (Iizumi et al., 2020) from 2001 to 2016 at a 0.5° resolution, and b) comparing the average of dry cropping season yield data from this study for the years 2003 to 2007 (representing crop yield in 2005) with rice yield data from Earthstat (Ray et al., 2012) for 2005 (obtained from the average of rice yield values from 2003 to 2007) at a regency scale.

Fig. 3. illustrates the spatial variation of the r-value between the gridded crop yield dataset from this study and the GDHY

dataset, while **Fig. 4.** displays the scatter plot and correlation value between the gridded crop yield dataset from this study and the Earthstat dataset. Although the correlation between the crop yield data from this study and the Earthstat dataset is high (R^2 = 0.79), the spatial variation of the r-value between the gridded crop yield data and the GDHY dataset shows variability. It is important to note that this dataset was developed using a similar approach to the GDHY dataset, which utilizes regency-scale crop yield data, whereas the GDHY dataset relies on FAO country-based crop yield data.
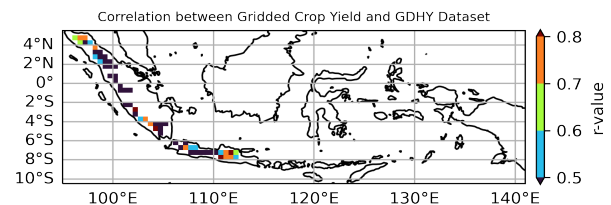
Fig. 3. Correlation value between the gridded crop yield (from this study) and GDHY dataset.
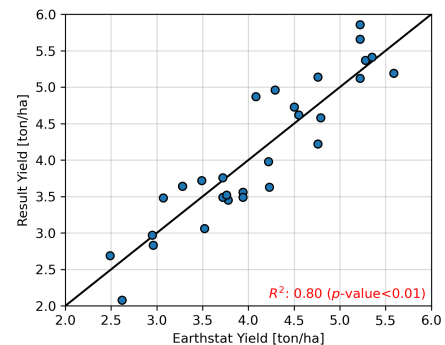
Fig. 4. Correlation between the gridded crop yield (from this study) and Earthstat dataset.

4 Conclusions

This study successfully developed the gridded crop yield data of paddy in Indonesia at 1-km resolution from 2001 – 2021, covering the first and second dry cropping season in Indonesia which accounts to 55% of annual rice production. The dataset has a relatively good correlation with established global crop yield data (GDHY and Earthstat). Supported by its finer resolution, this dataset can be used for detailed risk assessment of various hazard affecting agricultural sectors (i.e.., flood and drought) which important to address the response variation across different region.

Reference

[1] Blomqvist L, Yates L and Brook B W 2020 Drivers of increasing global crop production: a decomposition analysis Environ. Res. Lett. 15 0940b6

[2] Iizumi, Toshichika, Masayuki Yokozawa, Gen Sakurai, Maria Isabel Travasso, Vladimir Romanenkov, Pascal Oettli, Terry Newby, Yasushi Ishigooka, and Jun Furuya. "Historical changes in global yields: major cereal and legume crops from 1982 to 2006." Global ecology and biogeography 23, no. 3 (2014): 346-357.

[3] Iizumi, T.; Sakai, T. The global dataset of historical yields for major crops 1981–2016. Sci. Data 2020, 7, 1–7.

[4] Ray D K, Ramankutty N, Mueller N D, West P C and Foley J A 2012 Recent patterns of crop yield growth and stagnation Nat. Commun. 3 1293.

The 12th International Symposium on Water Environment Systems
----- with Perspective of Global Safety   (Nov. 21st ~ 22nd , 2024)

GP-RSS & SyDE
Tohoku University

Table A.1. A Summary of Established Gridded Historical Yield Dataset.

No	Dataset	Crop Types	Spatial Coverage and Resolution	Temporal Coverage and Resolution	Methods
1	M3Crops (Monfreda et al., 2008)	175 crops	Global; 0.083° (national or sub-national)	Circa 2000	Census
2	SPAM[1] (Yu et al., 2010)	26 crops	Global; 0.083°	Circa 2010	Census and model
3	GAEZ[2] (Fischer et al., 2021)	23 crops	Global; 0.083°	Circa 2010	Census and model
4	Ray2012 (Ray et al., 2012)	4 crops	Global; 0.083° (national or sub-national)	Annual (1961 – 2008)	Census
5	GDHY[3] (Iizumi & Sakai., 2020)	4 crops	Global; 0.5°	Seasonal (1982 – 2016)	Census and model
6	GGCMI[4] phase 1 (Muller et al., 2019)	19 crops	Global; 0.5°	Annual (1901 – 2012)	Model

[5] [1] Spatial Production Allocation Model.
[6] [2] Global Agro-Ecological Zoning.
[7] [3] Global Dataset of Historical Yields of major crops.
[8] [4] Global Gridded Crop Model Intercomparison.

The 12th International Symposium on Water Environment Systems
----- with Perspective of Global Safety   (Nov. 21st ~ 22nd , 2024)

GP-RSS & SyDE
Tohoku University

Predicting typhoon rainfall using image-based similarity of atmospheric fields

○ Jose Angelo HOKSON[1*], Shinjiro KANAE[2] & Yusuke HIRAGA[1]

[1]Department of Civil Engineering, Tohoku University, Miyagi 980-8579, Japan.
[2]Department of Civil and Environmental Engineering, Institute of Science Tokyo, Tokyo 152-8550, Japan.
*E-mail: hokson.jaa@gmail.com

Abstract

As climate change is expected to intensify typhoon-related rainfall, enhancing prediction capabilities is more crucial than ever. Statistical methods complement traditional numerical weather prediction models, offering additional insights that improve prediction accuracy. One such method, the analog method, uses past typhoon data (e.g., atmospheric fields) to predict current or future rainfall. In this study, we explore the use of the image-based Structural Similarity Index (SSIM) for identifying analog typhoons. Our findings show that SSIM achieves rainfall prediction accuracy comparable to previous studies and outperforms a prior method using cosine similarity, a metric comparing data in vector form. This underscores the potential of image-based similarity metrics in advancing hydrometeorological forecasting and contributing to broader geoscience applications.

Keywords: image-based similarity, typhoon rainfall, statistical prediction

1 Introduction

Typhoon-induced rainfall can lead to disasters such as flooding and landslides, making accurate prediction crucial for disaster preparedness. However, accurately predicting typhoon rainfall remains a significant challenge [1]. Advancements in both numerical and statistical methods are needed to improve these predictions. One statistical approach that has been studied extensively in recent years is the analog method [2]. This method uses past typhoons as predictors for current or future ones. If the characteristics of a current typhoon—such as its track or atmospheric fields—resemble those of past typhoons, the rainfall patterns from these past events can be used to predict the rainfall of the present typhoon.

In the analog method, a similarity measure is often employed to compare typhoon characteristics. For atmospheric fields, [3] successfully used cosine similarity to predict typhoon rainfall in China. While cosine similarity effectively captures pattern similarity, it has limitations, particularly in its inability to account for differences in absolute values.

This study explores the use of an image-based similarity measure called Structural Similarity Index (SSIM) to identify analogous typhoons for typhoon rainfall prediction.

2 Materials and methods

Using atmospheric field data from the Japan Meteorological Agency's Japanese 55-year Reanalysis [4] and rainfall data from the APHRODITE Monsoon Asia Daily Precipitation dataset [5], we predicted typhoon rainfall by following the procedure outlined in Fig. 1. The similarity measure SSIM, specifically its dissimilarity counterpart SSIM$_s$, is applied at the parameter level. These values are then averaged to calculate the overall dissimilarity between the atmospheric fields of the target typhoon and past typhoons. The rainfall of
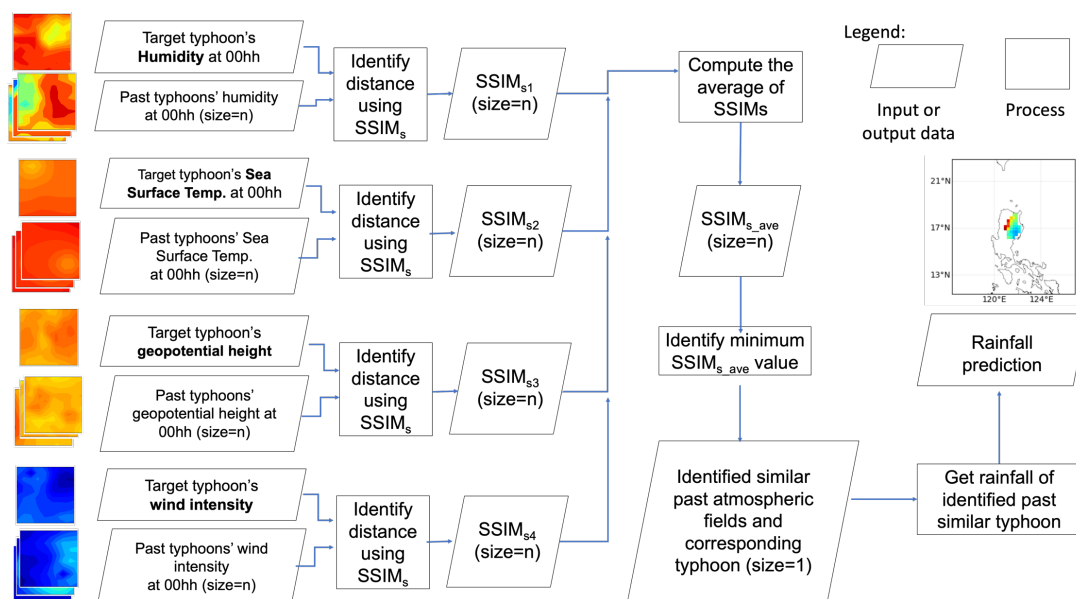

Fig. 1. Rainfall prediction methodology. n is equal to 4053 samples.

The 12th International Symposium on Water Environment Systems
----- with Perspective of Global Safety   (Nov. 21st ∼ 22nd , 2024)

GP-RSS & SyDE
Tohoku University

the past typhoon with the minimum $SSIM_{s\_ave}$ serves as the predicted rainfall for the target typhoon.

SSIMs values range from 0 to 2, with 0 indicating the closest resemblance. Mathematically, SSIMs [6] is expressed as:

$$SSIM(X,Y) = 1 - \frac{(2\mu_x\mu_y+C_1)(2\sigma_{xy}+C_2)}{(\mu_x^2+\mu_y^2+C_1)(\sigma_x^2+\sigma_y^2+C_2)}$$

where μ_x and μ_y represent the mean values of matrices X and Y, while σ_x^2 and σ_y^2 are their respective variances. The term σ_{xy} denotes the covariance of X and Y. Constants C_1 and C_2 are set to 0.01 and 0.03 respectively [6], are included to prevent instability when the denominator is close to zero.

3 Results and discussion

Overall, SSIM effectively identified similar atmospheric fields across 36 test targets and 4,053 past typhoons (example in Fig. 2). When comparing rainfall prediction results, SSIM outperformed the conventional cosine similarity distance (CSD)—a dissimilarity measure derived from cosine similarity—in terms of accuracy, based on root mean square error (RMSE) and correlation coefficient.

The rainfall prediction performance of SSIM was evaluated using two strategies for selecting analog (similar) typhoons: (1) using only the rainfall from the most similar typhoon (analog rank 1), and (2) using an ensemble of rainfall from the top Z most similar typhoons (analog ranks 1-Z). When using only analog rank 1, the performance of SSIM and CSD was comparable, with average RMSE values of 54 mm for SSIM and 53 mm for CSD, and average correlation values of 0.46 for SSIM and 0.44 for CSD. However, with an ensemble approach, SSIM consistently outperformed CSD in terms of average RMSE when using two or more ensemble members, and in terms of average correlation coefficient when using nine or more ensemble members. For instance, with 10

ensemble members (analog ranks 1-10), the RMSE and correlation values were 44 mm and 0.70 for SSIM, compared to 40 mm and 0.67 for CSD. These findings indicate that the advantages of SSIM become increasingly pronounced when multiple similar typhoons are considered, which is logical given that no single typhoon will perfectly match another.

The superior performance of SSIM in rainfall prediction is rooted in the differences in how similar atmospheric fields are selected (example in Fig. 2). CSD predominantly focuses on pattern similarity, specifically on the directional changes between two 2-dimensional fields. In contrast, SSIM balances both pattern and magnitude (in terms of range and averages). For instance, CSD may consider the upper-right figure in Fig. 2 more similar to the upper-left figure than the upper-middle right figure due to greater pattern similarity, paying less attention to value differences. SSIM, on the other hand, considers the upper-middle figure more similar, despite lower pattern similarity, because of the closer minimum and range values.

4 Conclusions

We have demonstrated the effectiveness of image-based Structural Similarity Index (SSIM) in identifying similar atmospheric fields, resulting in comparable or even better typhoon rainfall predictions compared to previous studies [1,3], including those that utilized conventional cosine similarity distance for analog identification [3]. This improved performance stems from SSIM's capability to balance the effects of both pattern and magnitude—through range and average—in the identification of similar atmospheric fields.

By treating atmospheric fields as images rather than mere numerical vectors, our approach opens new possibilities not only in meteorological prediction but also in the broader field of geoscience. Given the escalating impacts of climate change and the rapidly advancing field of computer science, there has never been a more opportune time to rethink our methodologies for handling spatial data in scientific research.

Reference

[1] Kim, H. J., Moon, I. J., & Kim, M., Statistical Prediction of Typhoon - Induced Accumulated Rainfall over the Korean Peninsula Based on Storm and Rainfall Data, Meteorological Applications, 27(1) (2019).

[2] Hokson, J. A., & Kanae, S., An Alternative Similar Tropical Cyclone Identification Algorithm for Statistical TC Rainfall Prediction in the Western North Pacific, Journal of Geophysical Research: Atmospheres, 129 (2024).

[3] Zhong, Y., Yu, H., Teng, W., & Chen, P, A dynamic similitude scheme for tropical cyclone quantitative precipitation forecast (in Chinese), J. Appl. Meteor. Sci., 20(1) (2009) 17–27.

[4] Japan Meteorological Agency/Japan, JRA-55: Japanese 55-year Reanalysis, Daily 3-Hourly and 6-Hourly Data [Dataset], Research Data Archive at the National Center for Atmospheric Research, Computational and Information Systems Laboratory, (2013) ,accessed: May 15, 2024.

[5] Yatagai, A., Kamiguchi, K., Arakawa, O., Hamada, A., Yasutomi, N., & Kitoh, A., APHRODITE: Constructing a Long-Term Daily Gridded Precipitation Dataset for Asia Based on a Dense Network of Rain Gauges. Bulletin of the American Meteorological Society, 93(9) (2012), 1401–1415

[6] Wang, Z., Bovik, A. C., Sheikh, H. R., & Simoncelli, E. P., Image quality assessment: From error visibility to structural similarity. IEEE Transactions on Image Processing, 13(4) (2004), 600–612.
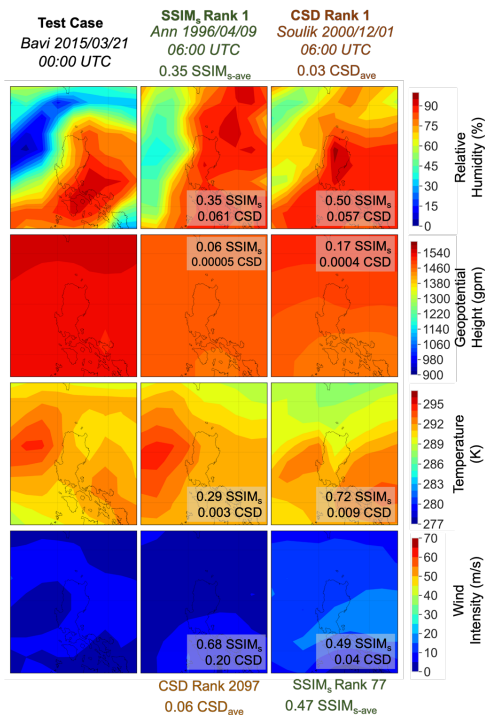
Fig. 2. Example atmospheric fields of 1 test typhoon and its most similar analogs based on SSIM and CSD.

The 12th International Symposium on Water Environment Systems
----- with Perspective of Global Safety   (Nov. 21st ~ 22nd , 2024)

GP-RSS & SyDE
Tohoku University

Sensitivity analysis of cloud seeding methods for rainfall suppression: A WRF model-based study of the 2014 Hiroshima rainfall event

○ Jacqueline Muthoni MBUGUA[1*], Yusuke HIRAGA[1]

[1]Department of Civil and Environmental Engineering, Tohoku University, Miyagi 980-8579, Japan.
[*]E-mail: mbugua.jacqueline.muthoni.e7@tohoku.ac.jp

Abstract

  This study explores the effectiveness of cloud seeding for rainfall suppression during the 2014 Hiroshima rainfall event using the WRF model. Sensitivity analyses were conducted across various atmospheric levels (Z = 20 to 34) for every alternate layer and four locations along the cross-section of heavy rainfall. Results show that seeding at lower levels (Z = 20 to 24) is more effective, with the best case showing an average reduction of -3 mm/3hr in rainfall greater than 100mm in control. These findings highlight the importance of targeting lower atmospheric layers for more efficient rainfall reduction, offering insights for future weather control practices.

Keywords: Senjo-Kousuitai; Hiroshima event, WRF model; Cloud seeding; Morrison 2-moment scheme.

1 Introduction

  Localized heavy rainfall events in Japan are typically caused by quasi-stationary band-shaped precipitation systems known as "senjo-kousuitai. These are meso-scale convective systems which are characterized by rainfall accumulation exceeding 200mm in three hours and the band-shaped area greater than 50km in length and 20km in width. A recent study reported that about 50 percent of the heavy rainfall events observed in Japan between 1989 and 2015 were Senjo-kousuitai, indicating the prevalence of this event's contribution to heavy rainfall [1].

  This often results in floods, landslides and loss of lives. In 2020, heavy rainfall caused by a senjo-kousuitai event in the Kyushu region led to extensive flooding in around 200 rivers, over 900 reported landslides, and the inundation of 130 km² of land. Similarly, the heavy rainfall event in Hiroshima in 2014 resulted in floods, landslides and the tragic loss of 75 lives. Although such events are rare, their impacts can be severe, underscoring the need for effective mitigation measures.

  This study, therefore, aims to explore feasible weather control practices to mitigate heavy rainfall disasters with a focus on the 2014 Hiroshima senjo-kousuitai. This event, driven by a large moisture flux over the Bungo Channel between Kyushu and Shikoku, was characterized by back-building convective clouds, where new cells continuously formed on the upwind side of the storm due to the abundant water vapor flux. The sustained inflow of moist, unstable air into the storm provided the necessary energy for the repeated formation of new convective cells, resulting in prolonged heavy rainfall.

  To simulate the event, the Weather Research and Forecasting (WRF) model, a mesoscale numerical weather prediction system, was employed. Sensitivity analyses were then conducted to determine the optimal vertical and spatial locations for weather control over-seeding practices aimed at rainfall reduction.

2 Methodology

  The rainfall event was simulated from 0000 UTC on August 19, 2014, to 0000 UTC on August 20, 2014. A summary of the model setup is provided in **Table 1**, based on configurations used in previous studies. [2], [3]. The National Center for Environmental Prediction Final (NCEP FNL) Global Data Assimilation System (GDAS) at 0.25-degree resolution was used to provide data for the initial and boundary conditions (ICBC). Meanwhile, the Mellor–Yamada–Nakanishi–Niino (MYNN2.5) scheme was applied for the Planetary Boundary Layer (PBL). The domain setting is shown in **Fig. 1**.

Table 1 Model settings

Grid Spacing [km]	d01: 25km, d02:5km, d03:1km 2-way nesting
Vertical layers	70
ICBCs	GDAS FNL 0.25°
Time step [s]	d01: 30, d02: 20, d03: 6.67
Microphysics	Morrison 2-moment
PBL	MYNN2.5
Cumulus	d01: Kain–Fritsch, d02: Kain–Fritsch, d03: None
Radiation	RRTMG
Simulation start time	0000 UTC August 19
Analysis time	1600 UTC August 19 onwards
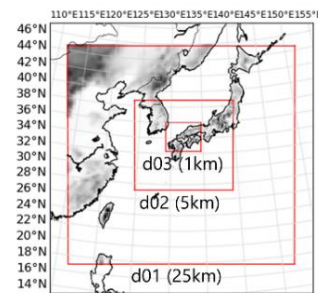
Fig. 1 Domain setting

2.1 Experimental settings for seeding

  After reproducing the rainfall event, an experimental setting was designed following Meyer's formula in the Morrison 2-moment scheme [4]. See Eq. (1).

$$n_c = exp\{-2.80 + 0.262 \times (273.15 - T)\} \times \beta \quad (1)$$

  where, n_c is the number of ice nucleus concentration per kilogram, T is the temperature in Kelvin and β is a unit less multiplier in this case (10^{11}).

Additional setup and considerations for seeding including the vertical layers seeded for sensitivity analysis are included in **Table 2**. Seeding locations are shown in **Fig. 2.**

The 12th International Symposium on Water Environment Systems
----- with Perspective of Global Safety   (Nov. 21st ~ 22nd , 2024)

GP-RSS & SyDE
Tohoku University

Table 2 Seeding setup and considerations

Parameter	Details
Vertical Layer (z)	Layers: 20, 22, 24, 26, 28, 30, 32, 34 Conditions: QCLOUD > 0 kg/kg, Temperature < 0ºC, Strong upward motion
Location	Presence of deep convective clouds, Grid dimensions: 6 km × 6 km, 4 seeding spots selected along the cross-section of heavy rainfall
Start Time	Beginning of heavy rainfall
Duration	3 hours (1600 - 1900 UTC) August 19th, 2014
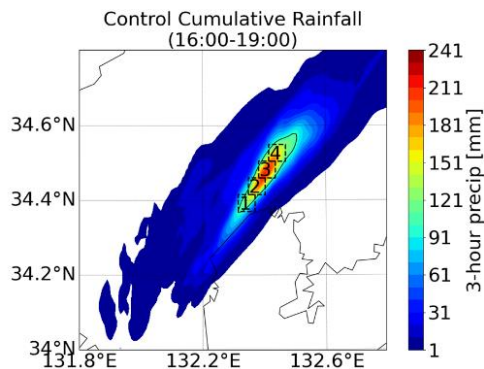
Fig. 2 Simulated cumulative rainfall (mm) from 16:00 to 19:00 UTC with 4 seeding locations

3. Results and discussion

To assess the effectiveness of over-seeding for rainfall reduction, we first evaluated the cumulative rainfall from 1600 to 1900 UTC in both the seeding and control (no seeding) simulations. The difference in rainfall was calculated by subtracting the seeding simulation results from the control. Our analysis focused on the region where rainfall exceeded 100 mm in the control, as indicated by the black solid line in **Fig. 2**. A summary of the results is presented in **Table 3**

Table 3 Over-seeding effect in rainfall reduction where rainfall was > 100mm in the control simulation

Locations/ layers	1 (west) [mm]	2 [mm]	3 [mm]	4 (east) [mm]
20 (5.7 km)	-2.5	-0.6	-0.9	-0.6
22 (6.4 km)	-2.1	-2.4	-2.9	-1.8
24 (7.2 km)	**-3.0**	**-3.0**	-1.3	-1.1
26 (7.9 km)	-2.3	-0.8	0.2	0.1
28 (8.6 km)	-0.8	-0.6	-0.8	-0.4
30 (9.3 km)	-0.6	-0.0	-0.7	-0.7
32 (10.0 km)	0.1	-0.4	-0.7	-0.1
34 (10.7 km)	0.0	-0.7	-1.3	-0.2

The results show that seeding at lower atmospheric levels (Z = 20 to 24) is more effective in reducing rainfall across all locations, likely due to more responsive cloud microphysical processes at these levels. In contrast, seeding at higher levels (Z = 28 to 34) had little to no impact, possibly due to weaker upward motion or insufficient cloud water content. Thus, targeting lower levels appears to be a more effective approach for rainfall reduction. Further investigation into the microphysical mechanisms at different altitudes is recommended.

Additionally, Seeding at Level 24 in Location 1 effectively reduced rainfall, as shown by the shift toward negative values in the histogram and a maximum reduction of -13.3 mm/3hr. The average reduction of -3.0 mm/3hr and blue areas in the difference map further confirm successful rainfall suppression at this level.
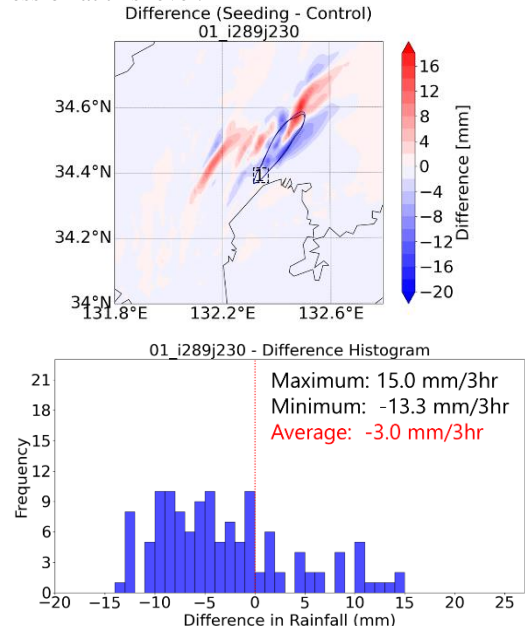
Fig. 3 Rainfall changes after overseeding location 1, z=24 in location of rainfall > 100mm in control

4 Conclusions

This study demonstrates that cloud seeding at lower atmospheric levels (Z = 20 to 24) is more effective in reducing rainfall. suggesting that targeting lower layers is crucial for effective rainfall suppression. Further research into the microphysical processes across different altitudes is recommended to optimize cloud-seeding techniques.

Reference

[1] K. Teruyuki, "Quasi-stationary band-shaped precipitation systems, named 'Senjo-Kousuitai', causing localized heavy rainfall in Japan," *J. Meteorol. Soc. Jpn.*, vol. 98, no. 3, pp. 485–509, 2020, doi: https://doi.org/10.2151/jmsj.2020-029.

[2] Kita M., Kawahara Y., Tsubaki R., and Nyunt C. T., "High-resolution downscaled simulation of heavy rainfall in Hiroshima in August 2014 using WRF," *J. Jpn. Soc. Civ. Eng. Ser B1 Hydraul. Eng.*, vol. 72, no. 4, p. I_211-I_216, 2016, doi: 10.2208/jscejhe.72.I_211.

[3] T. Oizumi, K. Saito, L. Duc, and J. Ito, "Ultra-high Resolution Numerical Weather Prediction with a Large Domain Using the K Computer. Part 2: The Case of the Hiroshima Heavy Rainfall Event on August 2014 and Dependency of Simulated Convective Cells on Model Resolutions," *J. Meteorol. Soc. Jpn. Ser II*, vol. 98, no. 6, pp. 1163–1182, 2020, doi: 10.2151/jmsj.2020-060.

[4] S. Yagi, Y. Suzuki, and K. Yokoyama, "Study of the Mitigation effect and acceleration risk on precipitation of torrential rains by cloud seeding with the forced-cooling technique," vol. 73, no. 4, p. I_259-I_264, 2017.

The 12th International Symposium on Water Environment Systems
----- with Perspective of Global Safety   (Nov. 21st ~ 22nd , 2024)

GP-RSS & SyDE
Tohoku University

Evaluation of ensemble post-processing methods to improve high-resolution short-term streamflow prediction based on LDAPS and WRF-Hydro

Yaewon LEE[1*], Bomi KIM[1] & Seong Jin NOH[1]

[1]Department of Civil Engineering, Kumoh National Institute of Technology, Gumi 39177, Republic of Korea.

*E-mail: yaewon99@kumoh.ac.kr

Abstract

To enhance water resource management and flood control, it is crucial to improve the accuracy and stability of runoff prediction. To achieve more reliable short-term hydrological prediction, each uncertainty source should be properly addressed. The WRF-Hydro modeling system is a physically-based hydrometeorological modeling system that can simulate floods, hydrological states, and the spatial distribution of water resources. In this study, the Local Data Assimilation and Prediction System (LDAPS) is applied to the distributed hydrological model WRF-Hydro to construct a high-resolution model with a 100-meter resolution for the Geumho River basin, a tributary of the Nakdong River. The results of a single simulation are compared with those of ensemble post-processing techniques including Bayesian Model Averaging (BMA) and Ensemble Model Output Statistics (EMOS) to evaluate the improvement in forecast accuracy and discuss limitations and applicability.

Keywords: WRF-Hydro; Ensemble; Ensemble post-processing; High-resolution; LDAPS

1 Introduction

The frequency of extreme rainfall events has been increasing due to recent climate change, leading to growing flood damage worldwide. South Korea is also experiencing an increased risk of extreme floods due to climate change [1], and accurate runoff prediction is essential to minimize such damage. Short-term hydrological forecasting is critical for real-time water resource management and flood response, making it necessary to improve prediction accuracy and stability.

The current weather forecasting system in Korea is classified according to prediction periods: ultra-short-term (KLAPS, 12 hours), short-term (LDAPS, 48 hours; RDAPS, 87 hours), and medium-term (GDAPS, 288 hours). Among these, LDAPS is a short-term prediction model providing 48-hour forecast information, which is highly applicable to hydrological prediction due to its ability to provide high-resolution detailed weather information. Using data from numerical weather prediction models as input for physics-based hydrological process models has the advantage of enabling high-resolution hydrological predictions. However, there are limitations due to systematic errors in numerical weather prediction models and parameter uncertainties in hydrological models.

To overcome these limitations, ensemble post-processing techniques have been actively studied [2]. Ensemble post-processing techniques such as BMA and EMOS have proven effective in improving prediction accuracy, particularly showing excellent performance in short-term prediction.

This study aims to improve the accuracy of short-term runoff prediction by establishing a coupled modeling system between LDAPS and WRF-Hydro and applying ensemble post-processing techniques BMA and EMOS. Specifically, we intend to quantitatively evaluate prediction accuracy and uncertainty through high-resolution modeling at 100m resolution and ensemble post-processing techniques.

2 Materials and methods

This study focuses on the Geumho River basin (area: approximately 2,092 km²), a tributary of the Nakdong River, with two streamflow measurement locations: Ansim Bridge and Kangchang Bridge (Fig. 1). The simulation periods were set for the heavy rainfall event in August 2020 and the Typhoon Hinnamnor event in September 2022.
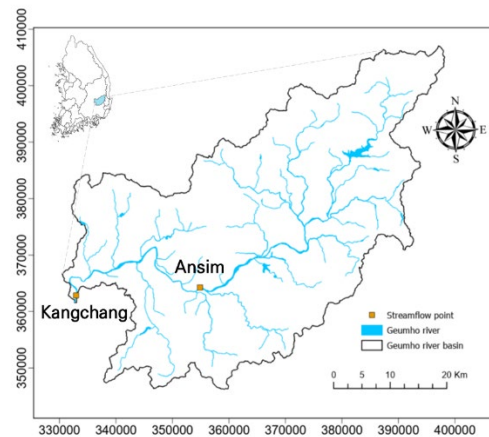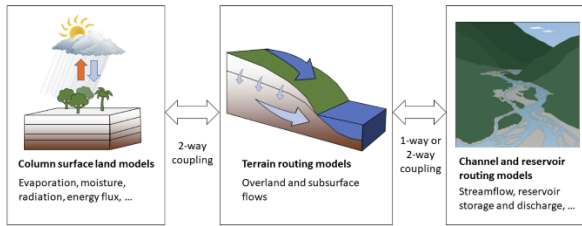

Fig. 1. Geumho river basin

WRF-Hydro was constructed with 100m spatial resolution (Fig. 2), utilizing eight meteorological variables from LDAPS. LDAPS provides 48-hour forecast information, with initial times set at 6-hour intervals (00:00, 06:00, 12:00, 18:00 UTC) to create up to eight ensemble members per hour during the 11-day simulation period.

For both events, each simulation performed 48-hour streamflow predictions starting at 00UTC (August 3, 2020, and September 1, 2022, respectively). The simulations continued for 11 consecutive days, allowing eight ensemble members to overlap at each time step.

The 12th International Symposium on Water Environment Systems
----- with Perspective of Global Safety   (Nov. 21st ～ 22nd , 2024)

GP-RSS & SyDE
Tohoku University

Fig. 2. Conceptual diagram of WRF-Hydro components

To improve the ensemble prediction results, BMA and EMOS techniques were applied [3]. Continuous Ranked Probability Score (CRPS) is used as the primary evaluation metric for the quantitative assessment of ensemble prediction results.

3 Results and discussion
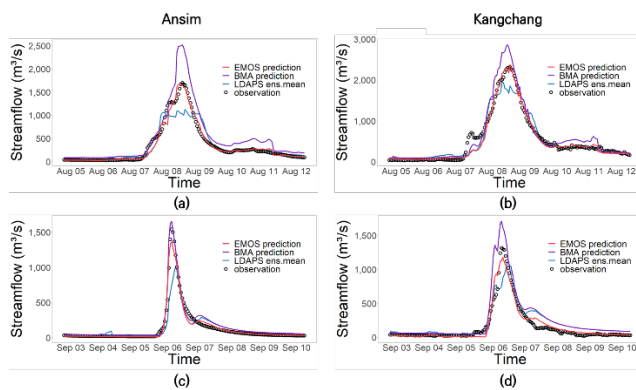
Fig. 3. Comparison of streamflow predictions at Ansim and Kangchang stations during (a), (b) August 2020 heavy rainfall event and (c), (d) September 2022 typhoon event [4]

As shown in Fig. 3(a-d), both EMOS and BMA techniques showed improved prediction performance compared to the LDAPS ensemble mean at Ansim and Kangchang stations for both events. Both ensemble post-processing techniques demonstrated results more similar to observed values than the LDAPS ensemble mean, providing more stable predictions even in low flow periods.

Table 1 Comparison of CRPS values for Raw ensemble*, BMA, and EMOS predictions [4]

		CRPS(m^3/s)		
		RAW	BMA	EMOS
Event 2020	Ansim	70.75	48.86	29.54
	Kangchang	99.92	70.54	52.70
Event 2022	Ansim	47.03	23.87	16.19
	Kangchang	72.38	34.11	29.30

* Raw ensemble represents LDAPS ensemble mean

Quantitative evaluation through CRPS analysis (Table 1) showed that both EMOS and BMA improved prediction performance, with EMOS performing better in all cases. For the 2020 event, error reductions of 31-58% were achieved, while the 2022 typhoon event showed even greater improvements with reductions of 49-66%.

4 Conclusions

This study established a high-resolution runoff prediction system by coupling WRF-Hydro with LDAPS for the Geumho River basin and applied ensemble post-processing techniques to derive the following conclusions:

- By coupling LDAPS with WRF-Hydro, a high-resolution modeling system with 100 m resolution was established, and runoff simulations were conducted for the August 2020 heavy rainfall event and the September 2022 Typhoon Hinnamnor event.

- Both BMA and EMOS ensemble post-processing techniques showed significant improvement in prediction accuracy compared to the LDAPS ensemble mean.

- CRPS analysis showed error reductions of 31-58% for the 2020 event and 49-66% for the 2022 event, with EMOS consistently outperforming BMA at both stations.

This study is expected to contribute to improving short-term runoff prediction accuracy. However, future research will require validation using more diverse rainfall events and long-term data.

Reference

[1] S. Kim, et al., Increasing extreme flood risk under future climate change scenarios in South Korea, Weather and Climate Extremes, 39 (2023) 100552.

[2] A. Muhammad, et al., Multi-model approaches for improving seasonal ensemble streamflow prediction scheme with various statistical post-processing techniques in the Canadian Prairie Region, Water, 10(11) (2018) 1604.

[3] Raftery, A.E., et al., Using Bayesian model averaging to calibrate forecast ensembles. Monthly Weather Review, 133(5) (2005) 1155-1174.

[4] Y.Lee, et al., Applicability of LDAPS and WRF-Hydro-based High-Resolution Ensemble Short-Term Flow Prediction, (2024) in prep.

The 12th International Symposium on Water Environment Systems
----- with Perspective of Global Safety   (Nov. 21st ~ 22nd , 2024)

GP-RSS & SyDE
Tohoku University

Developing deep learning-based urban inundation prediction model with physical information for real-time applications

Hyuna WOO[1*], Minyoung KIM[1], Hyeonjin CHOI[1], Seongjin NOH[1]

[1]Department of Civil Engineering, Kumoh National Institute of Technology, Gumi 39177, Republic of Korea.

[*]E-mail: hwoo@kumoh.ac.kr

Abstract

The increasing frequency and intensity of extreme rainfall events resulting from climate change expose urban areas to an elevated risk of severe flooding. Although traditional physics-based models provide accurate predictions for urban floods, their high computational demands restrict their use in real-time applications. This study proposes a convolutional neural network (CNN) based deep learning model for the generation of high-resolution inundation predictions. The model is trained on simulations of urban floods from synthetic rainfall scenarios generated by a physics-based model, and validated against historical extreme rainfall events. The results demonstrate that the proposed deep learning model achieves comparable accuracy to conventional physics-based models while significantly reducing computational time, thereby enabling near real-time predictions. This represents a significant enhancement to operational flood forecasting capabilities, supporting rapid decision-making in urban flood management systems.

Keywords: Deep learning; Physical information; Urban inundation; Flood prediction; Artificial intelligence.

1 Introduction

Climate change has intensified extreme rainfall events, leading to increased urban flood damage, especially in areas with extensive impervious surfaces due to urbanization. Urban flooding can occur and propagate rapidly, potentially causing significant loss of life and economic damage making accurate and timely predictions essential. Traditionally, flood prediction has relied on physics-based models that using Shallow Water Equations (SWE). Although these models provide accurate predictions, they require substantial computational resources, particularly for high-resolution analysis, limiting their application in real-time prediction. Due to these computational constraints, there is growing interest in developing deep learning approaches as an alternative solution.

Various artificial intelligence techniques, including Artificial Neural Networks (ANN), Convolutional Neural Networks (CNN), Long Short-Term Memory networks (LSTM), and Generative Adversarial Networks (GAN) have been used to extract spatiotemporal characteristics of hydrological information and predict flood extent or water levels.

This study aims to develop a CNN-based deep learning model that can rapidly replicate urban flood spatial distribution results of physics-based models. Using the CADDIES model's simulation data for the Oncheon basin, we evaluate the model's performance against historical flood events while analyzing the impact of rainfall time series window settings on accuracy.

2 Materials and methods

This study employed the Oncheon basin, located in Busan Metropolitan City, as the study area. The basin has extensive impervious surfaces due to urban development, which leads to significant flood damage from both fluvial flooding, caused by river overflow during extreme rainfall events, and pluvial flooding, resulting from insufficient drainage capacity.
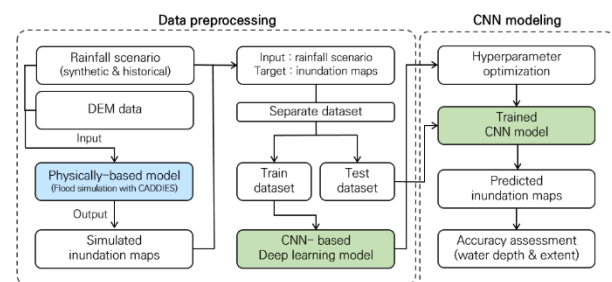

Fig. 1. Flowchart of the deep learning-based urban flood modeling

The methodology of this study's CNN-based urban flood prediction model consisted of two principal phases (Fig.1). First, a physics-based model was employed to generate flood information, including inundation depth and extent, which populated the dataset for the deep learning model. The physics-based model simulations were conducted using synthetic and historical rainfall scenarios, along with topographic data, as inputs. Subsequently, the deep learning model was trained to input rainfall information and output flood information, with optimized hyperparameters. The model's performance was evaluated by comparing it with the physics-based model simulation results. For the physics-based model, we applied the WCA2D version of the CADDIES model (Guidolin et al., 2016), a cellular automata-based 2D urban flood analysis model. CADDIES utilizes a grid-based numerical calculation method capable of relatively fast computation. Using this model, we constructed flood simulation training data by simulating synthetic rainfall scenarios based on probability rainfall.

The 12th International Symposium on Water Environment Systems
----- with Perspective of Global Safety   (Nov. 21st ~ 22nd , 2024)

GP-RSS & SyDE
Tohoku University

For the simulation inputs, we employed a Digital Surface Model (DSM) with a 10 m spatial resolution, incorporating both river cross-section survey data and road network information specific to the Oncheon basin. Synthetic rainfall scenarios were generated for the Busan region using probability rainfall data with a 17-hour duration. The temporal distribution of rainfall followed a normal distribution [2]. For model validation, we selected historical rainfall events from 2014 and 2020 that resulted in flooding in the study area. These events occurred during two periods: 07:00-23:00 on August 25, 2014, and 14:00 on July 23, 2020, to 06:00 on July 24, 2020.

3 Results and discussion

This study compared the maximum flood depth simulation results from a CNN-based deep learning model and the physics-based CADDIES model for historical rainfall events that occurred in 2014 and 2020 in the Oncheon basin (Fig.2). The maximum flood depth simulation results represent the highest depth value for each grid cell across all simulation time steps.
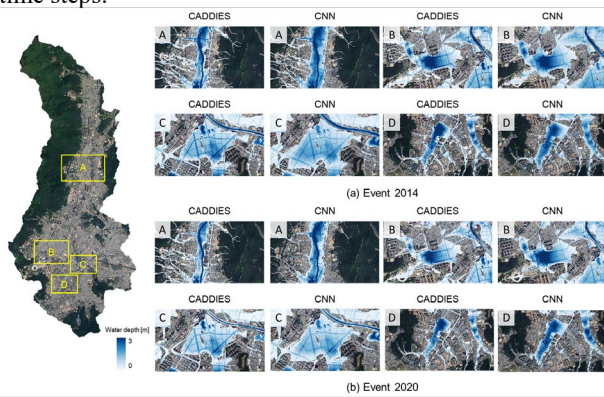
Fig. 2. Comparison of simulated maximum inundation using CADDIES and CNN models: (a) event 2014 (b) event 2020

The CNN model effectively reproduced CADDIES flood patterns in most urban areas, particularly on roads and in lowlands, although it showed some overestimated flood depth in area A due to complex flooding dynamics involving both internal drainage and river overflow. Performance analysis demonstrated high accuracy with Hit Rates (HR) of 0.98 and 0.93 for 2014 and 2020 events, with false alarms mainly occurring mainly along flood boundaries. The model performed better for the 2014 event (Critical Success Index (CSI)=0.85) than for the 2020 event (Critical Success Index (CSI)=0.76), likely due to the latter's more complex double-peak rainfall pattern. While the CNN model exhibited a tendency to slightly overestimate flood areas—a common characteristic in deep learning flood models—it maintained acceptable accuracy with RMSE values around 0.22-0.23 m (Table 1).

Table 1 Verification results of the events 2014 and 2020

	Event 2014	Event 2020
HR	0.98	0.93
FAR	0.12	0.19
CSI	0.85	0.76
RMSE	0.22	0.23

The computational efficiency comparison between the models showed that while the CADDIES model required 140 seconds with parallel computing (using 12 CPU cores) or 600 seconds with sequential computing to simulate a single rainfall event, the CNN model took only 15 seconds to generate flood maps after a 40-second training period (Table 2). This represents a substantial reduction in computation time—97.5% compared to sequential and 89.29% compared to parallel computing with the CADDIES model. These results demonstrate the CNN model's potential for real-time flood prediction applications, particularly considering that CADDIES itself is already computationally efficient compared to conventional physics-based models. However, future research should focus on improving the model's capacity to represent complex physical processes in diverse topographic conditions.

Table 2 Average runtimes of the CADDIES and CNN models for simulating a flood event (17 hours)

Model	CADDIES (sequential)	CADDIES (parallel)	CNN
Runtimes	600 sec	140 sec	15 sec

4 Conclusions

This study developed and validated a CNN-based deep learning model for the rapid prediction of urban floods. The model was trained using physics-based CADDIES model simulations of synthetic rainfall scenarios. The model exhibited high accuracy in reproducing historical flood events from 2014 and 2020 in the Oncheon basin, with a hit rate above 0.92 and a critical success index above 0.76. The CNN model significantly reduced computational costs, reducing simulation time by 97.5% compared to conventional physics-based models while maintaining reliable accuracy. This indicates the possibility of near real-time, high-resolution flood mapping, although future research should concentrate on enhancing the model's capacity to represent intricate physical processes in diverse urban settings.

Reference

[1] H. Woo, H. Choi, M. Kim, and S. Noh, Estimating urban inundation using physics-informed deep learning: a case study of the Oncheon-cheon catchment, under review.

[2] Y. Wang, A. S. Chen, G. Fu, S. Djordjević, C. Zhang, and D. A. Savić, An integrated framework for high-resolution urban flood modelling considering multiple information sources and urban features, Environmental Modelling & Software, 107 (2018) 85-95.

The 12th International Symposium on Water Environment Systems
----- with Perspective of Global Safety　(Nov. 21st ~ 22nd , 2024)

GP-RSS & SyDE
Tohoku University

Evaluating Downstream Flood Hazards Using Dam Break Simulation: A Case Study of Khlong Luang Rachalothorn Reservoir, Thailand

○ Jinnaphrot Chalatthanyakit [1], Jirawat Kanasut [1] Prem Rangsiwanichpong[1*]

[1]Department of Environmental Engineering, Faculty of Engineering, Kasetsart University, Thailand.
[*]E-mail: prem.r@ku.th.

Abstract

This study aims to simulate dam failure and flood wave propagation from the Khlong Luang Rachchaloet Reservoir, focusing on its impact on downstream areas. The study area extends from Ko Chan Subdistrict, Ko Chan District, Chonburi Province, to the confluence of Khlong Omkaeo in Tha Kham Subdistrict, Bang Pakong District, Chachoengsao Province. To analyze the potential dam failures, the HEC-RAS mathematical model was employed, simulating scenarios where increased inflows raise the reservoir's water level, leading to potential failures of the dam and associated structures. The analysis considered various flood return periods, including 50, 100, 500, 1,000, and 10,000 years, with two types of dam failure mechanisms: piping failure and overtopping failure. The results reveal that the triangular-shaped piping failure mechanism produces the highest flood discharge, reaching 2,862.62 cubic meters per second. This leads to flooding over an area of approximately 198 square kilometers (123,750 rai), with average flood depths ranging from 0.49 to 0.95 meters. Additionally, the study found that floodwaters from a dam failure would take about 48 hours and 10 minutes to reach the community in Ko Chan Subdistrict. The findings of this research are crucial for creating detailed flood hazard maps for downstream areas, providing valuable information for local authorities. These maps can serve as a basis for evacuation planning and effective disaster management strategies, helping to mitigate the risks and potential impacts of future dam failure events. By understanding the behavior of flood wave propagation following dam failure, this study contributes to enhancing the preparedness and resilience of the affected communities.

Keywords: Dam Break; Disaster; HEC-RAS; Natural Hazard; Thailand

1 Introduction

The Khlong Luang Ratchachonlothorn Reservoir, a medium-sized irrigation project, is located in Ko Chan Subdistrict, Ko Chan District, Chonburi Province, Thailand. Completed in 2015, this reservoir features an earthfill dam constructed with a zoning earthfill dam structure. Currently, the reservoir's capacity has been expanded from 98 million cubic meters to 126.33 million cubic meters, helping slow down water flow to downstream areas during the rainy season. This mitigates flooding risks for Ko Chan, Phanat Nikhom, and Phan Thong districts and supports growth across all sectors in the eastern region of Thailand.

Study and analysis of the volume of water flowing through the cracks of the dam in different recurrence years using the HEC-RAS mathematical model to simulate the collapse of the Khlong Luang Ratchalothorn reservoir.

2 Materials and methods

This research centers on the Khlong Luang Ratchalothorn Reservoir, a medium-sized irrigation project located in Ko Chan Subdistrict, Ko Chan District, Chonburi Province, Thailand. The project is situated within the Khlong Luang River basin, which covers an area of approximately 819.55 square kilometers. The basin resembles the shape of a leaf and is surrounded by mountain ranges, creating a unique and varied topography that influences the hydrological and ecological characteristics of the reservoir. This reservoir plays a vital role in supporting agricultural activities and water management within the region, making it an essential focus for studying sustainable water resource management and environmental impacts in central Thailand.
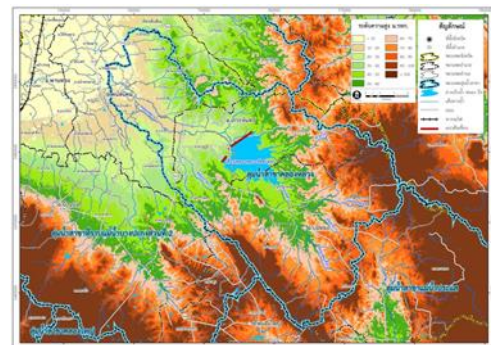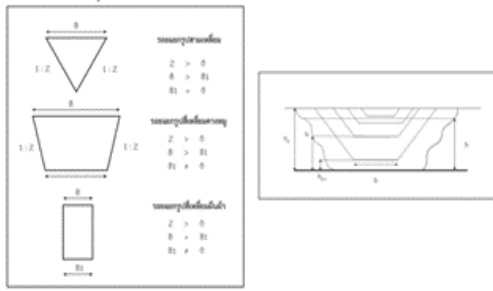

Fig. 1. Stay Area

1) Data collection, including physical data of Khlong Luang Ratchalothorn Reservoir, daily rainfall data, daily, monthly, annual runoff data, DEM data, and river cross-section data

2) Analysis of the reliability of rainfall data using the (Double Mass Curve Analysis) method

3) Calculate the flood graph in various recurrence cycles by calculating the design of rainstorms from the relationship graph between rainfall intensity (IDF) using data from 1991-2021, analyzing continuous rainfall for 3 days of the highest rainfall from the analysis (Gumbel Distribution) and creating a flood graph from rainstorms using the Unit Hydrograph technique by modifying Synder's method. Calculate further and apply it to excess rainfall (design rainfall excess) to calculate the flood graph.

4) Analyze the cross-section of the dam collapse in the overtopping form, which will simulate the shape of the crack as a triangle, a trapezoid, with the crack increasing faster from the dam crest or the dam core level. Specified Value,hf)

The 12th International Symposium on Water Environment Systems
----- with Perspective of Global Safety   (Nov. 21st ~ 22nd , 2024)

GP-RSS & SyDE
Tohoku University

of the dam core, the separate flow value(Qb) is calculated by the Broad-Crested Weir equation.

Fig. 2. Failure pattern due to water overflow across the crack

5) Analysis of the dam failure section of the piping type will model the condition of the orifice as a rectangular fracture with side slope (Z=0). The dam failure will be modeled as the condition at the initial center of the fracture (hp). The flow through the fracture (Qb) will be calculated by the orifice or board-crested weir equation which is based on the relationship between the water level in the dam and the top level of the orifice.
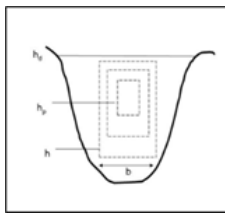
Fig. 3. Failure pattern due to water leakage through the dam

6) Simulate flood conditions in the downstream area of the reservoir using the HEC-RAS model in the case of Khlong Luang Ratchalothorn Reservoir using a mathematical model with 3 main steps: study of the volume of water flowing into the reservoir (inflow hydrograph), hydraulic study to study the movement of flood waves, and use of geographic information system to compile physical characteristics of the area for analysis in the hydraulic model.
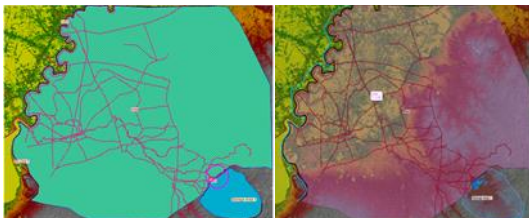
**Fig. 4. Shows how to create a HEC-RAS model of the dam and reservoir.**

3 Results and discussion

From the simulation results of the flow conditions of the river downstream in the case of the collapse of Khlong Luang Ratchalothorn Reservoir using the HEC-RAS model, the analysis results of the dam collapse cross-section in the overtopping form found that at the 10,000-year recurrence cycle, the rectangular form had the highest flow rate of 2348.89 cubic meters/second.

At the time of the highest flow of 47 hours and 12 minutes, at the water level in the reservoir +36.45 m. MSL, the flooded area was 181.10 (sq.km.)

The analysis results of the dam collapse cross-section in the piping failure form, the triangle form had the highest flow rate of 2862.62 cubic meters/second, at the time of the highest flow of 48 hours and 10 minutes, at the water level in the reservoir +36.45 m. MSL, the flooded area was 198.01 (sq.km.)
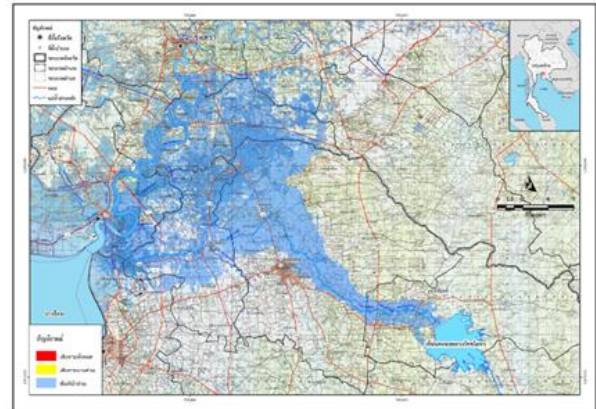
Fig. 5. Flood map downstream of Khlong Luang Ratchalothorn Reservoir

4 Conclusions

This study evaluated the simulation results of flow and flood conditions downstream of the Khlong Luang Ratchalothorn Reservoir collapse using the HEC-RAS model. The results of the analysis of flow rates through the triangular failure pattern in the case of 10,000-year piping failure were used to display the results of the analysis of the maximum water level in this case in the form of a flood map downstream of the dam after the collapse of the Khlong Luang Ratchalothorn Reservoir. This resulted in a flooded area downstream of 198 sq.km. or 123,750 rai, with an average depth of 0.49–0.95 m. The movement of water from the collapse of the dam to the Koh Chan community, Koh Chan Subdistrict, Koh Chan District, Chonburi Province took 48 hours and 10 minutes. From the results, the extent of the flood map downstream can be determined to be used as a guideline for evacuation planning and management.

Reference

Narumon Nawayon 2012. Simulation of the Srinakarin Dam Disaster. Master's thesis. Kasetsart University. Bangkok.

Suttisak Soralamp and Worakorn Mairiang. 2007. Dam Safety Documents. Dam Disaster. Geotechnical and Foundation Engineering Research and Development Center. Department of Civil Engineering. Faculty of Engineering. Kasetsart University. Bangkok.

Wongduean Jaithiangtham and Wandee Thaisayam 2022. Simulation of Flood Conditions in the Downstream Area in the Case of the Collapse of the Muak Lek Reservoir. Master's thesis. Kasetsart University. Bangkok

Hydrologic Engineering Center. Using HEC-RAS for Dam Break Studies.

The 12th International Symposium on Water Environment Systems
----- with Perspective of Global Safety   (Nov. 21st ~ 22nd , 2024)

GP-RSS & SyDE
Tohoku University

Future Projections of Dengue Fever Risk in Chiang Mai Under Climate Change

○ Prem RANGSIWANICHPONG[1*], Banramee KABTAWONG[1] & Thapthai CHAITHONG[2]

[1]Department of Water Resources Engineering, Kasetsart University, Bangkok 10900, Thailand.
[2]Department of Geography, Kasetsart University, Bangkok 10900, Thailand.
[*]E-mail: Prem.r@ku.th.

Abstract

  This study analyzes the influence of global climate change on existing and future dengue fever risks in Chiang Mai Province, Thailand, an area prone to health problems caused by environmental changes. Applying Global climate Models (GCMs) and Random Forest analysis, the study projections dengue fever incidence under several climatic scenarios for the future decades. The analysis integrates climatic data with epidemiological models to explore how changes in temperature and precipitation may influence dengue risk. The results reveal a strong link between key climate variables and dengue outbreak patterns, emphasizing the importance of environmental factors in the disease's spread. The findings suggest that rising global temperatures and shifts in rainfall patterns will likely increase the risk of dengue outbreaks in the future. This study underscores the urgent need to incorporate climate change into public health planning and offers a framework for predicting disease risks in the context of global climate change.

Keywords: Dengue Fever; Global Climate Models; Mosquito; Random Forest; Thailand.

1 Introduction

  The aim of this research is to apply advanced modeling tools to assess the effect of climate change on dengue fever risk dynamics in Chiang Mai province applying 20 Global Climate Models (GCMs) and Random Forest analysis. The transmission of dengue, facilitated by Aedes mosquitoes, is highly sensitive to climatic factors like temperature and precipitation, which influence mosquito breeding, life cycles, and virus transmission rates. Previous studies, including those by Hales et al. (2002) and Morin et al. (2013), have shown that climate change can expand the geographical distribution of dengue by creating favorable conditions for mosquito proliferation. Moreover, Bhatt et al. (2013) emphasized that climate change could exacerbate the global dengue burden, with over half of the world's population at risk. The integration of GCMs with machine learning approaches such as Random Forest, a method praised for its ability to handle complex, nonlinear relationships, offers a powerful tool for forecasting disease outbreaks. Research by Carlson et al. (2016) and Banu et al. (2014) demonstrated the effectiveness of these models in accurately predicting dengue transmission by analyzing climate and environmental data. By focusing on future climate-driven dengue scenarios, this study aims to provide critical insights into areas of heightened disease risk and inform targeted public health strategies. Understanding these dynamics is vital for developing effective interventions as the global climate continues to shift, posing increasing challenges for controlling vector-borne diseases like dengue.

2 Study Area

  Chiang Mai Province, located in northern Thailand, features diverse geography from mountainous terrains to fertile valleys, with a tropical savanna climate. Its climate is marked by a wet season from May to October, influenced by the southwest monsoon, and a dry season from November to April. This weather pattern fosters ideal breeding conditions for Aedes mosquitoes, the main vectors of dengue fever. Dengue outbreaks in the region align with the rainy season, when mosquito breeding increases. Studies, such as by Cummings et al. (2004), emphasize the role of geography and climate in influencing dengue's spread, highlighting the need for targeted public health strategies to manage the disease effectively.
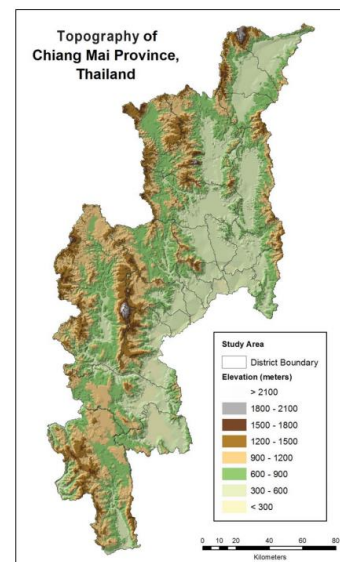
Fig. 1. Topography of Chiang Mai Province.
(Sources: Thebpanya, P., Hatfield, S.L., Lee, J. (2019))

3 Methodology

  This study employs an analytical approach using Global Climate Models (GCMs) to predict future climate conditions in Chiang Mai Province, which are crucial for assessing potential changes in dengue fever risk due to climate change. GCMs are advanced tools designed to simulate Earth's climate systems, offering projections for temperature, precipitation, and other climatic variables across different

The 12th International Symposium on Water Environment Systems
----- with Perspective of Global Safety   (Nov. 21st ~ 22nd , 2024)

GP-RSS & SyDE
Tohoku University

greenhouse gas emission scenarios. After generating climate forecasts, the study utilizes the Random Forest algorithm, a reliable machine learning method recognized for its accuracy and capability in managing complex data, to model dengue fever risk. This algorithm examines the relationship between climate factors predicted by GCMs and historical dengue incidence, identifying trends and accurately forecasting future outbreaks. This approach effectively combines climate projections with epidemiological data to project dengue fever risks under evolving climate conditions.

4 Results and discussion

Climate Projections:

Recent climate change studies specifically forecasted for Chiang Mai province reveal pressing insights about future environmental conditions in the area. Analysis based on Shared Socioeconomic Pathways (SSPs) emphasizes expected impacts on temperature, including shifts in average, maximum, and minimum levels, along with projected changes in precipitation. In the SSP1-2.6 scenario, aiming for significant pollution reductions, a moderate average temperature rise of 0.76°C is anticipated. Under the SSP2-4.5 scenario, which assumes medium changes, an increase of 1.31°C is expected. More concerning is the SSP3-7.0 and SSP5-8.5 pathways, with substantial emissions increases, where temperatures could rise by 2.17°C and 2.88°C, respectively. Maximum and minimum temperatures also show notable increases: SSP1-2.6 projects rise of 0.71°C and 0.6°C, while SSP5-8.5 foresees significant increases of 2.5°C in both. In terms of precipitation, SSP1-2.6 forecasts a modest 2.4% increase, while SSP5-8.5 predicts a drastic 41.49% rise, suggesting intensified rainfall patterns.
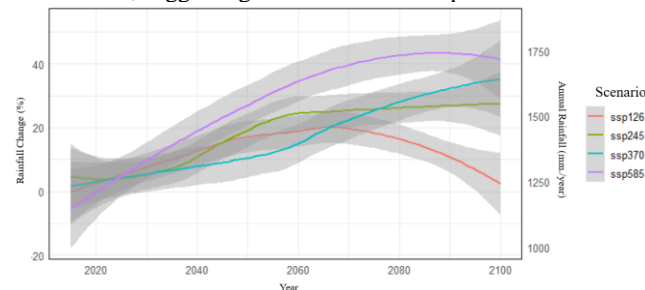

Fig. 2. Projected Rainfall Trends Under SSPs Scenarios.

Dengue Fever Infection Prediction:

Recent research aimed at predicting dengue fever infections in Chiang Mai has employed the Random Forest Regressor method. The parameters set for the Random Forest included n_estimators = 6, max_depth = 100, min_samples_split = 2, min_samples_leaf = 1, and max_features = sqrt. The analysis revealed that Monthly Minimum Temperature emerged as the most crucial predictor of dengue outbreaks, corroborating the findings of Mordecai et al. (2017), which highlighted the significant influence of minimum temperatures on mosquito breeding and survival rates. Global climate change is expected to have a considerable effect on future trends in dengue fever infections. This study examined infection projections across different Shared Socioeconomic Pathways (SSPs), spanning from SSP1-2.6 to SSP5-8.5. Each scenario suggests a rise in infection rates moving forward, with SSP5-8.5 predicting the most significant increase, reaching an infection rate of 149.09 per 100,000 people, which represents a 114.58% rise.
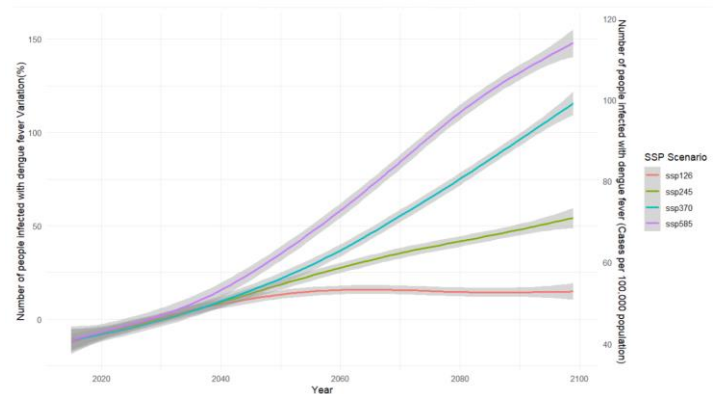

Fig. 3. Projected Dengue Fever Infection Trends.

4 Conclusions

This study evaluated the effectiveness of the CMIP6 global climate models, specifically 20 different models, in forecasting rainfall and temperature trends in Chiang Mai Province. Among these, the MIROC-ES2L model demonstrated the best performance for rainfall predictions, achieving an R² value of 0.61. Rainfall is projected to increase by 2.4% under the SSP1-2.6 scenario and by 41.49% under the SSP5-8.5 scenario. Regarding temperature, the CNRM-CM6-1 model exhibited the highest accuracy with an R² of 0.76, forecasting temperature increases of 0.76°C under SSP1-2.6 and 2.88°C under SSP5-8.5. Additionally, the study utilized the Random Forest model to predict dengue fever cases, identifying monthly minimum temperature as the most significant predictor. By the year 2100, dengue cases are projected to rise to 149.09 per 100,000 individuals, representing a 114.58% increase under the SSP5-8.5 scenario. Therefore, adapting to climate change, particularly in terms of public health responses and disease control strategies, will be essential moving forward.

Reference

[1] Hales, S., de Wet, N., Maindonald, J., & Woodward, A. (2002). Potential effect of population and climate changes on global distribution of dengue fever: an empirical model. Lancet, 360(9336), 830-834.

[2] Morin, C. W., Comrie, A. C., & Ernst, K. (2013). Climate and dengue transmission: Evidence and implications. Environmental Health Perspectives, 121(11-12), 1264-1272.

[3] Bhatt, S., Gething, P. W., Brady, O. J., et al. (2013). The global distribution and burden of dengue. Nature, 496(7446), 504-507.

[4] Carlson, J., Dougherty, E., & Getz, W. (2016). An ecological assessment of the pandemic threat of Zika virus. PLoS Neglected Tropical Diseases, 10(8), e0004968.

[5] Banu, S., Hu, W., Hurst, C., & Tong, S. (2014). Dengue transmission in the Asia-Pacific region: Impact of climate change and socio-environmental factors. Tropical Medicine & International Health, 19(5), 596-607.

[6] Cummings, D. A. T., Irizarry, R. A., Huang, N. E., et al. (2004). Travelling waves in the occurrence of dengue haemorrhagic fever in Thailand. Nature, 427(6972), 344-347.

[7] Thebpanya, P., Hatfield, S.L., Lee, J. (2019). Visualizing Dialect Variation on a 3-D Interpolated Map: A Case Study in Chiang Mai, Thailand. In: Brunn, S., Kehrein, R. (eds) Handbook of the Changing World Language Map. Springer, Cham. https://doi.org/10.1007/978-3-319-73400-2_90-1.

[8] Mordecai EA, Cohen JM, Evans MV, Gudapati P, Johnson LR, Lippi CA, et al. (2017) Detecting the impact of temperature on transmission of Zika, dengue, and chikungunya using mechanistic models. PLoS Negl Trop Dis 11(4): e0005568. https://doi.org/10.1371/journal.

The 12th International Symposium on Water Environment Systems
----- with Perspective of Global Safety   (Nov. 21st ~ 22nd , 2024)

GP-RSS & SyDE
Tohoku University

Multiphase dolomitization in Kingriali formation of Namal Gorge section in Western Salt Range, Pakistan

Asim Hussain[1*],Dr Emadullah khan[2]

Abstract

Kingriali Formation at Namal Gorge Section in Salt Range, Mianwali is selected for research study. Research is based on geochemical analysis and petrographic analysis. Lithologically it consists of light grey to brownish thin to thick-bedded, massive, and fine to coarse-grained dolostone and dolomitic limestone with interbedded shale, marl, and dolomite. Petrographic observation revealed three types of dolomites which includes i) fine grained anhedral dolomite (D1) ii) medium grained subhedral to anhedral dolomite (D2) and coarse grained euhedral dolomite (D3) . Para genetic sequence of Kingriali Formation revealed several other digenetic events which are micritization, compaction, dissolution, calcitization and fracturing. Calcite veins, elephant skin weathering and brecciation was also observed in the studied formation. The stable oxygen isotopic signatures of D1 ranges from -2 to -2.8‰ VPDB and that of Carbon ranges from 0.8 to 1 ‰ VPDB, D2 oxygen isotopic signatures is -2.9 to -1.5‰ . VPDB, while its Carbon isotopic values ranges from 0.4 to 0.6 ‰. Dolomite D3 oxygen isotopic signatures ranges from -3.3 to -3.7‰ VPDB and its Carbon isotopic values ranges from 0.9 % to 1‰ VPDB this indicate Carbon and isotopic values lie within the late Triassic marine signatures. Elemental analysis of all 3 types of dolomite was carried out for Manganese (Mn), Iron (Fe), Sodium (Na) and Strontium (Sr) in all the three types of dolomite that were identified during the petrographic study. Based on our field observation, petrographic analysis and geochemical analysis it is suggested that the dolomite is formed by evaporation and burial dolomitization.

Keywords: 1; geochemical analysis 2; petrographic analysis 3; micritization 4; elephant skin weathering

1 Introduction

The genesis of dolomite has been a very confusing problem for geoscientists. Fault-related dolomites were usually the focus of hydrocarbon exploration because their quality of reservoir is very good. As a potential hydrocarbon reservoir dolomite or dolomitic rock is a very important rock. The process of dolomitization in carbonate rocks happended once deposition occurred, and they were always developing during different stages of burial diagenesis as dolomitization and the Lower Cretaceous Judea Formation [1]. More researchers work revealed that the dolomites were because of multiple phase dolomitization not because of a single process [3].

Globally 50% or more are very important carbonate rocks which are used as hydrocarbon reservoirs, specifically dolomitic rock. Integrated studies of carbonate rocks give an idea that dolomite can exist in many forms. World proven oil and gas carbonates reservoirs have porous dolostones and it is also believed by some researchers that it is affected by the dolomitization fluids [2].

2 Materials and methods

2.1 Thin section preparation and microscopy:

27 samples were selected for thin section preparation. The prepared thin sections were stained using Dickson (1996) modified staining technique, thin sections were half stained with Potassium Ferricyanide and Alizarin Red S solution. Then thin sections were studied using a plane-polarized microscope. Photomicrographs were captured using a DP-21 camera which is attached to the plane polarized microscopy.

2.2   Geochemical Methods:

2.2.1   Stable Isotope Analysis (O & C):

It provides information on environmental variability in salinity, temperature, and isotope composition of the host water and at the end carbon cycling. Standard isotopes were compared with bulk isotopic composition of a sample, and it is expressed as a difference between the sample and between the international standards that is VPDB (Vienna Pee Dee Belemnites for carbonates). The standard isotopes $\delta 13C$ and $\delta 18O$ are used for the said purpose. This method deals with measuring isotopes of carbon that is 13C and 12C and oxygen 18O &16O and is expressed in permil or percentage.

8 samples of different dolomite phases were selected, which are recognized by petrographic examination. Analysis was carried out in PINSTECH laboratory Islamabad. The carbonate samples show reaction with Phosphoric acid at 500°C which do rapid evolution of CO2 in the carbonate preparation line. The calibration values of 13C and 18O is assigned from the isotope ratio of the belemnite.
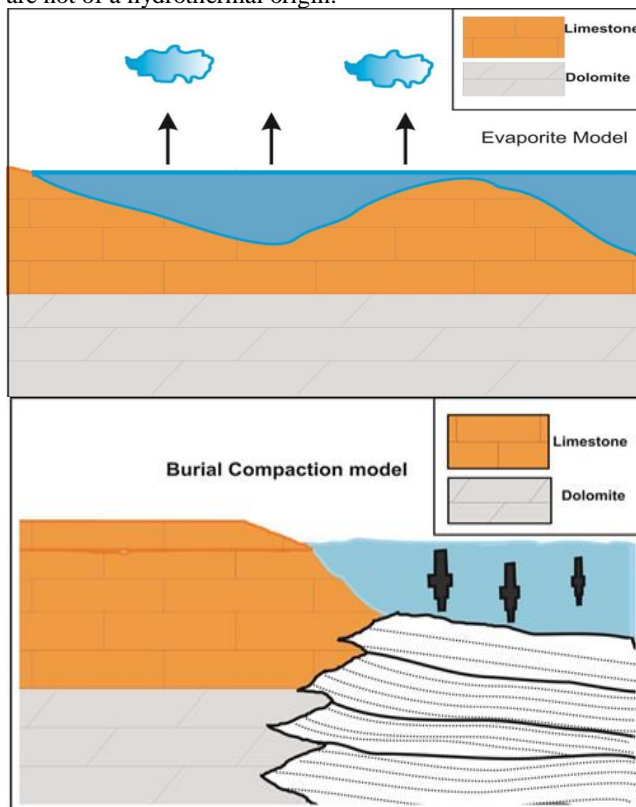
2.2.2   X-ray fluorescence (XRF) Spectrometry analysis:

XRF analysis is used for quantitative analysis of trace elements which is inside a particular rock sample on Teflon filter. The X-ray peaks and it quantitate the concentration with calibration parameters by collaborating it. XRF analysis of 5 samples was carried out at National Physical and Standards Laboratory Islamabad.

3 Results and discussion

Dolomite (D1 and D2) are formed in evaporitic environment and lies in original marine signatures. Dolomite (D3) shows low isotopic values because it is altered because of high temperature and it is formed at burial environment. Six samples of different dolomite phases were analyzed with the aim to find the elemental composition. The major and trace elements abundance will

The 12ᵗʰ International Symposium on Water Environment Systems
----- with Perspective of Global Safety   (Nov. 21ˢᵗ ~ 22ⁿᵈ , 2024)

GP-RSS & SyDE
Tohoku University

give important 36 proofs to the process of dolomitization. In dolomite D3 the Fe value is high as compared to dolomite D2 and D3 so it means it is formed in evaporatic environment. If the iron value is less it means it is formed at deep burial environment. Na concentration of D3 is lower than that of other 2 types of dolomites suggesting that dolomites lost Na in the course of diagenesis exhibiting the features of burial dolomitization. Sr is always related to a variety of rock-forming minerals like that calcite and dolomite. Mn concentration gives us idea that the dolomites are not of a hydrothermal origin.

variety of rock forming minerals like calcite and dolomite. Mn(170ppm to 1400ppm) concentration gives us idea that the dolomites are not of a hydrothermal origin.

Reference

[1] Ibrahem Y, Morozov VP, Sudakov V. Dolomitization of the lower cretaceous carbonate reservoir in the Euphrates Graben, Syria. Petroleum Science. 2021 Oct;18(5):1342–56.

[2] Ronchi P, Masetti D, Tassan S, Camocino D. Hydrothermal dolomitization in platform and basin carbonate successions during thrusting: A hydrocarbon reservoir analogue (Mesozoic of Venetian Southern Alps, Italy). Marine and Petroleum Geology. 2012 Jan;29(1):68–89.

[3] Al-Aasm IS, Packard JJ. Stabilization of early-formed dolomite: a tale of divergence from two Mississippian dolomites. Sedimentary Geology. 2000 Mar;131(3–4):97–108.

4 Conclusions

Detailed field observations and petrographic study indicates that there are several diagenetic events that were involved in the modification of Kingriali Formation from Precursor limestone to present day dolomite. Paragenetic sequences includes micritization, compaction, dissolution, cementation, fracturing, neomorphism is developed for kingriali Formation which revealed the complete history. Petrographic study revealed 3 kinds of dolomite namely fine-grained anhedral dolomite (D1), medium-grained subhedral dolomite (D2) and coarse-grained euhedral dolomite (D3). Different diagenetic events i.e brecciation, dissolution, compaction, cementation, development of ooids, fracturing, neomorphism, micritization were observed. Elemental analyses were done to find composition of elements. In dolomite D3 the Fe value is high as compared to dolomite D1 and D2 indicating it is formed in evaporitic environment. If the iron value is less, indicating that it is formed at deep burial environment. Na concentration of D3 is lower than that of other 2 types of dolomites suggesting that dolomites lost Na during diagenesis exhibiting the features of burial dolomitization. Sr is always related to a

The 12th International Symposium on Water Environment Systems
----- with Perspective of Global Safety   (Nov. 21st ~ 22nd , 2024)

GP-RSS & SyDE
Tohoku University

Suspended sediment transport in the Abukuma River estuary

○ Sheikh Hefzul BARI[1], Mayu TATENO[1], Yoshiyuki YOKOO[1]

[1]Graduate School of Symbiotic Science and Technology, Fukushima University, Fukushima 960-1296, Japan
*E-mail: shbari.bd@gmail.com.

Abstract

This study investigated the characteristics of suspended sediment in the Abukuma River estuary, Japan. Field measurements revealed a predominance of fine-grained sediments (clay and silt) with occasional coarser material (sand). The mineral composition of the suspended sediment samples was dominated by silicates, primarily silica and aluminum. Particle size distribution exhibited a positively skewed unimodal pattern, with a significant portion of particles concentrated in the 4-5 µm range. Strong correlations between surface and cross-sectional suspended sediment concentrations justified the use of surface measurements as a representative of cross-sectional suspended sediment concentration. Turbidity was found to be a reliable proxy for estimating suspended sediment concentration. Power function relationships between discharge and suspended sediment, including total sediment and its components (clay, silt, and sand), demonstrated varying degrees of association. Discharge and suspended sediment concentration relations during a storm event suggested sequential flushing of suspended sediments. The power law relationship between discharge and suspended sediment indicates the need for alternative modeling approaches, particularly for sand. It is anticipated that continued monitoring and data analysis will contribute to a more comprehensive understanding of sediment dynamics and their implications for coastal landforms in the Abukuma River estuary.

Keywords: suspended sediment; particle size distribution; estuary, sediment dynamics; turbidity, hysteresis.

1 Introduction

Sediment transport is a critical factor in river ecosystems, influencing landscapes, economies, and societal well-being [1]. While computational estimation is possible for coarse sediment, fine sediments have more complex dynamics and often require observed data [2]. Additionally, suspended sediment (SS) concentration fluctuates with discharge, influenced by factors like erosion characteristics, transportation, and deposition [1, 3-4]. High-flow events, in particular, contribute significantly to overall SS loads.
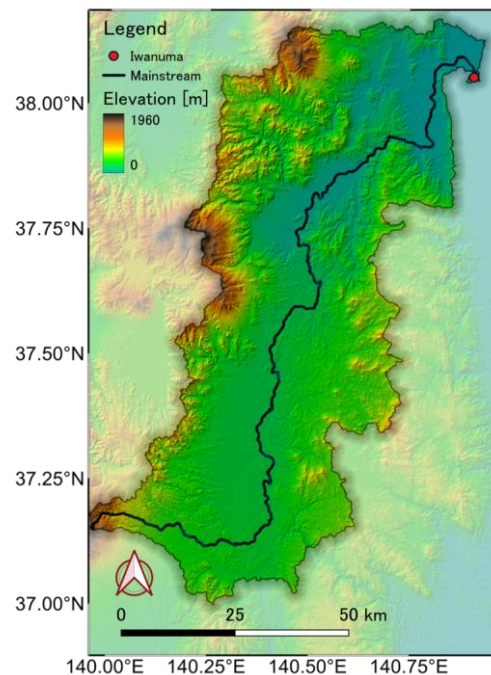
Characterizing SS dynamics is essential as it helps understanding enduring trends, the impact of high episodes, and the broader effects on ecology, geomorphology, as well as infrastructure [5]. Sediment properties, including particle size distribution and mineralogy, offer insights into transport processes, source tracking, and potential environmental impacts [5-6]. Fine sediments have the capacity to adsorb aquatic pollutants. This characteristic highlights their importance in understanding water quality.

Accurate SS estimation and characterization require continuous data with a high sampling frequency. While traditional grab sampling methods have limitations to serve this purpose, alternative approaches, such as turbidity-based surrogate methods, offer a promising solution for near-continuous data collection. However, the relationship between water turbidity and SS needs site-specific calibration for effective field application.

The Abukuma River, a crucial economic resource in the Tohoku Region of Japan, lacks comprehensive research on estuarine SS dynamics. Existing studies suggest changes in sediment supply and highlight the need for updated research. This study aims to improve our understanding of estuarine SS dynamics by implementing a comprehensive sampling strategy, investigating turbidity as a surrogate for SS, and analyzing sediment properties.

2 Materials and methods

The Abukuma watershed (Fig. 1) covers an area of 5400 km². The river originates from the Nasu Mountains in Nishi-Shirakawa-gun, Fukushima prefecture, before it drains into the Pacific Ocean. The main channel runs northward for a length of 236 km (derived from SRTM 30 m DEM) making it the 2nd and 6th longest river in the Tohoku region and Japan, respectively. It has a flume shaped morphology with a steep slope in the headwater region.


Fig. 1: The mainstream (black line) and Iwanuma sampling point in the Abukuma River basin.

The 12th International Symposium on Water Environment Systems
----- with Perspective of Global Safety   (Nov. 21st ~ 22nd , 2024)

GP-RSS & SyDE
Tohoku University

To understand the SS characteristics in the estuary region of the river, we performed a sampling program in 2023. Samples were collected from Iwanuma, Miyagi, about eight kilometers from the river mouth. Collected samples were then analyzed to determine the concentration, mineralogical composition and particle size distribution.

3 Results and discussion

One of the crucial steps in getting representative SS measurements from a river section is to locate the most suitable sampling point. The selection of the most representative sampling point varies depending on the cross-sectional properties of the river. We used a total of 10 spatially varying points to find a representative point. Fig. 2 provides a visual representation of the river's geometry at the sampling location. The results indicate that surface water SS taken from 70 meters from the left bank represents the cross-sectional average adequately.
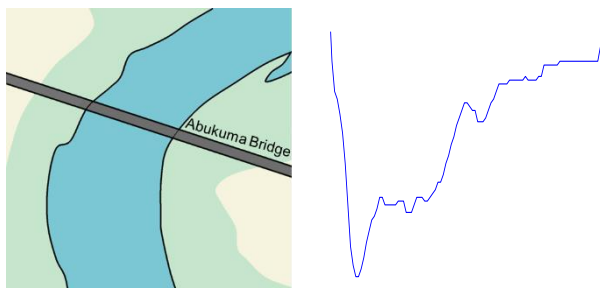
Fig. 2: Top view (left) and cross-sectional view (right) of the Abukuma River at the Iwanuma sampling point.

Once the representative location was identified, total SS and its constitutional components (clay, silt and sand) were modeled using the most widely used power function. The results show a reasonable fit except for sand. This is because sand is mostly transported during a highflow event, which better fits to a linear relationship compared to a power function.
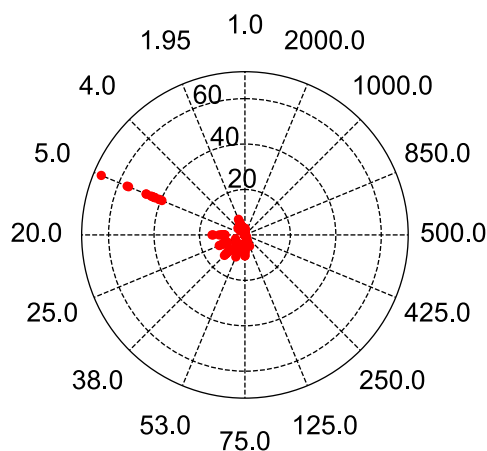
Fig. 3. Contribution (%) of different particle classes to total suspended sediment (SS). The radial axis represents different particle size classes (in µm) and concentric circles indicate contribution values (%).

The SS was mainly composed of clay and silt, totaling sand contributions less than 10% through the sampling period. We discovered that particles within 5µm size make up nearly half of the total SS (Fig. 3). The mineralogical compositions of the SS samples were granite, suggesting that weathering of granitic rocks is the major contributor to the SS. It becomes apparent that a major source can be expected, most likely from the granite-rich Abukuma Mountain on the eastern bank. The unimodal particle size distribution, peaking in the smaller size range, best fits the Normal Inverse Gaussian Distribution tested against all the distributions available in Scipy (a Python package).

4 Conclusions

This study examined the suspended sediment concentration (SSC), composition, and particle size distribution (PSD) in the Abukuma River estuary. A single sampling location provided an accurate depiction of the cross-sectional SSC. A strong correlation between turbidity and SSC was found, suggesting turbidity is a reliable indicator of SSC. While the suspended sediment contained some sand, it mainly consisted of silt and clay. During flood events, finer particles were transported first, followed by coarser materials. The PSD was skewed towards smaller particle classes, with a median size below 5 µm. These findings highlight the need for further investigation into suspended sediment dynamics and suggest implementing long-term monitoring programs for the river.

Reference

[1] Bari, S.H., Yokoo, Y., Leong, C., A brief review of recent global trends in suspended sediment estimation studies, Hydrological Research Letter, 18 (2024) 51–57.

[2] Colby, B.R., Fluvial sediments- a summary of source, transportation, deposition, and measurement of sediment discharge (No. 1181- A), Bulletin (1963), U. S. Govt. Print. Off.

[3] Haygarth P.M., Condron L.M., Heathwaite A.L., Turner B.L., Harris G.P., The phosphorus transfer continuum: Linking source to impact with an interdisciplinary and multi-scaled approach, Science of the Total Environment, 344 (2005) 5–14.

[4] Thompson J., Cassidy R., Doody D.G., Flynn R., Assessing suspended sediment dynamics in relation to ecological thresholds and sampling strategies in two Irish headwater catchments, Science of the Total Environment, 468–469 (2014) 345–357.

[5] Vercruysse, K., Grabowski, R.C., Rickson, R.J., Suspended sediment transport dynamics in rivers: Multi-scale drivers of temporal variation, Earth-Science Reviews, 166 (2017) 38–52.

[6] Xu, J., Grain-size characteristics of suspended sediment in the Yellow River, China, Catena, 38 (1999) 243–263.

The 12th International Symposium on Water Environment Systems
----- with Perspective of Global Safety   (Nov. 21st ~ 22nd , 2024)

GP-RSS & SyDE
Tohoku University

Implementation of disaster prevention education method using three-dimensional digital space: Focusing on the subject's independence

○ Keitaro SUSUKIDA[1*], Keisuke ONO[1] & Akira KIKUCHI[1]

[1] Department of Civil Engineering, Graduate School of Engineering, Tohoku Institute of Technology,
Miyagi 982-8577, Japan.
*E-mail: m244807@st.tohtech.ac.jp

Abstract

In Japan, where water-related disasters are becoming more severe and more frequent, it is important to be aware of the risk of flooding, to think of it as if it was one's own, and to act proactively. The study involved creating 3D educational content on disaster prevention using the popular video game Minecraft and implementing the effectiveness of the content at an actual educational site. The results of the questionnaire survey showed that the total percentage of "4" and "5" for the question of the need to independently consider whether flooding occurs increased by 16% before and after the class. These results suggest that 3D spatial disaster education content is an effective tool for encouraging subject's independence.

Keywords: disaster prevention; three-dimensional digital space; minecraft; video game; education

1 Introduction

In recent years, water-related disasters have become more severe and more frequent throughout Japan, and the need for soft measures against water-related disasters has increased. According to a proposal by the MLIT in 2023, in order to minimize the damage caused by water-related disasters, it is important for residents to recognize their own flood risks, to think of it as if it was their own, and to act proactively[1]. In addition, in relation to think of it as if it were one's own, Suzuki et al. (2022) study revealed that active learning on disaster prevention consists of five processes: "pay attention, get interested, acquire knowledge, understand correctly, and take action "[2]. In addition, a study by Ono et al. (2024) suggests that disaster education using a 3D space is effective in eliciting the subject's interest[3]. However, it is not yet clear how disaster education in a 3D space can be effective in making people think of it as if it was one's own.

Therefore, this study combines 3D city data with Minecraft, a globally popular video game, to create disaster education content utilizing 3D digital space (hereinafter referred to as "3D space"). Disaster education will also be conducted using this content at junior high schools to survey its educational effectiveness.

2 Materials and methods

(1) Content of disaster prevention education

On August 29, 2024, disaster education using 3D spatial disaster education contents was conducted at Kanan Junior High School in Morioka City, and the effectiveness of the contents was surveyed using a questionnaire in the class. The number of subjects was 52 in total from two classes of second-year junior high school students.
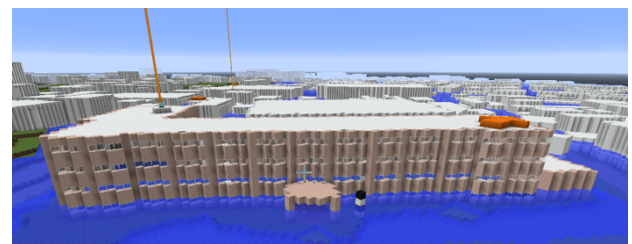
The content of the class is to form groups of three, and have the first two students check the expected flood depth in Morioka City in the event of the heaviest rainfall in history in a 3D space. Then, Another member of the group was asked to learn how to protect the city from flooding by building a levee in 3D space.

(2) Questionnaire Content

This study focuses on the three questions shown in Table 1. In designing the questionnaire, questions from the survey by Sato et al. (2011) were referenced[4]. The questionnaire was distributed before and after the class to investigate changes in disaster awareness resulting from the use of this content. Responses were collected using a five-point scale.

Table 1 Questions asked in this survey

	Question Content	**Purpose of a Question**
Q1	Do you think you need to carefully consider "on your own" if flooding will occur during a heavy rain?	Independence of decision making during heavy rain
Q2	Do you think that during one of the heaviest rainfalls in history, it is difficult to completely prevent flooding and that "doing prevention measures yourself" is important?	Importance of "doing prevention measures yourself"
Q3	Do you think it is important for the national, prefectural, and municipal governments to carry out disaster prevention activities to protect towns from heavy rain and flooding?	Importance of disaster prevention activities carried out by the municipalities

Fig. 1. School reproduced in 3D space

The 12th International Symposium on Water Environment Systems
----- with Perspective of Global Safety   (Nov. 21st ~ 22nd , 2024)

GP-RSS & SyDE
Tohoku University

3 Results and discussion

The results of the questionnaire are shown below.

Regarding Q1, Figure 2 shows that before the class, 52% of the respondents selected "4" and 32% selected "5", which indicate the need to independently consider whether flooding occurs, while after the class 40% selected "4" and 48% selected "5", indicating a 12% decrease in the percentage of "4" and a 16% increase in the percentage of "5" between before and after class. The total percentage of "4" and "5" increased by 4%. The 16% increase in "5" suggests that this content is a tool that increases the need for subjects to independently consider whether flooding.

Regarding Q2, Figure 3 shows that before the class, 56% of the respondents selected "4" and 0% selected "5", which are relatively important "doing prevention measures yourself", while after the class, 60% selected "4" and 0% selected "5", with the percentage of "4" increasing by 12% before and after the class, while the percentage of "5" remained almost unchanged. The total percentage of "4" and "5" increased by 11%. After the class, 0% of the respondents selected "5" and the total percentage change of "4" and "5" was also small, 3D space was not found to promote independent disaster prevention behavior.

Regarding Q3, Figure 4 shows that 60% of the respondents selected "4" and 0% selected "5" for the importance of disaster prevention activities conducted by the municipalities before the class, while 53% selected "4" and 0% selected "5" after the class, indicating a 7% decrease in the percentage of "4" and no change in the percentage of "5" before and after class. The total percentage of "4" and "5" decreased by 7%. After the class, 0% of the respondents selected "5" and the change in the total percentage of "4" and "5" was small, suggesting that the 3D space did not seem to influence the importance of disaster prevention activities conducted by the municipalities.

4 Conclusions

In this study, disaster-prevention education contents utilizing 3D space were used to verify their effectiveness in actual educational settings. The results suggest that this content is a tool that increases the need for subjects to independently consider whether flooding occurs, but it was not found to be effective in promoting independent disaster prevention behavior and increasing the importance of disaster prevention activities conducted by the municipalities. In the future, we would like to study factor analysis of interest and motivation for using this content using more specialized factor analysis.
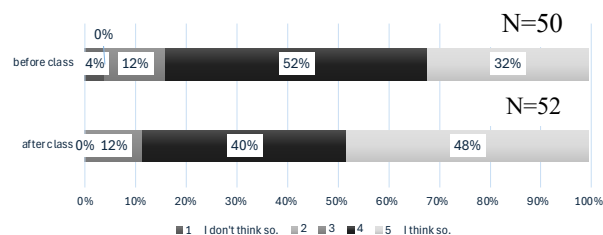
Acknowledgement

Fig. 2. Do you think you need to carefully consider "on your own" if flooding will occur during a heavy rain?
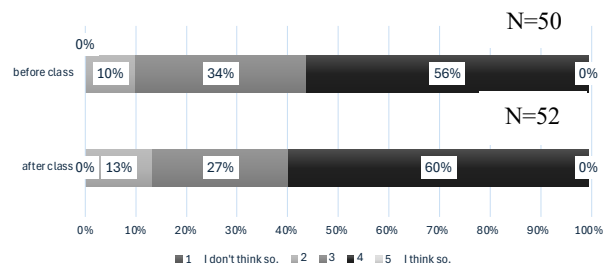

Fig. 3. Do you think that during one of the heaviest rainfalls in history, it is difficult to completely prevent flooding and that "doing prevention measures yourself" is important?
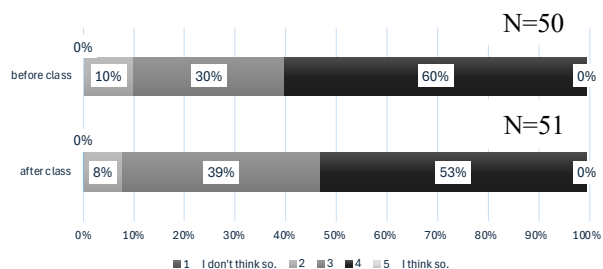

Fig. 4. Do you think it is important for the national, prefectural, and municipal governments to carry out disaster prevention activities to protect towns from heavy rain and flooding?

Reference

[1] MLIT, Study Group on taking Flood Risk Personally and Increasing the Number of Actors Working on Watershed Flood Control, https://www.mlit.go.jp/river/shinngikai_blog/suigairisk2/, accessed 2024-10-22.

[2] Hikari SUZUKI and Masahiro MURAKAMI, A Study on Educational Methods that Learning with Self-Directed and Proactive Manner about Disaster Reduction, Journal of Disaster Education, Vol. 2，No.2（2022）, pp.53-64.

[3] Keisuke ONO, Keitaro SUSUKIDA, Akira KIKUCHI and Yasutaka KOUSAKA, Development and Implementation of Disaster Education Content For Flood Using Open 3D City Models and Minecraft, Japanese Journal of JSCE（Global Environment）, 2024.

[4]Shinsuke SATOH, Akira KIKUCH1, Ayako TANIGUCHI, Shinichiroh HAYASHI, Masato NISHI, Nobutomo OSANAI, Hideyuki ITOH, Katsuya YAMORI, Satoshi FUJII, The Meta-Message Effect of Disaster Information, Kyoto University Research Notes, Disaster Information, No.9（2011）, pp.172-179.

The 12th International Symposium on Water Environment Systems
----- with Perspective of Global Safety   (Nov. 21st ~ 22nd , 2024)

GP-RSS & SyDE
Tohoku University

Effectiveness analysis of 3D disaster education content using text mining of free response questionnaire data

○ Mutsuki KODAMA[1*], Keitaro SUSUKIDA[1] , Keisuke ONO[1] & Naoyuki TOMARI[1]

[1]Department of Civil Engineering and Management, Tohoku Institute of Technology,
Miyagi 982-8577, Japan.
*E-mail: s2114111@st.tohtech.ac.jp

Abstract

The free response section of a questionnaire survey conducted at a junior high school on disaster education using 3D urban data and Minecraft was analyzed. Frequently occurring words and co-occurrence networks were created to examine whether students themselves perceive disaster education as a personal matter. The results showed that 'levee,' 'think,' and 'flood' were the most frequently mentioned words, indicating a high level of interest. Furthermore, the co-occurrence of 'myself' and 'community' suggests that disaster prevention education regarding flooding is indeed perceived as a personal matter.

Keywords: Flood inundation; Class evaluations; Free-text descriptions; Co-occurrence networks

1 Introduction

According to the MLIT press release in August 2023, titled "Making Water-Related Disasters a Personal Matter and Increasing the Number of Entities Involved in Basin Flood Control: Aiming for All-Out Basin Flood Control," it is stated that the risk of increased flood flows due to climate change cannot be addressed solely through measures implemented in river basins. It is emphasized that basin flood control needs to be promoted not only by administrative agencies but also by private companies and local residents. In order for flood control in river basins to be promoted, it is required that flood disasters be regarded as personal matters by not only government agencies but also private companies and local residents, who need to engage in flood control efforts in river basins.[1]

In addition, a gap is identified between "knowing" and "acting" on flood disasters, and in order to narrow this gap, it is necessary for an understanding of one's own relationship with flood disasters and the countermeasures against them to be deepened.[2]

Disaster prevention education content was developed by Ono et al. (2024), enabling the flooding risk level of one's own neighborhood to be checked using Minecraft, a platform widely used by elementary and junior high school students. This was achieved by utilizing PLATEAU, a project led by the MLIT to develop 3D urban models. A lecture was conducted using the content, and the educational effects were suggested. It was revealed that the developed content enables children to actively learn about the flooding risk in their local areas while enjoying themselves, and that it tends to draw out the children's interest and curiosity. However, it has not been verified how the children's interest in and concern for learning are enhanced, nor how the learning is perceived by them as a personal matter.[3]

In this study, a delivery class will be conducted using Minecraft content, and the educational effects of the class will be checked. Frequently occurring words and phrases will be extracted from the free response sections of the class evaluation questionnaires, and a co-occurrence network analysis will be conducted to examine the educational effects. The purpose of this study is for the effectiveness of the disaster education content to be surveyed, and future issues to be clarified through the analysis of the free response columns, contributing to more effective disaster education in the future.

2 Materials and methods

(1) Conditions of the class

On August 29, 2024, a class on disaster prevention was conducted at Morioka City Kanan Junior High School, located in the upper reaches of the Kitakami River. The target group consisted of two classes of second-year junior high school students (52 students in total): Class 3 (27 students) and Class 4 (25 students).

The flow of the class began with a pre-study class questionnaire, followed by the checking of the depth of inundation in Minecraft, which reproduced the surrounding area, and the learning about the degree of danger of inundation. In addition, a levee was created by placing blocks on the Kitakami River, which was reproduced in Minecraft, and a simulation of the situation when the river flow rate increases was conducted. The changes in flood damage before and after the countermeasures were confirmed. Finally, group work was conducted on the question of whether levees should be built as a local flood control measure, based on indicators such as construction cost and the degree of dependence on voluntary disaster prevention activities, and a review questionnaire was administered after the class.

(2) Effectiveness Analysis Methodology

The analysis was based on the results of a questionnaire that was collected during a delivery class held at Kanan Junior High School in Morioka City. Specifically, the free response section of the post-lesson review questionnaire (Figure 1) was analyzed. The free-response section of the class review questionnaire was analyzed using the KH Coder software for quantitative analysis of text data.
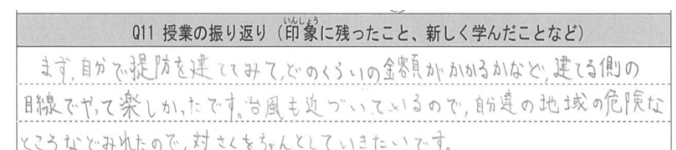

Figure 1 Example of free response section

The 12th International Symposium on Water Environment Systems
----- with Perspective of Global Safety   (Nov. 21st ~ 22nd , 2024)

GP-RSS & SyDE
Tohoku University

3 Results and discussion

A simple tabulation of the text from the class evaluation questionnaire (free response section) was conducted, and 69 sentences were identified. The number of extracted words was 1,724 (695 different words). After preprocessing, 370 words (266 different words) were used for the analysis, and this data was utilized for the analysis. The top 50 extracted words and their number of occurrences are shown in Table 1.

The top 50 words were found to account for more than 40% of the total, which was considered sufficient to grasp the overall content of the free descriptions in the class evaluation questionnaires. The most frequently appearing words were "levee" (25 times), "think" (23 times), and "flood" (16 times). The process of building a levee in their community on Minecraft to prevent flooding was considered the most interesting topic by the junior high school students. In addition, many free responses section regarding flood control in their own communities were observed.

A co-occurrence network diagram (Jaccard coefficient 0.2) is shown in Figure 2. In the co-occurrence network diagram, words that are relatively strongly connected are automatically detected and grouped together. Additionally, the lines are drawn relatively thicker according to the strength of co-occurrence. In Figure 2, the words have been divided into six groups (1, 2, 3, 4, 5, 6). Group (1), which contains the most frequently occurring words, will be discussed. The fact that "levee" and "think," the most frequent words, are strongly co-occurring in the text confirms that the process of creating levees on Minecraft deepened the participants' knowledge of the dangers of water-related disasters and disaster prevention. Additionally, focusing on group (6), "self" and "community" are found to co-occur. By reproducing flooding in their own neighborhoods, it has been recognized that the disaster prevention education against flooding was perceived by the children as their own personal matter.

4 Conclusions

In this study, the free response section from the questionnaires obtained from the delivery lectures held at junior high schools were analyzed. Co-occurrence analysis was also used to determine the extent to which the knowledge of disaster prevention was considered by the students as their own personal matter. The results suggest that the process of building a levee using Minecraft was found to be an interesting topic for the students and that disaster education based on the theme of their own community was regarded as a personal matter. In this study, the results were analyzed using the frequent word list and co-occurrence network, but in the future, other analysis methods will be considered to improve the accuracy of the analysis.
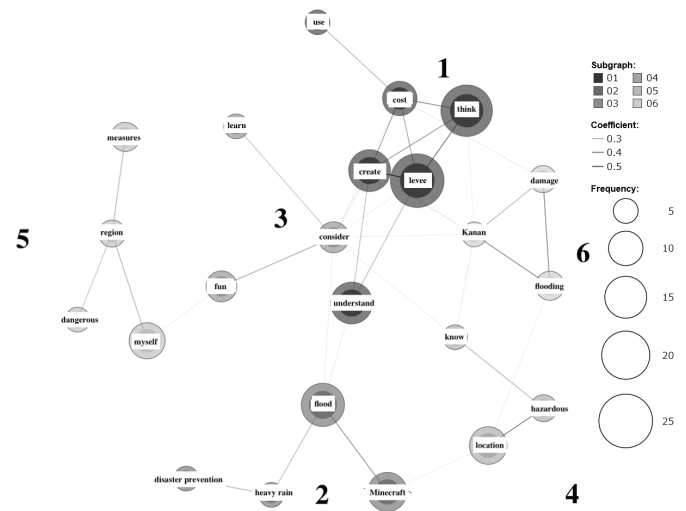
Acknowledgments

Figure 2 Co-occurrence network diagram

Table 1 Frequently appearing words table in the class evaluation questionnaire (free response section)

No	Word	times	No	Word	times	No	Word	times
1	levee	25	18	Kanan	5	35	this time	3
2	think	23	19	learn	5	36	remain	3
3	flood	16	20	dangerous	5	37	nature	3
4	create	15	21	use	5	38	protect	3
5	understand	15	22	heavy rain	5	39	live	3
6	Minecraft	13	23	know	5	40	water	3
7	location	12	24	disaster prevention	5	41	river	3
8	myself	11	25	impression	4	42	Daijiji	3
9	cost	10	26	today	4	43	important	3
10	fun	8	27	disaster	4	44	prevent	3
11	consider	8	28	reality	4	45	demerit	2
12	game	7	29	protectable	4	46	map	2
13	flooding	7	30	class	4	47	merit	2
14	measures	7	31	district	4	48	town	2
15	hazardous	6	32	difficult	4	49	school	2
16	region	6	33	learning	3	50	environment	2
17	damage	6	34	enjoy	3			

Reference

[1] MLIT, Study Group for Making Flood Risk a Personal Matter and Increasing the Number of Actors Engaged in Basin Flood Control https://www.mlit.go.jp/river/shinngikai_blog/suigairisk2/

[2] MLIT, Hokkaido Regional Development Bureau, Goshi-Toribetsu River Basin Flood Control Council (March 8, 2024) https://www.hkd.mlit.go.jp/hk/koumu/

[3] Keisuke ONO, Keitaro SUSUKIDA, Akira KIKUCHI, Yasutaka KOUSAKA Development and Implementation of Disaster Education Content for Flood using Open 3D City Models and Minecraft (in press)

The 12th International Symposium on Water Environment Systems
----- with Perspective of Global Safety   (Nov. 21st ~ 22nd , 2024)

GP-RSS & SyDE
Tohoku University

Can sampling during rain events improve the detection rate of eDNA metabarcoding?

◯ Chen XU[1*], Kei Nukazawa[2]

[1] Graduate School of Engineering, University of Miyazaki, 889-2192, Japan.
[2] Faculty of Engineering, University of Miyazaki, 889-2192, Japan
[*]E-mail: hh19054@student.miyazaki-u.ac.jp

Abstract

  eDNA analysis has been applied to monitor aquatic and terrestrial species. However, eDNA of the species with a small abundance or less contact with water bodies is barely detected and may cause a false negative result. To address this issue, sampling that includes eDNA materials transported from terrestrial realms via surface runoff would be promising. Here we sampled stormwater during different heavy rain events to simultaneously detect aquatic species as well as terrestrial species that do not frequently contact aquatic realms. Samples were obtained at the three rivers, the Mizunashi, Oka, and Tagami Rivers in May, Sep, Nov 2022, June 2023 (9 samples in total). In addition, we also sampled stream water on a normal day without antecedent rainfall events. We applied DNA metabarcoding to identify the vertebrate species using slightly modified universal vertebrate primers 12SV5. As a result, eDNA analysis identified four vertebrate classes: Actinopterygii, Mammalia, Aves, and Amphibia across all sites in the Mizunashi River and Tagami River, rainfall greatly increased the detection of terrestrial mammals and amphibian taxa. However, in the Oka River, the dilution caused by rainfall reduced the detectable of fish.
Keywords: eDNA metabarcoding; vertebrate; rainfall; turbid water.

1 Introduction

  Environmental DNA (eDNA) analysis is being applied as a new biological survey method for species detection. The concept of eDNA refers to DNA released by organisms in the environment (e.g., sea, lakes, and soil) through skin fragments, mucus, and excreta. By using species-specific primers or universal primers to analyze environmental samples, the presence of species can be determined. Moreover, it is unnecessary for eDNA analysis to make direct contact with the species. Compared to traditional biological survey methods, eDNA analysis has the advantages of being non-invasive and causing less environmental impact [1].

  eDNA can be extracted from various media such as air, soil, water, and even pollen or insects. Depending on the species being studied, each type of medium has its own advantages. Among them, river water demonstrates the potential for rapid monitoring of biodiversity. Because rivers connect upstream and downstream, as well as land and water, most substances ultimately accumulate in rivers. Therefore, research is underway to simultaneously detect aquatic and terrestrial species using river water samples. Although many studies have confirmed that detecting terrestrial species from water bodies is possible, there is a prerequisite: terrestrial species must release their DNA into the water. Terrestrial species can directly release DNA into the water through drinking, swimming, or excreting in the water. However, such behavior cannot be predicted, and the DNA released into the water will degrade due to environmental factors, making it difficult to detect species with smaller populations or lower DNA release rates [2].

  Surface runoff occurring during rainfall can transport materials from land into water bodies. If terrestrial species release DNA into water bodies through such indirect process, assessing the organisms at terrestrial realms in a given watershed would be feasible based on the eDNA approach. However, the increase in flow rate caused by rainfall can dilute and disrupt the eDNA signals. Therefore, the aim of
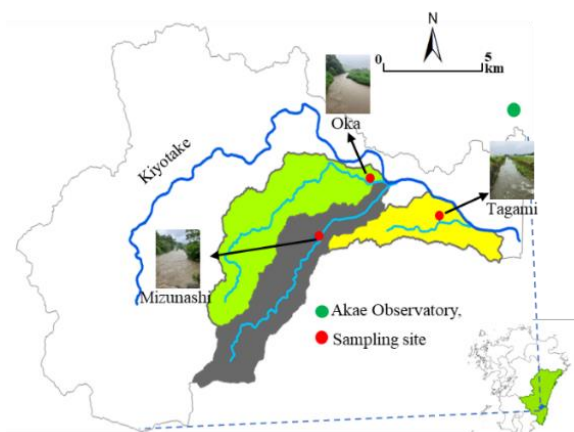

Fig 1 Study area

this study is to explore whether rainfall samples can complement non-rainfall samples to enhance detection rates of both aquatic and terrestrial species.

2 Materials and methods

  The study area included three rivers within the Kiyotake River catchment in Miyazaki Prefecture, southwestern Japan, i.e., the Mizunashi, Oka, and Tagami Rivers. We sampled 1 L of stream water at the three sites during different rainfall events; May and November 2022 and May 2023 in the Mizunashi River, May and Sep 2022 and June 2023 in the Oka River, And Sep and Nov 2022 and June 2023 in the Tagami River. The sampling of 1 L stream water without antecedent rainfall events were performed in Nov 2022 (hereafter, normal samples).

  The water samples were filtered using a glass fiber filter with a pore size of 0.7 μm. Since the samples of stormwater had high turbidity, potentially containing a large amount of organic matter and other PCR inhibitors, DNA was extracted

The 12ᵗʰ International Symposium on Water Environment Systems
----- with Perspective of Global Safety   (Nov. 21ˢᵗ ~ 22ⁿᵈ , 2024)

GP-RSS & SyDE
Tohoku University
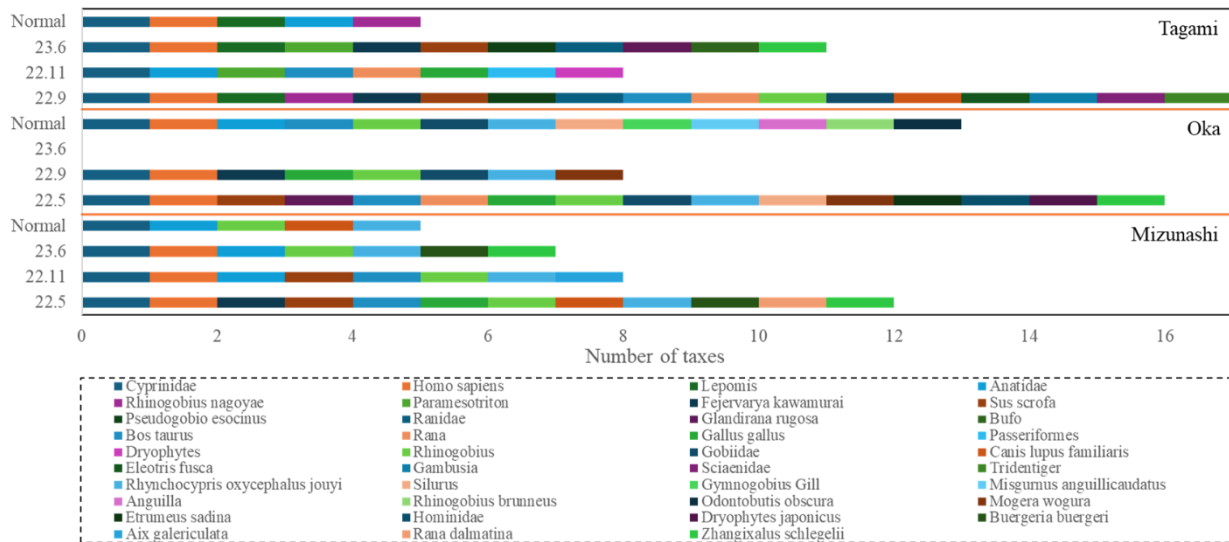
Fig 2. The result of eDNA metabarcoding

using the DNeasy PowerSoil Kit, which is known to minimize effects of inhibition for such turbid samples (Mikami, Xu, Nukazawa, unpublished).

After the extraction step, we applied DNA metabarcoding to identify the vertebrate species by amplifying ~100 bp using slightly modified universal vertebrate primers 12SV5 (Forward prime: YAGAACAGGCTCCTCTAG, Reverse prime: TTAGATACCCCACTATGC, adapted from Riaz et al.) [3]. The prepared DNA library was sequenced using next-generation sequencing (NGS) on the MiSeq system (Illumina) to determine the nucleotide sequences. Subsequently, a similarity analysis of the DNA sequences was conducted to create the Amplicon Sequencing Variants (ASVs) with the highest similarity. The Basic Local Alignment Search Tool (BLAST) was used to search for species with the highest similarity to each sequence in the National Center of Biotechnology Information (NCBI) database. For taxonomic groups that could not be identified at the species level, the genus, family, or order were determined.

3 Results and discussion

The sequencing libraries generated approximately 931,837 raw reads. Following sequence filtering and assignment processes, the four samples in the Mizunashi River retained 55,465 reads for fish (48.4%), 48,690 reads for terrestrial mammals (42.5%), 5,256 reads for birds (4.6%), and 5,156 reads for amphibians (4.5%). The three samples in the Oka River retained 113,004 reads for fish (64.2%), 48,571 reads for terrestrial mammals (27.6%), 5,084 reads for birds (2.9%), and 9,402 reads for amphibians (5.3%). The sample collected in June 2023 showed no detection. The four samples in the Tagami River retained 54,523 reads for fish (52.5%), 19,349 reads for terrestrial mammals (18.6%), 4,412 reads for birds (4.2%), and 25,619 reads for amphibians (24.7%). In the Mizunashi River, 14 taxa were detected: Actinopterygii (2 species, 1 genus, 1 family), Mammalia (3 species), Aves (2 species, 1 family), and Amphibia (4 species). In the Oka River, 23 taxa were found: Actinopterygii (5 species, 4 genera, 2 families), Mammalia (4 species, 1 family), Aves (1 species, 1 family), and Amphibia (4 species, 1 genus). Similarly, in the Tagami River, 23 taxa were recorded: Actinopterygii (3 species, 4 genera, 3 families), Mammalia

(4 species, 1 family), Aves (1 species, 1 family, 1 order), and Amphibia (3 species, 4 genera, 1 family).

In the Mizunashi River, compared with Normal samples, more taxa were identified during rain events. Except for Canis lupus familiaris, which was not detected in the samples from November 2022 and June 2023, and Anatidae in May 2022, the five taxa commonly detected under normal conditions were almost all detected during rainfall periods. In the Oka River, the normal and rainfall samples showed different detection trends. Among the 13 taxa detected in the normal samples, only 5 were found in all rainfall samples. In particular, the detectable taxa of fish drop from 10 to 6. In the 16 taxa detected in May 2022, 9 taxa were not found in the normal samples. The results from the Tagami River were similar to those from the Mizunashi River, with rainfall greatly enhancing the detection rate. Only 5 taxa were detected in the normal sample, whereas as many as 17 taxa were detected during rainfall in September 2022. Amphibian taxa were detected only during rainfall periods at all locations.

4 Conclusions

Compared with normal samples, more taxa were identified during rain events. Surface runoff occurring during rainfall facilitated the detection of terrestrial mammals and amphibian taxa. In the Oka River, the detectable taxa of fish drop from 10 to 6, rainfall increased the flow, diluting the eDNA, which may have reduced detectability.

Reference

[1] Darling. et.al., From molecules to management: Adopting DNA-based methods for monitoring biological invasions in aquatic environments. *Environ. Res.*, 111 (2011) 978-988

[2] Mayvusseau., et al., The Multiple States of Environmental DNA and What Is Known about Their Persistence in Aquatic Environmental. Environ. Sci Technol 56 (2022) 5322-5333

[3] Riaz. et al., ecoPrimers: inference of new DNA barcode markers from whole genome sequence analysis. Nucleic Acids Research, 39 (2011) e145

The 12th International Symposium on Water Environment Systems
----- with Perspective of Global Safety   (Nov. 21st ~ 22nd , 2024)

GP-RSS & SyDE
Tohoku University

What are the differences between the two rivers in different climatic zones? -Focusing on the Abukuma River and Mogami River in Japan-

○ Erina YAMAGATA[1*], Koji KODERA[2] & Seiki KAWAGOE[1]

[1]Faculty of Symbiotic Systems Science and Technology, Fukushima University, Fukushima 960-1296, Japan.
[2] Department of Geography, Faculty of Letters, Hosei University, Tokyo 102-8160, Japan.
[*]E-mail: erinayamagata220@gmail.com

Abstract

The differences in water quality responses of the Mogami and Abukuma Rivers, which are located in snow covered areas but have different climatic zones, were compared based on various environmental factors. The results may be applicable to watershed management that takes into account changes in the water environment caused by climate change. We compared topography, land cover, and surface geology as environmental factors affecting water quality. We found that human and volcanic activities have different effects on water quality in the Abukuma and Mogami river basins. The results of the study also showed that water quality and flow rates changed during the snowmelt season from March to June, indicating that the water environment is changing due to climate change. In the future, we will clarify the characteristics of the response to climate change in rivers and reflect them in watershed management by specifying and elaborating these response characteristics and systematizing the process.

Keywords: water environment; river basin; snow melt; land use; climate change.

1 Introduction

The Tōhoku region of Japan is characterized by different climates on the eastern side of the Pacific Ocean and western side of the Sea of Japan. The Ou Mountains, which run north-south through the center of the Tōhoku region, separates the individual monsoon influences, resulting in a distinct climate. The Tohoku region itself is located in the northern part of the Japanese archipelago and has one of the highest snowfalls on a global scale. Depending on these climatic characteristics, natural and artificial water cycle systems have been formed, and society and industry have developed.

The watershed management has been carried out according to the water cycle systems. On the other hand, as well known by IPCC AR6(2023) and other reports, global warming effects due to greenhouse gases have been pointed out. Even under the maximum effort scenario, a reasonable impact is expected. Therefore, climate change and changes in the hydrological cycle and water environment associated with climate change are also likely to occur. In particular, it has been pointed out that the impact of climate change on the water environment is greater in snowy regions (Kazama & Oki 2006). The Tohoku region is also expected to have a greater impact, and may be forced to modify its watershed management. In addition to basin flood control, which has been promoted in recent years, watershed management may need to focus on the conservation of the water environment.

To quantitatively estimate the impact of climate change and discuss specific measures, several models have been used to predict changes in temperature rise, precipitation, etc. (Hasebe and Kodera 2007, Zierl and Bugmann 2005, etc.). It is necessary to clarify (1) and (2) below in order to promote watershed management based on mitigation and adaptation to climate change as soon as possible, referring to various examples of previous studies.

1) Specific and detailed characteristics of the response of various environmental factors (topography, geology, land use, etc.) to climate change in the region

2) Systematization of the process to determine how some elements respond and how large the impact is, with comparisons among climates.

In this study, we compared the differences in the water environments of two large river basins in the Tohoku region, the Mogami River (hereafter referred to as "Mo") and the Abukuma River (hereafter referred to as "Ab"), which are located in different climatic zones, including snow covered areas. They are typical Japanese rivers that repeatedly flow through basins and constrictions. Mo is a first-class river with a length of 229 km (7th in Japan) and a basin area of 7,040 km^2 (9th in Japan), and flows into the Sea of Japan from Mount Nishi-Azuma (2,035 m above sea level). The Ab is a first-class river with a length of 239 km (6th in Japan) and a basin area of 5,400 km^2 (11th in Japan), and flows into the Pacific Ocean from Mount Asahidake (1,835 m above sea level).

2 Materials and methods

In this study, " water environment factors" such as land use, geology, and hydrology were determined using GIS. The hydrological data were sampled from field surveys. The Ab basin was basically surveyed once a month from October 2019 to September 2020, and the Mo basin from March 2021 to July 2023. A total of 61 sites were surveyed in Ab basin and 53 sites in the Mo basin, where air temperature (AT), water temperature (WT), electrical conductivity (EC), pH, and RpH were measured. The data of the major dissolved constituents were obtained from ion chromatography. We then compared the water environmental factors.

3 Results and discussion

The Ab basin is approximately 1,640 km^2 smaller than the Mo basin (Table 1). However, its population is about 400,000 larger than that of the Mo basin. Therefore, the land use in the Ab basin is dominated by areas with high human activity (e.g., building, paddy field and other agricultural land), which

The 12th International Symposium on Water Environment Systems
----- with Perspective of Global Safety   (Nov. 21st～22nd , 2024)

GP-RSS & SyDE
Tohoku University

Table 1 Comparison of basic information

	Abukuma	Mogami	Unit
Catchment area	5,400	7,040	km²
Length	239	229	km
Watershed shape factor	0.09	0.13	
River basin population	1,360	960	×1,000
Highest elevation	1835	2035	m
Average elevation	402.2	430.6	m
Land use			
Paddy fields	14.9	14.0	%
Other agricultural land	12.1	5.5	%
Forests	60.0	70.8	%
Buildings	7.3	5.1	%
Others	5.8	4.6	%
Geology			
No.1	Non-volcanic sedimentary rocks 43.9	Igneous rocks 29.2	%
No.2	Granite 31.4	Non-volcanic sedimentary rocks 28.9	%
No.3	Igneous rocks 22.9	Sediments 24	%
Survey results, main stream			
Average AT	19.1	17.1	℃
Average WT	15.9	12.9	℃
Average EC	175.9	108.7	µS/cm
Average pH	7.4	6.9	
Average RpH	7.6	7.2	

account for 34.3% of the total area, more than that of the Mo basin (24.6%). The mean elevation was lower in the Ab basin. Regarding the surficial geology, granite is widely distributed on the right bank of Ab, accounting for 31.4% of the total area. In the Mo basin, igneous rocks accounted for 29.2%.

The survey results show that AT, WT, EC, pH, and RpH are higher in the Ab basin; EC is 67.2 µS/cm higher, indicating a higher supply of ions to the main stream. Ion chromatography results indicate that there is both volcanic and human-caused ion supply in the two basins. The human-caused ion supply is considered to be significant in the upper reaches of the Ab basin and near Koriyama City, and in the Mo basin near Yonezawa City (Fig. 1). Domestic wastewater from urban areas and wastewater from sewage treatment facilities may have an impact (Yamagata and Kodera 2023). As for the volcanic ion supply, there are active volcanoes in both watersheds, and volcanic-derived substances are supplied to the rivers, causing an increase in EC in the main stream (Fig. 1). In particular, the increase in sulfate ions is particularly remarkable, and this is attributed to the merging of tributaries that contain large amounts of sulfate ions into the main stream. The pH also changed, with Ab dropping by 0.2 and Mo dropping by 0.25. Moreover, in the Mo basin, EC clearly decreased during the snowmelt season, indicating that snow accumulation during winter had a considerable impact on water quality (Fig. 2), while the Ab basin showed no significant changes during the snowmelt season. These results indicate that although Ab and Mo have similar topographical features, they differ in water quality, with Ab being affected by human influence > natural influence and Mo by natural influence > human influence. These differences are likely to be reflected in the water quality changes that are expected to result from climate change, and we believe that our findings are important for effective watershed management.

4 Conclusions

Although the Abukuma and Mogami Rivers have similar topographical features, their water quality characteristics differ due to human activity and natural environmental
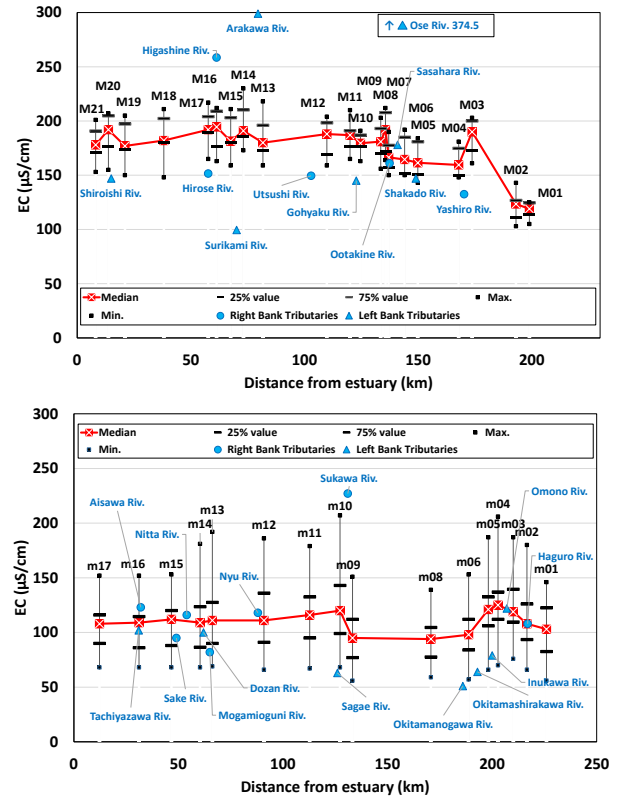
Fig. 1. Longitudinal changes in EC in the main stream Abukuma River (above) and Mogami River (below)
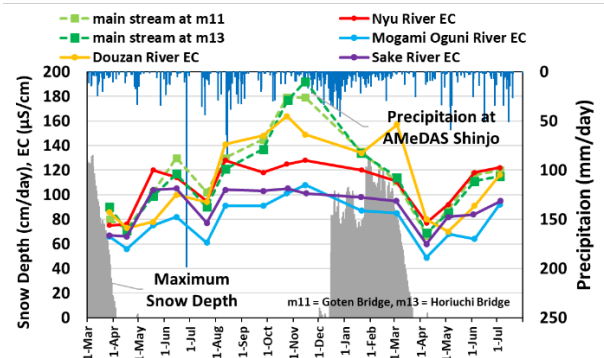
Fig. 2. EC changes during the snowmelt season in the Mogami River basin near Shinjo City

influences. This suggests the possibility of different effects of climate change. We would like examine these influences in detail in the future.

Reference

[1] Kazama, S. and Oki, T., Impacts of Global Warming on Water Resources, Chikyu Kankyo, (2006) 11, 1, 59-65.
[2] Hasebe, T. and Kodera, K., Runoff Characteristics of the Mogami River, Hydrography Research Report, (2007) 11, 29-40.
[3] Zierl, B. and Bugmann, H., Global change impacts on hydrological processes in Alpine catchments, Water Resources Research, (2005) 41, 2, 1-13.
[4] Yamagata, E. and Kodera, K., Watershed characteristics and river water quality in the Abukuma River basin, Journal of the Japanese Society of Physical Hydrology, (2023) 5, 1, 3-15.

The 12th International Symposium on Water Environment Systems
----- with Perspective of Global Safety   (Nov. 21st ~ 22nd , 2024)

GP-RSS & SyDE
Tohoku University

Analysis of Future Changes and the Impact of Historical Warming on Localized Heavy Rainfall Using the Pseudo-Global Warming Method

○ Ryotaro TAHARA[1*], Yusuke HIRAGA[1] & So KAZAMA

[1] Department of Civil and Environmental Engineering, Tohoku University, Sendai 980-8579, Japan.
[*]E-mail: tahara.ryotaro.q7@dc.tohoku.ac.jp

Abstract

In August 2022, extreme rainfall impacted Japan's Tohoku and Hokuriku regions, causing record-breaking precipitation and significant damage, particularly in Niigata and Yamagata Prefectures. Like this localized heavy rainfall with "Senjo-Kousuitai", the frequency and intensity of heavy rainfall in northern Japan are expected to increase with climate change. This study aims to analyze future changes in localized extreme rainfall and the effects of historical global warming on the August 2022 event using the pseudo-global warming (PGW) method. The PGW approach simulates future and historical climate scenarios by adding climate deltas, derived from global climate model (GCM) outputs, to initial and boundary conditions. The study employed the WRF-ARW model to simulate rainfall in the Arakawa River Basin under different climate conditions: present-day (CTRL-run), future projections (2050s-MRI-run, 2090s-MRI-run), and historical warming (1860s-MRI-run). Results indicate that maximum hourly rainfall increased by 24.5% in the 2090s-MRI-run compared to the CTRL-run, with enhanced cumulonimbus development due to elevated atmospheric water vapor. Historical warming may have led to a 22.9% increase in 48-hour accumulated rainfall in this rainfall event that occurred in 2022. These findings provide insights into climate change impacts on extreme rainfall and inform disaster management strategies for northern Japan.

Keywords: Weather and Research and Forecasting model (WRF); Senjo-Kousuitai; Climate Change.

1 Introduction

In August 2022, extreme rainfall occurred in Japan's Tohoku and Hokuriku regions, particularly affecting Niigata and Yamagata Prefectures. Known as "Senjo-Kousuitai," the band-shaped heavy rainfall led to record-breaking precipitation levels, exceeding 600 mm in 24 hours in some areas [1]. The event was driven by a quasi-stationary front and low-pressure system over the Sea of Japan, with warm, moist air flowing from the Pacific, resulting in significant flooding and damage, especially in the Mogami River Basin. Northern Japan has experienced a rise in heavy rainfall events in recent years, highlighting the need for better understanding and preparedness against climate-related changes.

Future projections suggest that northern Japan is likely to experience more frequent and intense rainfall because of climate change, with rising air and sea surface temperatures in the region contributing to increased levels of atmospheric water vapor [2]. Despite these projections, northern Japan remains inadequately prepared for such disasters compared to western regions like Kyushu, because it has relatively less experience with historical heavy rainfall events.

The study used the pseudo-global warming (PGW) method to analyze future changes in localized heavy rainfall, focusing on the August 2022 event. This method allows for event-specific climate change impact analysis and helps estimate future rainfall trends in regions with limited historical data. The PGW approach was also applied to assess the influence of historical global warming on the intensity of this extreme rainfall, providing insights into how past warming has contributed to the event's severity. The findings aim to enhance understanding of climate change effects on extreme rainfall and improve disaster preparedness in northern Japan.

2 Materials and methods

The study utilized the Advanced Research version of the Weather Research and Forecasting Model (WRF-ARW) version 4.1.2, a fully compressible non-hydrostatic mesoscale weather forecast model. Fig.1. shows the computational domains and the target basin. Three computational domains with two inner domains were configured, with resolutions of 12 km, 4 km, and 1.3 km from the outermost to the innermost domain. The analysis focused on the Arakawa River Basin in Niigata Prefecture, where flooding and landslides occurred.

Initial and boundary conditions for the model were based on data from the NCEP Global Data Assimilation System (GDAS) FNL operational global analysis, which offers data from July 2015 onwards at 6-hour intervals, with 0.25° horizontal resolution and 34 vertical levels. Physics parameterization schemes were chosen according to a sensitivity analysis by Hiraga and Tahara (2024) [3], which aimed to reconstruct heavy rainfall events in northern Japan. The Goddard 4-ice scheme and Grenier–Brethrton–McCaa scheme were selected as the microphysics and planetary boundary layer schemes, respectively [4, 5]. The Kain-Fritsch cumulus parameterization was used for the coarser outer domain (d01) where explicit cumulus convection was not feasible.
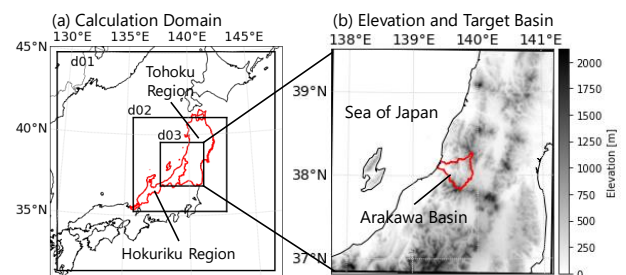

Fig. 1. (a) Calculation domain and (b) target basin.

The 12th International Symposium on Water Environment Systems
----- with Perspective of Global Safety   (Nov. 21st ~ 22nd , 2024)

GP-RSS & SyDE
Tohoku University

The pseudo-global warming (PGW) method was used to create initial and boundary conditions (ICBC) for future and historical climate scenarios by adding the differences between current and future or historical climates ("climate delta") to the ICBC. This method calculates the climate delta using a global climate model (GCM) outputs and adds it to the ICBC in a numerical model, generating "warming experiments." Comparing these experiments with a reconstructed event (CTRL-run) allows for evaluating the impact of global warming on specific weather events. The study used future climate estimation data of MRI-ESM2-0 under the SSP2-4.5 scenario, which predicts a 3.0°C global temperature rise by the end of the 21st. This scenario is considered more realistic compared to extreme ones like SSP5-8.5. As historical climate data, the same GCM's simulation output from 1850 to 2014 was used. Climate differences included monthly mean air and sea surface temperatures, while relative humidity and wind speed were kept constant, as previous research indicates no significant future changes in these variables. The monthly mean future and historical climate deltas were computed for the 2041–2060 period (2050s), 2081–2100 period (2090s), and 1850–1869 period (1860s) periods as the differences from the 2015–2024 period (2020s). Compared to "CTRL-run", each PGW simulation result is referred to as the "1860s-MRI-run", "2050s-MRI-run", and "2090s-MRI-run".

3 Results and discussion

Fig.2. shows the time series of basin-average hourly precipitation for the Arakawa River Basin. Compared to the CTRL-run, the maximum hourly precipitation increased in the 2050s-MRI-run and 2090s-MRI-run. Notably, the maximum hourly precipitation in the 2090s-MRI-run showed a significant increase compared to the CTRL-run (24.5%). The time series patterns did not exhibit a linear increase or decrease relative to the CTRL-run, showing variability in both spatial and temporal patterns. Additionally, the 48-hour accumulated precipitation increased by 3.6% from the CTRL-run to the 2050s-MRI-run, while the accumulated precipitation in the 2090s-MRI-run decreased compared to the CTRL-run (not shown). The hourly precipitation for the 1860s-MRI-run was similar to that of the CTRL-run, but historical warming may have led to a 22.9% increase in 48-hour accumulated rainfall in this rainfall event that occurred in 2022.
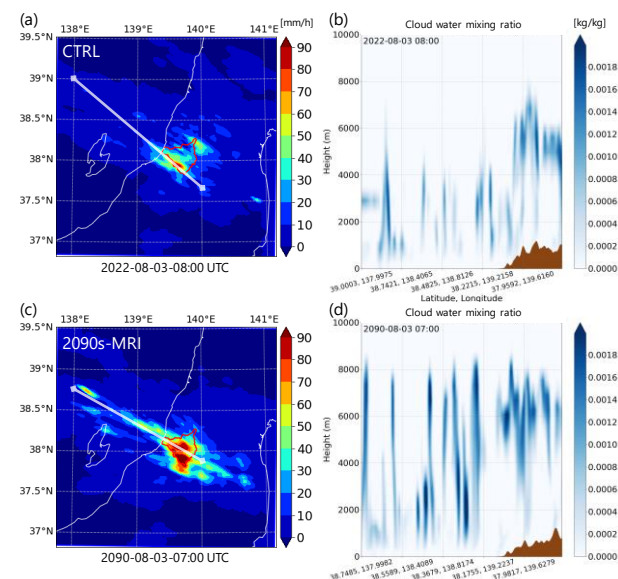
Fig.3. shows the distribution of maximum hourly precipitation for the CTRL-run and 2090s-MRI-run, along with vertical cross-sections of the cloud water mixing ratio. Compared to the CTRL-run, the 2090s-MRI-run exhibits a higher development of cumulonimbus clouds. This enhancement in cumulonimbus development may be attributed to the increase in water vapor associated with warming and strong convergence (not shown). On the other hand, convergence in the 2090s-MRI-run did not persist in the Arakawa River Basin and shifted southward of the basin, resulting in no contribution to the increase in accumulated precipitation.

Reference

[1] Japan Meteorological Agency (JMA). 2022. Heavy rainfall caused by the front from August 1 to 6. https://www.data.jma.go.jp/obd/stats/data/bosai/report/2022
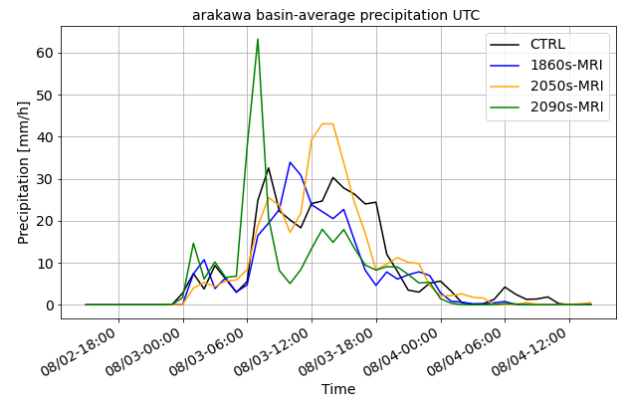
Fig. 2. Basin-average hourly precipitation (Arakawa River).

Fig. 3. (a) (c) maximum hourly precipitation distribution, (b) (d) vertical cross-section of cloud water mixing ratio ((a) (c) CTRL-run, (b) (d) 2090s-MRI-run).

/20220822/jyun_sokuji20220801-0806.pdf (accessed 11 July 2024).

[2] Naka, Y., & Nakakita, E. 2023. Comprehensive future projections for the line-shaped convective system associated with Baiu front in Japan under RCP scenarios using regional climate model and pseudo global warming experiments. Frontiers in Earth Science, 11, 1093543.

[3] Hiraga, Y., & Tahara, R. 2024. Sensitivity of Localized Heavy Rainfall in Northern Japan to WRF Physics Parameterization Schemes. Available at SSRN 4901639.

[4] Tao, W. K., Wu, D., Lang, S., Chern, J. D., Peters‐Lidard, C., Fridlind, A., & Matsui, T. 2016. High‐resolution NU‐WRF simulations of a deep convective‐precipitation system during MC3E: Further improvements and comparisons between Goddard microphysics schemes and observations. Journal of Geophysical Research: Atmospheres, 121(3), 1278-1305.

[5] Grenier, H., & Bretherton, C. S. 2001. A moist PBL parameterization for large-scale models and its application to subtropical cloud-topped marine boundary layers. Monthly Weather Review, 129(3), 357-377.

The 12th International Symposium on Water Environment Systems
----- with Perspective of Global Safety   (Nov. 21st～22nd , 2024)

GP-RSS & SyDE
Tohoku University

Effects of wetland loss on the regional temperature: Case study of 2023 heatwave event in Southeast Asia

○ Chang LIU[1*], Yusuke HIRAGA[1] & So KAZAMA[1]

[1] Graduate School of Civil Engineering, Tohoku University, Sendai 980-8579, Japan
*E-mail: chang.liu.t5@dc.tohoku.ac.jp.

Abstract

Wetland loss has been a problem over the last few centuries due to the development of human society. Wetlands not only have important effects on both the local ecosystem and hydrological cycle but also have a significant impact on the regional climate. In 2023, during the summer season, a historical heat wave hit the Asia area with many countries recording the highest temperature in recent history. While the wetland loss in the area may not be the leading factor that caused this event, it certainly contributed, and it is important for us to estimate the potential effect. This study utilizes numerical modeling approach to represent the effect of wetlands in regional climate. Two approaches to represent wetland inside WRF model were proposed. The result shows a significant cooling effect up to 4 to 6 degrees kelvin through the representation of the wetland. The result of this study can become part of the guideline for future wetland development plans in the world.

Keywords: wetland loss, heat wave, regional climate, Noah-MP, WRF Model

1 Introduction.

Heatwaves have become widespread across the world and more intense over the past decades due to the progress of global warming. A heatwave is a prolonged period of excessively hot weather, typically accompanied by high humidity. Heatwaves have significant impacts on human health, infrastructure, agriculture, and the environment. Heat waves can be more devastating in developing countries like Cambodia, where most of the people are physical workers and farmers. In 2023 extreme heatwave struck Southeast Asia where all the countries broke their highest temperature records with measurements exceeding 42 °C, and Thailand set the region's new record of 49 °C. If extreme heatwave events become more and more often in the future, it would be beneficial for us to understand the main factors causing heatwaves. This study aims to find the relationship between wetlands and heatwave events using a numerical modelling approach.

2 Materials and methods

2.1 WRF model

This study used the Advanced Research version of the Weather Research and Forecasting Model (WRF(ARW)), version 4.1.2 coupled with Noah-Mulitiparameterization Land Surface Model (Noah-MP LSM) to simulate the surface physical condition at the same time.

2.2 Study Area

This study focuses on Cambodia in the lower Mekong region where the loss of wetland has been significant due to the development of the city and farmland in the country. With the lack of observation weather data in the area, numerical model could be a viable approach to analyze the regional climate conditions. The wetland cover data is taken from the report provide by WWT in lower Mekong region in Cambodia. (WWT 2023)

2.3 Input data

ERA5 global reanalysis data was used for the model input for both atmosphere and surface requirements. The ERA5 dataset has a resolution of 31 km whereas the ERA5-Land dataset has a resolution of 9km. It is one of the ideal datasets to use in the WRF simulation, especially in areas like Cambodia where gridded weather data is very limited.

2.4 Model calibration

Observation data is very limited in the Cambodia area. Since the simulated heatwave event is very recent, there are no available analyzed data as well. In this case, hourly temperature data from the Phnom Phen Airport which located in the city of Phnom Phen north to the lower Mekong wetland area was used to compare with the model output.

The model setting for the calibration run is listed in Table 1.

Table 1. Model settings for the calibration

Number of domains	2
Resolution	2500m (domain d01) 500m (domain d02)
Number of grid points	184x184 (domain d01) 256x261 (domain d02)
Map projection	Mercator
Land surface physics	Noah-MP LSM
Simulated period	2023/5/1-2023/5/30

In this case, hourly temperature data from the Phnom Phen Airport was used to compare with the model output. Fig. 1. shows the comparison between the modelled surface temperature result and the observation data from the airport station over the hottest day within the one-month simulated period. The correlation coefficient between the two data sets over a month is 0.89, which shows a strong correlation between the two data sets
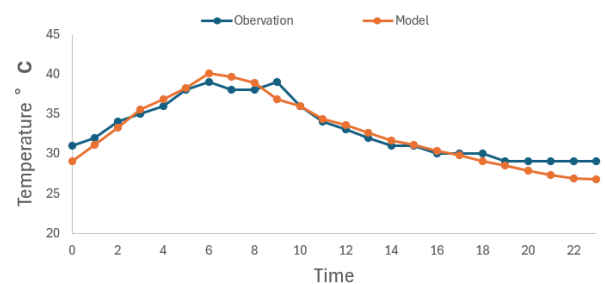
Fig. 1. Temperature comparison between model results and observation at Phnom Phen Airport station

2.5 Wetland in WRF model

The 12th International Symposium on Water Environment Systems
----- with Perspective of Global Safety   (Nov. 21st ~ 22nd , 2024)

GP-RSS & SyDE
Tohoku University

Wetland is not well represented in the WRF model as shown by Zhang et al. (2022). They proposed a wetland modification in the WRF model based on a wetland water capacity calculated through elevation. However, this approach does have the drawback of not being able to define wetland area manually. This study proposes two approaches to represent wetland through manipulating the land use and soil moisture parameters inside WRF model. The first approach assumes the wetland to have high soil moisture with no surface water. In this approach the land use of the wetland area is changed from the default forest and cropland to wetland classification in the model, and the initial soil moisture in the area is changed to 100%. The second approach assumes the wetland to be a waterbody with surface water. In this approach the land use is changed to waterbody for the wetland area.

The model setting for the wetland scenarios are listed in Table 2. Three simulations were performed under this base setup. The first simulation is performed without any modifications to serve as a baseline for the model's performance. The second and third simulation uses the first and second approach to represent wetland in two different ways. Both approaches to represent wetland as well as the baseline simulation use the same basic setups to keep the results consistent. The domain setup for the simulation is shown in Fig 2. The setup to includes the wetland area in lower Mekong region in Cambodia as provided in the WWT report in domain d02.

**Table 2. Model settings for the wetland scenarios**

| Number of domains	3
Resolution	7500m (domain d01)
	1500m (domain d02)
	500m (domain d03)
Number of grid points	100x100 (domain d01)
	121x121 (domain d02)
	100x100 (domain d03)
Map projection	Mercator
Land surface physics	Noah-MP LSM
Simulated Period	2023/5/5-2023/5/20
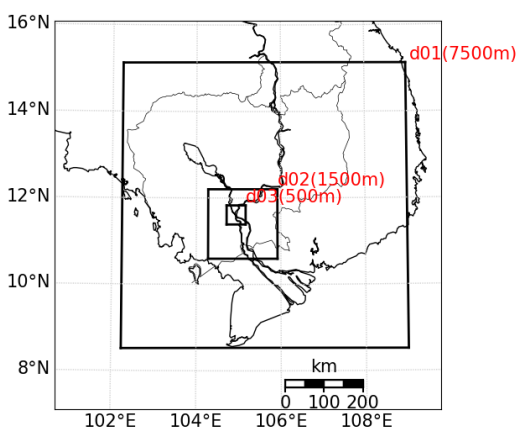
Fig. 2. Domain setup in the model

3 Results and discussion

Surface temperature difference between the baseline simulation and the two wetland approaches at the time where the highest temperature was observed at the Phnom Phen Airport during the heatwave in domain d02 is shown in Fig. 3 and Fig. 4. The wetland area is shown in the black outlines.
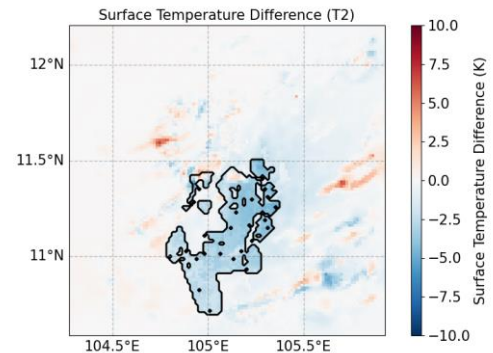
Fig. 3. Surface temperature difference between the baseline simulation and the first wetland approach
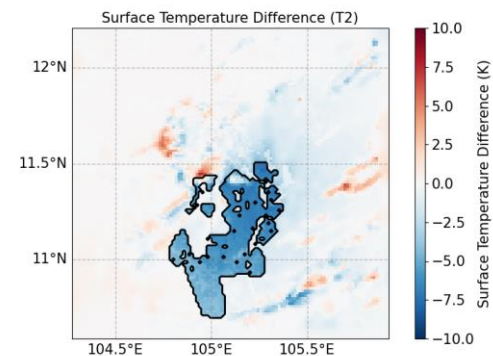
Fig. 4. Surface temperature difference between the baseline simulation and the second wetland approach

From the result we can see that the first wetland approach results in a temperature reduction in the wetland area ranging from 2-4 degrees kelvin whereas the second wetland approach results in a reduction ranging from 4-6 degrees kelvin. This difference is due to the soil moisture in the wetland area during the simulation which is the biggest contributing factor to surface temperature reduction. Since the water in the soil increased the heat capacity of the ground and it's able to soak up the heat that would otherwise go to the surrounding atmosphere. In the first approach, the soil moisture during the simulation is around 40% in the wetland area whereas in the second approach soil moisture stained at 100%.

4 Conclusions

From the result we can observe a major cooling effect through the representation of wetland in the WRF model. These approaches can be used to evaluate the effect of wetlands in regional temperature. Furthermore, both approaches to represent wetland displayed a radiating effect outside the wetland area. This radiating effect could be further analyzed to evaluate the cooling effect of wetland to the surrounding area.

Reference

[1] Zhang, Z., Chen, F., Barlage, M., Bortolotti, L. E., Famiglietti, J., Li, Z., ⋯ Li, Y. (2022). Cooling effects revealed by modeling of wetlands and land‐atmosphere interactions. Water Resources Research, 58(3). doi:10.1029/2021wr030573

[2] WWT, 2023. The status of wetland habitats in the Cambodia Lower Mekong Delta. WWT, Slimbridge, UK.

The 12th International Symposium on Water Environment Systems
----- with Perspective of Global Safety   (Nov. 21st~22nd , 2024)

GP-RSS & SyDE
Tohoku University

High-resolution spatial estimation of soil moisture using UAV aerial photography and machine learning algorithms

○ Takuya MATSUMOTO[1*], Yusuke HIRAGA[1] & Shunsuke AITA[1]

[1] Department of Civil Engineering, Environmental Tohoku University, Miyagi 980-8579, Japan.
*E-mail: matsuoto.takuya.s2@dc.tohoku.ac.jp.

Abstract

This study utilized UAV aerial photography and machine learning algorithms to estimate the spatial distribution of soil moisture content at high resolution. The measurements were performed at the vineyard with steep slope in Miyagi, Japan (Ryomi Vineyard & Winery). The soil moisture content data from 55 sites acquired by TDR measurements were augmented to 5,500 using the UAV aerial photography. Based on the large number of samples, the random forest algorithm was applied to estimate the spatial distribution of soil moisture content with high accuracy, resulting in the determination coefficient of 0.96.

Keywords: *soil moisture; machine learning; UAV; viticulture*

1 Introduction

The management of water content is crucial for the healthy growth of crops, it is desirable to accurately estimate the soil moisture content of agricultural land. In particular, the growth of wine grapes is strongly influenced by soil moisture content. High quality grapes can be produced under low moisture, or high-water stress conditions. Conventional methods for estimating soil moisture in the field include deterministic methods[1] such as solving the Richards equation based on Darcy's law and the equation of continuity, and methods based on water balance calculations[2]. However, the application of the Richards equation requires the specification of representing moisture characteristics (e.g., vanGenuchten model) and the establishment of ground surface boundary conditions, which are difficult to set in actual fields with heterogeneous soils[3]. In methods based on water balance calculations, we essentially attempt to estimate soil moisture by building a field-scale tank model, making it difficult to estimate the detailed spatial distribution in the field.

In recent years, sensors that measure permittivity, such as the TDR (Time Domain Reflectometry) method, became common. There is a lot of research that has been conducted on estimating soil moisture content in the field by applying machine learning algorithms based on meteorological conditions and other factors[3][4]. There have been many attempts to estimate soil moisture in the field using machine learning algorithms, but there have been few examples of such estimations being conducted for wine grapes vineyards.

This study aimed to construct a model to estimate the spatial distribution of soil moisture content in wine grapes vineyards with high resolution by utilizing UAV aerial images and machine learning algorithms for limited TDR observations.

2 Region and methods

2.1 Region and measurements

This study focuses on Ryomi Vineyard & Winery in Taiwa town, Kurokawa district, Miyagi Prefecture. Aerial images with UAV and soil moisture measurements with TDR were conducted on May 17, 2023. In this study, a MATRICE 200 equipped with the MicaSense's RedEdge-M sensor was used as the UAV. Multispectral images were acquired for
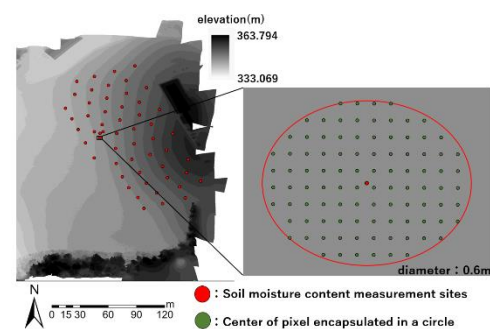
Fig. 1. Expanded soil moisture content measurement

blue (B: 450 nm), green (G: 560 nm), red (R: 650 nm), Rededge (RE: 730 nm), and near infrared (NIR: 840 nm). GNSS (Global Navigation Satellite System) surveying was conducted using the Promark100 (manufactured by GEOSURF) with the rapid static method. The latitude, longitude, and elevation data of the ground control markers were acquired using this method, and the elevation distribution of the target field was obtained. Soil moisture measurements were conducted at a depth of approximately 30 cm within the field. 55 sites were selected in a grid pattern within the target area to measure soil moisture content (**Fig. 1**).

2.2 Methods

In this study, we attempted to extend the dataset for the application of machine learning algorithms. Following the method proposed by Morishita and Ishizuka[4], a circular buffer with a diameter of 0.6 meters was created around each measurement point. Assuming that the soil moisture content within each buffer was uniform, the soil moisture measurement data were expanded accordingly.

In this study, A random forest regression model was constructed using the soil moisture measurement dataset. The objective variable was the spatial distribution of soil moisture content within the field, and the explanatory variables were the digital values of blue, red, green, rededge, and near-infrared images obtained by UAV aerial photography and elevation. We constructed a random forest learner by splitting dataset into two subsets: 80% of the data are used for training, and 20% of the data are used for testing. We calculated the determination coefficient (R^2) as

The 12th International Symposium on Water Environment Systems
----- with Perspective of Global Safety   (Nov. 21st ~ 22nd , 2024)

GP-RSS & SyDE
Tohoku University

Table 1. Accuracy and feature importance of model for estimating spatial distribution of soil moisture content

determination coefficient	feature importance					
	B	G	R	RE	NIR	elevation
0.96	0.07	0.07	0.04	0.03	0.03	0.80

a measure of model accuracy. Additionally, the spatial distribution of the estimated soil moisture content was compared with the distribution of NDVI (the Normalized Difference Vegetation Index). The NDVI was calculated using the following equation (1).

$$NDVI = \frac{NIR - R}{NIR + R} \quad (1)$$

NIR: Pixel values in the near-infrared band
R: Pixel value of red band
 The NDVI values range from -1 to 1, with values closer to 1 indicating higher vegetation activity.

3 Results and discussion

  The determination coefficient and feature importance of the explanatory variables are shown in **Table 1**. The determination coefficient was 0.96, indicating that the model can estimate soil moisture content with high accuracy. From the feature importance shown in **Table 1**, it is evident that elevation is the most critical parameter. This is consistent with the hypothesis that information on elevation at each point in the field is important for estimating soil moisture content in sloped vineyards. This insight will be valuable for applying similar methods to vineyards in future studies.
  Fig. 2 shows the estimated spatial distribution of soil moisture content. The elevation within the field varies significantly, ranging from approximately 333 meters to 360 meters, and the soil moisture content changes according to the degree of slope. Areas with higher soil moisture content from north to south correspond to locations where the slope becomes gentler at the base of the incline. Additionally, areas in the southeast of the study region with lower soil moisture content are associated with convex topography, suggesting good drainage. Furthermore, in the northwest of the study area, it can be observed that in addition to elevation, the variation in NDVI corresponds to the variation in soil moisture content. This suggests that areas with less active vegetation may experience higher ground temperatures and greater surface evaporation. However, further detailed analysis is required to fully understand the relationship between NDVI and soil moisture content. In the future, it will be necessary to validate how the model developed in this study generalizes across different seasons and weather conditions. For instance, in viticulture, the water requirements before and after the veraison stage differ, making it crucial to develop a model that can be applied universally across different growth stages.

4 Conclusions

  This part is Conclusions. This study aimed to develop a model that estimates the time series and spatial distribution of soil moisture content in a vineyard for wine production with high resolution by utilizing UAV aerial imagery and machine learning algorithms, despite limited TDR observations and easily measurable meteorological
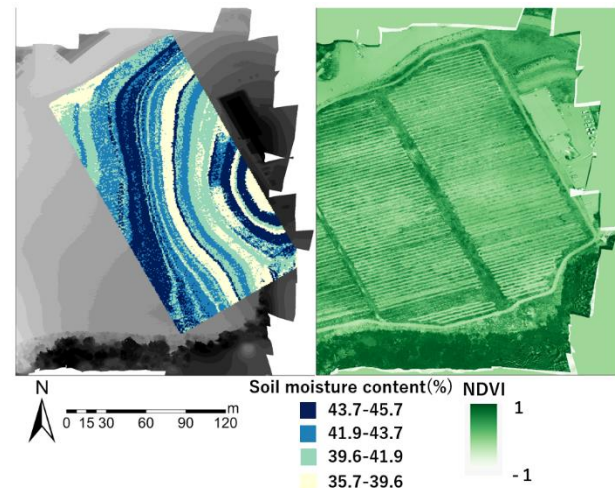
Fig. 2. Spatial distribution estimates of soil moisture content and NDVI distribution

conditions. By combining soil moisture content data obtained from TDR measurements with UAV observations and applying the Random Forest algorithm, a model was developed that estimates the spatial distribution of soil moisture content with high accuracy, achieving a coefficient of determination of 0.96. In the developed spatial distribution estimation model, elevation was identified as the most important parameter. This finding is consistent with the hypothesis that information on the elevation at each point in the field is crucial for estimating soil moisture content in fields with steep slopes. In the future, we aim to propose a method for accurately and generally estimating soil moisture content by developing higher-precision soil moisture estimation models and evaluating their applicability to other vineyards for wine production.

Reference

  [1] Sugawara, T., Sayama, T. and Takara, K.: An analytical solution of Richard's equation for soil with groundwater table, Journal of the Japan Society of Civil Engineers Ser B1 (Hydraulic Engineering), Vol. 74, Issue 4, pp. I_1-I_6, 2018.
  [2] Ohta, K. and Shinogi, Y.: Soil moisture balance analysis of upland field by the tank model method, Journal of the Agricultural Engineering Society, Vol. 58, Issue 7, pp. 675-679, a1, 1990.
  [3] Moroizumi, T. and Kubota, S.: Prediction of soil water content using multiple regression model with time series data, Transactions of The Japanese Society of Irrigation, Drainage and Rural Engineering, Vol. 82, Issue 1, pp. 47-52, 2014.
  [4] Morishita, M. and Ishitsuka, N.: Estimation of soil moisture distribution in soybean field using UAV, Journal of the Japanese Agricultural Systems Society, Vol. 36, Issue 4, pp. 55-61, 2020.

The 12th International Symposium on Water Environment Systems
----- with Perspective of Global Safety   (Nov. 21st ～ 22nd , 2024)

GP-RSS & SyDE
Tohoku University

Modeling The Interaction of Flood Hazard and Society in Citarum Watershed, Indonesia: A Socio-hydrological Perspective

○ Muthiah SADIDAH[1*], Daisuke KOMORI[1]

[1]Graduate School of Environmental Studies, Tohoku University, Miyagi 980-8572, Japan.
[2]Green Goals Initiative Laboratory, IRIDES building, Tohoku University, Miyagi 980-8572, Japan.
[*]E-mail: Muthiah.sadidah.t2@dc.tohoku.ac.jp

Abstract

In this study, the SH modeling of flooding in Karawang has provided valuable insights into the memory dynamics and impacts of flood events. Two important effects related to flood damage, the "adaptation effect" and the "levee effect," were investigated. The adaptation effect was found in the target area driven by accumulated societal memory of past flood events. On the other hand, the reduction in flood memory led to a slight increase in damage when river flooding occurred in 2019 after the absence of floods following the 2016 event. Therefore, the levee effect was not found instead the adaptation effect remained in the target area. In addition, in the process of this study, a new method of extracting memory loss rate has been proposed. This method was conducted using significance tests focusing on memory using a certain initial value of memory loss rate as a benchmark. This method resulted in a range of memory loss rates of this study (0.05 until 0.42). Using this range with memory loss rates of previous study to be compared with GDP (Gross Domestic Product) gave this study new insights. This comparison involved looking at how economic factors, as indicated by GDP, connect with the way people remember flood events. This analysis helps us gain a deeper understanding of how economic conditions influence the way people remember floods, and it provides valuable insights into the wider socio-economic consequences of flood memory patterns.

Keywords: socio-hydrological modeling; socio-hydrology; flood hazard; society.

1 Introduction

Based on National Agency for Disaster Countermeasure of Indonesia (BNPB), Karawang regency is the most flooding-prone area in Citarum watershed with the highest number of flood events compared to the upper areas. Recent research has explored the impact of human interventions to floods including urbanization, land-use change, etc [Di Baldassarre et al., 2009; Heine and Pinter, 2012; Remo et al., 2012]. However, all these works have been looking only at one side of the interaction between floods and societies [Di Baldassarre et al., 2013].

This study aims to develop a socio-hydrology model to quantitatively explain the coevolution of human-flood systems. We proposed a dynamic analysis using socio-hydrological (SH) model to Indonesia. The SH model was applied in Karawang Regency of Citarum Watershed which is known as the largest watershed in West Java, Indonesia. In addition, no prior research has employed the SH model in Indonesia, specifically within the Karawang Regency.

2 Materials and methods

This research used hydrological (water level) and societal data (population data); this research also used historical flood event data derived from Based on National Agency for Disaster Countermeasure of Indonesia (BNPB).

The SH model, developed by Di Baldassarre in 2015, used a set of differential equations to understand the interactions between human activity, technology, and flooding. The model uses the variable F to represent the severity of a flood event, the variables and parameters used in Equations (1) are W: high water level, H_-: flood protection level before the flooding event, ξH: proportion of flood level enhancement due to the presence of levees and αH: parameter

$$F = 1 - \exp\left(-\frac{W + \xi_H H_-}{\alpha_H}\right) if\ W + \xi_H H_- > H_- \quad (1)$$

$$\frac{dD}{dt} = \rho_d\big(1 - D(1 + \alpha_D M)\big) - \Delta(\Psi(t))FD_- \quad (2)$$

$$\frac{dH}{dt} = -\Delta(\Psi(t))R - K_T H \quad (3)$$

$$\frac{dM}{dt} = \Delta(\Psi(t))FD_- - \mu_S M \quad (4)$$

Fig.1. Socio-hydrological modeling equations

related to the slope of the floodplain and the resilience of the human settlement. The Equations (2)– (4) show the dynamics of the human-floodplain system. The D, H and M represent the population density, flood protection level and flood memory of the community respectively. The parameters in the set of equations are ρD: mean relative growth rate, αD: ratio preparedness/awareness, κT : protection level decay rate and μS : memory loss rate, $\Delta(\Psi(t))$: a function which is always 0 and becomes 1 in flood occasion.

3 Results and discussion

Figure 2(b) provides a detailed view of the cyclical dynamics of flood memory ("M") within communities, reflecting changes in awareness and response to flood risks. The graph depicts two main phases: the amplification phase (marked with blue arrows) and the attenuation phase (highlighted with green arrows). In the amplification phase, flood memory increases, often seen in communities with high-risk awareness following recent flood events. These communities are likely to retain or even enhance their vigilance towards flood preparedness. Conversely, during the attenuation phase, flood memory decreases, typically

The 12ᵗʰ International Symposium on Water Environment Systems
----- with Perspective of Global Safety   (Nov. 21st ～ 22ⁿᵈ , 2024)

GP-RSS & SyDE
Tohoku University

occurring in communities with lower awareness or a diminished focus on flood risks, possibly due to a lack of recent flood events or a fading of past experiences over time. The results of SH model applied in Karawang Regency show that flood events happened in 2013 and 2014 result in damage ratio (the ratio of people evacuated and modelled flood damage) around 1. These consecutive flood events accumulated societal memory and lead to a decreased damage resulted in 2016 flood event with damage ratio 0.43. Consequently, it is speculated that the damage from river flooding has reduced due to the accumulation of memories as the effect of flood events in 2013 and 2014, this situation is called adaptation effect. On the other hand, a decrease in flood memory occurred in 2019, this is resulted by no flood events after 2016 flood. In addition, it can be seen in Figure 2, a river flooding occurred in 2020 has damage ratio 0.5 which is slightly increased from damage ratio in 2016 (0.43). However, in comparison to damage change that occurred in adaptation effect, the decrease of memory in this case is not significant. Therefore, it is speculated that there is no levee effect found in this study as society still maintains the adaptation effect.

This research used a significance test to assess whether the observed changes in the memory loss rate, as determined by my model, genuinely reflect variations in the damage ratio or
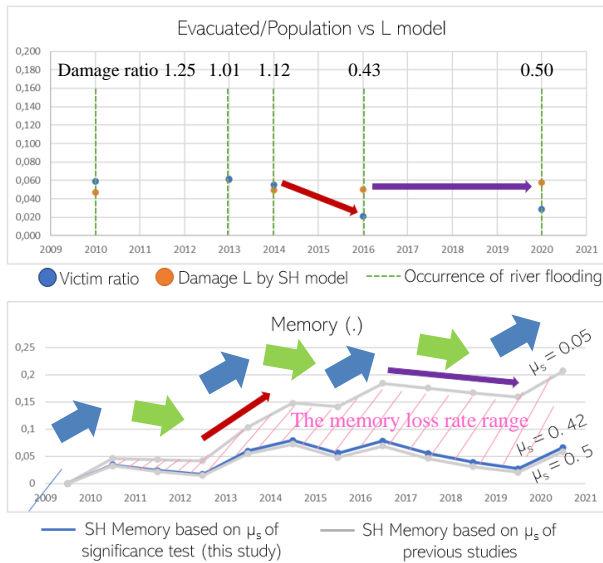

Fig.2. SH model results and memory loss rate range

if they could have occurred randomly. The findings indicate that the memory loss rate of this study ranged from 0.05 to 0.42. This calculation of memory loss rate range has not been applied in the previous study and one of the findings in this study. The visualization can be seen in Figure 2.

This study examines the fading of memory regarding past flood events in relation to the economic status (GDP) of different countries, interpreted through a socio-hydrological perspective. Figure 3 categorizes these countries into two groups based on their GDP levels. In lower-GDP countries, memory loss rates concerning flood events are generally low, indicating that communities tend to remember floods more vividly. This can be attributed to the fact that these countries prioritize economic growth and often lack robust flood protection systems. Socio-hydrological models reveal that, in the absence of effective flood defenses, communities face

recurrent flood impacts, which embed these events deeply in social memory. The limited infrastructure in these areas makes flood experiences an enduring part of daily life.

As GDP increases, a shift in socio-hydrological patterns is observed. In higher-GDP countries, the tendency to forget past flood events is more pronounced. Socio-hydrological models suggest that this is due to the presence of advanced flood protection systems, which reduce the frequency and severity of flood events. With greater security, the immediate need to retain memories of floods diminishes, leading to a gradual fading of these memories. Furthermore, these safer regions often attract residents from other areas who lack prior
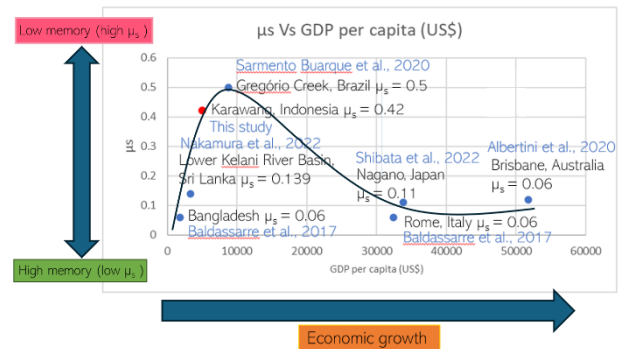

Fig.3. Memory loss rate Vs GDP per capita (US$)

experience with local flooding, accelerating the overall decline in flood memory among the population.

Interestingly, beyond a certain GDP threshold, the memory loss rate appears to decrease again. This suggests that in highly developed countries with strong economies, there is a renewed focus on flood risk awareness and disaster preparedness. Advanced initiatives such as flood education, early warning systems, and land-use policies are likely to contribute to a reinforced collective memory of flood risks. This final stage highlights how economically stable countries invest not only in flood prevention but also in maintaining public awareness of flood risks, demonstrating a more complex socio-hydrological relationship between economic growth, flood protection, and memory retention.

4 Conclusions

Overall, adaptation effect has been found in this study. Moreover, in the process of this study, a new method of extracting memory loss rate has been proposed. This method was conducted using significance test. Using this range with memory loss rates of previous study to be compared with GDP (Gross Domestic Product) gave this study new insights about how economic factors, as indicated by GDP, connect with the way people remember flood events.

Selected References

[1] Di Baldassarre, G., Viglione, A., Carr, G., Kuil, L., Salinas, J.L. and Blöschl, G., 2013. Socio-hydrology: conceptualising human-flood interactions. Hydrology and Earth System Sciences, 17(8), pp.3295-3303.
[2] Di Baldassarre, G., Viglione, A., Carr, G., Kuil, L., Yan, K., Brandimarte, L. and Blöschl, G., 2015. Debates—Perspectives on socio-hydrology: Capturing feedbacks between physical and social processes. Water Resources Research, 51(6), pp.4770-4781.

The 12th International Symposium on Water Environment Systems
----- with Perspective of Global Safety   (Nov. 21st ~ 22nd , 2024)

GP-RSS & SyDE
Tohoku University

The Impact of Sea Level Rise and Wave Driven by Climate Change on Indonesia Coastal Flood Condition

○ Daniel MARTUA[1*], Keiko UDO[1]

[1]Department of Civil and Environmental Engineering, Tohoku University, Miyagi 980-0845, Japan.
[*]E-mail: danielmartua10@gmail.com.

Abstract

Coastal flooding, exacerbated by rising sea levels and changing wave conditions due to climate change, poses a significant impact on Indonesia's coastal areas. This study assesses potential flood inundation from tides, storm surges, and wave setups for both present-day and projected conditions up to 2100 using the FLOWTUB model. The simulations utilize 30m FABDEM data combined with extreme water levels, including present and future sea levels, 100-year return period extreme water levels, and present and future wave setups. Two scenarios, SSP1-2.6 and SSP5-8.5, are used to model future conditions, which are then overlaid with population projections for the present and 2100. The results indicate that current flooding affects approximately 14,000 km², with the most vulnerable regions along Java and Sumatra's northern coasts impacting around 3 million people. By 2100, the flooded area could increase by 185% under the SSP1-2.6 scenario and by 378% under SSP5-8.5. Population exposure is projected to rise to 4.1 million under SSP1-2.6 and 5.2 million under SSP5-8.5. These projections highlighted the importance of understanding future flood conditions and implementing effective coastal management strategies in Indonesia.
Keywords: Coastal Flood, Exposed Population, Climate Change

1 Introduction

Coastal flooding, a phenomenon caused by the water levels rising beyond their normal condition, poses a serious threat to coastal areas in Indonesia. Especially during the rainy season and when tropical storms hit, coastal flooding can cause water inundation along the coastline, damage buildings, and endanger the lives of communities. Cities like Jakarta, Surabaya, and several other major urban areas are most vulnerable to the effects of tidal flooding [9]. Climate change, which leads to rising sea levels and changes in wave conditions worldwide, exacerbates the vulnerability of coastal areas to tidal flooding [10]. According to data from the National Disaster Management Agency (BNPB), the incidence of tidal flooding increased by 46 percent between 2020 and 2023. Given these conditions, it is crucial to understand the current state of tidal flooding in Indonesia and, with climate change in mind, to assess the potential severity of future tidal floods. This study aims to evaluate the potential flood inundation conditions caused by tides, storm surges, and wave setups, as well as the population affected. Additionally, the study assesses future conditions due to ongoing climate change.

2 Materials and methods

The coastal flood simulation in this study is based on the FLOWTUB Model, using the Digital Elevation Model (DEM) [5] and Water Level as inputs. Specifically, the study uses the 30m resolution FABDEM (Forest and Buildings removed Copernicus DEM) [3] for the DEM input. Water level is a combination of mean sea level, extreme water level, and wave set-up, each derived from different datasets. The resulting flood inundation is then overlaid with population data for 2020 and projected 2100 populations.[1]

The mean sea level to evaluate is based on the initial DEM used in this study. The elevation on the sea surface for this DEM is zero based on the mean sea surface at the year 2000, then added with sea level projection to produce the 2020 water level. For future conditions, this study uses all 2 SSP scenarios produced by IPCC [4]. This study uses the sea level rise by 2100 across SSP1-2.6 and SSP5-8.5 scenarios to show the probable worst conditions during the last decade.

For the extreme water level, this study uses the COAST-RP [2]. This dataset shows the probabilistic value of combined tropical and extratropical cyclone surge levels and tidal levels with various return periods. This study uses the 100-year return period. To obtain future projections, the extreme value is coupled with the sea level rise projection. [6]

The wave datasets for this study is using significant wave height data from the 140-yr wind-wave climate simulations (1961–2100) forced with surface wind speed and sea ice concentration from two CMIP6 GCMs under SSP1-2.6 and SSP5-8.5 scenarios. [7] Then, the significant wave height datasets are statistically calculated to produce the 95th percentile during the 2005-2014 period and the 2090-2100 period. The wave set-up is estimated by the empirical equation [8], which is the function of beach face slope and offshore significant wave height. The beach face slope uses the sub-aerial coastal slope. [1]

3 Results and Discussions

3.1 Present Flood Conditions

The total flooded area for the present condition within the 100-year return period is approximately 14000 km². The high flooded areas are mostly distributed on Java's northern coast and Sumatra's northern coast. Several other locations, such as the eastern part of Kalimantan, the western part of Sulawesi, and some parts of Papua, also faced relatively high flooded areas. Regarding the wave condition, the southern coast of Java and the western coast of Sumatra—both exposed to the Indian Ocean—show higher wave heights (above 2.0 meters), reaching 3.5 meters or more in some regions. The situation is clearer if we look at Indonesia's population exposed to coastal floods. Nationwide, the population exposed to coastal floods is approximately 3 million. The western part of Indonesia, particularly Java and Sumatra, is densely populated but has relatively smaller flood-affected areas than

The 12th International Symposium on Water Environment Systems
----- with Perspective of Global Safety   (Nov. 21st ~ 22nd , 2024)

GP-RSS & SyDE
Tohoku University

some areas in the eastern part of Indonesia. Based on this result, the coastal manager should prioritize the regions with a large extent on their flood mitigation planning, including densely populated areas like Java, where even small-scale floods could lead to significant human and economic losses. For regions with large flood extent but lower populations such as Kalimantan and Papua, the strategies may focus on managing the spread of flooding and mitigating its impact on ecosystems

3.2 Future Flood Conditions

The future flood conditions are very related to the sea level rise condition and the future wave changes. Within the SSP1-2.6 Regional Sea Level Rise (RSLR) scenario by 2100, The sea level rise is primarily in the range of 0.3 to 0.5 meters, with some areas experiencing higher sea level rise but generally on moderate values. On the other hand, the SSP5-8.5 shows a value between 0.6 to 1 meter. The future aver 95th percentile from 2090-2100 of significant wave height shows that there is minimal change in nearshore wave heights under the SSP1 scenario compared to historical data, suggesting a stable condition near the coasts with low to moderate wave heights. On the other hand, The SSP5 scenario shows a noticeable increase in nearshore wave heights.

It is well known that the SSP5-8.5 might produce more severe flooded areas compared to the SSP1-2.6 and other SSP scenarios. The nationwide change in the flooded areas is around 53% for SSP1-2.6 and 97% for SSP5-8.5, with the spatial variability for the flooded area change. The notable province with the highest percentage of change is Jambi. The SSP5-8.5 scenario shows a 378% increase in flooded areas compared to the present, while SSP1-2.6 shows a 185% increase. Jakarta, as the capital city of Indonesia, shows an 83% increase under SSP1-2.6, but in the SSP5-8.5 scenario, it reaches 146%, indicating a severe future flood condition for the capital city that is already prone to flooding in the present condition.

Based on the population projection data used for Indonesia, both SSP1 and SSP5 projections follow a similar population projection in the first decade or two, with populations growing modestly. After 2035, SSP5's population starts to decline faster and more sharply than SSP1. However, in general, the population projections under SSP5 are mostly higher compared to SSP1 in most provinces. This situation might impact the projected exposed population by 2100. Nationwide, the number of exposed populations for the SSP1-2.6 scenario is around 5.2 million, and around 4.1 million under the SSP5-8.5 scenario. If we look into some provinces, for example, in Jakarta, the exposed populations are estimated at around 430 thousand for the SSP5 scenario and 350 thousand for the SSP1 scenario. Other provinces, such as Jawa Tengah and Jawa Timur, which show moderately flooded areas under the previous climate scenarios, also have relatively high population projections under both SSPs. These population projections and flood condition data are important basic knowledge to understand the potential impact of future floods in Indonesia. Some areas have large population projections, which, caused by large flooded areas and dense populations, are suggested for urgent climate adaptation and mitigation strategies. Infrastructure investments, flood defenses, and relocation planning may be critical.

4 Conclusions

The present situation of Indonesian coastal floods is important to assess and the future condition of this disaster. The present flood situation inundated approximately 14000 km^2 and could be increased 2-4 times higher. The huge amount of exposed population in the present condition (3 million) might be increased to around 5.2 million by 2100. This situation needs to be addressed by the government and coastal manager for any mitigation, such as infrastructure investments, flood defenses, and relocation planning.

Reference

[1] Almar, Rafael, Roshanka Ranasinghe, Erwin W. J. Bergsma, Harold Diaz, Angelique Melet, Fabrice Papa, Michalis Vousdoukas, et al. 2021. "A Global Analysis of Extreme Coastal Water Levels with Implications for Potential Coastal Overtopping." Nature Communications 12 (1). doi:10.1038/s41467-021-24008-9.

[2] Dullaart, Job C. M., Sanne Muis, Nadia Bloemendaal, Maria V. Chertova, Anaïs Couasnon, and Jeroen C. J. H. Aerts. 2021. "Accounting for Tropical Cyclones More than Doubles the Global Population Exposed to Low-Probability Coastal Flooding." Communications Earth & Environment 2 (1). doi:10.1038/s43247-021-00204-9.

[3] Hawker, Laurence, Peter Uhe, Luntadila Paulo, Jeison Sosa, James Savage, Christopher Sampson, and Jeffrey Neal. 2022. "A 30 m Global Map of Elevation with Forests and Buildings Removed." Environmental Research Letters 17 (2): 024016. doi:10.1088/1748-9326/ac4d4f.

[4] (IPCC), Intergovernmental Panel on Climate Change. 2023. Climate Change 2021 – The Physical Science Basis: Working Group I Contribution to the Sixth Assessment Report of the Intergovernmental Panel on Climate Change. Cambridge University Press.

[5] Kasmalkar, Indraneel, Dennis Wagenaar, Alina Bill-Weilandt, Jeanette Choong, Sonali Manimaran, Tian Ning Lim, Maricar Rabonza, and David Lallemant. 2024. "Flow-Tub Model: A Modified Bathtub Flood Model with Hydraulic Connectivity and Path-Based Attenuation." MethodsX 12 (June): 102524. doi:10.1016/j.mex.2023.102524.

[6] Kirezci, Ebru, Ian R. Young, Roshanka Ranasinghe, Sanne Muis, Robert J. Nicholls, Daniel Lincke, and Jochen Hinkel. 2020. "Projections of Global-Scale Extreme Sea Levels and Resulting Episodic Coastal Flooding over the 21st Century." Scientific Reports 10 (1). doi:10.1038/s41598-020-67736-6.

[7] Meucci, Alberto, Ian R. Young, Mark Hemer, Claire Trenham, and Ian G. Watterson. 2023. "140 Years of Global Ocean Wind-Wave Climate Derived from CMIP6 ACCESS-CM2 and EC-Earth3 GCMs: Global Trends, Regional Changes, and Future Projections." Journal of Climate 36 (6): 1605–1631. doi:10.1175/jcli-d-21-0929.1.

[8] Stockdon, Hilary F., Rob A. Holman, Peter A. Howd, and Asbury H. Sallenger Jr. 2006. "Empirical Parameterization of Setup, Swash, and Runup." Coastal Engineering 53 (7): 573–588. doi:10.1016/j.coastaleng.2005.12.005.

[9] Syafitri, Annisa Widya, and Agus Rochani. 2021. "Analysis of the Causes of Tidal Flooding in Coastal Areas Case Study: North Jakarta, East Semarang, Brebes Regency, Pekalongan." Jurnal Kajian Ruang 1 (1): 16–28.

The 12th International Symposium on Water Environment Systems
----- with Perspective of Global Safety (Nov. 21st ~ 22nd , 2024)

GP-RSS & SyDE
Tohoku University

[10] Toimil, Alexandra, Iñigo J. Losada, Pedro Díaz-Simal, Cristina Izaguirre, and Paula Camus. 2017. "Multi-Sectoral, High-Resolution Assessment of Climate Change Consequences of Coastal Flooding." Climatic Change 145 (3–4): 431–444. doi:10.1007/s10584-017-2104-z.

[11] Wang, Xinyu, Xiangfeng Meng, and Ying Long. 2022. "Projecting 1 Km-Grid Population Distributions from 2020 to 2100 Globally under Shared Socioeconomic Pathways." Scientific Data 9 (1). doi:10.1038/s41597-022-01675-x.

The 12th International Symposium on Water Environment Systems
----- with Perspective of Global Safety   (Nov. 21st~22nd , 2024)

GP-RSS & SyDE
Tohoku University

Understanding relationship between land use change and fluvial inundation frequency in Chiang Mai, Thailand

○ Zhaolong GU[1*], Daisuke KOMORI[2] & Sartsin Phakdimek[1]

[1]Graduate School of Environmental Studies, Tohoku University, Miyagi 980-0845, Japan.
[2]International Research Institute of Disaster Science, Tohoku University, Miyagi 980-8572, Japan.
*E-mail: gu.zhaolong.r5@dc.tohoku.ac.jp.

Abstract

This study evaluates the impact of urbanization on flood risks in Chiang Mai, Thailand, from two critical perspectives: land-use changes and social reactions. It categorizes 10 Frequent Flood-prone Areas into "persistent," "second-half," and "first-half" zones based on the frequency of flood events before and after 2005. A key focus is on how the transformation of paddy fields into impermeable urban surfaces has reduced water retention and exacerbated flood risks. The Rainfall-Runoff-Inundation (RRI) model was employed to simulate flood inundation under various rainfall scenarios, calculating Exposure (E) and Hazard (H) and coupling them with the IPCC framework to quantify the relationship between Risk (R), Exposure, Hazard, and Vulnerability (V). Additionally, field surveys revealed differences in flood risk awareness and adaptation strategies across the zones, with "first-half" areas showing reduced risks due to long-term adaptation, while "second-half" zones faced higher risks due to recent urbanization. This comprehensive approach integrates both land-use and social dimensions to provide a clearer understanding of urbanization's effects on flood risks.

Keywords: Flood risk; Rainfall-Runoff-Inundation model; IPCC Flood Risk Formula; Socio-hydrology; Field survey.

1 Introduction

Urbanization has dramatically transformed landscapes globally, leading to increased environmental challenges. One such challenge is flood risk, which has become particularly acute in rapidly urbanizing regions. As cities expand, natural landscapes such as wetlands, paddy fields, and forests are replaced by impermeable urban surfaces, resulting in increased runoff, reduced water retention, and heightened flood hazards. This pattern has been observed in many developing regions, where urban planning related to flood often lags behind rapid urban expansion.

Chiang Mai, located in northern Thailand, has experienced rapid urbanization over the past few decades. Historically, the city was surrounded by paddy fields and natural water retention areas, which played a vital role in managing seasonal floodwaters, especially during the monsoon season. However, the expansion of urban areas has transformed these natural landscapes, resulting in more frequent and severe flood events.

The objective of this study is to assess the impact of urbanization on flood risk in Chiang Mai. The research focuses on how land-use changes, particularly the conversion of paddy fields into urban areas, have influenced flood risk, and how these changes interact with social responses to urbanization-induced flooding.

The novelty of this research lies in two aspects: (1) A comprehensive approach that integrates both land-use changes and social awareness of flood risks, offering a fuller understanding of how urbanization impacts flood vulnerability; and (2) A focus on Frequent Flood-prone Areas, providing a more accurate assessment of flood risk changes in response to urbanization, rather than concentrating on extreme flood events.

2 Materials and methods

This study utilizes a multi-method approach to assess the impact of urbanization on flood risks in Chiang Mai, Thailand.

1. Frequent flood-prone areas identification and land-use change analysis: frequent flood-prone areas were identified and categorized into "persistent," "first-half," and "second-half" zones based on changes in flood frequency before and after 2005. GIS-based analysis was used to examine land-use changes, particularly the conversion of paddy fields into urban areas, which reduced natural water retention and increased flood risks.
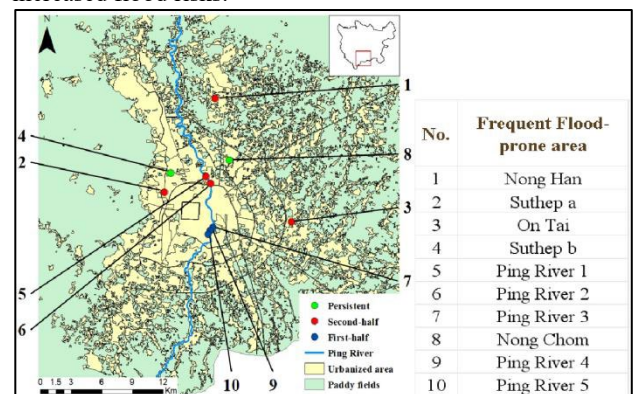
**Fig. 1. Distribution of 10 flood-prone areas.**

2. Quantification of the factors contributing to flood occurrences in Frequent Flood-prone areas: To study the flood dynamics, the Rainfall-Runoff-Inundation (RRI) model was employed, simulating inundation under various rainfall conditions. The model assessed Exposure (E) and Hazard (H), which, when integrated with the IPCC Flood Risk Framework, quantified the overall flood risk by linking it to Vulnerability (V) and Risk (R).

3. Field survey: Surveys are conducted to capture residents' flood awareness and environment information in various

The 12th International Symposium on Water Environment Systems
----- with Perspective of Global Safety   (Nov. 21st ~ 22nd , 2024)

GP-RSS & SyDE
Tohoku University

flood-prone areas. These social insights are crucial to understanding how urbanization has affected flood risk from a socio-hydrological perspective.

3 Results and discussion

Based on the characteristics of exposure and vulnerability changes in 10 frequent flood-prone areas, this study found that in the "Second-half" flood-prone areas (2006-2018), these regions generally exhibit higher vulnerability changes and greater exposure levels.
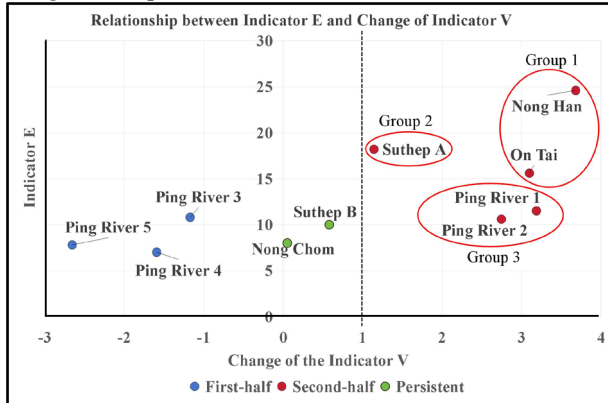
Fig. 2. Diagram of the relationship between V change and indicator E in "Second-half" Frequent Flood-Prone Areas.

The land-use change analysis showed that in the "Second-half" frequent flood-prone areas, significant land-use changes occurred during the urbanization process. These changes, particularly the conversion of high-exposure paddy fields into urban land, had a substantial impact on the flood risk characteristics of these areas.

| Frequent flood-prone areas	First half		Second half		Whole period	
	9 cells	25 cells	9 cells	25 cells	9 cells	25 cells
Group 1	16.67%	26.00%	50.00%	40.00%	66.67%	66.00%
Group 2	55.56%	24.00%	22.22%	48.00%	66.67%	72.00%
Group 3	44.44%	40.00%	5.56%	8.00%	50.00%	48.00%

Table 1 Land-use change of 3 groups in "Second-half" Frequent Flood-Prone Areas.

In contrast, land use changes in "First-half" and "Persistent" areas were less significant compared to "Second-half" areas, and thus have made a smaller contribution to flood risk.

Frequent flood-prone areas	First half		Second half		Whole period	
	9 cells	25 cells	9 cells	25 cells	9 cells	25 cells
Persistent	11.11%	22.00%	11.11%	20.00%	22.22%	42.00%
First-half	16.67%	34.00%	5.56%	8.00%	22.22%	42.00%

Table 1 Land-use change of 3 groups in "Second-half" Frequent Flood-Prone Areas.

The field survey revealed that the trend in flood awareness among residents in "Persistent" and "First-half" areas over time differs from that in "Second-half" areas. When combined with environmental information, the study suggested that human interventions in flood response measures are the primary factor influencing the impact of urbanization on flood risk in "Persistent" and "First-half" areas.
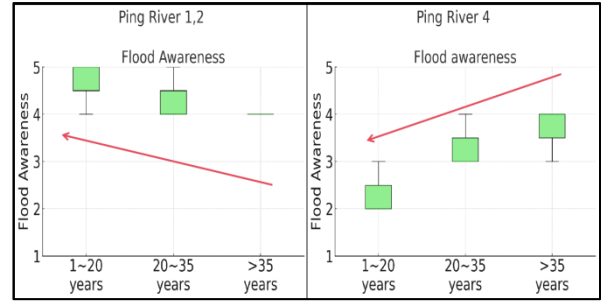
Fig. 3. The box-line figure of Flood Awareness of Ping River 1,2 (Second-half); Ping River 4 (First-half).

4 Conclusions

This study examined the impact of urbanization on flood risk in Chiang Mai, Thailand, with a focus on both land-use changes and social responses. Using flood simulation models and field surveys, the research identified and classified 10 frequent flood-prone areas, analyzing how urban expansion−particularly the conversion of paddy fields into urban land−has aggravated flood risk.

Quantification of the factors contributing to flood occurrences in Frequent Flood-Prone Areas showed that in "Second-half" flood-prone areas, vulnerability increased significantly after 2005 due to large-scale land-use changes.

In contrast, flood risk patterns in "First-half" and "Persistent" flood-prone areas remained relatively stable, with vulnerability driven more by human activities than by land-use changes. Field surveys revealed that residents' awareness of flood risks and their responses varied depending on the length of residency and the development stage of the flood-prone areas. The study concludes that urbanization, particularly land-use changes, is a key factor contributing to increased flood risk in Chiang Mai. However, social responses and adaptation efforts also play a crucial role in shaping flood vulnerability, suggesting that future flood management strategies should consider both environmental and social factors.

Reference

[1] Kulsrisombat, N. (2008). De Facto Urban Regeneration: A Case Study of Chiang Mai City, Thailand. In: Kidokoro, T., Harata, N., Subanu, L.P., Jessen, J., Motte, A., Seltzer, E.P. (eds) Sustainable City Regions:. cSUR-UT Series: Library for Sustainable Urban Regeneration, vol 7. Springer, Tokyo.

[2] Komori, D.; Nakaguchi, K.; Inomata, R.; Oyatsu, Y.; Tachikawa, R.; Kazama, S. Topographical Characteristics of Frequent Urban Pluvial Flooding Areas in Osaka and Nagoya Cities, Japan. Water 2022, 14, 2795.

[3] Tachikawa, Inomata, Oyatsu, Komori (2022) The distribution and characteristic on frequent flooded area of inland inundation in Nagoya City, Civil Engineering Society Proceedings G (Environment), 78 (5), pp. I_371-I_377, 2022.

[4] Sayama, T., Tatebe, Y., Iwami, Y., & Tanaka, S. (2014). Hydrologic sensitivity of flood runoff and inundation: 2011 Thailand floods in the Chao Phraya River basin. Natural Hazards and Earth System Sciences Discussions, 2, 7027-7046.

The 12th International Symposium on Water Environment Systems
----- with Perspective of Global Safety   (Nov. 21st ~ 22nd , 2024)

GP-RSS & SyDE
Tohoku University

Effects of updating frequency and observation network density in hydrological data assimilation

◯ Kumudu Madhawa KURUGAMA[1*], So KAZAMA[1], Yusuke HIRAGA[1]

[1]Department of Civil and Environmental Engineering, Tohoku University, Miyagi 980-8579, Japan
*E-mail: kurugama.arachchige.kumudu.madhawa.r4@dc.tohoku.ac.jp

Abstract

  Precise flood predictions have the potential to minimize socioeconomic losses; however, uncertainties in inflows from precipitation forecasts often lead to substantial prediction errors. Recent research indicates that assimilating independent flood observations can help reduce the inherent uncertainty in hydrological modeling. This study explores the optimal configuration for discharge assimilation within a spatially distributed hydrological model. The Ensemble Kalman Filter (EnKF) was applied to update the states in the spatially distributed LISFLOOD hydrological model. Using a process-based model for routing provides a more realistic representation of time delay and flow attenuation. At each time step, the discharge and states are assumed to depend solely on the preceding time step, following the Markov property. A synthetic twin experiment was conducted for a subsection of the Fraser River basin, in British Columbia, Canada. We assessed the impact on the simulated discharge of (1) different configurations of spatially distributed discharge gauges and (2) the filtering frequency. The results showed that assimilating interior gauges at higher frequencies enhances hydrological predictions at the catchment outlet.

Keywords: Data assimilation; hydrological modeling; ENKF; uncertain observation.

1 Introduction

  Hydrological forecasting plays an essential role in water resource management, especially for applications requiring accurate predictions to mitigate flood risks and manage water distribution [1]. Over recent decades, advances in data assimilation (DA) have improved forecasting accuracy by integrating real-time observational data into model simulations, offering enhanced initial conditions for hydrological models [2]. This fusion of observation and simulation helps reduce uncertainties, a critical factor for effective decision-making in dynamic environments. Most current hydrological forecasting systems rely on lumped models that aggregate data across a catchment, often simplifying spatial variability [3]. However, distributed hydrological models such as the LISFLOOD model, which integrates spatially distinct data points, offer a finer representation of catchment characteristics. Ensemble methods have enhanced their effectiveness, particularly the Ensemble Kalman Filter (EnKF), which leverages data from various points within the catchment [4]. By updating model states with high temporal resolution, the EnKF helps maintain model reliability across changing environmental conditions. This study focuses on optimizing DA in a distributed hydrological model, assessing how prediction accuracy varies with different updating frequencies and observational network densities through a synthetic twin experiment using ENKF. Through this approach, this study seeks to identify the best configurations to enhance prediction accuracy and applicability across various hydrological scenarios.

2 Study area and data set

  The methodology proposed in this study is applied to a sub-basin of the Fraser River basin, in British Columbia, Canada. The study area covers the river section from the Nechako tributary in the North to the Quesnel tributary in the South. The Basin outlet is indicated as "A" and discharge was
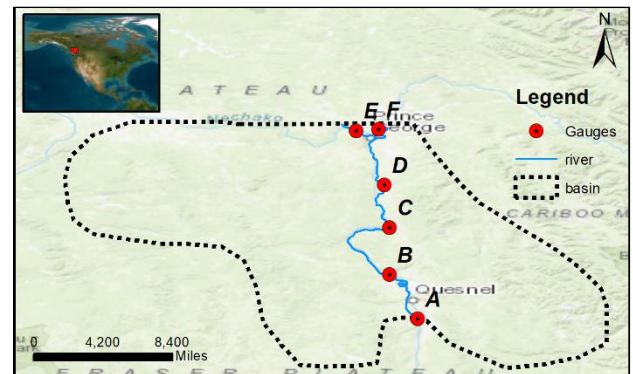
Fig. 1. Study area

recorded at six different points (Fig. 1), and different combinations of these locations were used in the assimilation process. For this proof-concept study, only data from the 2016-2017 period was used.

3 Methodology

  EnKF is a Monte Carlo data assimilation method that updates model states by integrating observation and model errors, accounting for uncertainties in meteorological forcing, model structure, and parameters. The general form of the EnKF is given as follows [5].

$$\psi^a = \psi^f + P^f H^t (HP^f H^t + R)^{-1}(d - H\psi^f) \quad (1)$$

$$d = H\psi^t + \in \quad (2)$$

Where ψ^t: model analysis, ψ^f: model simulation, P^f: model error covariance matrix of the model, R: observation error covariance matrix H: observation operator. The synthetic experiment was conducted to assess the EnKF's capability to update the process-based LISFLOOD model states through spatial discharge assimilation. To generate the ensembles (50 ensemble members), the precipitation data was scaled and perturbed with a white noise (~N (1,0.15)). To maintain clarity in the experimental setup, model parameters were kept constant and

The 12th International Symposium on Water Environment Systems
----- with Perspective of Global Safety   (Nov. 21st ~ 22nd , 2024)

GP-RSS & SyDE
Tohoku University

not updated. In an open-loop simulation (without DA), the model was initially driven by uncertain precipitation inputs, with daily timestep. This generated an ensemble of simulated discharges, from which a single complete realization was randomly chosen as the true discharge ($Q_{true,k}$). To obtain synthetic perturbed discharge observation ($Q_{syn,k}$) a normally distributed error with heteroscedastic variance was added to $Q_{true,k}$ [6]. In the synthetic experiment, three schemes of perturbed discharge observations were assimilated: Case 1 uses only the downstream observation (A), Case 2 includes only the upstream observation (F), and Case 3 incorporates all six discharge gauges. Moreover, the effect of updating frequencies for 30, 10, 5, and 1-day filtering steps were used.

3 Results and discussion

The results were evaluated using the Nash-Sutcliffe efficiency at outlet point A. The NSE between the synthetic observed discharge and the predicted discharge of the 50 ensemble members for the four updating frequencies is shown in Table 1.

Table 1 This is a table sample.

Frequency (days)	Case I (NSE)	Case 2 (NSE)	Case 3 (NSE)
1	0.947	0.946	0.958
5	0.943	0.942	0.958
10	0.930	0.931	0.957
30	0.887	0.885	0.890

The results indicate that, with a 1-day updating frequency, Case 3 outperformed the other two cases. Although the differences between Cases 1 and 2 are minimal, the slight variation in their NSE values favors Case 1. A similar performance trend was seen with the 5-day assimilation frequency simulations. However, at a 10-day assimilation frequency, Case 2 showed a slightly higher NSE than Case 1, though still lower than Case 3. All three cases performed poorly with the 30-day assimilation frequency simulations. Overall, performance generally improved with higher assimilation frequencies. The results showed that assimilating spatially distributed observations, rather than relying on single point-based assimilation, has a greater impact on enhancing discharge predictions. This is due to the spatially distributed data providing a more comprehensive representation of the watershed's conditions.

4 Conclusions

We examined the sensitivity of the data assimilation process to factors like updating frequency and the number of interior discharge gauge locations, which were incorporated into a spatially distributed LISFLOOD hydrological model through the EnKF. Our synthetic experiment demonstrated that adding more interior gauges improves hydrological forecasts at the catchment outlet. This is intuitive, as each discharge observation provides upstream information, enhancing the posterior forecast. However, this experiment was limited to input uncertainty alone, and only the discharge state variable was updated during analysis. Future research could expand this by incorporating uncertainties in initial states and model parameters, as well as structural uncertainties, for a more comprehensive analysis.

Reference

[1] Gong, Junfu, et al., State Updating in a Distributed Hydrological Model by Ensemble Kalman Filtering with Error Estimation, Journal of Hydrology, 620(2023), p. 129450.

[2] Dumedah, Gift, and Paulin Coulibaly.,Evolutionary Assimilation of Streamflow in Distributed Hydrologic Modeling Using In-Situ Soil Moisture Data, Advances in Water Resources,53(2013), pp. 231–41.

[3] Revilla-Romero, Beatriz, et al., Integrating Remotely Sensed Surface Water Extent into Continental Scale Hydrology. Journal of Hydrology, 543(2016), pp. 659–70.

[4] Revilla-Romero, B., et al., Evaluation of the Satellite-Based Global Flood Detection System for Measuring River Discharge: Influence of Local Factors, Hydrology and Earth System Sciences, 18(2014), pp. 4467–84.

[5] Roth, Michael, et al., The Ensemble Kalman Filter: A Signal Processing Perspective, EURASIP Journal on Advances in Signal Processing, 56(2017), pp.1-16.

[6] Lee, Haksu, et al., Assimilation of Streamflow and in Situ Soil Moisture Data into Operational Distributed Hydrologic Models: Effects of Uncertainties in the Data and Initial Model Soil Moisture States, Advances in Water Resources, 34(2011), pp. 1597–615.

The 12th International Symposium on Water Environment Systems
----- with Perspective of Global Safety   (Nov. 21st ~ 22nd , 2024)

GP-RSS & SyDE
Tohoku University

Development of hazard assessment methods capable of simulating the discharge of large woody debris at dam catchments

Y Liu, Y Abe, S Phakdimek, D Komori*

[1]Department of Environmental Engineering, Environmental University, Miyagi 980-8579, Japan.
[2]Department of Water Environment, Engineering University, Miyagi 980-8579, Japan.
liu.yunhao.r6@dc.tohoku.ac.jp.

Abstract

This study represents the volume of large wood debris (LWD) that exports to dam catchments in Japan under different rainfall return periods using an annual-scale approach. The hazard was assessed using the following procedure, based on the model developed by Komori et al. (2022): (1) rainfall analysis to determine the return levels of precipitation within the catchment area, (2) simulation of potential large wood debris recruitment volumes using a rainfall-induced analytical shallow landslide model, and (3) estimation of expected, maximum, and minimum large wood debris discharge volumes using the double storage function with a lumped hydrological method at the catchment scale. The simulation results were validated against observed volumes in various domains. This method successfully modeled the theoretical large wood debris discharge volumes for eight dam catchments across northern and southern Japan, providing a data foundation for dam managers to conduct further risk analysis and disaster prevention.

Keywords: large wood debris; slope stability analysis; landslide; storage function model.

1 Introduction

Large wood debris can be defined as a combination of downed trees, branches, roots, stumps and snag, usually considered to be greater than 0.1 m in diameter (Vanderwel et al., 2016). Large amounts of large wood debris can also bring a significant risk to river basin infrastructure and human habitation. Landslide is a significant potential source of large wood debris. In addition, accompanied by global warming, landslide and floods events are gradually increasing due to the frequent occurrence of extreme rainfall, therefore, to forecast the volume of large wood debris discharge will become increasingly important in current meteorological conditions.

Due to the lack of observed data and the significant error of the current hazard assessment method (Yano et al., 2020), an approach that considers large wood debris transport mechanism is needed for hazard assessment. Komori (2022) proposed an integrated large wood debris discharge model that accounts for large wood debris transport processes and has been validated across 134 dam reservoirs in Japan. This study will develop a large wood debris hazard assessment method for dam catchments in Japan based on this approach.

2 Materials and methods

The methodology of this research includes two parts: First one is the hazard identification for estimating the landslide and the potential volume of large wood recruitment. The second one is probability assessment that calculating the potential volume of large wood export to dam reservoir.
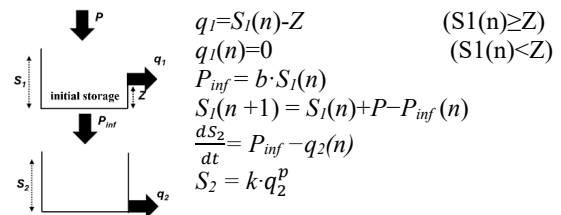
Generalized Extreme Value (GEV) distribution is a statistical model which is widely used for hazard assessments of hazards including floods and landslides research. In this study, the GEV method was used to calculate the precipitation return level within catchment area under different return levels. The historical precipitation dataset was prepared from Radar- AMeDAS rainfall of the JMA are available from the public data source, and the spatial resolution is 1km.

$$x_T = \mu + \frac{\sigma}{\xi} \left[(-\log(1 - \frac{1}{T}))^{-\xi} \right]$$

Where x_T is the extreme rainfall intensity value (mm/hour), T is the return period (T=3,5,8,15,17,20,25,30 ······ 200 years, n is the number of observations, ξ, μ and σ is the shape parameter, the location parameter and the scale parameter respectively, they were determined by Log-Likelihood Function.

Precipitation return level is used to groundwater and infiltration depth(m), The rainfall-induced shallow landslide analysis model was utilized in this study; for detailed methodology, refer to Komori et al. (2022).

Annually potential volume of large wood debris will be input for double storage function model (Komori et al.,2022), which presents storage, transport and discharge processes in a dam catchment:

$$q_1 = S_1(n) - Z \quad (S1(n) \geq Z)$$
$$q_1(n) = 0 \quad (S1(n) < Z)$$
$$P_{inf} = b \cdot S_1(n)$$
$$S_1(n+1) = S_1(n) + P - P_{inf}(n)$$
$$\frac{dS_2}{dt} = P_{inf} - q_2(n)$$
$$S_2 = k \cdot q_2^p$$

Fig.1. Framework of double storage function model (Modified from Komori and Abe et al., 2024)

Where P is annual large wood recruitment (m³), S is storage at the tank (m³), P_{inf} is large wood exported into next tank (m³), q_1 is overflow from the tank1 (m³), q_2 is baseflow from the tank2 (m³), Z is capacity of tank1 (m³). n is time (in years), b, k and p are model parameters.

The simulation period for this model spans from 1996 to 2021, with the initial storage in the first tank set to zero by default. When the model is applied to hazard assessment, the storage volume in the first tank prior to the start of the simulation period must be considered. Specifically, the actual storage volume present in each dam catchment before 1996 is expected to be determined. For each dam catchment, the

The 12th International Symposium on Water Environment Systems
----- with Perspective of Global Safety   (Nov. 21st~ 22nd , 2024)

GP-RSS & SyDE
Tohoku University

framework for determining the expected initial storage percentage is shown as following:
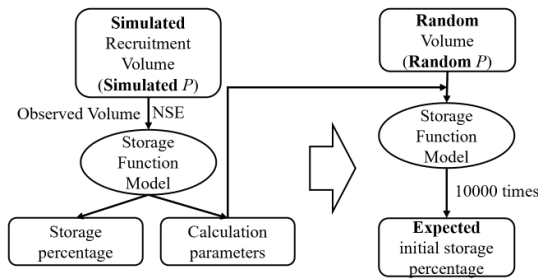

Figure.2. Framework of expected storage percentage determination

The storage percentage in each dam catchment area can be determined by the framework on the left side. By setting many random volumes similar to the simulated recruitment volume and using the obtained parameters, the expected storage percentage in the first tank can be determined, representing the initial storage percentage at the beginning of simulation period, it allows for the estimation of the expected discharge volume.

3 Results and discussion

This method requires observed volumes of large wood debris (LWD) to determine the parameters of the storage function model; therefore, this study selected four dam catchments (Kamuro , Tase, Kanayama, Gassan) in north Japan and four (Nukui, Onbe, Tsugawa, Katagiri) in south Japan as target area, within large wood debris discharge volume records from Ministry of Land, Infrastructure, Transport and Tourism . The locations are shown as follows:
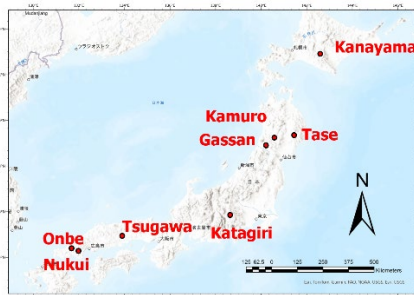

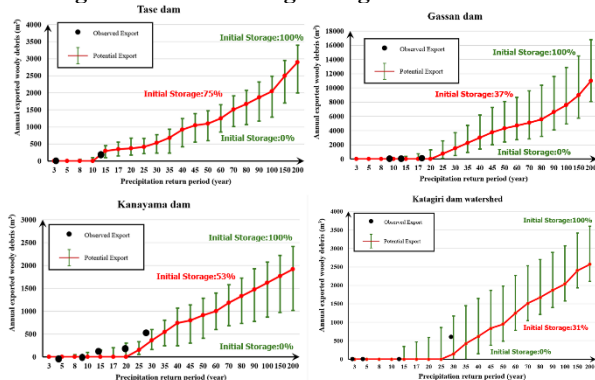**Fig. 3. Locations of eight target dam reservoirs**

Fig. 4. Large wood debris hazard assessment of four target dam reservoirs north Japan

Where the line located in the middle represents the annual expected volume of large wood debris exported to Katagiri dam by using the expected initial storage percentage in first tank, the corresponding maximum and minimum points represent the maximum and minimum volume by setting the
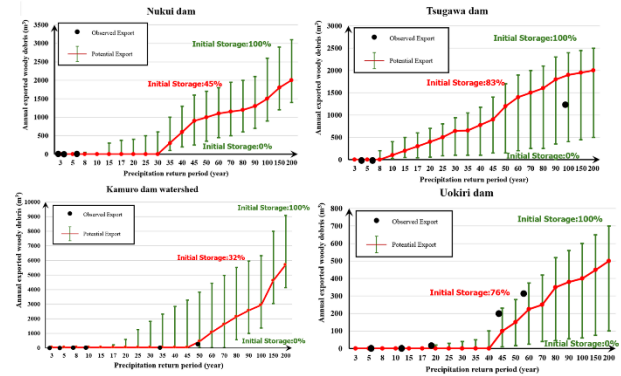

Fig. 5. Large wood debris hazard assessment of four target dam reservoirs sorth Japan

initial storage percentage as 100% and 0%, respectively. This result was validated by the observed volume of large wood debris represented by dots.

Compared to the northern dam catchments, the southern catchments, although smaller in area (which may result in a lower volume of LWD during the recruitment process), are more likely to experience higher rainfall return periods and possess a higher initial storage percentage. As a result, they tend to exhibit a greater volume of LWD discharge.

Using the Katagiri Dam catchment as an example, additional information can be derived from figure 4. It can be determined that the Katagiri dam reservoir will receive large wood debris at a minimum rainfall return period of 15 years, corresponding to a precipitation return level of 253 mm/24 hours. When the precipitation return period approached 30 years, the observed large wood debris volume was 610 m^3, which falls within the simulated range. The result also showed the maximum annual discharge volume of large wood debris under different precipitation return period.

4 Conclusions

This research aimed to develop a hazard assessment method of large wood debris based on an integrated large wood discharge model proposed by Komori (2022). Through historical rainfall analysis, slope stability analysis, determination of calculation parameters for the storage function model, and estimation of initial expected storage, a hazard assessment method of large wood debris applicable to dam catchments in Japan was developed.

Reference

[1] Ruiz-Villanueva V, Piégay H, Gurnell A M, et al. Recent advances quantifying the large wood dynamics in river basins: New methods and remaining challenges[J]. Reviews of Geophysics, 2016, 54(3): 611-652.

[2] Yano S, Shogaki T, Yato S, et al. Development of Logistic Regression Model for Slope Failure and Estimation of Driftwoods Generation in Marumori Town due to the East Japan Typhoon 2019[J]. Journal of Japan Society of Civil Engineers, Ser. B1 (Hydraulic Engineering), 2020, 76(1): 253-263.

[3] Komori D, Sukegawa Y, Chaithong T, et al. Modelling of large wood export at a watershed scale[J]. Earth Surface Processes and Landforms, 2022, 47(2): 688-696.

The 12th International Symposium on Water Environment Systems
----- with Perspective of Global Safety   (Nov. 21st ~ 22nd , 2024)

GP-RSS & SyDE
Tohoku University

Effects of Climate Change and Population Change on Exposed Population to Fluvial Flood, Pluvial Flood, and Slope Failure

◯ Tomoaki MATSUURA[1*], So KAZAMA[1]

[1]Department of Environmental Engineering, Environmental University, Miyagi 980-8579, Japan.
*E-mail: matsuura.tomoaki.p7@dc.tohoku.ac.jp

Abstract

Future changes in the population exposed to fluvial flood, pluvial flood, and slope failure due to climate and population change were evaluated for SSP1-1.9, SSP1-2.6, SSP2-4.5, SSP3-7.0, and SSP5-8.5, respectively. Exposed population due to fluvial flood and pluvial flood was defined as the population residing in the area where 45 cm or more of inundation occurred. Exposed population to slope failure was defined as the population living in the area where the probability of slope failure exceeded 80%. Exposed population change rate was higher for all SSPs in the order of pluvial flood, fluvial flood, and slope failure, and exposed population increase change for pluvial flood was particularly pronounced for SSPs 5-8.5. Exposed population was shown to be more strongly affected by population change than by climate change.

Keywords: *exposed population, climate change, population change, SSP*

1 Introduction

Record-breaking heavy rains occur every year in Japan, resulting in frequent heavy rainfall-related disasters such as flooding and sediment disasters caused by fluvial flood and pluvial flood. In the future, there are concerns that heavy rainfall disasters will become even more frequent due to the expected increase in precipitation caused by climate change. In addition, public investment is expected to decrease in the future due to a decline in tax revenues caused by a decrease in population and an increase in public welfare expenses caused by a declining birthrate and an aging population. Effective utilization of land with low disaster risk and effective investment in disaster prevention with limited financial resources are important issues for Japan in the future. To this end, it is necessary to quantitatively evaluate the relationship between the distribution of flood risk over the entire country and the future population distribution. Since the future population distribution can be assumed to be other than the scenarios described above, the exposed population will differ depending on the scenario. Therefore, it is important to estimate the exposed population based on more population distribution scenarios. To predict the impacts of climate change, a shared socioeconomic pathway (SSP) scenario, which assumes future socioeconomic development trends, combined with radiative forcing is assumed. There are five basic socioeconomic scenarios: SSP1-1.9, SSP1-2.6, SSP2-4.5, SSP3-7.0, and SSP5-8.5. In this study, we estimated future changes in the exposed population due to fluvial flood, pluvial flood, and slope failure for the whole of Japan, and assessed the risk of future disasters due to heavy rainfall, with the aim of accumulating knowledge on the population exposed to disasters according to the assumed population distribution.

2 Data set

2.1 Population data

Population scenarios (Version 2) for a tertiary mesh (approximately 1 km x 1 km) for each Japanese SSP developed by the National Institute for Environmental Studies (NIES) were used. Population data for the year 2100 for each SSP were used as future population data. The SSPs used were SSP1, SSP2, SSP3, and SSP5. Population scenarios (2nd edition) for the tertiary mesh were also used for the population data in 2015 (base year).

2.2 Rainfall and climate scenario data

Yamamoto *et al.* [1] developed rainfall distributions (hereafter referred to as "Probability Flood-Contributing Rainfall Distributions") at arbitrary locations on a 5th order mesh (approximately 250 m x 250 m) with spatial resolution, which generate extreme values of discharge for each return period. The probability flood-contributing rainfall distributions for 30, 50, 100 and 200-year return periods developed by Yamamoto *et al.* [1] were used in this study to calculate flood hazard data. Extreme value rainfall data (spatial resolution: 3th order mesh) from Kawagoe *et al.*[2] Extreme rainfall data for recurrence periods of 5, 10, 30, 50, 100, and 200 years were used to calculate hazard data for pluvial flood and slope failure. Five global climate models (GCMs) were used from NIES2020: MRI-ESM2-0, MIROC6, ACCESS-CM2, IPSL-CM6A-LR, and MPI-ESM1-2-HR. The spatial resolution was 3th order mesh, and two time periods were used: 1981-2000 (base climate) and 2081-2100 (2100 time period).

3 Analysis Method

Fluvial flood analysis was conducted based on the method of Yanagihara *et al.* [3] . The spatial resolution was 5th order mesh. The rainfall distribution of the probable flood contribution was uniformly distributed for 24 hours. Flood analysis was conducted using the rainfall distributions of 30, 50, 100, and 200-year return periods, respectively, and inundation depths were calculated. For details, see Yanagihara *et al.* [3] Pluvial flood analysis was conducted based on the method of Yanagihara *et al* .[3] The spatial resolution was 5th order mesh. Extreme rainfall data for 5-, 10-, 30-, 50-, and 100-year return periods were used for the

inundation depths. For details, see Yanagihara *et al.* [3] The slope failure probability data for all of Japan at daily precipitation levels of 0, 50, 100, 150, 200, 250, 300, and 500 mm from Kawagoe *et al.* [4] The spatial resolution was cubic mesh. The slope failure probabilities corresponding to the extreme rainfall data (spatial resolution: 3th order mesh) for the 5-, 10-, 30-, 50-, 100-, and 200-year return periods of Kawagoe *et al.* [2] were calculated by linear interpolation.

Exposed population due to fluvial flood and pluvial flood is defined as the population living in the area where inundation of 45 cm or more occurs, which is inundation above the floor level. Exposed population due to slope failure was defined as the population living in areas where the probability of slope failure was greater than 80%. This is because the study by Kawagoe *et al.* [4] shows that actual slope failures occur within areas where the probability of slope failure is greater than 80%. The exposed population was evaluated as an annual expected value.

4 Results and Discussion

Fig.1. shows the rate of change in the exposed population by SSP due to climate change. The rates of change in the exposed population for each GCM are calculated based on the mean value of the exposed population estimated for each GCM. Error bars indicate the standard deviation from the mean of all GCMs. The exposed population increased in all SSPs. The increase was especially significant in the case of pluvial flood. The exposed population change rates were higher in the order of pluvial flood, fluvial flood, and slope failure, respectively. On the other hand, when the population change was taken into account (see Fig.2.), the exposed population decreased in all SSPs. In addition, Figure 3 shows that the exposed population decreased in all SSPs except SSP 5-8.5 when both climate change and population change were taken into account. This indicates that population change is more dominant than climate change for the exposed population. As for Fig.3., the exposed population to pluvial flood in SSP5-8.5 increased by about 35%. In the case of slope failure, the exposed population decreased in all SSPs. The high rate of change in the population exposed to pluvial flood may be due to the smaller population loss in urban areas compared to other areas. Pluvial flood increases the depth of inundation in low lying areas, generally in urban areas, while slope failure occurs in mountainous areas. Fluvial Flood occurs in both urban and rural areas. In particular, SSP5-8.5 is a scenario in which the population is concentrated in metropolitan areas and is more concentrated in areas at high risk of internal flooding. As a result, the rate of change in the exposed population is positive despite a decrease in the population, suggesting that the exposed population has increased.

5 Conclusion

The main findings of this study are as follows. For all SSP, the rates of change in the exposed population, including positive and negative, were higher for pluvial flood, fluvial flood and slope failure, in that order. Exposed population was shown to be more strongly affected by population change than by climate change.
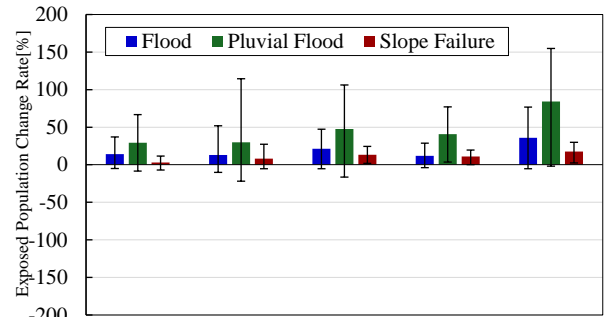

Fig.1. Exposed population change rate by SSP due to climate change
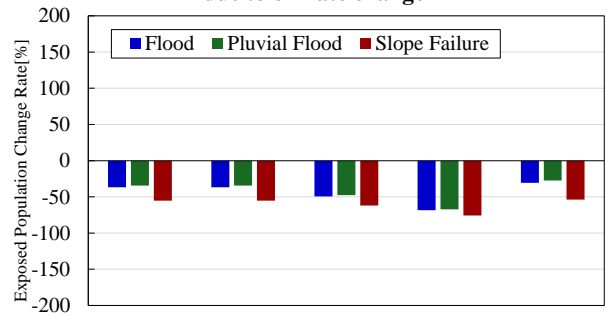

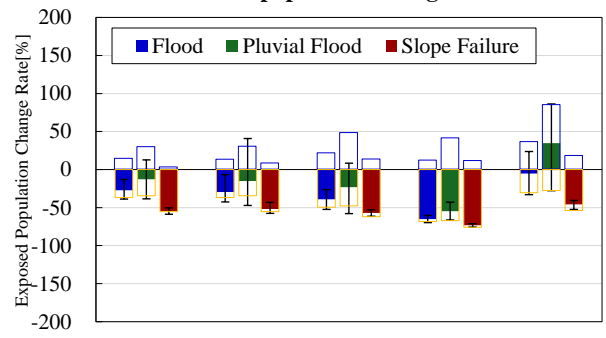Fig.2. Exposed population change rate by SSP due to population change

Fig.3. Exposed population change rate by SSP due to climate and population change

Reference

[1] Yamamoto, T., Kazama, S., Touge, Y., Yanagihara, H., Tada, T., Yamashita, T., and Takizawa, H.: Evaluation of flood damage reduction throughout Japan from adaptation measure taken under a range of emissions mitigation scenarios. *Climate Change*，Vol.165，No.60，2021.

[2] Kawagoe, S.,Kazama, S. and Sarukkalige, R.: Probabilistic modeling of rainfall induced landslide hazard assessment, *Hydrology and Earth System Sciences*，Vol.14, pp.1047-1061，2010.

[3] Yanagihara, H., Kazama, S., Yamamoto, T., Ikemoto, A., Tada, T., Touge, Y.: Nationwide evaluation of changes in fluvial and pluvial flood damage and the effectiveness of adaptation measures in Japan under population decline. *International Journal of Disaster Risk Reduct*, Vol.110, 2024, 104605, ISSN 2212-4209.

[4] Kawagoe, S., Esaka, Y., Ito, K., & Hijoka, Y. : Estimated Sediment Hazard Damage Using General Circulation Model Outputs in the Future. *Journal of Japan Society of Civil Engineers*, Ser. G (Environmental Research), Vol.70, No.5, pp. I_167-I_175, 2014.

The 12th International Symposium on Water Environment Systems
----- with Perspective of Global Safety   (Nov. 21st ~ 22nd , 2024)

GP-RSS & SyDE
Tohoku University

SRGAN-based downscaling of GRACE groundwater storage for improved aquifer management

◯ Sakina AHMED[1*], Yusuke HIRAGA[1] & So KAZAMA[1]

[1]Department of Civil and Environmental Engineering, Tohoku University, Miyagi 980-8579, Japan.
*E-mail: ahmed.sakina.r5@dc.tohoku.ac.jp

Abstract

Groundwater is a critical freshwater resource that supports agricultural, industrial, and domestic activities, necessitating continuous monitoring for sustainable water resource management. The Gravity Recovery and Climate Experiment (GRACE) mission has made substantial contributions to tracking regional-scale water mass changes. However, its coarse resolution limits its applicability to localized aquifers. This study proposes a deep learning approach to downscale GRACE-derived groundwater storage data using Super Resolution Generative Adversarial Network (SRGAN) combined with inception modules and a transformer, enhancing its utility for small-scale aquifer analysis. The downscaled data will provide valuable guidance for sustainable water policies, localized climate adaptation strategies, and informed water allocation decision making.

Keywords: Groundwater; Downscaling; GRACE; SRGAN; Bangkok.

1 Introduction

Groundwater is a valuable asset, particularly in regions with high water demand where climate change vulnerability and population growth exert pressure on water sources. As a major source of freshwater, groundwater has been extensively extracted for agricultural and industrial activities in the vicinity of Bangkok. Excessive and unregulated groundwater extraction in the past has placed significant stress on certain aquifers, resulting in severe land subsidence. To prevent such adverse effects, proper regulation and mitigation policies based on continuous monitoring must be implemented for sustainable water resource management. However, conventional monitoring requires on-site measurements of well water levels, which are often expensive, time-consuming, and inefficient for large-scale aquifers. Satellite-based monitoring methods, such as the Gravity Recovery and Climate Experiment (GRACE) mission, provide monthly measurements of Earth's gravity field, which are converted into variations in terrestrial water storage (TWS), with changes in groundwater storage (GWS) constituting one of its components. However, GRACE's coarse resolution (~300 km) limits its applicability in detecting localized groundwater changes in aquifer systems. Recent advancements in deep learning techniques, such as Super Resolution Generative Adversarial Networks (SRGAN) [1], have demonstrated their capabilities in climate downscaling for wind, rainfall, and sea surface temperature. Several deep learning approaches, such as Convolutional Long Short-Term Memory (ConvLSTM) and the Keras Sequential model [2,3], have also been applied to downscale GRACE to a finer resolution. However, to the authors' knowledge, no prior studies have applied SRGAN for GRACE downscaling. This study aims to propose a methodology to downscale GRACE-derived GWS from a 0.25° resolution to a 0.05° resolution by utilizing several hydrological and vegetation parameters to evaluate changes in GWS obtained from a mascon solution, facilitating its application in small-scale aquifer management and decision making.

2 Study area

The study area comprises seven provinces situated atop a clay layer in the lower Chao Phraya River delta (Fig. 1). The Chao Phraya lower groundwater basin includes eight hydraulically connected aquifers, consisting of unconsolidated alluvial deposits confined within clay layers. Groundwater is predominantly extracted from the third and fourth aquifers, as the upper two are too saline, and the deeper ones require prohibitively expensive drilling [4]. The climate is classified as tropical monsoon, with a mean annual rainfall of approximately 1,400 mm. Maximum temperatures in the dry season can exceed 38 °C between March and May.
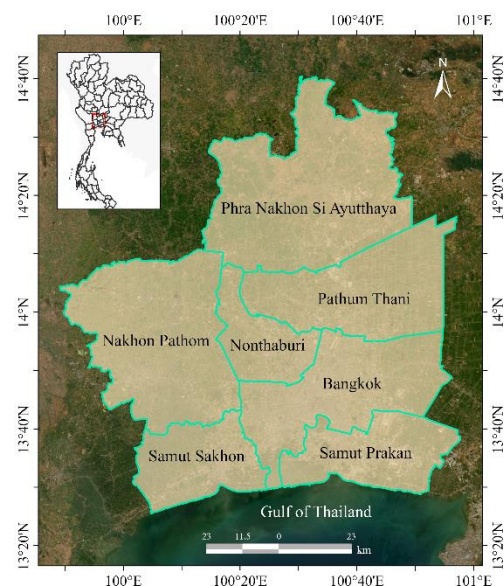

Fig. 1. Bangkok vicinity

3 Proposed methodology

The GRACE/GRACE-FO monthly mascon solution was obtained from the Center for Space Research (CSR) with spatial resolutions of 0.25° and 0.5°, covering the periods

The 12th International Symposium on Water Environment Systems
----- with Perspective of Global Safety (Nov. 21st ~ 22nd , 2024)
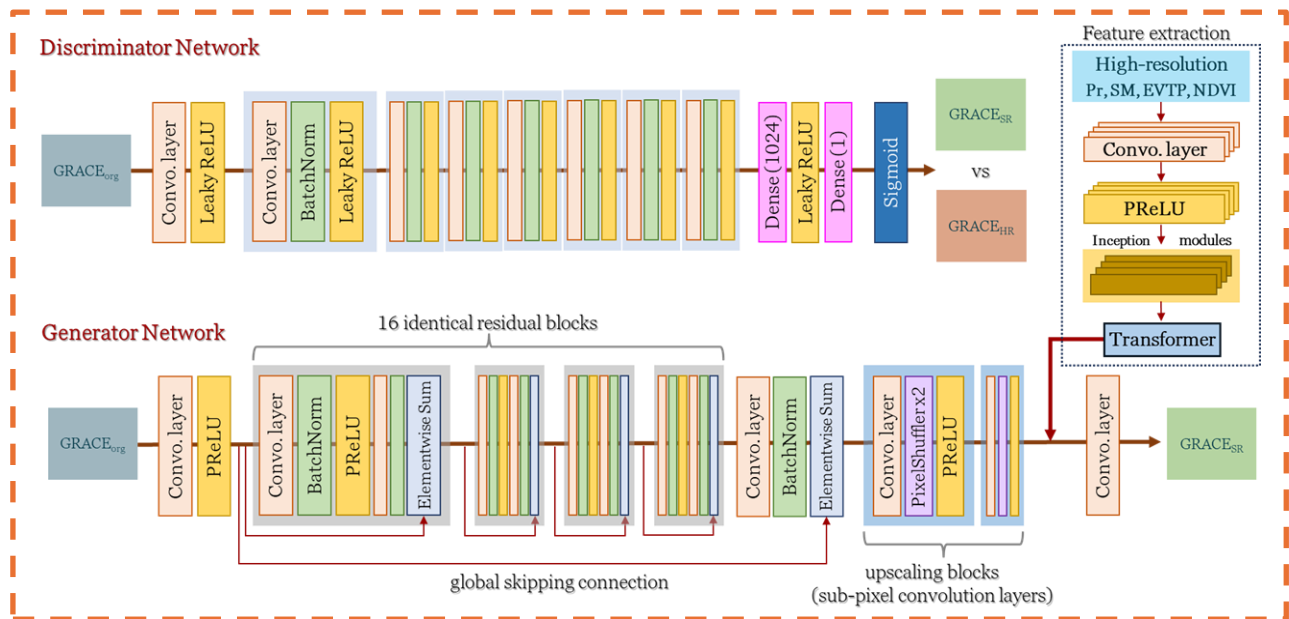
GP-RSS & SyDE
Tohoku University

from April 2002 to June 2016 and April 2002 to December 2023, respectively. The GRACE-derived GWS was calculated by subtracting canopy water, storm surface runoff, and soil and root zone moisture components from the Global Land Data Assimilation System (GLDAS) from GRACE's TWS. CHIRPS rainfall, SMAP soil moisture, and MODIS evapotranspiration and NDVI were upscaled to monthly resolutions of 0.05° and 0.25° to serve as correlated variables to improve downscaling performance. The SRGAN model consists of a generator network, which downscales low-resolution data (GRACE$_{org}$) to make it indistinguishable from real high-resolution data (GRACE$_{HR}$), and a discriminator network, which differentiates between the synthesized high-resolution data (GRACE$_{SR}$) and GRACE$_{HR}$. The two networks are trained recursively, formulated mathematically as a minimax optimization problem. The implementation of transformer and inception modules enables the detection of spatial features at multiple scales, leading to more accurate downscaling. Due to the unavailability of 0.05° GRACE data for direct validation, we followed the approach in [5], downscaling from 0.5° to 0.25° before downscaling to 0.05°. The data inputs were divided into 70% for training and 30% for testing. Four evaluation metrics: R^2, RMSE, MAE, and the correlation coefficient, will be calculated to assess downscaling accuracy. The proposed SRGAN network structures are illustrated in Fig. 2 below.

3 Merits of SRGAN-based downscaling

The proposed methodology allows for a finer spatial representation of GWS variations, which is highly beneficial in detecting early signs of groundwater drought and depletion at local scales. It also supports better-informed decisions on water allocation and enables localized climate adaptation strategies, such as rainwater harvesting and aquifer recharge, to ensure sustainable water supplies. This is critical for regions facing intense groundwater extraction, as it helps protect and optimize local groundwater resources and aids in crafting targeted policies.

Reference

[1] Ledig, C., Theis, L., Huszár, F., Caballero, J., Cunningham, A., Acosta, A., ... & Shi, W. (2017). Photo-realistic single image super-resolution using a generative adversarial network. In Proceedings of the IEEE conference on computer vision and pattern recognition (pp. 4681-4690).

[2] Foroumandi, E., Nourani, V., Huang, J. J., & Moradkhani, H. (2023). Drought monitoring by downscaling GRACE-derived terrestrial water storage anomalies: A deep learning approach. Journal of Hydrology, 616, 128838.

[3] Pulla, S. T., Yasarer, H., & Yarbrough, L. D. (2023). GRACE Downscaler: a framework to develop and evaluate downscaling models for GRACE. Remote Sensing, 15(9), 2247.

[4] Bremard, T. (2022). Monitoring land subsidence: The challenges of producing knowledge and groundwater management indicators in the Bangkok metropolitan region, Thailand. Sustainability, 14(17), 10593.

[5] Gu, S., Zhou, Y., Zhao, L., Ma, M., She, X., Zhang, L., & Li, Y. (2024). A Fast Generative Adversarial Network Combined with Transformer for Downscaling GRACE Terrestrial Water Storage Data in Southwestern China. IEEE Transactions on Geoscience and Remote Sensing.

Fig. 2. Proposed SRGAN downscaling framework, detailing the architectures of the generator and discriminator networks

The 12th International Symposium on Water Environment Systems
----- with Perspective of Global Safety   (Nov. 21st ~ 22nd , 2024)

GP-RSS & SyDE
Tohoku University

Relationship between long-term river-to-coast sediment supply and channel characteristics

◯ Shimon SUZUKI[1] & Keiko UDO[1*]

[1]Department of Civil and Environmental Engineering, Tohoku University, Miyagi 980-8579, Japan.
[*]E-mail: keiko.udo.c1@tohoku.ac.jp

Abstract

This study carried out a one-dimensional mixed grain size riverbed fluctuation analysis for rivers with different channel characteristics in Japan to understand the sediment supply from the river to the coast quantitatively and by grain size. Sensitivity analysis of several cases of sediment upstream edge boundary conditions showed a linear relationship between long-term sediment inflow from the upstream edge and sediment supply to the coast. The slope and intercept of the regression line showed different values for each river and varied by grain size. These results suggest that differences in river bed slope and bed material affect the sediment supply to the coast.

Keywords: sediment transport; grain size distribution; one-dimensional model; boundary conditions

1 Introduction

Rapid beach erosion in Japan occurred as a result of human activities such as the construction of dams and coastal structures especially during the rapid economic growth period in the 1960s. In particular, one of the main causes of beach erosion is the interception or disappearance of large amounts of sediment on land due to gravel mining in the river channel and sediment deposited by dams [1].

To predict beach erosion based on more realistic future climate change, the sediment budget of past sandy beaches needs to be quantitatively clarified. Furthermore, due to the different transport patterns, transport, and deposition for each grain size, evaluating the sediment supply by grain size is important. In this case, riverbed fluctuation calculations are often used to quantify the sediment supply from the river to the coast. The sediment inflow at the upstream edge, which is required for the calculation of river bed fluctuations, should be input as sediment transport data obtained from field observations. Observations of bedload and suspended load have been carried out in Japan, but the observation points and data sampling periods are limited and the accumulated observation data is difficult to use as input conditions for riverbed fluctuation calculations, so the method of giving the equilibrium sediment transport at the upstream edge is generally used [2]. However, because the equilibrium sediment transport is determined by the riverbed slope and bed material at the upstream edge, it does not take into account the effects of changes in sediment dynamics upstream, such as sediment yield due to large-scale slope failure in mountainous areas and human activities such as dams and land use changes.

In this study, several cases of sediment inflow from the upstream edge in rivers with different channel characteristics in Japan were analyzed and the sediment transport characteristics of each river were compared. The objective is to evaluate the relationship between sediment inflow and supply in each river and the relationship between sediment supply from the river to the coast and the river channel characteristics.

2 Materials and methods

This study uses the one-dimensional mixed-grain riverbed fluctuation analysis model of Takebayashi and Fujita [3] to calculate riverbed fluctuations over a long-term and large range. The amount of bedload is obtained from the equation of Ashida, Egashira and Liu [4]. The equation of Lane and Kalinske [5] is used for the reference concentration of suspended load at equilibrium, and the Rubey [6] equation is used for the fall velocity of suspended load.

Table 1 shows the analysis conditions for each river basin. The calculation conditions were determined similarly to the Yoshinogawa River calculations shown in Nakahara [7] to compare our results of Abukumagawa and Abegawa rivers with them. The measured data on riverbed level and bed materials as initial conditions were provided by the

Table 1 Analysis conditions for each river basin.

Conditions	Abukumagawa river	Abegawa river	Yoshinogawa river [7]
Analysis section	0.8 km - 37.2 km	0.0 km - 22.0 km	0.0 km - 77.8 km
Analysis period	2000 - 2019	2012 - 2022	1965 - 1999
Targeted runoff events	≥1,000 m³/s	≥100 m³/s	≥1,000 m³/s
Measurement point of discharge at the upstream edge in the calculation	Marumori	Usizuma	Ikeda (Mu-Tei)
Measurement point of water level at the downstream edge in the calculation	Arahama	normal depth	Komatsujima
Year of measured initial riverbed	2000	2012	1965
Year of measured initial bed material	2000	2012	1996, 1997
Grain size	13 (silt ~ gravel)	13 (silt ~ cobbles)	18 (silt ~ cobbles)
Δt	1 s	1 s	1 s
Δx	200 m	250 m	200 m

The 12th International Symposium on Water Environment Systems
----- with Perspective of Global Safety (Nov. 21st ~ 22nd , 2024)
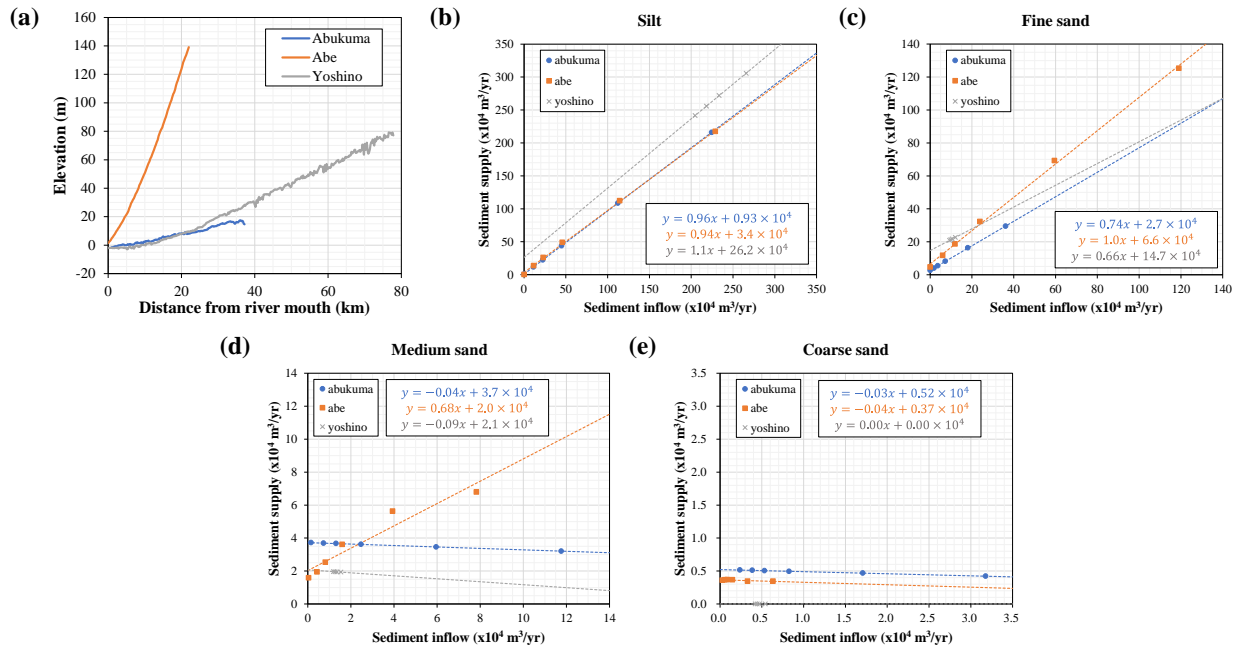
GP-RSS & SyDE
Tohoku University

Fig. 1. Riverbed level of three rivers (a), the relationship between sediment inflow and supply by grain size (b)~(e).

respective offices of the Ministry of Land, Infrastructure, Transport and Tourism (MLIT).

Six upstream boundary conditions of sediment size distributions were set and analysis was conducted to evaluate the relationship between sediment inflow from the upstream edge and sediment supply to the coast in the Abukuma and Abe Rivers. The conditions were the inflow of the equilibrium sediment volume from the upstream edge and the inflow of 0, 0.5, 2, 5, and 10 times the equilibrium sediment volume.

3 Results and discussion

Figure 1 shows the riverbed level of the three rivers within the analysis section and a comparison of the relationship between the sediment inflow from the upstream edge and the sediment supply to the coast for each river by grain size. There is an almost 1:1 relationship between inflow and supply for the silt content. This is obvious since the silt content is transported as a wash load. The intercept value was the largest in the Yoshino River, suggesting that the intercept varies with the amount of silt deposited in the river channel.

For fine sand, the slope of the Abe River is approximately equal to 1, suggesting that the fine sand inflow from the upstream edge is transported directly to the river mouth. On the other hand, the Abukuma River and the Yoshino River have slopes of less than 1, suggesting that some of the fine sand inflow from the upstream edge is deposited in the river channel.

For medium sand, the slopes of the Abukuma and Yoshino Rivers are close to 0, while the Abe River shows a proportional relationship. The regression lines for fine and medium sand had different characteristics between the rapid Abe River and the gentle Abukuma and Yoshino Rivers. Differences in riverbed slope probably affect fine and medium sand transport patterns.

For coarse sand, the slopes of all rivers are close to 0. Therefore, this suggests that most of the coarse sand inflow from the upstream edge is deposited in the river channel.

4 Conclusions

This study conducted a one-dimensional riverbed fluctuation analysis in the Abukuma, Abe, and Yoshino Rivers with different river channel characteristics. The long-term sediment inflow from the upstream edge and the supply from the river to the coast were compared by grain size. The slope and intercept of the regression line differed between rivers and between grain sizes. These results suggest that differences in riverbed slope and bed material affect sediment supply to the coast.

Reference

[1] Udo, K., Takeda, Y. and Yokoo, Y.: Relationship between potential sediment supply from river to sea and beach erosion in Japan, *Journal of Japan Society of Civil Engineers, Ser. B2 (Coastal Engineering)*, Vol. 72, Issue 2 (2016), pp. I_799-I_804.

[2] Yamamoto. K.: Comprehensive sediment management plan - Toward a sound sediment system, Gihodo Shuppan (2014), pp. 193-253.

[3] Takebayashi, H. and Fujita, M.: One dimensional bed deformation analysis with general cross-section on bed composed of cohesive and non-cohesive materials, *Journal of the Japan Society of Erosion Control Engineering*, Vol. 64, Issue 2 (2011), pp. 3-14.

[4] Ashida, K., Egashira, S., and Liu, B.: Numerical method on sediment sorting and bed variation in meander channels, *Proceedings of Hydraulic Engineering*, Vol. 35 (1991), pp. 383-390.

[5] Lane, E. W. and Kalinske, A. A.: Engineering calculations of suspended sediment, *Transactions-American Geophysical Union*, Vol. 22 (1941), pp. 603-607.

[6] Rubey, W. W.: Settling velocities of gravel, sand, and silt particles, *American Journal of Science*, Vol. 25, No. 148 (1933), pp. 325-338.

[7] Nakahara, D.: Impact Assessment of Gravel Mining and Dam Reservoirs on Long-Term Sediment Dynamics in Yoshinogawa River, Japan, Graduate School of Engineering, Tohoku University, Master's Thesis (2024).

The 12th International Symposium on Water Environment Systems
----- with Perspective of Global Safety (Nov. 21st ~ 22nd, 2024)

GP-RSS & SyDE
Tohoku University

Modeling Post-Wildfire Hydrological Responses: Assessing Flood Risk Amplification in California's Watersheds

○ Wasitha Dilshan[1*], Yusuke Hiraga[1] & So Kazama[1]

[1]Department of Environmental Engineering, Environmental University, Miyagi 980-8579, Japan.
[*]E-mail: munipurage.wasitha.randeepa.ranga.dilshan.p5@dc.tohoku.ac.jp.

Abstract

Rising global temperatures have been connected to a surge in extreme weather events and widespread wildfires. Although the effect of wildfires on downstream flood discharge is critical for flood risk management, there remains a gap in understanding this influence at the watershed scale. This study investigates the effects of wildfires on downstream flood discharge across 30 watersheds in California. Using the Soil and Water Assessment Tool (SWAT), we simulated daily discharge over a 20-year period, achieving strong model performance with R^2 values of 0.67-0.86 and Nash-Sutcliffe Efficiency (NSE) values of 0.65-0.86. Comparing observed flood discharge with simulated unburned conditions, our analysis reveals a significant increase in post-fire discharge, with an average 17.1% rise observed in 83.3% of watersheds during the first post-fire year. Statistically, a strong positive correlation (R^2=0.74; $p < 0.01$) exists between increased discharge and the percentage of burned watershed area. By adjusting Curve Numbers (CN) in SWAT, we quantified wildfire impacts, finding CN increments ranging from 16.5% to 30%, depending on burn severity and land use. A linear relationship was also established between wildfire area and CN increment, with a slope of 0.39, refining post-fire flood simulations.

Keywords: Curve Number; Flood risk; Peak discharge; SWAT model; Wildfire.

1 Introduction

Wildfires have emerged as a critical issue, significantly altering watershed hydrology, increasing erosion and runoff, and elevating flood risks [1]. Understanding the interaction between intense rainfall and wildfires is crucial for effective flood risk reduction. The increasing trend of compound disaster events, combining wildfires and extreme rainfall, presents complex challenges for disaster management [2]. California's water management has faced significant challenges due to frequent droughts and atmospheric river events, leading to water shortages and flood risks, exacerbated by climate change. California's water management infrastructure, including dams and reservoirs, is vital for collecting and storing runoff but is compromised by wildfires, which intensify discharge and sediment load. Evaluating the long-term viability of water management strategies requires considering wildfire impacts. Research has addressed various aspects of this issue [3,4], but studies on pluvial floods at short time scales remain limited. Recent investigations highlight how wildfire patterns impact water supply watersheds, affecting water availability and quality.

Given these limitations and the growing importance of understanding wildfire impacts on hydrology, this research aims to analyze how wildfires affect downstream discharge in California's watersheds. The study will focus on several key aspects: quantifying how wildfires alter watershed-scale post-fire peak discharge volumes and developing predictive models for peak discharge scenarios under various hypothetical conditions. Therefore, this study aims to understand the impact of wildfires by: (a) quantifying changes in post-fire peak discharge volumes at the watershed scale, and (b) identifying the relationships between wildfire characteristics and post-fire downstream peak discharge enhancements.

2 Materials and methods

2.1 Study Area

California's diverse landscape, spanning from the Sierra Nevada to coastal plains, experiences wide-ranging elevations, microclimates, and precipitation patterns. Annual rainfall varies from 20 cm in deserts to 200 cm in coastal mountains, influenced by topography and atmospheric rivers. The Sierra Nevada snowpack is essential for water resources, while temperatures vary across regions. Climate change is intensifying precipitation variability, complicating water management. This study examines 30 minimally managed California watersheds (169.9–1370.6 km²), each affected by major wildfires, with over 5% of their area burned.
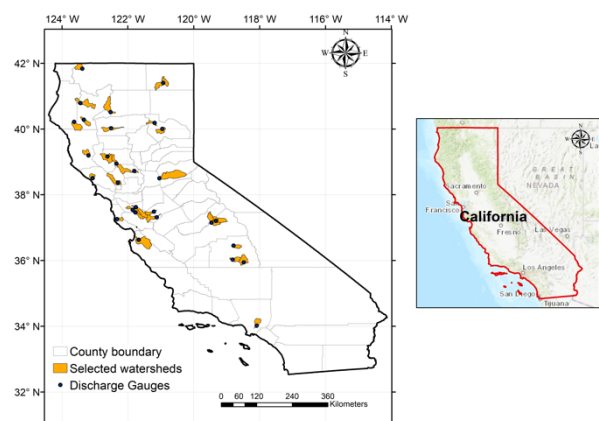

Fig. 1. Study Area.

2.2 Peak discharge estimation

This study employs the SWAT hydrological model to investigate the impacts of wildfires on peak discharge in California watersheds. SWAT model was calibrated for each

The 12th International Symposium on Water Environment Systems
----- with Perspective of Global Safety   (Nov. 21st ~ 22nd , 2024)

GP-RSS & SyDE
Tohoku University

watershed before and after the fire event using daily time steps. Despite good overall model performance in pre-fire simulations, some peak discharge events were underestimated. To account for model uncertainty, an error term was calculated based on pre-fire simulation underestimations.

The research methodology involved simulating a "no fire" scenario using pre-fire model parameters for each watershed. The maximum underestimation from the pre-fire model was adopted as the upper error limit for reconstructed post-fire hydrographs. Any observed peak discharge exceeding this limit was considered significantly impacted by wildfire. This approach was validated across all 30 watersheds, and discharge increments were compared with basin-scale fire characteristics, including average burn severity, percentage of area burned, major land use class affected, and wildfire location.

To quantify wildfire impact on peak discharge, the study adjusted the Curve Number (CN) in the SWAT model. The watershed average CN was manually adjusted to match observed and simulated discharge volumes for the first and largest post-fire flood events in the immediate post-fire year, with a 5% target margin of error. The required CN increase for these events was then compared across different watersheds and fire characteristics.

3 Results and discussion

The SWAT model simulation of pre-fire discharge yielded strong statistical performance across all watersheds, with R^2 and Nash coefficient values exceeding 0.65 during both calibration and validation periods. The study quantified wildfire-induced changes in peak discharge volumes during the post-fire period for each watershed. Our analysis showed that the most substantial increase in discharge volume occurred in the first year after a fire, averaging 17.1%, with 83.3% of watersheds experiencing peak increases. In the following years, discharge increments gradually decreased but remained above pre-fire levels.

The results revealed significant correlations between CN increments and factors such as burn severity, land use, burn scar location, and the percentage of watershed area burned. CN increments ranged from 16.5% to 30% based on burn severity and event type, with mixed forests showing the largest increments.
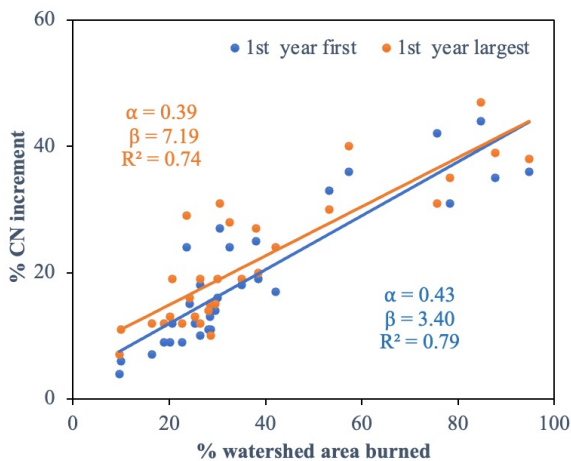
Fig. 2. Relationship between watershed area burned and Curve Number increment for the selected watersheds.

Strong positive correlations were identified between CN increases and the percentage of burned watershed area (R^2 values of 0.79 and 0.74 for largest and first peak discharge events, respectively). A novel linear relationship, CN increment = α × (wildfire area burned) + β, was developed, with α and β values varying by event type.
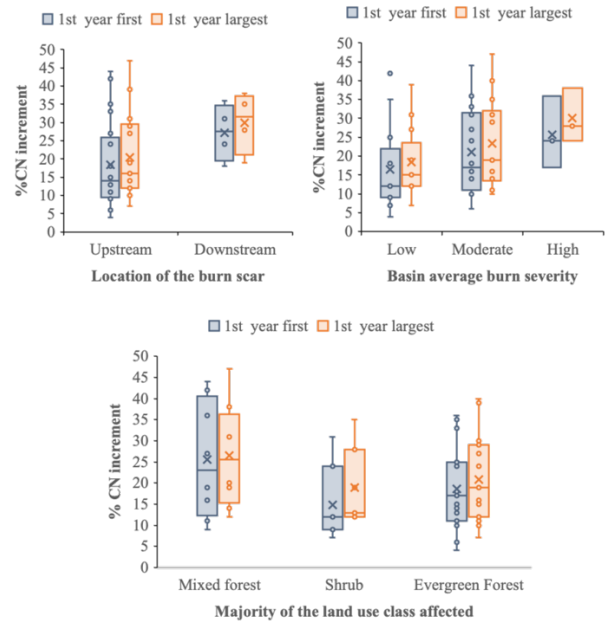
Fig. 3. Post-fire % CN increment under different fire characteristics, for 1st and largest peak flow events in immediate post-fire year.

4 Conclusions

This study uncovers complex interactions between wildfire characteristics, land use, and hydrological response, with variations in CN increments across land use types and fire locations providing key insights for tailored watershed-scale post-fire management. However, limitations include model uncertainty, data resolution constraints, and a narrow watershed selection. Future research should expand to watersheds with significant water infrastructure, examine seasonal impacts and snowmelt processes, link soil properties to burn severity, integrate climate projections, and improve peak discharge prediction methods.

Reference

[1] Bowman, D.M.J.S., Kolden, C.A., Abatzoglou, J.T., Johnston, F.H., van der Werf, G.R., Flannigan, M., 2020. Vegetation fires in the Anthropocene. Nature Reviews Earth & Environment, 1(10), 500–515.

[2] Touma, D., Stevenson, S., Swain, D. L., Singh, D., Kalashnikov, D. A., & Huang, X. (2022). Climate change increases risk of extreme rainfall following wildfire in the western United States. Science Advances, 8(13).

[3] Havel, A., Tasdighi, A., Arabi, M., 2018. Assessing the hydrologic response to wildfires in mountainous regions. Hydrology and Earth System Sciences, 22(4), 2527–2550.

[4] Williams, A.P., Livneh,..., Rinaldo, A., 2022. Growing impact of wildfire on western US water supply. Proceedings of the National Academy of Sciences, 119(10).

The 12th International Symposium on Water Environment Systems
----- with Perspective of Global Safety   (Nov. 21st ~ 22nd , 2024)

GP-RSS & SyDE
Tohoku University

An Integrated Evaluation of the Potential for Hydropower Generation and Flood Damage Reduction in Irrigation Reservoirs Across Japan

○ Atsuya IKEMOTO [1*], So KAZAMA[1] ,Takeo YOSHIDA[2], & Ryosuke ARAI[3]

[1]Department of Civil and Environmental Engineering, Graduate of School of Engineering, Tohoku University, Miyagi 980-8579, Japan.*E-mail: ikemoto.atsuya.s1@dc.tohoku.ac.jp
[2] National Agriculture and Food Research Organization
[3] Sustainable System Research Laboratory, Central Research Institute of Electric Power Industry,

Abstract

This study aims to evaluate integrated potential benefit both flood damage reduction effect and hydropower generation nationwide in Japan. We use two-dimensional inundation analysis model to evaluate flood damage reduction effect and artificial neural network model (ANN model) to estimate flow regime of each irrigation reservoir flow regime. As a results, The flood damage reduction benefit was 4,58 billion yen/year by using all irrigation reservoirs in Japan. The hydropower generation benefit was 1.80 billion yen/year. In total, these benefits are 6.38 billion yen. The flood damage reduction benefit accounts for 71.8%. The irrigation reservoirs maintenance for adaptation measures and mitigation measures is required in Hyogo prefecture because flood damage reduction benefits and hydropower generation benefit are almost equal.

Keywords: *adaptation measures, mitigation measures, irrigation reservoirs, hydropower generation, flood control*

1 Introduction

Adaptation and mitigation measures need to be implemented urgently to reduce risks caused by accelerating global warming [1]. In Japan, the concept of River Basin Disaster Resilience and Sustainability by All [2], which includes integrated water management, aims to utilize irrigation facilities as an adaptation strategy. Additionally, as a mitigation strategy, the expansion of renewable energy sources helps slow global warming by reducing greenhouse gas emissions. Both flood control and energy development efforts are expected to make use of agricultural water facilities. In Japan, irrigation reservoirs have traditionally been used exclusively for irrigation activities, such as supplying water to paddy fields. Expanding the use of these reservoirs for other purposes poses certain risks; however, previous studies have independently demonstrated the benefits of using irrigation dams and reservoirs for flood control and hydropower generation at the municipal level. Despite the potential advantages, the number of irrigation reservoirs utilized for these purposes remains very limited in Japan [3], [4]. This study aims to evaluate the integrated potential benefits of both flood damage reduction and hydropower generation on a nationwide scale in Japan.

2. Dataset

2.1 Data for inundation analysis and calculation damage cost

Rainfall data, land use data, elevation data, and irrigation reservoir data used for inundation analysis were the same as those utilized by Ikemoto et al. [5]. Land use and elevation data are stored in the National Land Numerical Information (NLNI) database. Irrigation dams data from the NLNI database [6] were incorporated into a disaster prevention support system for irrigation reservoirs, enabling comprehensive consideration of agricultural water facilities throughout Japan.

2.2 Data for estimation of basin regime

Rainfall data, snow data, and evapotranspiration data, which were inputs to the ANN model, were obtained from APHRO_JP V1207 [7] and APHRO_JP V1801. Monthly atmospheric data, including precipitation data, temperature data, snow depth data, sunshine duration data, and global solar radiation data, stored in the NLNI database, were also used. Geological, soil, and topographical data, likewise available in the NLNI database, were input as well.

3. Methods

3.1 Inundation analysis

We used a two-dimensional inundation analysis model, as validated by Yanagihara et al. [8], for the inundation analysis. The spatial resolution of the model is approximately 250 m. The rainfall data were distributed evenly across 24 hours for the analysis. The effect of damage cost reduction through the use of irrigation reservoirs was estimated by incorporating the reservoir volume into the analysis. The volume is considered the limit of water storage, representing the water storage capacity per unit area. The limit of water storage capacity in each grid cell was calculated by dividing the total reservoir storage in each mesh by the mesh area. In cells with existing irrigation reservoirs, inundation occurs when the cumulative inundation depth over specific time steps exceeds the water storage capacity limit.

3.2 Calculation damage cost

The damage cost in each mesh was estimated based on inundation depth by referring to the Flood Control Economic Survey Manual (Draft) [9]. Finally, the total damage cost was calculated by summing the damage costs in each mesh. The damage was assumed to occur in areas including paddy fields, crop yields, houses, offices, and golf courses. The expected annual damage cost was calculated by averaging the damage costs for each flood scale. In this study, four flood scales were used, corresponding to return periods of 30, 50, 100, and 200 years.

The 12th International Symposium on Water Environment Systems
----- with Perspective of Global Safety   (Nov. 21st ~ 22nd , 2024)

GP-RSS & SyDE
Tohoku University

3.3 Methods for estimating hydropower and benefit

The basin regimes in each irrigation reservoir were estimated using an ANN model [10] developed to estimate river regimes in unobserved basins in Japan. The output data includes mean annual streamflow and Q_D values: Q_{D95}, Q_{D185}, Q_{D275}, and Q_{D355}, representing the number of days per year on which daily streamflow exceeds specific thresholds. The model parameters were adjusted to maximize the correlation between observed and estimated data. Flow regime curves for each irrigation reservoir were determined based on the approximation formula proposed by Nakane [11]. Hydropower generation potential was calculated by applying inflow data to Eq. (1).

$$P = \gamma \rho g Q H_e = 0.8 \cdot \gamma \rho g Q H \qquad (1)$$

where, P : hydropower generation[W], γ : utilization efficiency, g : gravitational acceleration[m/s^2], Q : discharge[m^3/s], H_e : effective head [m], H : total head[m]. γ is adopted 0.529. Outflow equals inflow to estimate maximum hydropower generation as power generation facility. Hydropower generation is economically valued by using 22.9 yen/kWh as fixed purchased price in 2020.

4. Results and discussion

The flood damage reduction benefit achieved by utilizing all irrigation reservoirs in Japan was estimated at 4.58 billion yen per year, while the hydropower generation benefit was estimated at 1.80 billion yen per year. Together, these benefits total 6.38 billion yen annually, with flood damage reduction accounting for 71.8% of the total. Figure 1 shows the total economic value, as the sum of flood damage reduction and hydropower generation benefits, for each prefecture in Japan. Values in brackets represent the percentage of flood damage reduction benefits within the total value. The top five prefectures are Hyogo with 1.11 billion yen per year (58.6%), Osaka with 1.08 billion yen per year (93%), Okayama with 350 million yen per year (89%), Tokyo with 260 million yen per year (100%), and Hiroshima with 240 million yen per year (91.7%). In Hyogo Prefecture, maintenance of irrigation reservoirs for both adaptation and mitigation measures is essential, as flood damage reduction and hydropower generation benefits are nearly balanced. In other prefectures, flood damage reduction benefits outweigh hydropower generation, indicating that maintenance for adaptation measures is primarily needed.

5. Conclusions

The reason why Tokyo's flood damage reduction cost benefit is higher than that of other prefectures, despite the smaller number of irrigation reservoirs, is due to the significant effect of reservoirs located upstream in the Tone River basin. In Kochi Prefecture, the benefit is 240 million yen per year (2%), where maintenance for mitigation measures is expected, as the hydropower generation benefit is greater than the flood damage reduction benefit.
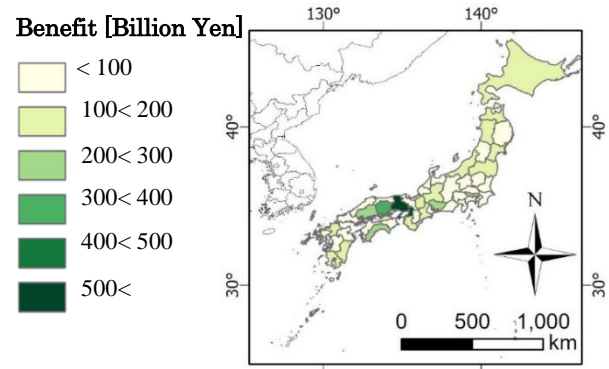

Fig.1 Benefits gained from flood damage reduction and hydropower generation

Reference

1) IPCC: Summary for Policymakers. In: Climate Change 2023: Synthesis Report.Contribution of Working Groups I, II and III to the Sixth Assessment Report of the Intergovernmental Panel on Climate Change [Core Writing Team, H. Lee and J. Romero (eds.)]. IPCC, Geneva, Switzerland, pp. 1-34, 2023.
2) Ministry of Land Infrastructure Transport and Tourism : River Basin Disaster Resilience and Sustainability by All Japan's New Policy on Water-related Disaster Risk Reduction, 2020.
3) Tanakamaru et al. : Simple Estimation Method of Flood Mitigation Effect of Irrigation Ponds, *Water, Land and Environmental Engineering*, Vol.88, No.9, pp. 737-740, 2020.
4) Goto et al. : Utilization of Agricultural Water Use Facilities Combining Small-scale Hydropower, *Technical report of the National Research Institute of Agricultural Engineering. WM*, Vol.180, pp.13-28,1988.
5) Ikemoto et al. : Evaluation of an adaptation strategy for flood damage mitigation under climate change through the use of irrigation reservoirs in Japan. *Water Resources Management*, 37(10), 4159–4175, 2023.
6) Ministry of Land Infrastructure Transport Tourism : National Land Numerical Information , https://nlftp.mlit.go.jp/ksj/other/agreement.html.
7) Kamiguchi et al.: Development of APHRO_JP, the first Japanese high-resolution daily precipitation product for more than 100 years, *Hydrological Research Letters*, Vol.4, pp.60–64, 2010.
8) Yanagihara et al. : REGIONAL EVALUATION OF POTENTIAL FLOOD DAMAGE REDUCTION BY PADDY FIELD DAM IN JAPAN, *Journal of Japan Society of Civil Engineers, Ser. G (Environmental Research)*, Vol. 77, No.5, pp. I_33-I_42, 2021.
9) Ministry of Land Infrastructure Transport Tourism : Manual for Economic Evaluation of Flood Control Investment(Draft), 2020
10) Arai et al: Streamflow maps for run-of-river hydropower developments in Japan. *Journal of Hydrology*, 607, 127512, 2022.
11) Nakane : Estimation of Discharge-Duration Curve, *National Research Center for Disaster Prevention*,Vol.31, pp.35-65, 1983.

The 12th International Symposium on Water Environment Systems
----- with Perspective of Global Safety   (Nov. 21th ~ 22th , 2024)

GP-RSS & SyDE
Tohoku University

Assessing the effectiveness of reducing the amount of damage to trees in river channels throughout Japan

Takaya KANEKO[1*], So KAZAMA[1]

[1]Department of Civil Engineering, Environmental Tohoku University, Miyagi 980-8579, Japan.
*E-mail: kaneko.takaya.q2@dc.tohoku.ac.jp.

Abstract

This study evaluated the effectiveness of in-channel vegetation clearing to reduce flood inundation damage in a first-class water system in Japan. Focusing particularly on trees, each river was divided into three sections, and the logging area was further subdivided into three zones for analysis. As a result, the Joganji, Tokachi, Iwaki, Saru, and Kurobe Rivers were found to be the water systems that reduced damage the most. The most effective cut-off points were located in the downstream areas, where 30% of the first class water systems were located. Conversely, 17% of the water systems showed no significant impact from cutting. These results suggest that tree cutting around urban areas can be an effective measure to reduce flood damage. However, careful consideration is required since tree felling increased the amount of damage in many locations.

Keywords: *adaptation, tree cutting, damage reduction*

1 Introduction

It has been shown that the increasing severity of flood damage is caused by global warming[1]. Various adaptation measures have been implemented to address this issue, but effective river channel management remains essential. Given the limitations of adaptation strategies alone, both adaptation and mitigation measures must be promoted. One adaptation measure that also incorporates mitigation is the removal of in-channel vegetation.

By cutting in-channel vegetation, the water-carrying capacity of streams is increased, thereby reducing flood damage. This approach can also prevent secondary disasters, such as the formation of driftwood. Since in-channel vegetation is widespread across Japan, it would be cost-prohibitive to remove all vegetation, making it crucial to focus on efficient removal points.

A previous study by Yanagihara et al.[2] analyzed the reduction in flood damage when all vegetation in river channels across Japan was removed. However, river vegetation includes both grasses and trees, with trees having a greater impact on flow capacity. Therefore, to optimize removal efforts, it is important to assess the flood damage reduction effect of cutting only trees. This study focuses on evaluating the effectiveness of tree removal in reducing flood damage across river channels throughout Japan.

2 Data set and methods

A vegetation map was used to differentiate between herbaceous and woody vegetation within the river channels. The Ministry of the Environment provides data on the distribution of vegetation across Japan through this map, which is based on dominant species and created at a scale of 1:50,000[3]. In this map, areas containing woody species are classified as such, while all other areas are categorized as herbaceous vegetation. To extract vegetation data specifically for river channels, we used the river channel mask developed by Yamamoto et al.[4].

For the flood inundation analysis, a two-dimensional unsteady flow model was applied with a spatial resolution of 250 meters. The impact of tree removal within the river channels was represented by changes in the roughness coefficient. Prior to tree removal, the roughness coefficient was calculated using Equation 1, as derived by Fujishita and Kure[5], which is based on the NDVI value. After logging, the roughness coefficient was uniformly set to 0.03, following the reference by Ishikawa et al.[6]. In non-vegetated areas, the roughness coefficient was set to 0.025, and for off-channel areas, coefficients were assigned according to land use.

$$\text{roughness} = \begin{cases} 0.037 (NDVI<0.6) \\ 0.079 \times NDVI - 0.01 (0.6 \leq NDVI \leq 0.8) \\ 0.053 (NDVI>0.8) \end{cases} \quad (1)$$

NDVI data from Sentinel-2 were obtained via Google Earth Engine for the period from September to November each year from 2019 to 2023. The inundation depths from the flood analysis were used to calculate damage, following the guidelines in the Flood Control and Economic Research Manual. Damage was calculated based on land use for rice fields, agricultural fields, building sites, and golf courses. The calculation formula is Equation 2.

$$Damage = \sum Asset\ value\ of\ flooded\ cells \quad (2)$$

$$\times\ Damage\ rate\ according\ to\ flood\ depth$$

To evaluate the impact of tree removal, tree harvesting areas were defined to compare the effects across different categories within each water system. The tree areas in each category were standardized to ensure equal areas, and the energy required for logging was kept consistent within each water system. The tree areas were ranked in descending order of elevation, and the harvesting sections (downstream, midstream, and upstream) were established by dividing the total tree area of each water system into three sections, starting from the downstream end.

The 12th International Symposium on Water Environment Systems
----- with Perspective of Global Safety   (Nov. 21th~22th , 2024)

GP-RSS & SyDE
Tohoku University

3 Results and discussion

The results of the calculated damage reduction ratios are shown in Figure 1. The horizontal axis represents the percentage of damage reduction when all trees in the cutting sections are harvested, while the vertical axis shows the percentage of damage reduction for each harvested area. The orange line indicates the damage reduction rate for total tree removal, with points above the line indicating that selective cutting in certain areas is more effective than cutting all areas. Conversely, points below the line suggest that selective cutting is less effective. The top five water systems with the highest damage reduction from in-channel tree removal were the Joganji(2.1%), Iwaki(1.2%), Tokachi (1.1%), Saru(1.1%), and Kurobe(0.87%) Rivers. In four of these five systems, downstream cutting was the most effective. The Saru River was the only system where total cutting resulted in higher damage reduction than selective cutting by section. On the other hand, the five water systems with the lowest damage reduction ratios were the Omono(-0.81%), Monobe(-0.77%), Yoshino(-0.51%), Shigenobu(-0.51%), and Shokotsu(-0.38%) Rivers, where cutting actually increased damage, resulting in negative damage reduction rates.

When each water system was divided into three sections, we evaluated which section would be most effective for reducing damage through tree removal. Figure 2 presents the results, showing that 31.2%, 18.3%, and 10.1% of the 109 water systems were most effectively cut in the downstream, midstream, and upstream sections, respectively. Additionally, 22.9% of the water systems saw the greatest benefit from cutting in all sections, while 17.4% experienced no benefit from tree removal. Notably, in about 30% of the water systems, logging in the downstream section was most effective, likely because urban areas—often located downstream—are more vulnerable to flood damage. In many cases, cutting in upstream areas led to increased damage downstream, as the flow that would have overflowed upstream was redirected downstream due to the removal of vegetation. In conclusion, selectively removing trees in urban-adjacent areas downstream is an effective strategy for reducing flood damage. However, it is essential to consider the impact on the entire water system, as in some cases tree removal can increase flood risks downstream.

4. Conclusion

In this study, we assessed the impact of clearing vegetation, particularly trees, from river channels on flood damage reduction across Japan. The results showed that the Joganji, Tokachi, Iwaki, Saru, and Kurobe Rivers had the highest damage reduction. The most effective cutting sites were primarily located in downstream areas, with 30% of Class 1 water systems situated in these regions. Conversely, 17% of the water systems showed no significant impact from vegetation removal.

In this analysis, the influence of trees was modeled as a roughness factor in the inundation simulation. However, it would be more accurate to treat trees as cross-sectional areas of river. In the future, a two-dimensional inundation analysis considering cross-sectional areas of river. will be conducted to more comprehensively evaluate the impact of tree removal.
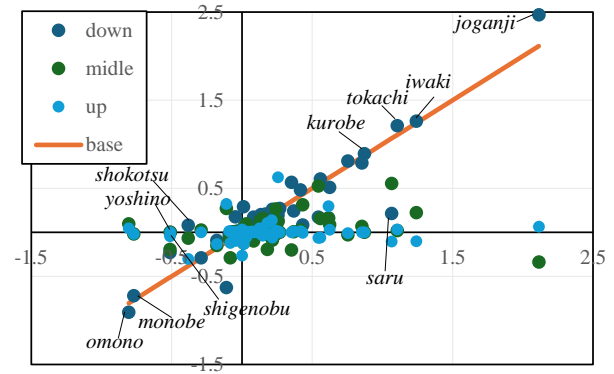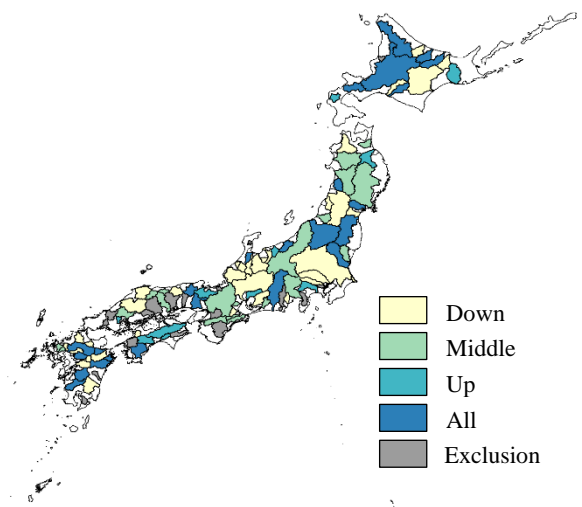

Fig. 1 Damage Reduction Rate

Fig. 2 Optimal cutting classification

References

[1] IPCC: Summary for Policymakers. In: Climate Change 2021: The Physical Science Basis. Contribution of Working Group I to the Sixth Assessment Report of the Intergovernmental Panel on Climate Change, pp. 4, Cambridge University Press, 2021.

[2] Yanagihara, H., Ikemoto, A. , Kazama, S., Kure, S. and Fujishita, R.: Evaluation of flood adaptation and mitigation measures based on the cutting sequence of river channel vegetation, *Journal of Japan Society of Civil Engineers*, Vol.80, Issue 16, 2024.

[3] Ministry of the Environment: 2nd Basic Survey Vegetation Survey Report, https://www.biodic.go.jp/kiso/fnd_f.html, last viewed on 2024/07/23.

[4] Yamamoto, T., Tada, T. and Kazama, S.: Datasets of Strahler Stream Order and Flood Plain Masks in Japan, *Journal of Japan Society of Hydrology and Water Resources*, Vol. 36, Issue 4, 2023.

[5] Fujishita, R. and Kure, S.: Evaluation of 1.5 degrees Celsius increase due to global warming and several adaptation measures for flood and erosion risks in rivers in Toyama prefecture, *Japan, Journal of Japan Society of Civil Engineers, Ser. G (Environmental Research)*, Vol. 79, Issue 5, 2023.

[6] Ishikawa, S., Kure, S., Kikuchi, D., Takeda, N. and Aoki, A.: Assessment of changes in streamflow due to global warming and evaluation of several adaptation measures in rivers in Toyama Prefecture, *Journal of Japan Society of Civil Engineers, Ser. G (Environmental Research)*,